Corso di dottorato di ricerca in:

"Scienze e Biotecnologie Agrarie"

Ciclo XXXVII

"Molecular and physiological insights into chloroplast function during phytoplasma infection in tomato"

Dottorando
Fernando Rodrigo de Oliveira Cantao

Supervisore
Prof. Fabio Marroni

Co-supervisore
Dott.ssa Simonetta Santi

Coordinatore
Prof. Stefano Bovolenta

Prof.ssa Rita Musetti

Anno (2025)

To God, for His unwavering guidance, strength, and wisdom throughout this journey. Without His grace, none of this would have been possible.

To my family, whose love, support, and encouragement have been my foundation. You have been my constant source of strength and inspiration, and I am deeply grateful for your endless patience and belief in me.

To my supervisors, for their invaluable mentorship, knowledge, and direction. Your guidance has shaped not only this work but also my professional and personal growth. Thank you for your dedication and commitment to my success.

Structure of Chapters

Chapter I - General Introduction and Aim of the work

1.1 Introduction

Phytoplasmas are cell wall-deficient bacteria belonging to the class *Mollicutes* (Hogenhout et al., 2008; Kirdat et al., 2023; Minato et al., 2014). In plants, phytoplasmas are found exclusively within sieve elements (Doi et al., 1967; Hogenhout et al., 2008; Musetti et al., 2023; van Bel & Musetti, 2019), which are highly specialized transport cells that offer a physical and chemical environment suitable for phytoplasmas (van Bel et al., 2022). Genomic analyses indicate that they evolved from Gram-positive bacteria through reductive evolution (Kube et al., 2008; Marcone, 2014; Oshima et al., 2013). As a result, phytoplasmas possess the smallest genome among all known plant-pathogenic bacteria, have limited metabolic pathways and their survival likely depends on plant resources, as they lack many essential genes required for cellular metabolism (Kube et al., 2012).

Phloem-feeding insects, mainly leafhoppers, planthoppers, and psyllids from the families *Cicadellidae*, *Derbidae*, and *Cixiidae* serve as the primary means of phytoplasma transmission, although these pathogens can also spread through vegetative propagation of infected plants (Hogenhout et al., 2008; Kirdat et al., 2023; Kumari et al., 2019; Minato et al., 2014). Phytoplasmas are known to induce diseases in a broad spectrum of host plants and have been reported in over 100 countries, as evident from the sequences available in the GenBank database (Kirdat et al., 2023). They cause significant economic and ecological impacts on species worldwide, including vegetables, spices, medicinal plants, and ornamentals (Bertaccini et al., 2022; Brooks et al., 2022; Drcelic et al., 2024; Lee et al., 2000; Wang et al., 2024). These pathogens cause severe plant malformations, such as witches' broom, dwarfism, phyllody (where floral organs transform into leaf-like structures), virescence (the greening of floral organs), and flower sterility (Christensen et al., 2005; Hogenhout et al., 2008; Yong, 2014). In many plants infected by

phytoplasmas, reduction in chlorophyll and carotenoid levels, along with the suppression of their biosynthesis are observed (Xue et al., 2018).

Recently Buoso et al., (2019) has shown that phytoplasma-infected tomato plants (cultivar Micro-Tom, MT) exhibited alteration on photosynthetic machinery (Buoso et al., 2019), including thylakoid organization, altered expression of genes involved in porphyrin/chlorophyll metabolism, photosynthetic light reactions, and flowering control, leading to a subsequent reduction in photosynthesis. Emerging findings have highlighted a crucial and previously underappreciated role for chloroplasts in coordinating a wide range of plant immune responses (Kachroo et al., 2021).

While oxygenic photosynthesis and primary metabolism remain central to chloroplast functions, these organelles are also capable of processing and responding to environmental cues by reprogramming the synthesis of primary and secondary metabolites (Serrano et al., 2016; Wang et al., 2020). In response to environmental and developmental cues, chloroplasts generate signals that modulate nuclear gene expression, a process known as chloroplast-to-nucleus retrograde signaling (Chan et al., 2016; de Souza et al., 2017; Loudya et al., 2024; Sowden et al., 2018; Wang et al., 2024). This altered gene expression often leads to changes in the production of proteins that are imported back into the chloroplast, impacting its development or function. It is now understood that chloroplast signaling extends beyond the regulation of chloroplast-specific proteins, influencing various aspects of plant physiology and development, including pathogen defense, through chloroplast-generated signals (Hogenhout et al., 2008). These signals also interact with other organelles, such as mitochondria and peroxisomes (Kuźniak & Kopczewski, 2020).

Chloroplasts are also well known for synthesizing phytohormone precursors (Wang et al., 2020), which play a key role in pathogen resistance (Bürger & Chory, 2019; Robert-Seilaniantz et al., 2011). Plant hormones are small organic molecules that play crucial regulatory roles in controlling plant growth and developmental processes (Wang et al.,

2020). They also play a role in regulating plant defense mechanisms against pathogens (Dermastia, 2019). Plant hormones function through intricate interaction networks, referred to as hormone crosstalk, which lead to physiological changes, including alterations in plant immunity (Kohli et al., 2013). The primary hormones involved in plant immune responses are salicylic acid (SA), jasmonic acid (JA), and ethylene (Dermastia, 2019). Additionally, chloroplasts are pivotal in plant immunity, serving as the site for the biosynthesis of several key signaling molecules, including reactive oxygen species (ROS) (Serrano et al., 2016).

One of the key challenges in managing phytoplasmas lies in its complex life cycle and its reliance on insect vectors (Kosovac et al., 2018). The wide range of plant and insect hosts makes phytoplasma outbreaks highly unpredictable. Additionally, the long incubation periods in both plants and insects often result in late detection, typically near crop harvest and after the phytoplasmas have already been spread by insect vectors. This complicates efforts to control or disrupt the disease cycle (Hogenhout et al., 2008). Furthermore, the lack of phytoplasma-resistant cultivars and the unavailability of effective chemical treatments make disease management even more challenging.

New perspectives in managing phytoplasmas focus on integrated pest management (IPM) approaches, which combine biological control, vector management, and molecular techniques, as well as the selection and screening of plants resistant to phytoplasma infection (Bianco, 2024; Osler et al., 2016). Furthermore, advances in genomics and molecular biology have opened opportunities to better understand the interactions between the phytoplasma, its host plants, and vectors, offering potential for the development of more targeted and sustainable control strategies (Bianco, 2024; Omenge et al., 2025).

1.1.2 Phytoplasmas: An overview

Despite their economic significance and distinctive biological characteristics, phytoplasmas-host interactions are still largely unknown (Musetti et al., 2023). This is primarily attributed to the challenges in culturing them *in vivo*, as well as difficulties in gene delivery and mutagenesis (Namba, 2011). Nevertheless, significant progress has been made in phytoplasma research over the past two decades. Published reviews provide a comprehensive understanding of phytoplasma studies, encompassing their taxonomy, etiology, transmission, and interactions with insect and plant hosts (Bertaccini et al., 2022; Hogenhout et al., 2008; Kirdat et al., 2023; Lee et al., 2000; Sugio et al., 2011; Wei & Zhao, 2022; Weintraub & Beanland, 2006).

Scientists have identified the main agents responsible for phytoplasma transmission, developed classification and detection methodologies, sequenced, and assembled 243 phytoplasma genomes to either complete or draft quality (Wang et al., 2024). Furthermore, researchers have delved into numerous potential phytoplasma effectors, shedding light on the molecular mechanisms through which these pathogens manipulate their hosts (Wang et al., 2024). The initial scientific documentation of a phytoplasma disease dates back two centuries to the observation of the mulberry dwarf disease outbreak in Japan (Ishiie, 1965). However, historical evidence of phytoplasma infection traces back approximately 1,000 years ago in China, where tree peonies (*Paeonia suffruticosa*) were cherished as the most captivating flowers for an extended period (Kirdat et al., 2023). Doi et al., (1967) discovered pleomorphic bodies within the phloem tissue of symptomatic plants, naming them Mycoplasma-like Organisms (MLOs) suggesting their potential involvement as causal agents. The causative agent of these diseases was demonstrated to be transmitted by phloem-feeding insects and through grafting. Additionally, its sensitivity to tetracycline reinforced the hypothesis that the disease agent was a prokaryote (as MLO) rather than virus (Doi et al., 1967; Ishiie, 1965).

Their findings sparked global exploration, linking numerous plant diseases to the persistent presence of MLOs (Bertaccini et al., 2022).

The term "phytoplasma" was formally introduced in 1992, with the establishment of the '*Candidatus* Phytoplasma' genus to encompass these prokaryotes, which lacked extensive genomic data at the time (Kirdat et al., 2023; The IRPCM Phytoplasma/Spiroplasma Working Team – Phytoplasma taxonomy group, 2004; Wang et al., 2024). The classification of an organism as a phytoplasma typically relies on six criteria: (1) it exhibits a pleomorphic structure devoid of cell walls under electron microscopy, (2) it resides in the phloem of plants and correlates with symptoms such as yellows and aberrating growth, (3) transmission occurs via phloem-feeding insects, (4) it shows sensitivity to tetracycline but resistance to penicillin, (5) chromosome size ranges from 530 to 1350 kb with a G + C content of no more than 30%, and (6) it shares genetic associations with mycoplasmas at the DNA level (Bertaccini et al., 2022; Kumari et al., 2019; The IRPCM Phytoplasma/Spiroplasma Working Team - Phytoplasma taxonomy group, 2004; Wang et al., 2024).

Phytoplasmas are obligate parasitic bacteria lacking cell walls, thrive in isotonic environments, i.e. sieve elements and insect hemolymph (Figures 1 and 2) and are mainly transmitted by phloem-feeding insects such as leafhoppers, planthoppers and psyllids (Asudi et al., 2021; Kumari et al., 2019). When insects feed on infected plants, phytoplasmas multiply within the salivary glands of these vectors and subsequently spread into the phloem of healthy plants through their bites as shown in Figure 1. In recent years, researchers attempted to isolate phytoplasmas from host plants and cultivate them in both liquid and solid mediums (Contaldo et al., 2016). However, despite these advancements, cultivation technique remains uncertain and difficult to implement. Thus, further refinement of the entire inoculation process is necessary. Moreover, dodder, a parasitic plant that derives nutrients from host plants' vascular tissue, can act as a vector for phytoplasmas (Chang & Chen, 2024; Kirdat et al., 2023).

Conventional horticultural practices such as grafting contribute to phytoplasma dissemination (Bertaccini, 2007; Tedeschi & Alma, 2006).

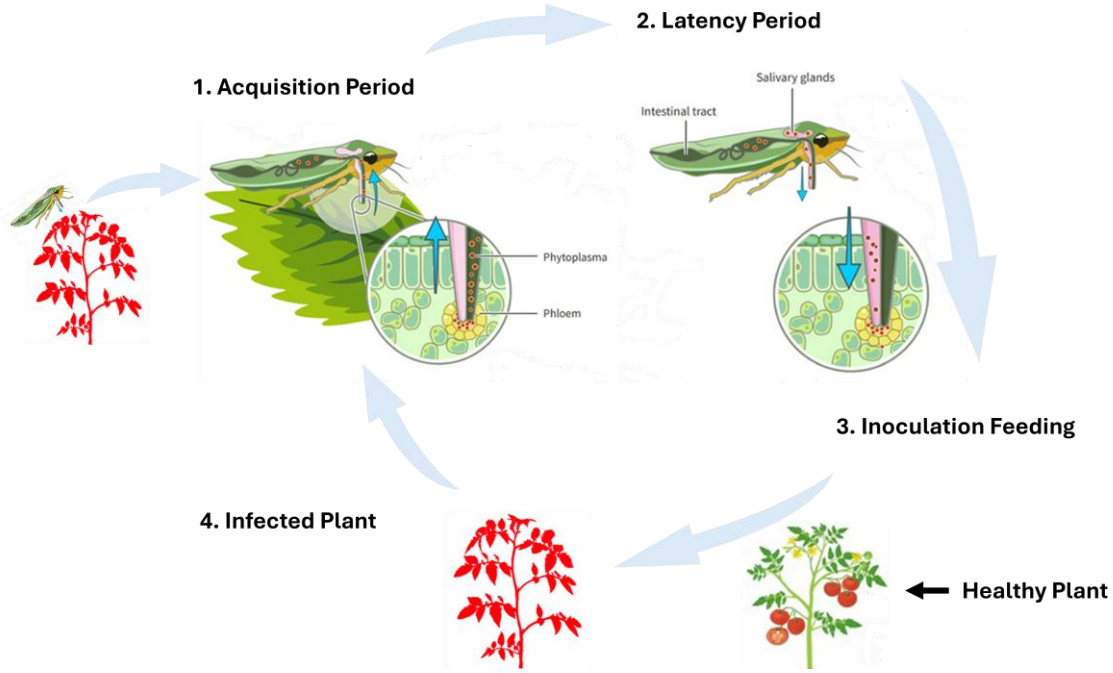

Figure 1. Cycle of phytoplasmas in plant hosts and insect vectors. A healthy leafhopper acquires phytoplasmas by feeding on an infected plant (acquisition feeding). After ingestion (acquisition period), a latency period is required, during which the phytoplasmas multiply and spread within the insect before it becomes capable of transmission. Once infectious, the insect can transmit phytoplasmas to healthy plants during feeding (inoculation feeding). In the host plant, phytoplasma multiplication and systemic colonization are associated with the development of characteristic disease symptoms (Adapted from Santos et al., 2025).

In their insect vectors, phytoplasmas inhabit the hemolymph, with a notable concentration in the salivary glands. Their relationship with both plants and insects is highly intricate, and they possess the ability to manipulate various metabolic pathways, often without adversely affecting the host's viability (Bertaccini et al., 2022).

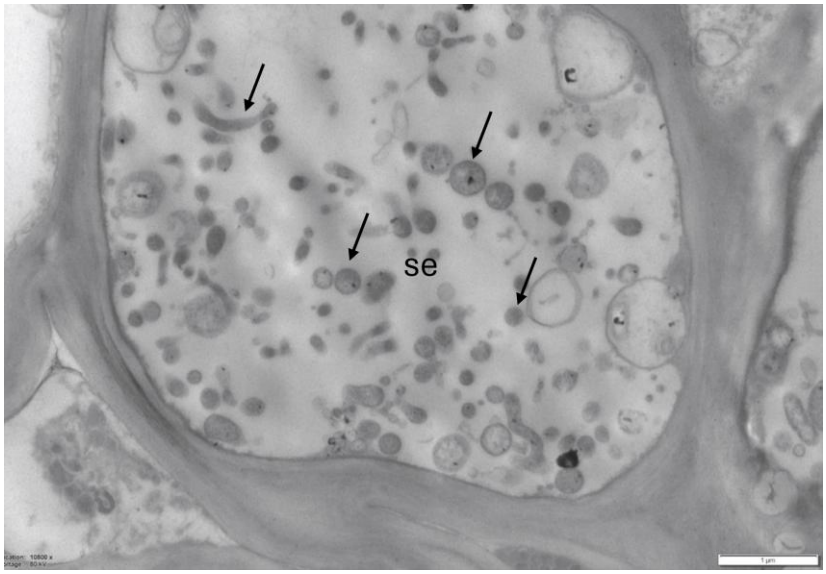

Figure 2. Transmission electron microscopy of phytoplasmas in sieve elements of tomato plants (*Solanum lycopersicum*) cultivar Micro-Tom affected by stolbur [the disease associated with the '*Candidatus* Phytoplasma solani' (*Ca*. P. solani')]. Phytoplasmas (black arrows), located in sieve elements, show a pleomorphic shape. se: sieve elements. Bar indicates 1 µm. Micrograph kindly provided by Professor Rita Musetti, TESAF - Dipartimento Territorio e Sistemi Agro-Forestali, Università degli Studi di Padova.

1.1.3 Phytoplasmas symptomatology

Phytoplasma infected plants display a wide range of symptoms, including yellowing, stunting, virescence, short internodes, phyllody, dwarfism, witches' broom, reduced leaf size, phyllody, greening of floral organs and sterility (Asudi et al., 2021; Buoso et al., 2019, 2022; Musetti et al., 2023; Wang et al., 2024). In severe cases, infection can lead to plant deterioration and death, inflicting significant harm on agricultural production (Asudi et al., 2021; Bertaccini et al., 2014). Phytoplasmas may trigger different symptoms depending on the host, or conversely, different phytoplasmas could prompt similar symptoms in diverse host species (Kumari et al., 2019). Figure 3 illustrates the symptoms of stolbur disease associated with '*Ca.* P. solani' in grapevine plants cv.

Chardonnay, grown in field conditions in Lucinico, GO, Italy (on the left). Symptoms include chlorosis, reduced shoot internodes, smaller leaf size, leaf rolling and yellowing. On the right, a tomato plant cv. Micro-Tom (MT) grown in hydroponic solution in controlled conditions, showing symptoms such as yellowing, phyllody, alterations in floral organ morphogenesis, and sterility.

Figure 3. Grapevine cv. Chardonnay grown in field conditions in Lucinico (GO) and on the right Micro-Tom (wild type) stolbur infected [the disease associated with the '*Candidatus* Phytoplasma solani' (*Ca*. P. solani')] grown in hydroponic solution in controlled conditions. Pictures taken by Fernando Cantao, 2022.

1.1.4 Plant-phytoplasma interactions

Phytoplasmas are phloem-restricted bacterial pathogens that establish intimate interactions with their host plants, profoundly reprogramming plant physiology to support their survival and proliferation. Like other biotrophic pathogens, phytoplasmas manipulate host cellular processes to suppress defenses and redirect nutrient flow (Buoso et al., 2019, 2022; Faulkner & Robatzek, 2012; Zhu et al., 2023). RNA-Seq and transcriptomic studies have revealed that phytoplasma infection leads to the differential regulation of genes across various metabolic pathways, including transcriptional

regulation, carbohydrate metabolism, photosynthesis, secondary metabolism, and cell wall remodeling (Buoso et al., 2019, 2022; Albertazzi et al., 2009; Dermastia et al., 2021; Hren et al., 2009). These alterations reflect the phytoplasma's strategy to hijack host cell functions and create a favorable niche for colonization.

A hallmark of phytoplasma infection is the disruption of sugar metabolism and transport (Marco et al., 2021; Santi et al., 2013). Genes involved in sucrose cleavage such as those encoding sucrose synthase, granule-bound starch synthase, and invertases are often upregulated, leading to an accumulation of sugar breakdown products in infected tissues (Santi et al., 2013a, b). In parallel, phytoplasmas interfere with sugar translocation, disturbing the source-sink dynamics within the host by modulating the activity of sugar transporters like members of the SWEET family, which mediate sugar efflux and redistribution between phloem cells and surrounding tissues (Beck et al., 2012; Eom et al., 2015; Marco et al., 2021). This redirection of photoassimilates is believed to be coordinated with pathogen-derived transport systems to ensure the acquisition of essential nutrients.

Phytoplasmas have undergone extensive genome reduction because of their obligate parasitic lifestyle, losing the capacity to synthesize many vital compounds, including amino acids, fatty acids, nucleotides, and sterols (Oshima et al., 2004; Tan et al., 2021). Instead, their genomes are enriched in genes encoding transporters, particularly ABC transporters, which enable the uptake of peptides, sugars, and other metabolites from the host cytoplasm (Oshima et al., 2004, 2013). This metabolic dependence is tightly linked to their localization within the nutrient-rich sieve elements of the phloem, where direct access to plant-derived metabolites supports their growth.

To manipulate host processes, phytoplasmas secrete a diverse array of effector proteins into both the apoplast and intracellular compartments. These effectors alter plant development, suppress immune responses, and rewire metabolic networks to optimize the host environment for colonization and systemic spread (Faulkner &

Robatzek, 2012; Zhu et al., 2023). Together, these strategies underscore the sophisticated interplay between phytoplasmas and their host plants and highlight the importance of transcriptional and physiological reprogramming during infection.

Plants can be infected by a wide range of pathogenic organisms that modify host cells to promote their own growth and spread. Pathogens use various strategies to suppress plant defenses, to extract nutrients from plant cells and to successfully colonize the host (Faulkner & Robatzek, 2012; Zhu et al., 2023). RNA-seq and gene expression studies have shown that numerous metabolic pathways are differentially regulated during phytoplasma infection (Abbà et al., 2014; Bertazzon et al., 2019; Buoso et al., 2019, 2022; Contaldo et al., 2023; Margaria et al., 2014; Pradit et al., 2019; Wang et al., 2018; Ye et al., 2017). These genes have been categorized based on their functions into the following groups: transcription factors and signal transduction, carbohydrate metabolism and photosynthesis, cell wall metabolism, protein and amino acid metabolism, secondary metabolism, and protein synthesis (Kirdat et al., 2023). Phytoplasmas rely on plant-derived nutrients, such as sugars and other metabolites, which are found in the apoplastic space between plant cells but are more abundant within host cells, enclosed by the cell wall (Kirdat et al., 2023) and plasma membrane (Kühn et al., 1997). To access these nutrients, pathogens must either degrade plant tissues and cells, as necrotrophic pathogens do, or manipulate living host cells to deliver nutrients, as seen in biotrophic pathogens (Faulkner & Robatzek, 2012).

The disruption of sugar metabolism in infected plants reflects the abnormal regulation of genes encoding key enzymes that use sucrose and other sugars as substrates in various biochemical reactions. Genes coding for sucrose synthase, granule-bound starch synthase, and invertase are upregulated during infection, indicating an increase in sugar cleavage products within cells (Santi et al., 2013a,b). Furthermore, phytoplasmas not only affect sugar synthesis and cleavage but also interfere with sugar

transport, altering the source-sink relationship across different plant organs (Kühn et al., 1997; Marco et al., 2021; Santi et al., 2013a,b).

Plant sugar transporters, such as Sugar Will Eventually Be Exported Transporters (SWEET) family, play roles in both intercellular and intracellular sugar translocation, with some acting in cells adjacent to the sieve elements (Beck et al., 2012; Eom et al., 2015; Zipfel et al., 2006), likely in coordination with pathogen-encoded transporters (Bernoux et al., 2011; Melotto et al., 2006). Many other transporters facilitate the exchange of sugars and other metabolites between sieve elements and surrounding cells along the phloem pathway (Aubry et al., 2019).

Residing in the nutrient-rich phloem tissues of plants, phytoplasmas have undergone reductive evolution (Tan et al., 2021). This is evident by the loss of numerous genes essential to free-living organisms, such as the tricarboxylic acid cycle, pentose phosphate pathway, sterol biosynthesis, fatty acid biosynthesis, de novo nucleotide synthesis, and the biosynthesis of most amino acids (Oshima et al., 2004). Conversely, phytoplasma genomes contain multiple copies of transporter-related genes, including ABC transporters, which facilitate the import of peptides, amino acids, and other nutrients into the cell (Oshima et al., 2004, 2013). This provides strong evidence that phytoplasmas are highly dependent on host plant-derived metabolites for their growth and successful infection. To facilitate this, they secrete a range of molecules, including effectors into both the extracellular apoplast and intracellular compartments.

1.1.5 Phytoplasma effectors and physiological responses

Phytoplasmas' capacity to infect and replicate within a diverse array of host cells indicates that these bacteria have evolved mechanisms to manipulate cellular processes in plant and insect vector (Drcelic et al., 2024; Hogenhout & Loria, 2008). In plant hosts, infection often leads to a range of symptoms that cause significant developmental changes (Martín-Trillo & Cubas, 2010). As *in vitro* cultivation of these bacteria remains

unsuccessful, studies on the mechanisms and strategies of pathogenicity and characterization of protein effector virulence rely mainly on functional genomics approaches (Drcelic et al., 2024).

As below reported, despite their limited metabolism (Music et al., 2019), phytoplasmas possess numerous genes encoding transporters that enable them to absorb sugars, amino acids, oligopeptides, and inorganic salts from their host cells, making them dependent on host-derived metabolites (Buoso et al., 2022; Chen et al., 2014; Kube et al., 2014). Also, phytoplasmas possess highly active secretion systems (Chen et al., 2014); it is estimated that most phytoplasmas secrete over a dozen proteins, likely functioning as effectors (Oshima et al., 2004; Wei et al., 2022).

According to Sugio et al., (2011), the secreted effector proteins target host cells, reprogramming plant development and defense responses. As endocellular parasites, phytoplasmas do not require a complex secretion system to deliver effectors across plant cell membranes (MacLean et al., 2011). Phytoplasmas secrete effectors directly into the cytoplasm of sieve cells via the Sec-dependent protein translocation pathway, where the signal peptide is cleaved off (Drcelic et al., 2024; Hogenhout & Loria, 2008; Kakizawa et al., 2004). Phytoplasma effectors are then transported symplastically, moving from the sieve elements to target other plant cells (Bai et al., 2009; Hoshi et al., 2009). As a result, these secreted proteins are thought to play a crucial role in the interactions between phytoplasmas and their host cells (Bai et al., 2009; Hogenhout & Loria, 2008; Oshima et al., 2011). Over the past 15 years, the roles of numerous effectors have been uncovered, and their functions are summarized in Table 1.

Table 1. Function and target of phytoplasma effectors (Wang et al., 2024).

Function	Effector	Phytoplasma	Host target	Reference
Witches' broom	SAP11	AY-WB/CaPM/WBDL	MdTCP16/MdTCP24/ MdTCP25/AtTCP4/AtTCP13	Al-Subhi et al., 2021; Chang et al., 2018; Mittelberger et al., 2022; Sugio et al., 2011
	SAP54	PaWB	SPLa	Cao et al., 2021
	TENGU	OY-M	ARF	Hoshi et al., 2009
	SWP1	'*Candidatus* Phytoplasma tritici'	BRC1	Wang et al., 2018
	Zaofeng 6	JWB	ZjTCP7	Chen et al., 2022
	SJP1 SJP2	JWB	ZjBRC1	Zhou et al., 2021
	SAP05	AY-WB	SPL GATA	Huang et al., 2021
	PM19_00189	CaPM	xxxxxxx	Boonrod et al., 2022
Leaf dysplasia	SAP11 PM19_00189	AY-WB CaPM	TCP	Boonrod et al., 2023; Strohmayer et al., 2021
Dwarfism	TENGU	OY-M	ARF	Hoshi et al., 2009; Sugawara et al., 2013
	SAP05	AY-WB	SPL GATA	Huang et al., 2021
	Zaofeng 3	JWB	MTF TCP	Chen et al., 2021
	SAP11	CaPM	Class II TCPs (TCP2-like, TCP13-like)	Tan et al., 2016
Disrupts cell integrity	PME2	CaPM	xxxxxxx	Mittelberger et al., 2019
Floral dysplasia	SAP54	AY-WB	MTF	MacLean et al., 2011
	PHYL1	AY-WB PnWB	MTF	Hu et al., 2015; Maejima et al., 2014;
	SAP11	MBSP	TB1/CYC TCP	Pecher et al., 2019
	TENGU	OY-M	ARF6/ARF8	Minato et al., 2014
	SJP3	JWB	MADS-box genes	Deng et al., 2021
	S54LP	SP	xxxxxxx	Singh & Lakhanpaul, 2020
Affects Hormones	SAP11	AY-WB CaPM	AtTCP1/AtTCP2	Janik et al., 2017; MacLean et al., 2011; Sugio et al., 2011
	TENGU	OY-M	ARF6/ARF8	Minato et al., 2014
	ATP_00189	CaPM	MdTCP24/MdTCP25	Janik et al., 2017
Volatile	SAP11	CaPM	NbOMT1	Tan et al., 2016
Insects attraction	SAP11	AY-WB	AtTCP1/AtTCP2	Sugio et al., 2011

	SAP54	AY-WB	MTF	MacLean et al., 2014; Orlovskis & Hogenhout, 2016
	PM19_00185	'*Ca*. Phytoplasma mali'	I and II TCP	Strohmayer et al., 2019, 2021
Immunity	SAP11	AY-WB	ELI3-1/PR1/LOX2	Lu et al., 2014
	SWP11	'*Ca*. Phytoplasma tritici'	H1N1/PR1/NPR1	Wang et al., 2018
	SWP12	'*Ca*. Phytoplasma tritici'	TaWRKY74	Bai et al., 2022
	SWP16	'*Ca*. Phytoplasma tritici'	SKP1	Wang et al., 2021
	ATP_00136 PME2	CaPM	xxxxxxxx	Mittelberger et al., 2019
	Zaofeng 6	JWB	xxxxxxxx	Chen et al., 2022
	ncSecP3/9/1214/ 16/22	'*Ca*. Phytoplasma ziziphi'	xxxxxxxx	Gao et al., 2023

The regulation of plant morphogenesis and the attraction of insect vectors are considered critical for the survival strategies of phytoplasmas, implying that inhibiting effector proteins could be a potential method to control phytoplasma infections (Oshima et al., 2023).

1.1.6 Plants immune system

In plants, there is an antagonistic relationship between immunity and growth, known as the growth-immunity trade-off (Kuźniak & Kopczewski, 2020; Sowden et al., 2018). Immune responses can temporarily suppress plant growth, while vigorous growth can impede defense mechanisms. This trade-off likely arises from the diversion of energy and metabolites derived from photosynthesis towards defense-related pathways rather than growth (Kuźniak & Kopczewski, 2020).

Our understanding of plant immunity has advanced significantly over the past 30 years (Kachroo et al., 2021). Following the cloning of plant disease resistance (R) proteins, researchers identified an innate immune system consisting of surface-localized pattern recognition receptors (PRRs) and intracellular nucleotide-binding leucine-rich repeat receptors (NLRs) (Ngou et al., 2022). PRRs detect conserved pathogen-associated molecular patterns (PAMPs) and trigger PAMP-triggered immunity (PTI), the first line of

active plant defense (Kachroo et al., 2021), while NLRs recognize specific pathogen effectors and initiate effector-triggered immunity (ETI), a second layer of immune response. In response, adapted pathogens have developed sophisticated strategies to suppress PTI using small molecules and protein effectors. To counter this, plants deploy R proteins that directly or indirectly recognize these effectors or the cellular disturbances they cause, activating ETI (Ngou et al., 2022). These discoveries led to the development of the classical zig-zag model of plant immunity (Ngou et al., 2022). However, it has become increasingly evident that this model is overly simplistic, and strong evidence now suggests an interdependence between PRR and R proteins for the effective activation of immune responses (Kachroo et al., 2021; Zhu et al., 2023). Despite structural differences, PRRs and NLRs share considerable overlaps in downstream signaling pathways, including mitogen-activated protein kinase (MAPK) cascades, calcium flux, bursts of ROS, transcriptional reprogramming, and phytohormone signaling (Nomura et al., 2012).

1.1.7 Chloroplasts: from photosynthesis to plant immune defense

A crucial and previously overlooked role of chloroplasts in orchestrating various plant immune responses has recently come to light (Kachroo et al., 2021). While oxygenic photosynthesis and primary metabolism remain central to chloroplast functions, these organelles also play a key role in integrating, decoding, and responding to environmental signals.

Beyond its classical function in photosynthesis, the chloroplast has emerged as a multifunctional signaling hub that integrates metabolic, developmental, and immune pathways, positioning it as a central regulator of plant adaptation and stress resilience (Geng et al., 2023; Nomura et al., 2012; Padmanabhan & Dinesh-Kumar, 2010). Upon pathogen recognition, plant immunity is activated through two distinct yet coordinated signaling pathways. The first is cytoplasmic, involving MAPK cascades and calcium (Ca^{2+}) signaling, which collectively reprogram nuclear gene expression. The second is

chloroplast-centered, mobilizing the production of ROS and key defense-related hormones such as salicylic acid (SA) and jasmonic acid (JA) (Nomura et al., 2012).

The chloroplast serves as both a generator and modulator of ROS during immune responses. Distinct ROS species originate from different sites within the chloroplast: singlet oxygen ($^1O_2$), primarily generated at Photosystem II under high light or stress conditions, and superoxide (O_2^-) and hydrogen peroxide (H_2O_2), mainly produced at Photosystem I (Crawford et al., 2018; Galvez-Valdivieso & Mullineaux, 2010; Wang et al., 2024). Additionally, the accumulation of tetrapyrrole intermediates such as protochlorophyllide, protoporphyrin IX, and uroporphyrinogen III can enhance $^1O_2$ formation, which, in turn, triggers SA biosynthesis through EXECUTER1 (EX1) and Genome Uncoupled 1 (GUN1) signaling nodes (Crawford et al., 2018; Geng et al., 2023). This mechanism tightly couples chloroplast redox status with immune hormone production.

Importantly, the chloroplast is not merely a passive target of immune signaling, it actively perceives and transduces pathogen-derived signals. For instance, PAMPs initiate a stromal Ca^{2+} wave involving the calcium sensor (CAS), which functions upstream of SA accumulation and gene activation (Nomura et al., 2012). This indicates a direct chloroplast-mediated route of immune activation during both PTI and ETI (de Torres Zabala et al., 2015; Serrano et al., 2016). These tightly regulated signaling circuits underscore the chloroplast's dual role as both a sensor and an executor of immune function, particularly through the production of ROS, salicylic acid precursors, and defense-related retrograde signals (Caplan et al., 2015; Medina-Puche et al., 2020).

In addition to its immunological role, the chloroplast is indispensable to primary and secondary metabolism. It houses pathways for the biosynthesis of fatty acids, amino acids, pigments, and various phytohormones, while also participating in nitrogen and sulfur assimilation (Richter et al., 2023; Wu & Bock, 2021). The chloroplast's evolutionary origin as a cyanobacterial endosymbiont led to a massive gene transfer to

the host nuclear genome (Archibald, 2009; Keeling, 2013), resulting in a small, retained plastid genome (~100 genes) and a large set of nucleus-encoded chloroplast proteins (NECGs) that must be post-translationally imported (Bock, 2017; Christian et al., 2020). This genomic division requires meticulous coordination between nuclear and plastid gene expression. Such coordination is achieved through bidirectional communication: anterograde signals direct plastid development and function from the nucleus, while retrograde signals transmit the developmental and functional state of the chloroplast back to the nucleus, enabling adaptive transcriptional responses (Dietz et al., 2019; Kleine & Leister, 2016a).

Retrograde signaling (RS) refers to the communication pathways through which chloroplasts modulate nuclear gene expression in response to developmental and environmental cues. RS operates in two primary modes: biogenic and operational. Biogenic RS predominates during chloroplast biogenesis: it is closely associated with plastid gene expression, protein homeostasis, and developmental signaling and has the purpose of coordinating nuclear gene expression during plastid development. It can be altered by disruptions in plastid transcription or translation, accumulation of tetrapyrrole intermediates (e.g., Mg-protoporphyrin IX or heme), and metabolic cues linked to lipid and antioxidant status, including α-tocopherol-binding proteins (Kleine & Leister, 2016b; Larkin, 2016; Pogson et al., 2008). In contrast, operational RS is the dominant mode in mature chloroplasts and responds to environmental or metabolic perturbations, including redox imbalances, disrupted photosynthetic electron transport, accumulation of ROS, and impaired carbon or nitrogen metabolism (Chan et al., 2016; Dietz et al., 2019; Foyer & Noctor, 2009). While biogenic signals coordinate organelle assembly, operational signals function primarily to maintain chloroplast homeostasis and adapt cellular processes to changing external or internal conditions.

An increasingly recognized third dimension of retrograde signaling (RS) involves chloroplast-derived metabolites, particularly carotenoid cleavage products known as

apocarotenoids. Compounds such as β-cyclocitral (β-CC), β-ionone, zaxinone, and anchorene act as signaling intermediates under oxidative or high-light stress and can modulate nuclear gene expression through pathways that appear to function at least partially independently of classical RS components such as GUN1 (Chan et al., 2016; D'Alessandro et al., 2018; Ramel et al., 2012). These apocarotenoids are considered operational RS molecules and reflect the growing complexity and crosstalk among different plastid-to-nucleus communication pathways. These molecules intersect with carotenoids play a dual role in reactive oxygen species (ROS) signaling pathways, contributing both to photoprotection and to plastid-to-nucleus communication (Colombo et al., 2016; D'Alessandro et al., 2018; Ramel et al., 2013). In addition to their functions as photoprotective compounds and retrograde signaling molecules, carotenoids also serve as precursors in the biosynthesis of several phytohormones (Al-Babili & Bouwmeester, 2015; Nambara & Marion-Poll, 2005). Carotenoids such as lycopene, β-carotene, xanthophylls, and zeaxanthin contain a conjugated polyene backbone that enables them to serve as vital light-harvesting pigments and photoprotective agents. Under excess light conditions, they quench excitation energy and dissipate it as heat, while also protecting Photosystem II (PSII) from photodamage by scavenging excited chlorophyll states (^{1}Chl*, ^{3}Chl*) and $^1O_2$, thereby limiting ROS formation (Wang et al., 2024). Carotenoid-derived signals are also implicated in responses to abiotic stress and pathogen attack (Chi et al., 2015; Wang et al., 2024). Indeed, loss of an early step in carotenoid biosynthesis results in a repression of Photosynthesis-Associated Nuclear Genes (PhANGs) and leads to arrested leaf development (Avendano-Vasquez et al., 2014).

Pathogens often exploit chloroplast-mediated signaling by targeting chloroplast functions through effector proteins, underscoring the organelle's strategic importance in plant defense (Yang et al., 2021). In turn, hormonal networks refine the immune response. While SA, JA, and ethylene are central to plant immune signaling (Dermastia,

2019), other phytohormones including abscisic acid, auxins, cytokinins, gibberellins, brassinosteroids, and peptide hormones act as modulators that fine-tune defense responses (Bari & Jones, 2009; Shigenaga et al., 2017; Shigenaga & Argueso, 2016). Given the chloroplast's role in the biosynthesis and signaling of multiple hormones, its contribution to immune regulation is likely both direct and highly integrative (Kachroo et al., 2021).

1.1.8 Retrograde and Anterograde Signaling: Insights from GENOMES UNCOUPLED

A breakthrough in understanding biogenic retrograde signaling emerged from an elegant genetic screen in *Arabidopsis thaliana* that identified GENOMES UNCOUPLED (GUN) mutants. These mutants display constitutive expression of Light Harvesting Complex genes associated with Photosystem II (LHCBs) even after treatment with norflurazon (NF), an inhibitor of carotenoid biosynthesis that disrupts chloroplast function (Loudya et al., 2024; Susek et al., 1993; Woodson et al., 2011; Wu & Bock, 2021), failing to fully repress also other PhANGs (Susek et al., 1993). The underlying assumption was that these mutant screens would uncover genes involved in retrograde communication pathways. Several mutants with deregulated expression of LHCBs and Ribulose-1,5-bisphosphate carboxylase/oxygenase small subunit (RBCS) genes were identified and termed "GUN mutants" the associated genes were mapped to six distinct loci in the *Arabidopsis* genome (Loudya et al., 2024; Wu & Bock, 2021).

The identification of GUN loci (Larkin et al., 2003; Loudya et al., 2024; Mochizuki et al., 2001; Strand et al., 2003) revealed the involvement of tetrapyrroles, particularly the repressive action of an intermediate in chlorophyll biosynthesis, Mg-protoporphyrin IX (Kropat et al., 1997; Loudya et al., 2024; Strand et al., 2003; Vasileuskaya et al., 2004; Wu & Bock, 2021; Zhang et al., 2015). However, it was later proposed that this mechanism might involve an activating molecule related to heme, whose synthesis increases when the chlorophyll branch of the tetrapyrrole pathway is blocked,

influencing PhANGs regulation (Larkin, 2016; Wu & Bock, 2021), disrupting retrograde signaling between plastids and the nucleus (Koussevitzky et al., 2007; Larkin et al., 2003; Mochizuki et al., 2001; Susek et al., 1993; Woodson et al., 2011). Emphasizing the importance of this pathway in biogenic signaling (Loudya et al., 2024; Wu & Bock, 2021), specifically, the GUN5 and GUN4 proteins play a role in magnesium chelation, which is a crucial step in the biosynthesis of Mg-protoporphyrin IX (Mg-ProtoIX), the first committed precursor of chlorophyll (Chan et al., 2016; Larkin et al., 2003). Defective chloroplasts in mutants affecting plastid protein synthesis (Pesaresi et al., 2006), import (Kakizaki et al., 2009) and quality control (Kato et al., 2007) highlight the necessity for coordination between chloroplastic protein processing and nuclear transcription.

The regulation of PhANGs in conjunction with protein import involves the related GOLDEN 2-LIKE (GLK) transcription factors, GLK1 and GLK2. These factors respond transcriptionally to plastid disturbances (Kakizaki et al., 2009; Waters et al., 2009) and directly bind to the promoters of several PhANGs (Waters et al., 2009). GLK1 and GLK2 operate independently of phytochrome signaling (Waters et al., 2009), Mg-ProtoIX, and ABI4 (Kakizaki et al., 2009). Any discussion of biogenic retrograde signaling would be incomplete without addressing the role of GUN1. Unlike other GUN proteins, GUN1 is not an enzyme directly involved in the tetrapyrrole biosynthetic pathway. Despite extensive research, its molecular and physiological functions as well as the mechanisms by which it modulates retrograde signaling remain largely unknown (Loudya et al., 2024). According to (Terashima et al., 2011), the fine-tuning of leaf development by retrograde signal is connected to light capture and photosynthesis in the chloroplast, as leaf morphology and architecture are influenced by factors like light intensity and gas exchange, which affect photosynthesis and overall chloroplast function. Chloroplasts relay information to the nucleus via retrograde signaling, using metabolites and proteins derived either from developing plastids (biogenic signals) or from mature chloroplasts under stress (operational signals). These cues modulate the expression of three main

classes of nuclear genes: PhANGs (photosynthesis-associated), SORGs (singlet oxygen-responsive), and PRANGs (plastid redox-associated) are shown in Figure 4.

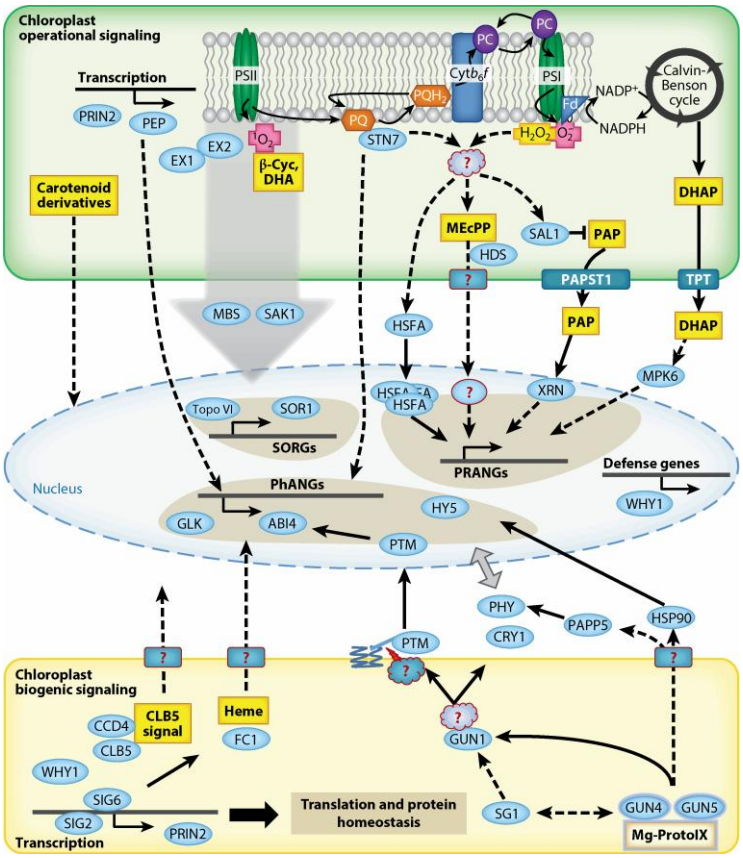

Figure 4. Chloroplasts communicate with the nucleus through retrograde signaling, using metabolite and protein signals that originate from two distinct contexts: biogenic signals from developing chloroplasts, and operational signals from mature chloroplasts responding to environmental stress. These signals regulate nuclear gene expression, broadly categorized into three groups: photosynthesis-associated nuclear genes (PhANGs), which encode components of photosynthetic protein complexes; singlet oxygen-responsive genes (SORGs), which are activated by singlet oxygen generated in photosystem II; and plastid redox-associated nuclear genes (PRANGs), which respond to shifts in plastid redox balance. In the associated diagram, solid arrows represent well-characterized signaling pathways, while dashed and shadowed arrows denote components whose mechanisms remain unresolved. Yellow boxes indicate retrograde signals, with blue ovals and rectangles representing proteins and transporters, respectively. For an in-depth review, see (Chan et al., 2016).

As a central hub in the plant's immune signaling network, the chloroplast is a key target for pathogens aiming to enhance their virulence. Chloroplast immunity is still an evolving field, with many open questions.

1.1.9 Micro-Tom genotypes: a model system for investigating the role of chloroplasts in phytoplasma infection

Micro-Tom (MT) is a dwarf cultivar of *Solanum lycopersicum* widely adopted as a model system in plant biology due to its small size, short life cycle (fruiting in ~60 days), and amenability to genetic transformation (Arie et al., 2007; Buoso et al., 2019, 2022). These features, combined with the availability of mutants affecting chloroplast development and light signaling, make MT an excellent platform for dissecting chloroplast functions in plant-pathogen interactions, including those involving phytoplasmas.

Chloroplasts are increasingly recognized as central players in plant immunity. Beyond their primary roles in photosynthesis and metabolism, they act as signaling hubs and targets of pathogen effectors (Sowden et al., 2018). During infection, plants can reprogram chloroplasts to initiate defense responses, including the production of ROS. While excessive ROS such as H_2O_2 can be damaging, they also function as signaling molecules that contribute to antimicrobial defense (Galvez-Valdivieso & Mullineaux, 2010). Over-reduction of PSII under stress or high light can lead to ROS generation including singlet oxygen $^1O_2$, O_2^- and hydroxyl radicals through the photoreduction of oxygen molecules (Krieger-Liszkay et al., 2011; Pospíšil et al., 2004; Yang et al., 2021). Such oxidative bursts, although harmful when uncontrolled, are tightly regulated by the plant and integrated into immune signaling cascades (Robert-Seilaniantz et al., 2011; Trotta et al., 2014).

The MT cultivar includes key mutants that deepen our understanding of chloroplast-related signaling. One such example is the *Aurea* mutant (*au*/*gun3*), defective in the

biosynthesis of phytochromobilin (PΦB) a tetrapyrrole-derived chromophore required for functional phytochromes (Terry & Kendrick, 1999). Since all phytochrome family members depend on PΦB, *Aurea* exhibits broad deficiencies in photoreceptor signaling, resulting in impaired photomorphogenesis, pale chlorophyll-deficient leaves, and elongated hypocotyls under white light (Koornneef et al., 1985; Muramoto et al., 2005; Terry, 1997). These phenotypes are particularly useful for exploring how chloroplast-derived signals, including those from the tetrapyrrole pathway (Figure 5), regulate nuclear gene expression and developmental programs.

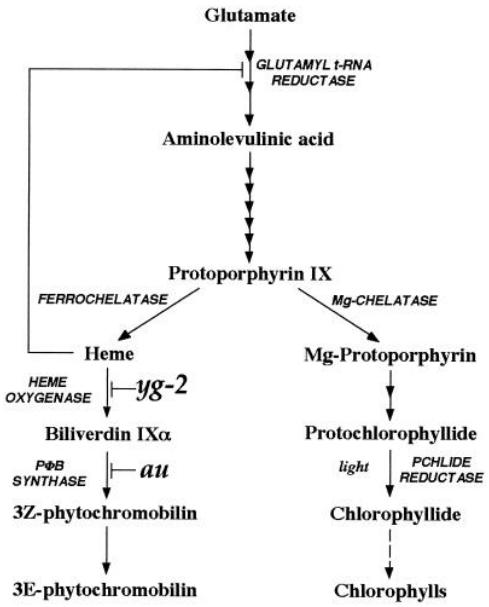

Figure 5. The tetrapyrrole-biosynthesis pathway (Terry & Kendrick, 1999).

Under white light, *Aurea* seedlings exhibit a pale yellow-green phenotype, a hallmark of defective chloroplast biogenesis and impaired de-etiolation (Koornneef et al., 1985; Terry & Kendrick, 1999) (Figure 6). Importantly, the *Aurea* mutant serves as a unique model to explore how perturbations in chloroplast-derived signaling influence systemic plant responses to phytoplasma infection. Although phytoplasmas are confined to the phloem (Christensen et al., 2005), they induce widespread physiological alterations,

including changes in plastid function and photosynthesis of many crops including apple (Bertamini et al., 2003); tomato Buoso et al., 2019, 2022); grape (Vitali et al., 2013; Endeshaw et al., 2012); jujube (Liu et al., 2016); coconut (Maust et al., 2003) and). In this context, the Micro-Tom system provides a genetically tractable platform to dissect the complex crosstalk between chloroplast signaling, hormonal regulation, and immune responses during phytoplasma challenge (Arie et al., 2007; Buoso et al., 2019).

Figure 6. Micro-Tom mutant *Aurea* (right) showing etiolation in the light, which leads to taller, chlorotic and less branched plants. The blue pipette tip is 8 cm. Picture from HCPD LAB-Esalq-USAP. Access on 09/26/2024 https://www.esalq.usp.br/tomato/

1.2. Aims

Building on previous findings from our research group that identified transcriptional changes in photosynthetic light reactions, porphyrin, and chlorophyll metabolism pathways in response to phytoplasma infection, this thesis aims to investigate the role of the chloroplast by highlighting the most affected pathways in plant-pathogen interactions. Specifically, we investigated how '*Ca*. P. solani' infection might affect chloroplast-to-nucleus communication and photosynthetic performance in tomato cv. Micro-Tom.

In the first part of this study, we re-analyzed an RNA-Seq dataset and performed gene co-expression network analysis to compare responses between infected and healthy plants. A multidisciplinary systems biology approach was employed, integrating ecophysiological, molecular, and biochemical analyses to characterize plant responses to phytoplasma infection.

The second part focused on the photomorphogenic Micro-Tom mutant *Aurea*, which is impaired in the synthesis of phytochromobilin due to a mutation in the *GUN3* gene, resulting in a deficiency of active phytochromes and altered light perception and signaling. Through comparative analyses between the wild-type genotype and the phytochrome-deficient *Aurea* mutant, we sought to deepen our understanding of how *'Ca.* P. solani' infection affects plant physiology in the absence of functional phytochromes. As part of the activities conducted during this PhD, we planned and implemented a series of experimental trials involving high-throughput RNA sequencing, biometric measurements, gas exchange analysis, chlorophyll fluorescence, and transmission electron microscopy (TEM) for ultrastructural characterization of chloroplasts. However, the present thesis includes only biometric and photosynthetic datasets.

1.3. References

Abbà, S., Galetto, L., Carle, P., Carrère, S., Delledonne, M., Foissac, X., Palmano, S., Veratti, F., & Marzachì, C. (2014). RNA-Seq profile of flavescence dorée phytoplasma in grapevine. *BMC Genomics*, *15*(1), 1088. https://doi.org/10.1186/1471-2164-15-1088

Albertazzi, G., Milc, J., Caffagni, A., Francia, E., Roncaglia, E., Ferrari, F., Tagliafico, E., Stefani, E., & Pecchioni, N. (2009). Gene expression in grapevine cultivars in response to Bois Noir phytoplasma infection. *Plant Science*, *176*(6), 792–804. https://doi.org/10.1016/j.plantsci.2009.03.001

Al-Babili, S., & Bouwmeester, H. J. (2015). Strigolactones, a Novel Carotenoid-Derived Plant Hormone. *Annual Review of Plant Biology*, *66*(1), 161–186. https://doi.org/10.1146/annurev-arplant-043014-114759

Al-Subhi, A. M., Al-Sadi, A. M., Al-Yahyai, R. A., Chen, Y., Mathers, T., Orlovskis, Z., Moro, G., Mugford, S., Al-Hashmi, K. S., & Hogenhout, S. A. (2021). Witches' Broom Disease of Lime Contributes to Phytoplasma Epidemics and Attracts Insect Vectors. *Plant Disease*, *105*(9), 2637–2648. https://doi.org/10.1094/PDIS-10-20-2112-RE

Archibald, J. M. (2009). The puzzle of plastid evolution. *Current Biology: CB*, *19*(2), Article 2. https://doi.org/10.1016/j.cub.2008.11.067

Arie, T., Takahashi, H., Kodama, M., & Teraoka, T. (2007). Tomato as a model plant for plant-pathogen interactions. *Plant Biotechnology*, *24*(1), 135–147. https://doi.org/10.5511/plantbiotechnology.24.135

Asudi, G. O., Omenge, K. M., Paulmann, M. K., Reichelt, M., Grabe, V., Mithöfer, A., Oelmüller, R., & Furch, A. C. U. (2021). The Physiological and Biochemical Effects on Napier Grass Plants Following Napier Grass Stunt Phytoplasma Infection. *Phytopathology*, *111*(4), Article 4. https://doi.org/10.1094/PHYTO-08-20-0357-R

Aubry, E., Dinant, S., Vilaine, F., Bellini, C., & Le Hir, R. (2019). Lateral Transport of Organic and Inorganic Solutes. *Plants (Basel, Switzerland)*, *8*(1), Article 1. https://doi.org/10.3390/plants8010020

Bai, B., Zhang, G., Li, Y., Wang, Y., Sujata, S., Zhang, X., Wang, L., Zhao, L., & Wu, Y. (2022). The "Candidatus Phytoplasma tritici" effector SWP12 degrades the transcription factor TaWRKY74 to suppress wheat resistance. *The Plant Journal: For Cell and Molecular Biology*, *112*(6), Article 6. https://doi.org/10.1111/tpj.16029

Bai, X., Correa, V. R., Toruño, T. Y., Ammar, E.-D., Kamoun, S., & Hogenhout, S. A. (2009). AY-WB phytoplasma secretes a protein that targets plant cell nuclei. *Molecular Plant-Microbe Interactions: MPMI*, *22*(1), Article 1. https://doi.org/10.1094/MPMI-22-1-0018

Bari, R., & Jones, J. D. G. (2009). Role of plant hormones in plant defence responses. *Plant Molecular Biology*, *69*(4), Article 4. https://doi.org/10.1007/s11103-008-9435-0

Beck, M., Heard, W., Mbengue, M., & Robatzek, S. (2012). The INs and OUTs of pattern recognition receptors at the cell surface. *Current Opinion in Plant Biology*, *15*(4), 367–374. https://doi.org/10.1016/j.pbi.2012.05.004

Bernoux, M., Ellis, J. G., & Dodds, P. N. (2011). New insights in plant immunity signaling activation. *Current Opinion in Plant Biology*, *14*(5), 512–518. https://doi.org/10.1016/j.pbi.2011.05.005

Bertaccini, A. (2007). Phytoplasmas: Diversity, taxonomy, and epidemiology. *Frontiers in Bioscience: A Journal and Virtual Library*, *12*, 673–689. https://doi.org/10.2741/2092

Bertaccini, A., Arocha-Rosete, Y., Contaldo, N., Duduk, B., Fiore, N., Montano, H. G., Kube, M., Kuo, C.-H., Martini, M., Oshima, K., Quaglino, F., Schneider, B., Wei, W., & Zamorano, A. (2022). Revision of the 'Candidatus Phytoplasma' species description guidelines. *International Journal of Systematic and Evolutionary Microbiology*, *72*(4), Article 4. https://doi.org/10.1099/ijsem.0.005353

Bertaccini, A., Duduk, B., Paltrinieri, S., & Contaldo, N. (2014). Phytoplasmas and Phytoplasma Diseases: A Severe Threat to Agriculture. *American Journal of Plant Sciences*, *05*(12), Article 12. https://doi.org/10.4236/ajps.2014.512191

Bertamini, M., Grando, M. S., & Nedunchezhian, N. (2003). Effects of Phytoplasma Infection on Pigments, Chlorophyll-Protein Complex and Photosynthetic Activities in Field Grown Apple Leaves. *Biologia Plantarum*, *46*(2), 237–242. https://doi.org/10.1023/b:biop.0000022258.49957.9a

Bertazzon, N., Bagnaresi, P., Forte, V., Mazzucotelli, E., Filippin, L., Guerra, D., Zechini, A., Cattivelli, L., & Angelini, E. (2019). Grapevine comparative early transcriptomic profiling suggests that Flavescence dorée phytoplasma represses plant responses induced by vector feeding in susceptible varieties. *BMC Genomics*, *20*(1). https://doi.org/10.1186/s12864-019-5908-6

Bianco, C. (2024). Plant-Growth-Promoting Bacteria. *Plants*, *13*(10), 1323. https://doi.org/10.3390/plants13101323

Bock, R. (2017). Witnessing Genome Evolution: Experimental Reconstruction of Endosymbiotic and Horizontal Gene Transfer. *Annual Review of Genetics*, *51*(1), Article 1. https://doi.org/10.1146/annurev-genet-120215-035329

Boonrod, K., Kuaguim, L., Braun, M., Müller-Renno, C., Ziegler, C., & Krczal, G. (2023). Identification of the Actin-Binding Region and Binding to Host Plant Apple Actin of Immunodominant Transmembrane Protein of 'Candidatus Phytoplasma mali.' *International Journal of Molecular Sciences*, *24*(2), Article 2. https://doi.org/10.3390/ijms24020968

Boonrod, K., Strohmayer, A., Schwarz, T., Braun, M., Tropf, T., & Krczal, G. (2022). Beyond Destabilizing Activity of SAP11-like Effector of Candidatus Phytoplasma

mali Strain PM19. *Microorganisms*, *10*(7), Article 7. https://doi.org/10.3390/microorganisms10071406

Brooks, D. R., Hoberg, E. P., Boeger, W. A., & Trivellone, V. (2022). Emerging infectious disease: An underappreciated area of strategic concern for food security. *Transboundary and Emerging Diseases*, *69*(2), Article 2. https://doi.org/10.1111/tbed.14009

Buoso, S., Musetti, R., Marroni, F., Calderan, A., Schmidt, W., & Santi, S. (2022). Infection by phloem-limited phytoplasma affects mineral nutrient homeostasis in tomato leaf tissues. *Journal of Plant Physiology*, *271*, 153659. https://doi.org/10.1016/j.jplph.2022.153659

Buoso, S., Pagliari, L., Musetti, R., Martini, M., Marroni, F., Schmidt, W., & Santi, S. (2019). 'Candidatus Phytoplasma solani' interferes with the distribution and uptake of iron in tomato. *BMC Genomics*, *20*(1), Article 1. https://doi.org/10.1186/s12864-019-6062-x

Bürger, M., & Chory, J. (2019). Stressed Out About Hormones: How Plants Orchestrate Immunity. *Cell Host & Microbe*, *26*(2), Article 2. https://doi.org/10.1016/j.chom.2019.07.006

Cao, Y., Sun, G., Zhai, X., Xu, P., Ma, L., Deng, M., Zhao, Z., Yang, H., Dong, Y., Shang, Z., Lv, Y., Yan, L., Liu, H., Cao, X., Li, B., Wang, Z., Zhao, X., Yu, H., Wang, F., … Fan, G. (2021). Genomic insights into the fast growth of paulownias and the formation of Paulownia witches' broom. *Molecular Plant*, *14*(10), Article 10. https://doi.org/10.1016/j.molp.2021.06.021

Caplan, J. L., Kumar, A. S., Park, E., Padmanabhan, M. S., Hoban, K., Modla, S., Czymmek, K., & Dinesh-Kumar, S. P. (2015). Chloroplast Stromules Function during Innate Immunity. *Developmental Cell*, *34*(1), 45–57. https://doi.org/10.1016/j.devcel.2015.05.011

Chan, K. X., Phua, S. Y., Crisp, P., McQuinn, R., & Pogson, B. J. (2016). Learning the Languages of the Chloroplast: Retrograde Signaling and Beyond. *Annual Review of Plant Biology*, *67*(1), 25–53. https://doi.org/10.1146/annurev-arplant-043015-111854

Chang, H.-C., & Chen, J.-C. (2024). An efficient grafting method for phytoplasma transmission in Catharanthus roseus. *Plant Methods*, *20*(1), 13. https://doi.org/10.1186/s13007-024-01139-w

Chang, S. H., Tan, C. M., Wu, C.-T., Lin, T.-H., Jiang, S.-Y., Liu, R.-C., Tsai, M.-C., Su, L.-W., & Yang, J.-Y. (2018). Alterations of plant architecture and phase transition by the phytoplasma virulence factor SAP11. *Journal of Experimental Botany*. https://doi.org/10.1093/jxb/ery318

Chen, W., Li, Y., Wang, Q., Wang, N., & Wu, Y. (2014). Comparative Genome Analysis of Wheat Blue Dwarf Phytoplasma, an Obligate Pathogen That Causes Wheat Blue

Dwarf Disease in China. *PLoS ONE*, *9*(5), Article 5. https://doi.org/10.1371/journal.pone.0096436

Chen, P., Chen, L., Ye, X., Tan, B., Zheng, X., Cheng, J., Wang, W., Yang, Q., Zhang, Y., Li, J., & Feng, J. (2022). Phytoplasma effector Zaofeng6 induces shoot proliferation by decreasing the expression of ZjTCP7 in Ziziphus jujuba. *Horticulture Research*, *9*, uhab032. https://doi.org/10.1093/hr/uhab032

Chen, Y.-M., Chien, Y.-Y., Chen, Y.-K., Liao, P.-Q., Tan, C.-M., Chiu, Y.-C., Tai, C.-F., & Yang, J.-Y. (2021). Identification of 16SrII-V Phytoplasma Associated with Mungbean Phyllody Disease in Taiwan. *Plant Disease*, *105*(9), Article 9. https://doi.org/10.1094/PDIS-12-20-2683-SC

Chi, W., Feng, P., Ma, J., & Zhang, L. (2015). Metabolites and chloroplast retrograde signaling. *Current Opinion in Plant Biology*, *25*, 32–38. https://doi.org/10.1016/j.pbi.2015.04.006

Christensen, N. M., Axelsen, K. B., Nicolaisen, M., & Schulz, A. (2005). Phytoplasmas and their interactions with hosts. *Trends in Plant Science*, *10*(11), Article 11. https://doi.org/10.1016/j.tplants.2005.09.008

Christian, R. W., Hewitt, S. L., Roalson, E. H., & Dhingra, A. (2020). Genome-Scale Characterization of Predicted Plastid-Targeted Proteomes in Higher Plants. *Scientific Reports*, *10*(1), Article 1. https://doi.org/10.1038/s41598-020-64670-5

Colombo, M., Tadini, L., Peracchio, C., Ferrari, R., & Pesaresi, P. (2016). GUN1, a Jack-Of-All-Trades in Chloroplast Protein Homeostasis and Signaling. *Frontiers in Plant Science*, *7*. https://doi.org/10.3389/fpls.2016.01427

Contaldo, N., Satta, E., Zambon, Y., Paltrinieri, S., & Bertaccini, A. (2016). Development and evaluation of different complex media for phytoplasma isolation and growth. *Journal of Microbiological Methods*, *127*, 105–110. https://doi.org/10.1016/j.mimet.2016.05.031

Contaldo, N., Zambon, Y., Galbacs, Z. N., Miloro, F., Havelda, Z., Bertaccini, A., & Varallyay, E. (2023). Small RNA Profiling of Aster Yellows Phytoplasma-Infected Catharanthus roseus Plants Showing Different Symptoms. *Genes*, *14*(5), 1114. https://doi.org/10.3390/genes14051114

Crawford, T., Lehotai, N., & Strand, Å. (2018). The role of retrograde signals during plant stress responses. *Journal of Experimental Botany*, *69*(11), 2783–2795. https://doi.org/10.1093/jxb/erx481

D'Alessandro, S., Ksas, B., & Havaux, M. (2018). Decoding β-Cyclocitral-Mediated Retrograde Signaling Reveals the Role of a Detoxification Response in Plant Tolerance to Photooxidative Stress. *The Plant Cell*, *30*(10), 2495–2511. https://doi.org/10.1105/tpc.18.00578

de Souza, A., Wang, J.-Z., & Dehesh, K. (2017). Retrograde Signals: Integrators of Interorganellar Communication and Orchestrators of Plant Development. *Annual Review of Plant Biology*, *68*, 85–108. https://doi.org/10.1146/annurev-arplant-042916-041007

de Torres Zabala, M., Littlejohn, G., Jayaraman, S., Studholme, D., Bailey, T., Lawson, T., Tillich, M., Licht, D., Bölter, B., Delfino, L., Truman, W., Mansfield, J., Smirnoff, N., & Grant, M. (2015). Chloroplasts play a central role in plant defence and are targeted by pathogen effectors. *Nature Plants*, *1*(6), Article 6. https://doi.org/10.1038/nplants.2015.74

Dermastia, M. (2019). Plant Hormones in Phytoplasma Infected Plants. *Frontiers in Plant Science*, *10*, 477. https://doi.org/10.3389/fpls.2019.00477

Dermastia, M., Škrlj, B., Strah, R., Anžič, B., Tomaž, Š., Križnik, M., Schönhuber, C., Riedle-Bauer, M., Ramšak, Ž., Petek, M., Kladnik, A., Lavrač, N., Gruden, K., Roitsch, T., Brader, G., & Pompe-Novak, M. (2021). Differential Response of Grapevine to Infection with "Candidatus Phytoplasma solani" in Early and Late Growing Season through Complex Regulation of mRNA and Small RNA Transcriptomes. *International Journal of Molecular Sciences*, *22*(7), 3531. https://doi.org/10.3390/ijms22073531

Dietz, K.-J., Wesemann, C., Wegener, M., & Seidel, T. (2019). Toward an Integrated Understanding of Retrograde Control of Photosynthesis. *Antioxidants & Redox Signaling*, *30*(9), Article 9. https://doi.org/10.1089/ars.2018.7519

Dodds, P. N., & Rathjen, J. P. (2010). Plant immunity: Towards an integrated view of plant-pathogen interactions. *Nature Reviews. Genetics*, *11*(8), Article 8. https://doi.org/10.1038/nrg2812

Doi, Y., Teranaka, M., Yora, K., & Asuyama, H. (1967). Mycoplasma- or PLT Group-like Microorganisms Found in the Phloem Elements of Plants Infected with Mulberry Dwarf, Potato Witches' Broom, Aster Yellows, or Paulownia Witches' Broom. *Japanese Journal of Phytopathology*, *33*(4), 259–266. https://doi.org/10.3186/jjphytopath.33.259

Drcelic, M., Skiljaica, A., Polak, B., Bauer, N., & Seruga Music, M. (2024). 'Candidatus Phytoplasma solani' Predicted Effector SAP11-like Alters Morphology of Transformed Arabidopsis Plants and Interacts with AtTCP2 and AtTCP4 Plant Transcription Factors. *Pathogens*, *13*(10), Article 10. https://doi.org/10.3390/pathogens13100893

Endeshaw, S. T., Murolo, S., Romanazzi, G., & Neri, D. (2012). Effects of Bois noir on carbon assimilation, transpiration, stomatal conductance of leaves and yield of grapevine (*Vitis vinifera*) cv. Chardonnay. *Physiologia Plantarum*, *145*(2), 286–295. https://doi.org/10.1111/j.1399-3054.2012.01576.x

Eom, J.-S., Chen, L.-Q., Sosso, D., Julius, B. T., Lin, I. W., Qu, X.-Q., Braun, D. M., & Frommer, W. B. (2015). SWEETs, transporters for intracellular and intercellular sugar translocation. *Current Opinion in Plant Biology*, *25*, 53–62. https://doi.org/10.1016/j.pbi.2015.04.005

Faulkner, C., & Robatzek, S. (2012). Plants and pathogens: Putting infection strategies and defence mechanisms on the map. *Current Opinion in Plant Biology*, *15*(6), Article 6. https://doi.org/10.1016/j.pbi.2012.08.009

Foyer, C. H., & Noctor, G. (2009). Redox Regulation in Photosynthetic Organisms: Signaling, Acclimation, and Practical Implications. *Antioxidants & Redox Signaling*, *11*(4), 861–905. https://doi.org/10.1089/ars.2008.2177

Galvez-Valdivieso, G., & Mullineaux, P. M. (2010). The role of reactive oxygen species in signalling from chloroplasts to the nucleus. *Physiologia Plantarum*, *138*(4), Article 4. https://doi.org/10.1111/j.1399-3054.2009.01331.x

Gao, X., Ren, Z., Zhao, W., & Li, W. (2023). Candidatus Phytoplasma ziziphi encodes non-classically secreted proteins that suppress hypersensitive cell death response in Nicotiana benthamiana. *Phytopathology Research*, *5*(1), Article 1. https://doi.org/10.1186/s42483-023-00166-0

Geng, R., Pang, X., Li, X., Shi, S., Hedtke, B., Grimm, B., Bock, R., Huang, J., & Zhou, W. (2023). PROGRAMMED CELL DEATH8 interacts with tetrapyrrole biosynthesis enzymes and ClpC1 to maintain homeostasis of tetrapyrrole metabolites in Arabidopsis. *New Phytologist*, *238*(6), 2545–2560. https://doi.org/10.1111/nph.18906

Hren, M., Nikolić, P., Rotter, A., Blejec, A., Terrier, N., Ravnikar, M., Dermastia, M., & Gruden, K. (2009). "Bois noir" phytoplasma induces significant reprogramming of the leaf transcriptome in the field grown grapevine. *BMC Genomics*, *10*(1). https://doi.org/10.1186/1471-2164-10-460

Hogenhout, S. A., & Loria, R. (2008). Virulence mechanisms of Gram-positive plant pathogenic bacteria. *Current Opinion in Plant Biology*, *11*(4), Article 4. https://doi.org/10.1016/j.pbi.2008.05.007

Hogenhout, S. A., Oshima, K., Ammar, E., Kakizawa, S., Kingdom, H. N., & Namba, S. (2008). Phytoplasmas: Bacteria that manipulate plants and insects. *Molecular Plant Pathology*, *9*(4), 403–423. https://doi.org/10.1111/j.1364-3703.2008.00472.x

Hoshi, A., Oshima, K., Kakizawa, S., Ishii, Y., Ozeki, J., Hashimoto, M., Komatsu, K., Kagiwada, S., Yamaji, Y., & Namba, S. (2009). A unique virulence factor for proliferation and dwarfism in plants identified from a phytopathogenic bacterium. *Proceedings of the National Academy of Sciences*, *106*(15), Article 15. https://doi.org/10.1073/pnas.0813038106

Hu, S.-F., Huang, Y.-H., Lin, C.-P., Liu, L.-Y. D., Hong, S.-F., Yang, C.-Y., Lo, H.-F., Tseng, T.-Y., Chen, W.-Y., & Lin, S.-S. (2015). Development of a Mild Viral Expression System for Gain-Of-Function Study of Phytoplasma Effector In Planta. *PLOS ONE*, *10*(6), Article 6. https://doi.org/10.1371/journal.pone.0130139

Huang, W., MacLean, A. M., Sugio, A., Maqbool, A., Busscher, M., Cho, S.-T., Kamoun, S., Kuo, C.-H., Immink, R. G. H., & Hogenhout, S. A. (2021). Parasitic modulation of host development by ubiquitin-independent protein degradation. *Cell*, *184*(20), Article 20. https://doi.org/10.1016/j.cell.2021.08.029

Ishiie, T. (1965). Dwarf Disease of Mulberry Tree. *Japanese Journal of Phytopathology*, *31*(Special1), Article Special1. https://doi.org/10.3186/jjphytopath.31.Special1_139

Janik, K., Mithöfer, A., Raffeiner, M., Stellmach, H., Hause, B., & Schlink, K. (2017). An effector of apple proliferation phytoplasma targets TCP transcription factors—A generalized virulence strategy of phytoplasma? *Molecular Plant Pathology*, *18*(3), Article 3. https://doi.org/10.1111/mpp.12409

Kachroo, P., Burch-Smith, T. M., & Grant, M. (2021). An Emerging Role for Chloroplasts in Disease and Defense. *Annual Review of Phytopathology*, *59*, 423–445. https://doi.org/10.1146/annurev-phyto-020620-115813

Kakizaki, T., Matsumura, H., Nakayama, K., Che, F.-S., Terauchi, R., & Inaba, T. (2009). Coordination of Plastid Protein Import and Nuclear Gene Expression by Plastid-to-Nucleus Retrograde Signaling. *Plant Physiology*, *151*(3), Article 3. https://doi.org/10.1104/pp.109.145987

Kakizawa, S., Oshima, K., Nishigawa, H., Jung, H.-Y., Wei, W., Suzuki, S., Tanaka, M., Miyata, S.-I., Ugaki, M., & Namba, S. (2004). Secretion of immunodominant membrane protein from onion yellows phytoplasma through the Sec protein-translocation system in Escherichia coli. *Microbiology (Reading, England)*, *150*(Pt 1), Article Pt 1. https://doi.org/10.1099/mic.0.26521-0

Kato, Y., Miura, E., Matsushima, R., & Sakamoto, W. (2007). White Leaf Sectors in *yellow variegated2* Are Formed by Viable Cells with Undifferentiated Plastids. *Plant Physiology*, *144*(2), Article 2. https://doi.org/10.1104/pp.107.099002

Keeling, P. J. (2013). The number, speed, and impact of plastid endosymbioses in eukaryotic evolution. *Annual Review of Plant Biology*, *64*, 583–607. https://doi.org/10.1146/annurev-arplant-050312-120144

Kirdat, K., Tiwarekar, B., Sathe, S., & Yadav, A. (2023). From sequences to species: Charting the phytoplasma classification and taxonomy in the era of taxogenomics. *Frontiers in Microbiology*, *14*, 1123783. https://doi.org/10.3389/fmicb.2023.1123783

Kleine, T., & Leister, D. (2016a). Retrograde signaling: Organelles go networking. *Biochimica Et Biophysica Acta*, *1857*(8), Article 8. https://doi.org/10.1016/j.bbabio.2016.03.017

Kleine, T., & Leister, D. (2016b). Retrograde signaling: Organelles go networking. *Biochimica et Biophysica Acta (BBA) - Bioenergetics*, *1857*(8), 1313–1325. https://doi.org/10.1016/j.bbabio.2016.03.017

Kohli, A., Sreenivasulu, N., Lakshmanan, P., & Kumar, P. P. (2013). The phytohormone crosstalk paradigm takes center stage in understanding how plants respond to abiotic stresses. *Plant Cell Reports*, *32*(7), Article 7. https://doi.org/10.1007/s00299-013-1461-y

Koornneef, M., Cone, J. W., Dekens, R. G., O'Herne-Robers, E. G., Spruit, C. J. P., & Kendrick, R. E. (1985). Photomorphogenic Responses of Long Hypocotyl Mutants

of Tomato. *Journal of Plant Physiology*, *120*(2), 153–165. https://doi.org/10.1016/S0176-1617(85)80019-5

Kosovac, A., Johannesen, J., Krstić, O., Mitrović, M., Cvrković, T., Toševski, I., & Jović, J. (2018). Widespread plant specialization in the polyphagous planthopper Hyalesthes obsoletus (Cixiidae), a major vector of stolbur phytoplasma: Evidence of cryptic speciation. *PLOS ONE*, *13*(5), Article 5. https://doi.org/10.1371/journal.pone.0196969

Koussevitzky, S., Nott, A., Mockler, T. C., Hong, F., Sachetto-Martins, G., Surpin, M., Lim, J., Mittler, R., & Chory, J. (2007). Signals from chloroplasts converge to regulate nuclear gene expression. *Science (New York, N.Y.)*, *316*(5825), Article 5825.

Krieger-Liszkay, A., Kós, P. B., & Hideg, É. (2011). Superoxide anion radicals generated by methylviologen in photosystem I damage photosystem II. *Physiologia Plantarum*, *142*(1), Article 1. https://doi.org/10.1111/j.1399-3054.2010.01416.x

Kropat, J., Oster, U., Rüdiger, W., & Beck, C. F. (1997). Chlorophyll precursors are signals of chloroplast origin involved in light induction of nuclear heat-shock genes. *Proceedings of the National Academy of Sciences of the United States of America*, *94*(25), Article 25. https://doi.org/10.1073/pnas.94.25.14168

Kube, M., Mitrovic, J., Duduk, B., Rabus, R., & Seemüller, E. (2012). Current View on Phytoplasma Genomes and Encoded Metabolism. *The Scientific World Journal*, *2012*, 1–25. https://doi.org/10.1100/2012/185942

Kube, M., Schneider, B., Kuhl, H., Dandekar, T., Heitmann, K., Migdoll, A. M., Reinhardt, R., & Seemüller, E. (2008). The linear chromosome of the plant-pathogenic mycoplasma "Candidatus Phytoplasma mali." *BMC Genomics*, *9*(1), Article 1. https://doi.org/10.1186/1471-2164-9-306

Kube, M., Siewert, C., Migdoll, A. M., Duduk, B., Holz, S., Rabus, R., Seemüller, E., Mitrovic, J., Müller, I., Büttner, C., & Reinhardt, R. (2014). Analysis of the Complete Genomes of Acholeplasma brassicae, A. palmae and A. laidlawii and Their Comparison to the Obligate Parasites from 'Candidatus Phytoplasma'. *Microbial Physiology*, *24*(1), Article 1. https://doi.org/10.1159/000354322

Kühn, C., Franceschi, V. R., Schulz, A., Lemoine, R., & Frommer, W. B. (1997). Macromolecular Trafficking Indicated by Localization and Turnover of Sucrose Transporters in Enucleate Sieve Elements. *Science*, *275*(5304), Article 5304. https://doi.org/10.1126/science.275.5304.1298

Kumari, S., Nagendran, K., Rai, A. B., Singh, B., Rao, G. P., & Bertaccini, A. (2019). Global Status of Phytoplasma Diseases in Vegetable Crops. *Frontiers in Microbiology*, *10*, 1349. https://doi.org/10.3389/fmicb.2019.01349

Kuźniak, E., & Kopczewski, T. (2020). The Chloroplast Reactive Oxygen Species-Redox System in Plant Immunity and Disease. *Frontiers in Plant Science*, *11*, 572686. https://doi.org/10.3389/fpls.2020.572686

Larkin, R. M. (2016). Tetrapyrrole Signaling in Plants. *Frontiers in Plant Science*, *7*. https://doi.org/10.3389/fpls.2016.01586

Larkin, R. M., Alonso, J. M., Ecker, J. R., & Chory, J. (2003). GUN4, a Regulator of Chlorophyll Synthesis and Intracellular Signaling. *Science*, *299*(5608), 902–906. https://doi.org/10.1126/science.1079978

Lee, I. M., Davis, R. E., & Gundersen-Rindal, D. E. (2000). Phytoplasma: Phytopathogenic mollicutes. *Annual Review of Microbiology*, *54*, 221–255. https://doi.org/10.1146/annurev.micro.54.1.221

Liu, Z., Zhao, J., & Liu, M. (2016). Photosynthetic responses to phytoplasma infection in Chinese jujube. *Plant Physiology and Biochemistry*, *105*, 12–20. https://doi.org/10.1016/j.plaphy.2016.04.003

Loudya, N., Barkan, A., & López-Juez, E. (2024). Plastid retrograde signaling: A developmental perspective. *The Plant Cell*, *36*(10), Article 10. https://doi.org/10.1093/plcell/koae094

Lu, Y.-T., Li, M.-Y., Cheng, K.-T., Tan, C. M., Su, L.-W., Lin, W.-Y., Shih, H.-T., Chiou, T.-J., & Yang, J.-Y. (2014). Transgenic plants that express the phytoplasma effector SAP11 show altered phosphate starvation and defense responses. *Plant Physiology*, *164*(3), Article 3. https://doi.org/10.1104/pp.113.229740

MacLean, A. M., Sugio, A., Makarova, O. V., Findlay, K. C., Grieve, V. M., Tóth, R., Nicolaisen, M., & Hogenhout, S. A. (2011). Phytoplasma Effector SAP54 Induces Indeterminate Leaf-Like Flower Development in Arabidopsis Plants. *Plant Physiology*, *157*(2), Article 2. https://doi.org/10.1104/pp.111.181586

Maejima, K., Iwai, R., Himeno, M., Komatsu, K., Kitazawa, Y., Fujita, N., Ishikawa, K., Fukuoka, M., Minato, N., Yamaji, Y., Oshima, K., & Namba, S. (2014). Recognition of floral homeotic MADS domain transcription factors by a phytoplasmal effector, phyllogen, induces phyllody. *The Plant Journal: For Cell and Molecular Biology*, *78*(4), Article 4. https://doi.org/10.1111/tpj.12495

Marco, F. D., Batailler, B., Thorpe, M. R., Razan, F., Le Hir, R., Vilaine, F., Bouchereau, A., Martin-Magniette, M.-L., Eveillard, S., & Dinant, S. (2021). Involvement of SUT1 and SUT2 Sugar Transporters in the Impairment of Sugar Transport and Changes in Phloem Exudate Contents in Phytoplasma-Infected Plants. *International Journal of Molecular Sciences*, *22*(2), Article 2. https://doi.org/10.3390/ijms22020745

Margaria, P., Ferrandino, A., Caciagli, P., Kedrina, O., Schubert, A., & Palmano, S. (2014). Metabolic and transcript analysis of the flavonoid pathway in diseased and recovered Nebbiolo and Barbera grapevines (*Vitis vinifera* L.) following infection by Flavescence dorée phytoplasma. *Plant, Cell & Environment*, *37*(9), 2183–2200. https://doi.org/10.1111/pce.12332

Minato, N., Himeno, M., Hoshi, A., Maejima, K., Komatsu, K., Takebayashi, Y., Kasahara, H., Yusa, A., Yamaji, Y., Oshima, K., Kamiya, Y., & Namba, S. (2014). The phytoplasmal virulence factor TENGU causes plant sterility by downregulating of the jasmonic acid and auxin pathways. *Scientific Reports*, *4*(1), Article 1. https://doi.org/10.1038/srep07399

Mittelberger, C., Hause, B., & Janik, K. (2022). The "Candidatus Phytoplasma mali" effector protein SAP11CaPm interacts with MdTCP16, a class II CYC/TB1 transcription factor that is highly expressed during phytoplasma infection. *PloS One*, *17*(12), Article 12. https://doi.org/10.1371/journal.pone.0272467

Mittelberger, C., Stellmach, H., Hause, B., Kerschbamer, C., Schlink, K., Letschka, T., & Janik, K. (2019). A Novel Effector Protein of Apple Proliferation Phytoplasma Disrupts Cell Integrity of Nicotiana spp. Protoplasts. *International Journal of Molecular Sciences*, *20*(18), Article 18. https://doi.org/10.3390/ijms20184613

Nambara, E., & Marion-Poll, A. (2005). ABSCISIC ACID BIOSYNTHESIS AND CATABOLISM. *Annual Review of Plant Biology*, *56*(1), 165–185. https://doi.org/10.1146/annurev.arplant.56.032604.144046

Marcone, C. (2014). Molecular biology and pathogenicity of phytoplasmas. *Annals of Applied Biology*, *165*(2), Article 2. https://doi.org/10.1111/aab.12151

Martín-Trillo, M., & Cubas, P. (2010). TCP genes: A family snapshot ten years later. *Trends in Plant Science*, *15*(1), Article 1. https://doi.org/10.1016/j.tplants.2009.11.003

Maust, B. E., Espadas, F., Talavera, C., Aguilar, M., Santamaría, J. M., & Oropeza, C. (2003). Changes in Carbohydrate Metabolism in Coconut Palms Infected with the Lethal Yellowing Phytoplasma. *Phytopathology®*, *93*(8), 976–981. https://doi.org/10.1094/phyto.2003.93.8.976

Medina-Puche, L., Tan, H., Dogra, V., Wu, M., Rosas-Diaz, T., Wang, L., Ding, X., Zhang, D., Fu, X., Kim, C., & Lozano-Duran, R. (2020). A Defense Pathway Linking Plasma Membrane and Chloroplasts and Co-opted by Pathogens. *Cell*, *182*(5), 1109-1124.e25. https://doi.org/10.1016/j.cell.2020.07.020

Melotto, M., Underwood, W., Koczan, J., Nomura, K., & He, S. Y. (2006). Plant Stomata Function in Innate Immunity against Bacterial Invasion. *Cell*, *126*(5), Article 5. https://doi.org/10.1016/j.cell.2006.06.054

Minato, N., Himeno, M., Hoshi, A., Maejima, K., Komatsu, K., Takebayashi, Y., Kasahara, H., Yusa, A., Yamaji, Y., Oshima, K., Kamiya, Y., & Namba, S. (2014). The phytoplasmal virulence factor TENGU causes plant sterility by downregulating of the jasmonic acid and auxin pathways. *Scientific Reports*, *4*(1), Article 1. https://doi.org/10.1038/srep07399

Mochizuki, N., Brusslan, J. A., Larkin, R., Nagatani, A., & Chory, J. (2001). *Arabidopsis genomes uncoupled 5* (*GUN5*) mutant reveals the involvement of Mg-chelatase H subunit in plastid-to-nucleus signal transduction. *Proceedings of the National Academy of Sciences*, *98*(4), Article 4. https://doi.org/10.1073/pnas.98.4.2053

Muramoto, T., Kami, C., Kataoka, H., Iwata, N., Linley, P. J., Mukougawa, K., Yokota, A., & Kohchi, T. (2005). The tomato photomorphogenetic mutant, aurea, is deficient in phytochromobilin synthase for phytochrome chromophore biosynthesis. *Plant & Cell Physiology*, *46*(4), 661–665. https://doi.org/10.1093/pcp/pci062

Musetti, R., Pagliari, L., Mian, G., De Oliveira Cantao, F. R., Bernardini, C., Santi, S., & Van Bel, A. J. E. (2023). The sieve-element endoplasmic reticulum: A focal point of phytoplasma-host plant interaction? *Frontiers in Microbiology*, *14*, 1030414. https://doi.org/10.3389/fmicb.2023.1030414

Music, M. S., Samarzija, I., Hogenhout, S. A., Haryono, M., Cho, S.-T., & Kuo, C.-H. (2019). The genome of "Candidatus Phytoplasma solani" strain SA-1 is highly dynamic and prone to adopting foreign sequences. *Systematic and Applied Microbiology*, *42*(2), Article 2. https://doi.org/10.1016/j.syapm.2018.10.008

Namba, S. (2011). Phytoplasmas: A century of pioneering research. *Journal of General Plant Pathology*, *77*(6), Article 6. https://doi.org/10.1007/s10327-011-0341-y

Ngou, B. P. M., Jones, J. D. G., & Ding, P. (2022). Plant immune networks. *Trends in Plant Science*, *27*(3), Article 3. https://doi.org/10.1016/j.tplants.2021.08.012

Nomura, H., Komori, T., Uemura, S., Kanda, Y., Shimotani, K., Nakai, K., Furuichi, T., Takebayashi, K., Sugimoto, T., Sano, S., Suwastika, I. N., Fukusaki, E., Yoshioka, H., Nakahira, Y., & Shiina, T. (2012). Chloroplast-mediated activation of plant immune signalling in Arabidopsis. *Nature Communications*, *3*(1), 926. https://doi.org/10.1038/ncomms1926

Omenge, K., Viscardo, O. C., De Oliveira Cantao, F. R., Santi, S., Van Bel, A. J. E., & Musetti, R. (2025). SEOR2 in Arabidopsis mediates Ca2+ dependent defense against phytoplasmas and reduction of plant growth. *Scientific Reports*, *15*(1), 17829. https://doi.org/10.1038/s41598-025-01374-8

Orlovskis, Z., & Hogenhout, S. A. (2016). A Bacterial Parasite Effector Mediates Insect Vector Attraction in Host Plants Independently of Developmental Changes. *Frontiers in Plant Science*, *7*. https://doi.org/10.3389/fpls.2016.00885

Oshima, K., Ishii, Y., Kakizawa, S., Sugawara, K., Neriya, Y., Himeno, M., Minato, N., Miura, C., Shiraishi, T., Yamaji, Y., & Namba, S. (2011). Dramatic Transcriptional Changes in an Intracellular Parasite Enable Host Switching between Plant and Insect. *PLoS ONE*, *6*(8), Article 8. https://doi.org/10.1371/journal.pone.0023242

Oshima, K., Kakizawa, S., Nishigawa, H., Jung, H.-Y., Wei, W., Suzuki, S., Arashida, R., Nakata, D., Miyata, S., Ugaki, M., & Namba, S. (2004). Reductive evolution suggested from the complete genome sequence of a plant-pathogenic phytoplasma. *Nature Genetics*, *36*(1), Article 1. https://doi.org/10.1038/ng1277

Oshima, K., Maejima, K., Isobe, Y., Endo, A., Namba, S., & Yamaji, Y. (2023). Molecular mechanisms of plant manipulation by secreting effectors of phytoplasmas. *Physiological and Molecular Plant Pathology*, *125*, 102009. https://doi.org/10.1016/j.pmpp.2023.102009

Oshima, K., Maejima, K., & Namba, S. (2013). Genomic and evolutionary aspects of phytoplasmas. *Frontiers in Microbiology*, *4*, 230. https://doi.org/10.3389/fmicb.2013.00230

Osler, R., Borselli, S., Ermacora, P., Ferrini, F., Loschi, A., Martini, M., Moruzzi, S., Musetti, R., Giannini, M., Serra, S., & Loi, N. (2016). Transmissible tolerance to European

stone fruit yellows (ESFY) in apricot: Cross-protection or a plant mediated process? *Phytoparasitica*, *44*(2), Article 2. https://doi.org/10.1007/s12600-016-0509-2

Padmanabhan, M. S., & Dinesh-Kumar, S. P. (2010). All Hands on Deck—The Role of Chloroplasts, Endoplasmic Reticulum, and the Nucleus in Driving Plant Innate Immunity. *Molecular Plant-Microbe Interactions®*, *23*(11), 1368–1380. https://doi.org/10.1094/MPMI-05-10-0113

Pecher, P., Moro, G., Canale, M. C., Capdevielle, S., Singh, A., MacLean, A., Sugio, A., Kuo, C.-H., Lopes, J. R. S., & Hogenhout, S. A. (2019). Phytoplasma SAP11 effector destabilization of TCP transcription factors differentially impact development and defence of Arabidopsis versus maize. *PLoS Pathogens*, *15*(9), Article 9. https://doi.org/10.1371/journal.ppat.1008035

Pfannschmidt, T., Terry, M. J., Van Aken, O., & Quiros, P. M. (2020). Retrograde signals from endosymbiotic organelles: A common control principle in eukaryotic cells. *Philosophical Transactions of the Royal Society of London. Series B, Biological Sciences*, *375*(1801), Article 1801. https://doi.org/10.1098/rstb.2019.0396

Pogson, B. J., Woo, N. S., Förster, B., & Small, I. D. (2008). Plastid signalling to the nucleus and beyond. *Trends in Plant Science*, *13*(11), Article 11. https://doi.org/10.1016/j.tplants.2008.08.008

Pospíšil, P., Arató, A., Krieger-Liszkay, A., & Rutherford, A. W. (2004). Hydroxyl Radical Generation by Photosystem II. *Biochemistry*, *43*(21), Article 21. https://doi.org/10.1021/bi036219i

Pradit, N., Rodriguez-Saona, C., Kawash, J., & Polashock, J. (2019). Phytoplasma Infection Influences Gene Expression in American Cranberry. *Frontiers in Ecology and Evolution*, *7*. https://doi.org/10.3389/fevo.2019.00178

Ramel, F., Birtic, S., Ginies, C., Soubigou-Taconnat, L., Triantaphylidès, C., & Havaux, M. (2012). Carotenoid oxidation products are stress signals that mediate gene responses to singlet oxygen in plants. *Proceedings of the National Academy of Sciences*, *109*(14), 5535–5540. https://doi.org/10.1073/pnas.1115982109

Ramel, F., Mialoundama, A. S., & Havaux, M. (2013). Nonenzymic carotenoid oxidation and photooxidative stress signalling in plants. *Journal of Experimental Botany*, *64*(3), 799–805. https://doi.org/10.1093/jxb/ers223

Richter, A. S., Nägele, T., Grimm, B., Kaufmann, K., Schroda, M., Leister, D., & Kleine, T. (2023). Retrograde signaling in plants: A critical review focusing on the GUN pathway and beyond. *Plant Communications*, *4*(1), 100511. https://doi.org/10.1016/j.xplc.2022.100511

Robert-Seilaniantz, A., Grant, M., & Jones, J. D. G. (2011). Hormone Crosstalk in Plant Disease and Defense: More Than Just JASMONATE-SALICYLATE Antagonism. *Annual Review of Phytopathology*, *49*(1), Article 1. https://doi.org/10.1146/annurev-phyto-073009-114447

Santos, A. A., Molligan, J., Plante, N., & Peréz-Lopéz, E. (2025). Strawberry Green Petal Disease Pathosystem in Québec, Canada. *Plant Health Cases*, phcs20250006. https://doi.org/10.1079/planthealthcases.2025.0006

Santi, S., De Marco, F., Polizzotto, R., Grisan, S., & Musetti, R. (2013a). Recovery from stolbur disease in grapevine involves changes in sugar transport and metabolism. *Frontiers in Plant Science*, *4*. https://doi.org/10.3389/fpls.2013.00171

Santi, S., Grisan, S., Pierasco, A., De Marco, F., & Musetti, R. (2013b). Laser microdissection of grapevine leaf phloem infected by stolbur reveals site-specific gene responses associated to sucrose transport and metabolism. *Plant, Cell & Environment*, *36*(2), 343–355. https://doi.org/10.1111/j.1365-3040.2012.02577.x

Serrano, I., Audran, C., & Rivas, S. (2016). Chloroplasts at work during plant innate immunity. *Journal of Experimental Botany*, *67*(13), 3845–3854. https://doi.org/10.1093/jxb/erw088

Shigenaga, A. M., & Argueso, C. T. (2016). No hormone to rule them all: Interactions of plant hormones during the responses of plants to pathogens. *Seminars in Cell & Developmental Biology*, *56*, 174–189. https://doi.org/10.1016/j.semcdb.2016.06.005

Shigenaga, A. M., Berens, M. L., Tsuda, K., & Argueso, C. T. (2017). Towards engineering of hormonal crosstalk in plant immunity. *Current Opinion in Plant Biology*, *38*, 164–172. https://doi.org/10.1016/j.pbi.2017.04.021

Singh, A., & Lakhanpaul, S. (2020). Detection, characterization and evolutionary aspects of S54LP of SP (SAP54 Like Protein of Sesame Phyllody): A phytoplasma effector molecule associated with phyllody development in sesame (Sesamum indicum L.). *Physiology and Molecular Biology of Plants: An International Journal of Functional Plant Biology*, *26*(3), Article 3. https://doi.org/10.1007/s12298-020-00764-8

Sowden, R. G., Watson, S. J., & Jarvis, P. (2018). The role of chloroplasts in plant pathology. *Essays in Biochemistry*, *62*(1), Article 1. https://doi.org/10.1042/EBC20170020

Strand, Å., Asami, T., Alonso, J., Ecker, J. R., & Chory, J. (2003). Chloroplast to nucleus communication triggered by accumulation of Mg-protoporphyrinIX. *Nature*, *421*(6918), Article 6918. https://doi.org/10.1038/nature01204

Strohmayer, A., Moser, M., Si-Ammour, A., Krczal, G., & Boonrod, K. (2019). ‘ *Candidatus* Phytoplasma mali’ Genome Encodes a Protein that Functions as an E3 Ubiquitin Ligase and Could Inhibit Plant Basal Defense. *Molecular Plant-Microbe Interactions®*, *32*(11), Article 11. https://doi.org/10.1094/MPMI-04-19-0107-R

Strohmayer, A., Schwarz, T., Braun, M., Krczal, G., & Boonrod, K. (2021). The Effect of the Anticipated Nuclear Localization Sequence of ‘Candidatus Phytoplasma mali’ SAP11-like Protein on Localization of the Protein and Destabilization of TCP

Transcription Factor. *Microorganisms*, *9*(8), Article 8. https://doi.org/10.3390/microorganisms9081756

Sugio, A., Kingdom, H. N., MacLean, A. M., Grieve, V. M., & Hogenhout, S. A. (2011). Phytoplasma protein effector SAP11 enhances insect vector reproduction by manipulating plant development and defense hormone biosynthesis. *Proceedings of the National Academy of Sciences of the United States of America*, *108*(48), Article 48. https://doi.org/10.1073/pnas.1105664108

Sugawara, K., Honma, Y., Komatsu, K., Himeno, M., Oshima, K., & Namba, S. (2013). The Alteration of Plant Morphology by Small Peptides Released from the Proteolytic Processing of the Bacterial Peptide TENGU. *Plant Physiology*, *162*(4), Article 4. https://doi.org/10.1104/pp.113.218586

Susek, R. E., Ausubel, F. M., & Chory, J. (1993). Signal transduction mutants of arabidopsis uncouple nuclear CAB and RBCS gene expression from chloroplast development. *Cell*, *74*(5), Article 5. https://doi.org/10.1016/0092-8674(93)90459-4

Tan, C. M., Li, C.-H., Tsao, N.-W., Su, L.-W., Lu, Y.-T., Chang, S. H., Lin, Y. Y., Liou, J.-C., Hsieh, L.-C., Yu, J.-Z., Sheue, C.-R., Wang, S.-Y., Lee, C.-F., & Yang, J.-Y. (2016). Phytoplasma SAP11 alters 3-isobutyl-2-methoxypyrazine biosynthesis in *Nicotiana benthamiana* by suppressing *NbOMT1*. *Journal of Experimental Botany*, *67*(14), Article 14. https://doi.org/10.1093/jxb/erw225

Tan, Y., Li, Q., Zhao, Y., Wei, H., Wang, J., Baker, C. J., Liu, Q., & Wei, W. (2021). Integration of metabolomics and existing omics data reveals new insights into phytoplasma-induced metabolic reprogramming in host plants. *PLOS ONE*, *16*(2), Article 2. https://doi.org/10.1371/journal.pone.0246203

Tedeschi, R., & Alma, A. (2006). Fieberiella florii (Homoptera: Auchenorrhyncha) as a Vector of "Candidatus Phytoplasma mali." *Plant Disease*, *90*(3), Article 3. https://doi.org/10.1094/PD-90-0284

Terashima, I., Hanba, Y. T., Tholen, D., & Niinemets, Ü. (2011). Leaf functional anatomy in relation to photosynthesis. *Plant Physiology*, *155*(1), Article 1. https://doi.org/10.1104/pp.110.165472

Terry, M. J. (1997). Phytochrome chromophore-deficient mutants. *Plant, Cell & Environment*, *20*(6), Article 6. https://doi.org/10.1046/j.1365-3040.1997.d01-102.x

Terry, M. J., & Kendrick, R. E. (1999). Feedback Inhibition of Chlorophyll Synthesis in the Phytochrome Chromophore-Deficient *aurea* and *yellow-green-2* Mutants of Tomato. *Plant Physiology*, *119*(1), 143–152. https://doi.org/10.1104/pp.119.1.143

The IRPCM Phytoplasma/Spiroplasma Working Team – Phytoplasma taxonomy group. (2004). 'Candidatus Phytoplasma', a taxon for the wall-less, non-helical prokaryotes that colonize plant phloem and insects. *International Journal of*

Systematic and Evolutionary Microbiology, *54*(4), Article 4. https://doi.org/10.1099/ijs.0.02854-0

Trotta, A., Rahikainen, M., Konert, G., Finazzi, G., & Kangasjärvi, S. (2014). Signalling crosstalk in light stress and immune reactions in plants. *Philosophical Transactions of the Royal Society of London. Series B, Biological Sciences*, *369*(1640), Article 1640. https://doi.org/10.1098/rstb.2013.0235

van Bel, A. J. E., & Musetti, R. (2019). Sieve element biology provides leads for research on phytoplasma lifestyle in plant hosts. *Journal of Experimental Botany*, *70*(15), 3737–3755. https://doi.org/10.1093/jxb/erz172

van Bel, A. J. E., Schulz, A., & Patrick, J. W. (2022). New mosaic fragments toward reconstructing the elusive phloem system. *Journal of Plant Physiology*, *275*, 153754. https://doi.org/10.1016/j.jplph.2022.153754

Vasileuskaya, Z., Oster, U., & Beck, C. F. (2004). Involvement of tetrapyrroles in inter-organellar signaling in plants and algae. *Photosynthesis Research*, *82*(3), Article 3. https://doi.org/10.1007/s11120-004-2160-x

Wang, L., Chen, W., Ma, H., Li, J., Hao, X., & Wu, Y. (2021). Identification of RNA silencing suppressor encoded by wheat blue dwarf (WBD) phytoplasma. *Plant Biology*, *23*(5), Article 5. https://doi.org/10.1111/plb.13257

Wang, J. Y., Haider, I., Jamil, M., Fiorilli, V., Saito, Y., Mi, J., Baz, L., Kountche, B. A., Jia, K.-P., Guo, X., Balakrishna, A., Ntui, V. O., Reinke, B., Volpe, V., Gojobori, T., Blilou, I., Lanfranco, L., Bonfante, P., & Al-Babili, S. (2019). The apocarotenoid metabolite zaxinone regulates growth and strigolactone biosynthesis in rice. *Nature Communications*, *10*(1), 810. https://doi.org/10.1038/s41467-019-08461-1

Wang, L., Leister, D., & Kleine, T. (2020). Chloroplast development and genomes uncoupled signaling are independent of the RNA-directed DNA methylation pathway. *Scientific Reports*, *10*(1), Article 1. https://doi.org/10.1038/s41598-020-71907-w

Wang, N., Li, Y., Chen, W., Yang, H. Z., Zhang, P. H., & Wu, Y. F. (2018). Identification of wheat blue dwarf phytoplasma effectors targeting plant proliferation and defence responses. *Plant Pathology*, *67*(3), Article 3. https://doi.org/10.1111/ppa.12786

Wang, R., Bai, B., Li, D., Wang, J., Huang, W., Wu, Y., & Zhao, L. (2024). Phytoplasma: A plant pathogen that cannot be ignored in agricultural production—Research progress and outlook. *Molecular Plant Pathology*, *25*(2), Article 2. https://doi.org/10.1111/mpp.13437

Waters, M. T., Wang, P., Korkaric, M., Capper, R. G., Saunders, N. J., & Langdale, J. A. (2009). GLK transcription factors coordinate expression of the photosynthetic apparatus in Arabidopsis. *The Plant Cell*, *21*(4), Article 4. https://doi.org/10.1105/tpc.108.065250

Wei, W., Inaba, J., Zhao, Y., Mowery, J. D., & Hammond, R. (2022). Phytoplasma Infection Blocks Starch Breakdown and Triggers Chloroplast Degradation, Leading to Premature Leaf Senescence, Sucrose Reallocation, and Spatiotemporal Redistribution of Phytohormones. *International Journal of Molecular Sciences*, *23*(3), Article 3. https://doi.org/10.3390/ijms23031810

Wei, W., & Zhao, Y. (2022). Phytoplasma Taxonomy: Nomenclature, Classification, and Identification. *Biology*, *11*(8), Article 8. https://doi.org/10.3390/biology11081119

Weintraub, P. G., & Beanland, L. (2006). INSECT VECTORS OF PHYTOPLASMAS. *Annual Review of Entomology*, *51*(1), Article 1. https://doi.org/10.1146/annurev.ento.51.110104.151039

Vitali, M., Chitarra, W., Galetto, L., Bosco, D., Marzachì, C., Gullino, M. L., Spanna, F., & Lovisolo, C. (2013). Flavescence dorée phytoplasma deregulates stomatal control of photosynthesis in *Vitis vinifera*. *Annals of Applied Biology*, *162*(3), 335–346. https://doi.org/10.1111/aab.12025

Woodson, J. D., Perez-Ruiz, J. M., & Chory, J. (2011). Heme Synthesis by Plastid Ferrochelatase I Regulates Nuclear Gene Expression in Plants. *Current Biology*, *21*(10), Article 10. https://doi.org/10.1016/j.cub.2011.04.004

Wu, G.-Z., & Bock, R. (2021). GUN control in retrograde signaling: How GENOMES UNCOUPLED proteins adjust nuclear gene expression to plastid biogenesis. *The Plant Cell*, *33*(3), Article 3. https://doi.org/10.1093/plcell/koaa048

Xue, C., Liu, Z., Dai, L., Bu, J., Liu, M., Zhao, Z., Jiang, Z., Gao, W., & Zhao, J. (2018). Changing Host Photosynthetic, Carbohydrate, and Energy Metabolisms Play Important Roles in Phytoplasma Infection. *Phytopathology®*, *108*(9), Article 9. https://doi.org/10.1094/PHYTO-02-18-0058-R

Yang, F., Xiao, K., Pan, H., & Liu, J. (2021). Chloroplast: The Emerging Battlefield in Plant–Microbe Interactions. *Frontiers in Plant Science*, *12*, 637853. https://doi.org/10.3389/fpls.2021.637853

Ye, X., Wang, H., Chen, P., Fu, B., Zhang, M., Li, J., Zheng, X., Tan, B., & Feng, J. (2017). Combination of iTRAQ proteomics and RNA-seq transcriptomics reveals multiple levels of regulation in phytoplasma-infected Ziziphus jujuba Mill. *Horticulture Research*, *4*(1). https://doi.org/10.1038/hortres.2017.80

Yong, E. (2014). Bacterial tricks for turning plants into zombies. *Nature*, nature.2014.15011. https://doi.org/10.1038/nature.2014.15011

Zhang, Z.-W., Zhang, G.-C., Zhu, F., Zhang, D.-W., & Yuan, S. (2015). The roles of tetrapyrroles in plastid retrograde signaling and tolerance to environmental stresses. *Planta*, *242*(6), Article 6. https://doi.org/10.1007/s00425-015-2384-3

Zhou, J., Ma, F., Yao, Y., Deng, M., Chen, M., Zhang, S., Li, Y., Yang, J., Zhang, N., Huang, J., Sun, Q., & Sun, J. (2021). Jujube witches' broom phytoplasma effectors SJP1 and SJP2 induce lateral bud outgrowth by repressing the ZJBRC1 -controlled

auxin efflux channel. *Plant, Cell & Environment*, *44*(10), Article 10. https://doi.org/10.1111/pce.14141

Zhu, J., Moreno-Pérez, A., & Coaker, G. (2023). Understanding plant pathogen interactions using spatial and single-cell technologies. *Communications Biology*, *6*(1), Article 1. https://doi.org/10.1038/s42003-023-05156-8

Zipfel, C., Kunze, G., Chinchilla, D., Caniard, A., Jones, J. D. G., Boller, T., & Felix, G. (2006). Perception of the bacterial PAMP EF-Tu by the receptor EFR restricts Agrobacterium-mediated transformation. *Cell*, *125*(4), Article 4. https://doi.org/10.1016/j.cell.2006.03.037

Chapter II - 'Candidatus Phytoplasma solani' Impairs Photosynthesis in Tomato via Disruption of Retrograde Signaling Pathways

Abstract - Phytoplasmas are obligate bacterial pathogens responsible for major yield losses across diverse economically important crops. Here, we investigate the impact of *'Candidatus* Phytoplasma solani*'* infection on chloroplast in *Solanum lycopersicum* cv. Micro-Tom. Combining transcriptomic profiling, gene co-expression network analysis and phenotyping, we show that infection leads to a profound disruption of photosynthetic capacity and marked alteration on plant growth and development. Transcriptomic data revealed downregulation of genes involved in the photosynthetic electron transport chain, carbon fixation, and chlorophyll biosynthesis, along with perturbations in hormone signaling, redox homeostasis, and defense pathways. Notably, phytoplasma infection impairs chloroplast-to-nucleus (retrograde) signaling, leading to the downregulation of key nuclear-encoded photosynthesis-associated genes and those involved in chloroplast proteostasis and light perception. Collectively, our findings demonstrate that chloroplasts serve as central hubs in the phytoplasma-host interaction, linking photosynthesis, immunity, and development and point to potential targets for enhancing plant resilience to phytoplasma infection.

2.1 Introduction

Phytoplasma infection affects photosynthesis at multiple levels. Transcriptomic analyses have revealed a broad suppression of genes involved in the photosynthetic electron transport chain, carbon fixation, and chlorophyll biosynthesis in tomato (Buoso et al., 2019, 2022), and grapevine (Dermastia et al., 2021; Hren et al., 2009). As the primary sites for photosynthesis, amino acid biosynthesis, lipid metabolism, and phytohormone production, chloroplasts play a central role in plant development and stress adaptation (Chen et al., 2018; Liebers et al., 2022).

Chloroplasts also have a critical role in plant immunity as a site to produce precursors of salicylic acid and jasmonic acid, defensive phytohormones (Nomura et al., 2012). Moreover, chloroplasts contribute to redox homeostasis, including the generation of

reactive oxygen species (ROS) and reactive nitrogen species, which are signals that in turn influence nuclear gene expression (retrograde signaling, RS) (Chan et al., 2016). An emerging role for chloroplasts in defense is reported, as well as in disease, being directly or indirectly target of pathogen effectors aimed to attenuate their immune response (Kachroo et al., 2021).

Disruption of chloroplast homeostasis by phytoplasmas induces ROS accumulation and alters phytohormone signaling, highlighting the organelle's role as a signaling hub during biotic stress (Miura et al., 2012). To investigate the chloroplast-centric physiological effects of '*Candidatus* Phytoplasma solani' ('*Ca*. P. solani') infection in tomato (*Solanum lycopersicum* cv. Micro-Tom), we employed a multidisciplinary approach integrating transcriptomic re-analysis, co-expression network modeling, and physiological assays. Additional physiological experiments were performed to validate the systemic impact of '*Ca*. P. solani' on photosynthesis, metabolism and overall plant growth and development.

Our findings demonstrate that '*Ca*. P. solani' infection disrupts chloroplast biogenesis and function, leading to visible morphological abnormalities and a pronounced reduction in photosynthetic efficiency. Moreover, the infection perturbs chloroplast-to-nucleus (retrograde) communication and compromises ROS detoxification, underscoring the central role of chloroplasts in coordinating photosynthesis, immunity, and development. Together, these results provide mechanistic insights into the molecular pathogenesis of phytoplasmas and lay the groundwork for strategies aimed at restoring chloroplast function and enhancing host resilience.

2.2 Materials and Methods

2.2.1 Plant Growth Conditions and Phytoplasma Detection

Tomato (*S. lycopersicum*, cv. Micro-Tom) seeds were collected from fruits of one single plant, placed between two layers of filter paper soaked in 1 mM $CaSO_4$ and germinated in dark at 22 °C. After seven days, uniform seedlings were transferred into pots filled with 2 liters of half strength nutrient solution containing 1.5 mM K_2SO_4, 3 mM KNO_3, 0.5 mM $MgSO_4$, 1.5 mM $CaCl_2$, 0.5 mM NaH_2PO_4, 25 µM H_3BO_3, 1 µM $MnSO_4$, 0.5 µM $ZnSO_4$, 0.3 µM $CuSO_4$, 0.05 µM $(NH_4)_6Mo_7O_{24}$, and 20 µM Fe-EDTA and pH adjusted to 6.0 with KOH. In the following four weeks the plants received the full-strength nutrient solution, which was kept aerated during the entire period by an air pumping system connected to the pots and replaced every four days. Plants were grown in a growth chamber at 23 ± 1°C, the photoperiod was maintained in 16 hours, with a photosynthetic photon flux density (PPFD) of 250 µmols m^{-2} s^{-1} at the canopy level. Then, healthy plants were grafted with shoot tips from phytoplasma-infected plants, using the lateral grafting technique on the base of the stem, while healthy plants were grafted with non-infected shoot tips, as described in (Buoso et al., 2019).

Plants were infected with '*Ca.* P. solani', a phytoplasma belonging to the stolbur subgroup 16SrXII-A (Quaglino et al., 2013), as previously described (Buoso et al., 2019, 2022). For molecular analysis, the leaf midribs and leaf laminae of the first fully expanded leaves designated as L2 and L3 (with L1 referring to the youngest, not fully expanded leaves) were collected five weeks after grafting from both infected and non-infected plants. L2 and L3 samples were carefully dissected using a scalpel to separate the midribs from the laminae, then immediately stored at -80 °C until use. Phytoplasma detection was carried out by RT-qPCR using specific primers designed on the 16SrRNA gene of '*Ca.* P. solani' (Santi et al., 2013b). The results of phytoplasma detection in the samples are presented in Supplemental files: Table S1. Biochemical and gas exchange investigations were performed using leaf discs or whole leaflets, as above detailed.

2.2.2 RNA-Seq

RNA-seq was previously performed on Micro-Tom leaf midribs, comparing healthy with '*Ca*. P. solani' infected plants, and further with Fe-deficient plants (Buoso et al., 2019). Briefly, leaf-midrib samples from two leaves (L2 and L3) from three plants were pooled and considered as one biological replicate. Three libraries for each condition (nine in total) were prepared from 200 ng of total RNA with the TruSeq stranded Total RNA library Prep Plant Kit (Illumina Inc., San Diego, CA, USA) and sequenced on the Illumina NextSeq500 platform as 75 bp single-end stranded reads. Reads used in the present study were downloaded from NCBI SRA database under BioProject ID: PRJNA548138.

The reads were mapped using STAR (Dobin et al., 2013) to a reference genome obtained combining a reference sequence for tomato and one for '*Ca*. P. solani'. The reference used for tomato was build SL3.0 and gene annotation ITAG3.20 (release date: August 08, 2018; https://ftp.ncbi.nlm.nih.gov/genomes/all/GCF/000/188/115/GCF_000188115.4_SL3.0, and that used for '*Ca*. P. solani' was the reference genome GCA_000970375 (https://www.ncbi.nlm.nih.gov/datasets/genome/GCF_000970375.1/). To maximize sample size, co-expression network analysis was conducted on all nine samples (see next paragraph). However, the differential expression analysis was focused on the comparison between phytoplasma-infected and healthy plants, the study of which is the aim of this work. Differentially expressed genes (DEGs) were identified using DESeq2 (Love et al., 2014) using a False Discovery Rate (FDR) of 0.05.

2.2.3 Weighted Gene Co-expression Network Analysis (WGCNA)

Following the re-analysis of the RNA-Seq data, a gene co-expression network analysis was conducted using a weighted correlation approach (WGCNA) implemented in the R package (Langfelder & Horvath, 2008). First, a matrix of adjacencies using the

WGCNA adjacency function was constructed by calculating Pearson correlation between all pairs of genes across all selected samples and raised it to a power β (soft threshold) of 17. The β = 17 parameter was chosen prior to constructing the adjacency matrix, based on the scale free topology criterion, using the function pickSoftThreshold (B. Zhang & Horvath, 2005). A Topological Overlap Matrix (TOM)-based dissimilarity was used as a measure to cluster gene expression profile. The function TOM similarity was used to compute similarity and then transformed into a dissimilarity object by subtracting it from 1 (B. Zhang & Horvath, 2005). The TOM dissimilarity matrix was used as an input for hierarchical clustering analysis, and the function cutreeDynamic, from the R package dynamicTreeCut, (Langfelder et al., 2008) was used to define network modules. Finally, modules with similar expression patterns were merged using the function mergeCloseModules from the package WGCNA; modules were deemed to be similar when their dissimilarity was less than 0.2. The module eigengene (ME) was considered as a representation of the gene expression profiles in a module, which was defined as the basic component of a given module (Langfelder & Horvath, 2008).

KEGG pathway and Gene Ontology enrichment analyses were performed using the ShinyGO web tool version 0.80; (Ge et al., 2020) on the full set of differentially expressed genes (DEGs) as well as separately for each co-expression module. Enrichment was assessed using an over-representation model with a Benjamini-Hochberg false discovery rate (FDR) threshold of ≤ 0.05 (Benjamini & Hochberg, 1995). Intra-module connectivity was calculated for each gene to identify putative hub genes.

2.2.4 Quantitative RT-PCR)

RNA was extracted from approximately 100 mg of powder with the Spectrum Plant Total RNA Kit (Sigma-Aldrich, St Louis, MO, USA) according to the manufacturer's instructions. RNA was reverse transcribed into cDNA with the QuantiTect Reverse Transcription Kit (Qiagen GmbH, Hilden, Germany). SsoFast EvaGreen Supermix 2x (Bio-

Rad Laboratories Inc., Hercules, CA, USA), the amount of cDNA synthesized from 2.5 ng of RNA, and specific primers (final concentration 400 nM each) were used in a total volume of 12 µL for all genes analyzed. Reaction was performed as described in De Marco et al., (2016) on a CFX96 instrument (Bio-Rad Laboratories, Richmond, CA, USA). Gene and primers sequences for expression analysis used for gene expression analysis and RNA-seq validation are presented in Supplemental files: Tables S2-3. The reference gene used for normalization was UPL3 (E3 ubiquitin-protein ligase), as described by De Marco et al. (2016).

2.2.5 Leaf pigments

Chlorophylls and carotenoids content were analytically determined as proposed by (Lichtenthaler, 1987) in the same set of leaves where GE analysis was performed (L2). Briefly, 0.025 g of leaf discs were placed in glass tubes wrapped with aluminum foil filled with 2 mL of acetone/ethanol (80% v/v) and kept at 4°C for 48 hours in dark condition for the pigment's extraction. Following the extraction 1,0 mL aliquots were taken, and the spectrophotometer absorbance readings performed at wavelengths of 663.2 and 646.8 nm for chlorophylls (Chla, Chlb and Chla+b) and 470 nm for carotenoids (carotene [c]+xanthophylls [x]), Car_{x+c}). The content of Chla, Chlb and car was determined according to the equations: chl_a: $12.25A_{663.2} - 2.79A_{646.8}$, Chl_b: $21.50A_{646.8} - 5.10A_{663.2}$, Chl_{a+b}: $7.15A_{663.2} + 18.71A_{646.8}$ and Car_{x+c}: $(1000A_{470} - 1.82Chl_a - 85.02Chl_b)/198$. The content of total chlorophylls and carotenoids was expressed in µg of pigment per gram (µg g^{-1}) of fresh matter (FM).

2.2.6 Gas exchange

Gas exchange (GE) parameters were measured in the fifth week after grafting on the terminal leaflet of the first fully expanded (L2) symptomatic leaf of the primary shoot in the infected and the corresponding in healthy plants as described by (Buoso et al., 2022).

The GE analysis was performed with a portable infrared gas analyzer, IRGA (LI-6400XT, LI-COR Biosciences, Lincoln, NE, USA) mounted with a 2 cm^2 fluorimeter chamber (LFC) coupled with a CO_2 injector in five plants in each condition. The measurements were performed in the morning, starting 3 h before the beginning of the light period.

Photosynthetic light response curves (A/PPFD) were generated in function of A, (carbon net assimilation [µmol CO_2 m^{-2} s^{-1}]) at different light intensities (PPFD, photosynthetic flux density). The curve started with a saturating PPFD level of 2000 photons µmol m^{-2} s^{-1}, and then it was reduced every 500 µmol photons m^{-2} s^{-1} to a value of 200 µmol m^{-2} s^{-1} photons (2000, 1500, 1000 and 500 µmol photons m^{-2} s^{-1}). At this rate, the spacing between values was reduced to determine the light compensation point (200 -100 - 50 - 20 - 0 µmol photons m^{-2} s^{-1}). The measurements were performed using the auto-program feature of the LI-6400 XT at 400 µmol CO_2 mol^{-1}.

The A/Ci curves, also known as CO_2 response curves, were measured varying the concentrations of Ci (intercellular CO_2 concentration [µmol CO_2 mol^{-1}]) under PPFD of 1200 µmol m^{-2} s^{-1} (Tanaka et al., 2013). Before recording measurements, the designated leaf was placed inside the LCF chamber head, and the CO_2 assimilation rate was allowed to stabilize at 1200 µmol photons m^{-2} s^{-1}, 400 µmol CO_2 mol^{-1}, leaf temperature was set in 25°C and 55% relative humidity. Once the photosynthesis rates stabilized (assessed by observing real time graphs), the A/Ci curve was generated using the auto-program feature of the LI-6400 XT to progress the CO_2 concentration through the following sequence of levels: 400, 300, 200, 100, 50, 400, 400, 600 µmol CO_2 mol^{-1}. At each CO_2 concentration, photosynthetic parameters were automatically recorded immediately upon stabilization, which was generally within span of two minutes. Two 400 µmol CO_2 mol^{-1} points were logged to allow the leaf to recover after being exposed to low CO_2 concentrations. The measurements were performed using the auto-program feature of the LI-6400 XT at 1200 µmol photons m^{-2} s^{-1}.

Besides A/Ci, and A/PPFD curves, photosynthetic parameters measured were as follows: A, (µmol CO_2 m^{-2} s^{-1}); stomatal conductance (*gs*, mol H_2O m^{-2} s^{-1}); transpiration (E, mmol H_2O m^{-2} s^{-1}); ratio between intercellular/atmosphere CO_2 (Ci/Ca), the instantaneous carboxylation efficiency (EiC) was calculated by dividing the net photosynthetic rate (A) by the intercellular CO_2 concentration (Ci). The electron transport rate (ETR) was measured simultaneously with the gas exchange and represented as µmol electrons m^{-2} s^{-1}. Measurements were taken with 400 µmol CO_2 mol^{-1} and 1200 µmol photons m^{-2} s^{-1}.

2.2.7 Characterization of the Oxidative Stress

Lipid peroxidation was determined as malondialdehyde (MDA) content using five plants, each one being considered as a biological replicate. The analysis was performed separately in leaf enriched midribs and lamina of the L2 leaves for each condition (healthy and infected), using the TBA (2-thiobarbituric acid) test. This method targets the end products of the lipid peroxidation process. Spectrophotometer readings were taken at 535 and 600 nm to obtain MDA values, which were calculated according to the equation described by (Heath & Packer, 1968). The amount of MDA was expressed as nmol g^{-1} mass of fresh matter (FM). The content of H_2O_2 was determined by potassium iodide (KI) reaction (Alexieva et al., 2001). The readings were performed in a spectrophotometer at 390 nm. The amount of H_2O_2 was expressed in µmol g^{-1} of FM.

2.2.8 Biomass allocation

The dry mass of roots, shoots and fruits was assessed in eight plants under each condition. Initially plants were sampled, separated by organs (roots, shoots, and fruits), and placed in an oven set at 65°C until the samples reached a constant weight. Subsequently, the dry mass was weighed using an analytical scale with an accuracy of

0.001 g. The harvest index (HI) was computed as the ratio of Fruit DM (Dry Mass) to Total DM.

2.2.9 Statistical analysis

Plant biometrics and gene expression data are expressed as mean values ± SE. Statistical analysis was performed, using one-way ANOVA followed by a Tukey test as post hoc multiple comparison ($P \leq 0.05$).

2.3 Results and Discussion

2.3.1 RNA-seq and weighted gene co-expression network analysis

To dissect the transcriptional architecture underlying tomato responses to '*Ca*. P. solani' infection, we constructed a weighted gene co-expression network using normalized RNA-Seq expression data. The analysis identified 10 co-expression modules (color-coded by WGCNA), each representing clusters of genes with highly correlated expression profiles. Figure 1a shows scale independence and connectivity as a function of β. Figure 1b shows the topological overlap using the 250 top expressed genes. Focusing on the top 250 highly expressed genes, analysis enhances biological relevance, reduces noise from lowly expressed genes and improves computational efficiency. Hierarchical clustering of gene expression data led to the identification of co-expressed gene modules based on the Topological Overlap Matrix (TOM). Using the dynamic tree cut algorithm, distinct modules were delineated, and subsequent merging steps resulted in a final set of ten co-expression modules (Figure 1c).

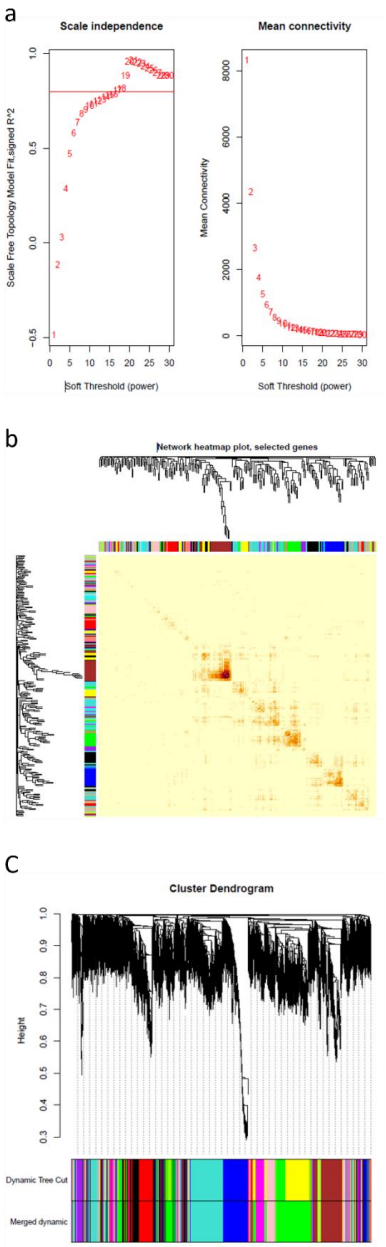

Figure 1. Co-expression network analysis. (a) Soft threshold for the identification of the best power for dividing co-expressed genes into different modules. The left panel shows the scale-free fit index (y-axis) as a function of the soft-thresholding power (x-axis). The right panel displays the mean connectivity (degree, y-axis) as a function of the soft-thresholding power (x-axis) (b) heatmap plot of the topological overlap in the gene network and clustering showing the correlation in expression among the 250 most expressed genes. Each row and column-correspond to a gene, light color denotes low

topological overlap, and progressively darker denotes higher topological overlap. (c) clustering dendrogram of genes. Gene clustering tree (dendrogram) obtained by hierarchical clustering of the adjacency-based dissimilarity. The colored row below the dendrogram indicates modules membership identified by the Dynamic Tree Cut method, before and after merging.

Figure 2a illustrates the correlations between the eigengenes of the network modules. Hierarchical clustering of the module eigengenes (ME) returned a dendrogram grouping together correlated eigengenes (Figure 2b).

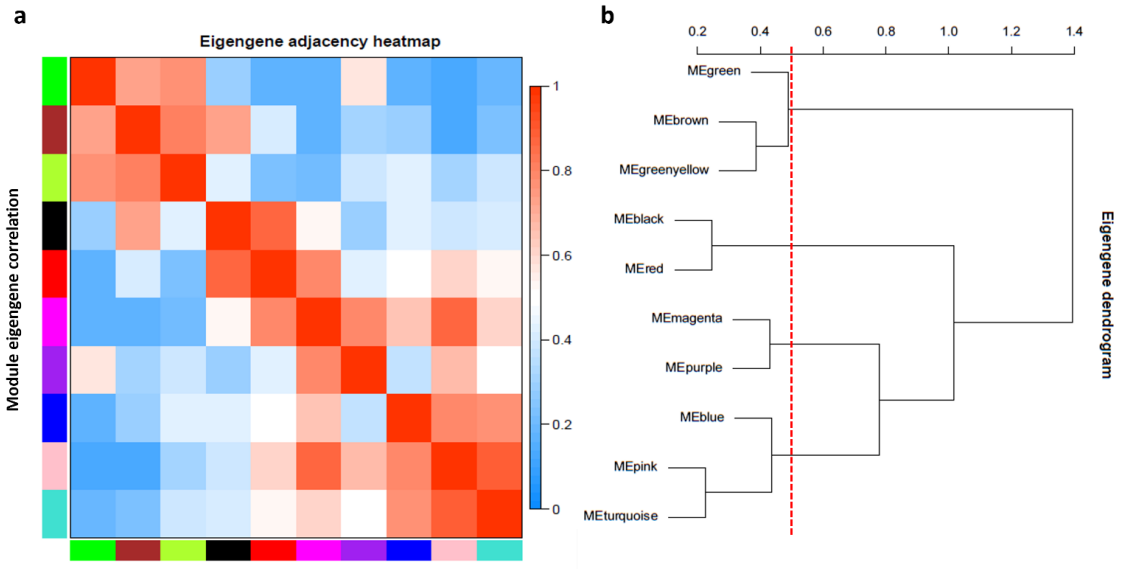

Figure 2. (a) Heatmap plot of the adjacencies in the eigengene network. Each row and column in the heatmap correspond to one module eigengene (labeled by color) or weight. In the heatmap, blue represents low adjacency (negative correlation), while red represents high adjacency (positive correlation). Squares of the red color along the diagonal are the meta-modules and (b) Hierarchical clustering of module eigengenes that summarize the modules found in the clustering analysis. Branches of the dendrogram (the meta-modules) group together eigengenes that are positively correlated. Larger co-expressed groups were formed based on a height cutoff of (0.50) represented by the red dotted line.

The size of the modules ranged from 761 genes in the greenyellow module to 4546 genes in the green module (Figure 3a). In terms of differentially expressed genes (DEGs), the magenta module contained the fewest, with only 0.18% DEGs, while the brown module had the most, comprising 34.62% DEGs (Figure 3b). Interestingly, nearly all '*Ca*. P. solani' transcripts (444 out of 447) were grouped within the blue module eigengene (ME), indicating a highly coordinated expression profile.

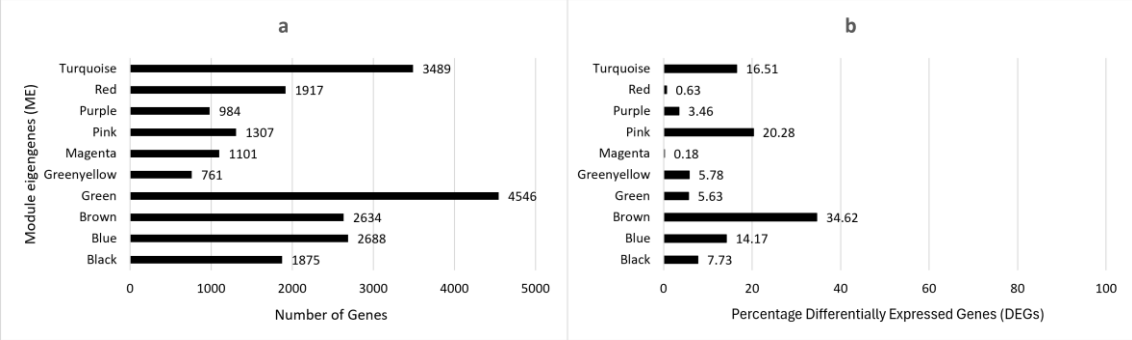

Figure 3. (a) List of modules and number of genes (b) percentage of differentially expressed plant genes (DEGs) in each module in response to phytoplasma infection in tomato cv Micro-Tom.

2.3.2 Enrichment analysis of differentially expressed genes (DEGs)

To explore the transcriptional response to phytoplasma infection, enrichment analysis was performed on the complete set of 2,627 differentially expressed genes (DEGs) (Figure 4), as well as individually within each module eigengene (ME) identified in the gene co-expression network. The most enriched terms in the whole set of DEGs included the KEGG pathway "sly00710, Carbon fixation in photosynthetic organisms" (Figure 4a) as demonstrated by (Buoso et al., 2019) and Gene Ontology (GO) terms such as "GO:0009416, Response to light stimulus" (biological process, BP) (Figure 4b), "GO:0009570, Chloroplast stroma" (cellular component, CC) (Figure 4c), and "GO:0005342), Organic acid transmembrane transporter activity" (molecular function, MF) (Figure 4d). Accordingly, Buoso et al. (2022) previously reported disruptions in ion

homeostasis in tomato leaf midribs, along with significant transcriptional changes in genes encoding ion transporters.

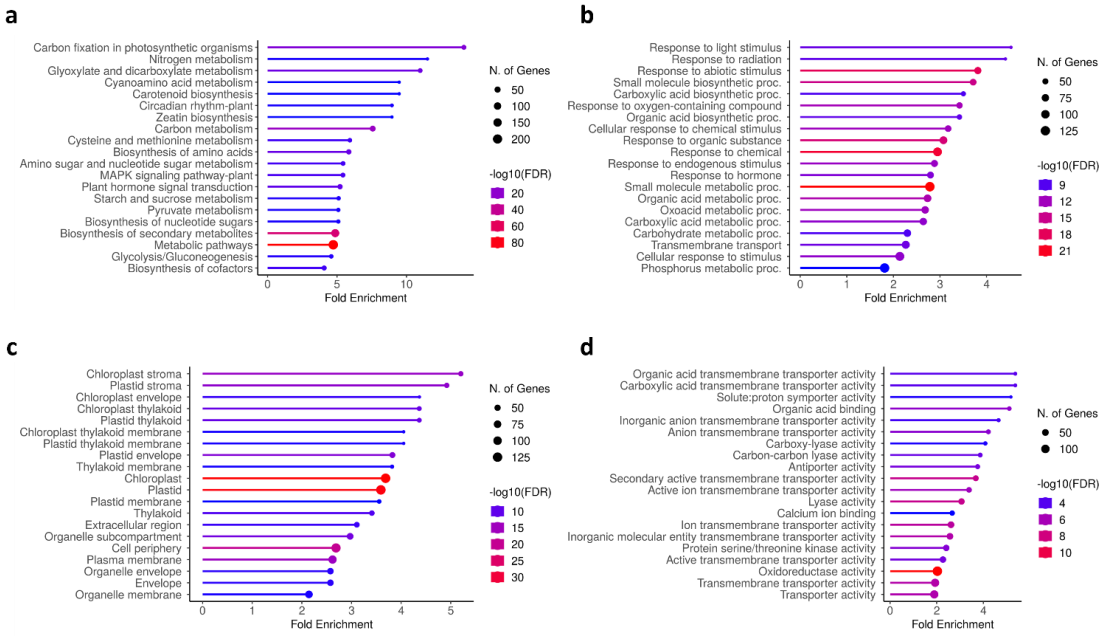

Figure 4. KEGG-enriched pathways and GO terms for all DEGs. (a) KEGG pathways, (b) biological process, (c) cellular component and (d) molecular function. Columns and rows represent fold enrichment; round size represents the number of genes; color bar from blue to red represents increasing significance in -log10 (FDR) in response to phytoplasma infection in tomato cv Micro-Tom.

Consistent with previous findings (Buoso et al., 2019, 2022), an overall impact of '*Ca*. P. solani' infection on chloroplast function and ion homeostasis in tomato leaf midribs was highlighted. We observed that the most part of enriched terms related to photosynthesis and both chloroplast structure and function was falling in the 'brown' ME, which also included the higher percentage of DEGs (Figure 3b). On the other hand, the 'blue' ME harbored *Solanum* and phytoplasma co-expressed genes. Based on these findings, we chose to focus our analysis on the brown and blue modules.

2.3.3 Co-expression analysis identified brown module genes associated with chloroplasts biogenesis and functions

Among the genes in the 'brown' ME, 34.62% (912 genes) were identified as differentially expressed (DEGs), with 112 genes up and 800 genes down regulated. Pathways and GO terms related to regulation of chloroplast biosynthesis and function were enriched within the DEGs in the brown module, as shown in Figure 5 and detailed in (Supplemental files: Tables S4-S7). Among the most significantly enriched pathways within this module were those related to primary and specialized metabolism, including carbon fixation (sly00710), carotenoid biosynthesis (sly00906), and porphyrin metabolism (sly00860), as well as nitrogen (sly00910) and sulfur metabolism (sly00920), zeatin biosynthesis (sly01230) (Figure 5a, Supplemental files: Table S4). The enrichment of biological processes further highlighted the involvement of key metabolic and stress-responsive pathways, such as tetraterpenoid (GO:0016109) and carotenoid metabolic processes (GO:0016117), along with responses to light stimulus (GO:0009416) and photosynthesis (GO:0015979) (Figure 5b, Supplemental files: Table S5). At the subcellular level, enriched GO terms associated with cellular components predominantly mapped to chloroplast-related structures, including the chloroplast thylakoid (GO:0009534, GO:0031976, GO:0009507, GO:0009579), and the chloroplast envelope (GO:0009941), as well as the stroma compartment (GO:0009570, GO:0009532) (Figure 5c, Supplemental files: Table S6). Enrichment analysis of molecular function GO terms (Figure 5d, Supplemental files: Table S7) revealed a significant representation of oxidoreductase activity and membrane transporters, underscoring the extensive reprogramming of transmembrane transport and redox homeostasis in response to *'Ca*. P. solani'.

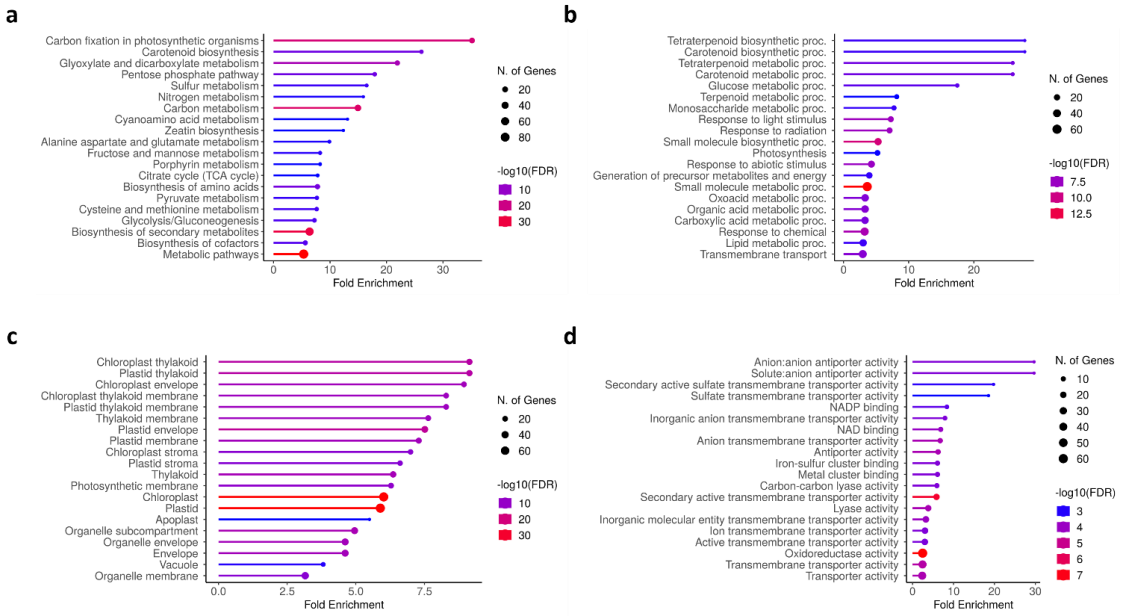

Figure 5. KEGG-enriched pathways and GO terms for DEGs of ME brown. (a) KEGG pathways, (b) biological process, (c) cellular component and (d) molecular function. Columns and rows represent fold enrichment; round size represents the number of genes; color bar from blue to red represents increasing significance in -log10 (FDR).

Gene expression profiling revealed a pronounced downregulation of genes within this module (Table 1). Several key genes were significantly downregulated, including glyceraldehyde-3-phosphate dehydrogenase A and B genes (LOC101266713, LOC101264004 respectively), glucose-6-phosphate 1-dehydrogenase (LOC101253589), ferredoxin (LOC101265784), cytochrome b6f complex iron-sulfur subunit (LOC101243864), ATP synthase gamma chain (LOC101253342), and ribulose bisphosphate carboxylase small chain 3B (LOC101268337) genes. These genes play essential roles in the thylakoid electron transport and carbon fixation in the Calvin cycle, and their repression indicates reduced chloroplast efficiency and a decline in photosynthetic ATP and NADPH production, crucial for carbon fixation and immune defense (Foyer & Noctor, 2009; Huang et al., 2020). The NADPH-cytochrome P450 reductase gene (LOC101247036), homologous to *Arabidopsis thaliana* AT4G30210

(*ATR2*), was significantly downregulated. This enzyme mediates electron transfer from NADPH to cytochrome P450 monooxygenases either directly or indirectly via cytochrome b5 proteins, thereby playing a pivotal role in CYP450-dependent metabolic processes (Sundin et al., 2014) and PROTON GRADIENT REGULATION 5 (*PGR5*, LOC101262255). *PGR5* has been identified as a key regulator of electron partitioning between linear electron flow (LEF) and cyclic electron flow (CEF) around photosystem I (PSI), a mechanism critical for maintaining PSI redox poise and preventing photoinhibition under fluctuating light conditions (Suorsa et al., 2012). Disruption of this process increases vulnerability to oxidative stress, potentially triggering ROS-mediated signaling and programmed cell death (Foyer & Noctor, 2005; Lill, 2009). Additionally, repression of chlorophyllide an oxygenase (LOC101244441), points to destabilization of light-harvesting complexes, further compromising. Finally, the reduced expression of key detoxification-related genes, such as glutathione reductase (GR, LOC100301931), reflects a weakened cellular capacity to maintain redox homeostasis during phytoplasma infection. Concurrently, the downregulation of 1-deoxy-D-xylulose-5-phosphate reductoisomerase (*DXR*, LOC543682) indicates impairment of the methylerythritol phosphate (MEP) pathway, which plays a central role in the biosynthesis of plastid-derived isoprenoids, including carotenoids, tocopherols, and other essential metabolites involved in photoprotection and stress tolerance. DXR catalyzes the first step committed of this pathway by converting 1-deoxy-D-xylulose 5-phosphate (DXP) into MEP. Previous studies using the DXR inhibitor fosmidomycin have highlighted the pathway's importance in tomato fruit pigmentation and overall plant growth (Rodríguez-Concepción et al., 2001). Given the role of isoprenoids in both development and defense, these transcriptional changes suggest that phytoplasma infection disrupts core metabolic pathways, compromising the plant’s ability to balance growth with an effective antioxidant response.

Table 1. Genes involved in electron transfer, carbon fixation and oxidative for the comparison infected vs. healthy plants.

Gene Symbol/ Locus ID	Transcript	Gene description	Module	Log2Fold Change	Average expression	FDR*
101266713	XM_004236801.3	glyceraldehyde-3-phosphate_dehydrogenase A, chloroplastic	brown	-1.14	11676	0.00
101264004	XM_004238398.4	glyceraldehyde-3-phosphate_dehydrogenase B, chloroplastic	brown	-1.02	3801	0.02
101253589	XM_004239197.4	glucose-6-phosphate 1-dehydrogenase, chloroplastic	brown	-0.66	946	0.01
101265784	XM_004248998.4	ferredoxin	brown	-2.18	666	0.00
101243864	NM_001317970.1	cytochrome b6-f complex iron-sulfur subunit, chloroplastic	brown	-0.89	6580	0.00
101253342	XM_004232663.2	ATP synthase gamma chain, chloroplastic	brown	-0.71	4426	0.00
101268337	XM_026029055.1	ribulose bisphosphate carboxylase small chain 3B, chloroplastic-like, transcript_variant_X1	brown	-1.33	33787	0.00
101247036	XM_004242883.4	NADP cytochrome P450 reductase	brown	-1.43	5540	0.02
101262255	XM_004247716.4	Protein PROTON GRADIENT REGULATION 5, chloroplastic	brown	-4.24	1366	0.00
101244441	XM_004250263.4	chlorophyllide a oxygenase, chloroplastic-like	brown	-3.22	1625	0.00
100301931	NM_001247314.2	Glutathione reductase, chloroplastic	brown	-1.25	1570	0.01
543682	NM_001247624.2	1-deoxy-D-xylulose-5-phosphate reductoisomerase	brown	-1.09	1433	0.00
LOC544106	XM_004243141.3	peroxisomal_(S)-2-hydroxy-acid_oxidase_GLO1,_transcript_variant_X1	pink	-1.18	27647	0.00

*False Discovery Rate

A widespread repression of genes involved in photosynthetic machinery was reported by (Buoso et al., 2019, 2022; Hren et al., 2009), indicating a profound disruption of photosynthetic (Bertamini et al., 2003; Endeshaw et al., 2012; Z. Liu et al., 2016; Maust et al., 2003; Vitali et al., 2013). These alterations likely contribute to the typical symptoms of phytoplasma infection, such as shoot proliferation (witches' broom), stunting, yellowing, phyllody (leaf-like flowers), and virescence (greening of

floral organs), commonly observed in infected plants (Bertaccini & Duduk, 2009; Hogenhout et al., 2008; MacLean et al., 2014; Sugio et al., 2011). These physiological alterations are likely the result of phytoplasma-induced disruptions in hormonal balance, nutrient dynamics, and both developmental and stress-related signaling pathways, as well as the complex interactions among them (Buoso et al., 2019; Dermastia, 2019).

2.3.4 Validation of genes involved in chlorophyll and carotenoid biosynthesis, gas exchange, electron transport, and carbon fixation

To gain deeper insights into the deleterious impact of '*Ca*. P. solani' infection on chloroplast functions, particularly regarding chlorophyll and carotenoid biosynthesis, gas exchange, electron transport, and carbon fixation we further assessed the expression profiles of key regulatory genes implicated in these processes via RT-qPCR (Figure 6). RT-qPCR analyses revealed a broad downregulation of photosynthesis-related genes, notably including GOLDEN2-LIKE 1 (GLK1; LOC101055587) a nuclear-encoded transcription factor that contributes to controlling plastid number and chlorophyll (Chl) content (Chen et al., 2016). Plastid abundance and Chl levels, which are shaped by environmental and genetic inputs, positively track photosynthetic capacity and photosynthate accumulation (Nguyen et al., 2014). Consistent with this, GLK transcription factors function as conserved regulators of chloroplast biogenesis (Zheng et al., 2024) and are central mediators of retrograde (chloroplast-to-nucleus) signaling during biogenesis, directly activating large sets of nuclear genes encoding chloroplast-localized, photosynthesis-related proteins (Hernández-Verdeja & Lundgren, 2024; Lupi et al., 2019; Wu & Bock, 2021). These targets include genes for chlorophyll biosynthesis, light harvesting, and CO_2 fixation (Chan et al., 2016; Waters et al., 2009a). *GLK1* promotes chloroplast development and upregulates photosynthesis-associated nuclear

genes (PhANGs) (Waters et al., 2009b), acting directly through light-responsive promoter elements (Waters et al., 2009a).

Light signaling tightly controls GLK expression. GLK1 and GLK2 are induced by red/far-red phytochromes and by blue light; the *glk1glk2* double mutant exhibits reduced Chl content and downregulation of photosynthesis genes under blue light, linking GLKs to cryptochrome-mediated greening (Waters et al., 2009a). In darkness, PIFs repress GLK1 by binding its promoter, whereas exposure to moderate light activates phytochromes (e.g., phyB), which in turn inactivate PIFs, relieving repression and permitting GLK1 expression (Waters et al., 2009b). Thus, GLK1 integrates photoreceptor inputs with chloroplast-derived retrograde cues to ensure that chloroplast biogenesis and photosynthetic gene expression proceed only under favorable conditions a framework that aligns with the observed RT-qPCR downregulation.

In tomato, SlGLKs play a crucial role in chloroplast development, with SlGLK1 being more active in leaves, while SlGLK2 primarily functions in fruits (Lupi et al., 2019; Nguyen et al., 2014). Overexpression of *SlGLKs* enhances chloroplast number and grana stacks, with a multiplicative effect on chlorophylls level only in green fruit. *SlGLK1* repression results in chlorotic leaves, demonstrating its importance in leaf plastid development, while *SlGLK2* repression has no leaf phenotype (Nguyen et al., 2014).

We examined the expression of genes acting downstream *GLKs* and possibly related to the pale-green phenotype of the infected plants. The genes involved in the first step of chlorophyll biosynthesis, the tetrapyrrole-binding protein encoding *GUN4* (LOC101252496) and the magnesium-chelatase subunit ChlH encoding *GUN5* (LOC101244176) are key genes in chlorophyll biosynthesis and involved in retrograde signaling (Wu & Bock, 2021). Both genes were significantly downregulated in the infected midribs compared to healthy (Figure 6). Tetrapyrroles, including porphyrins, are essential for key biological processes such as respiration and photosynthesis, functioning in light absorption, electron transport, and oxygen binding (Shimizu et al.,

2019). Their biosynthesis occurs in plastids and branches from protoporphyrin IX into two main pathways: the chlorophyll branch, producing chlorophylls a and b, and the heme branch, leading to phytochromobilin that is the chromophore for red/far-red light-sensing phytochromes (Bae & Choi, 2008; Griffin & Toledo-Ortiz, 2022). In the chlorophyll branch, *CHLH/GUN5* encodes the ChlH subunit of magnesium chelatase, catalyzing the conversion of protoporphyrin IX to magnesium protoporphyrin IX (Mg-ProtoIX), while *GUN4* encodes an activator of ChlH that enhances Mg-ProtoIX accumulation (Jarvis & López-Juez, 2013; Larkin et al., 2003; Mochizuki et al., 2001). Mg-ProtoIX has been proposed with heme as a key retrograde signal (Wu & Bock, 2021) involved in the repression of PhANGs, such as Light Harvest Complex (LHCB) and ribulose bisphosphate carboxylase small chain (*RbcS*) (Griffin & Toledo-Ortiz, 2022). The downregulation of *CHLH* that we observed in the infected leaf-midribs is probably correlated to a low level of Mg-ProtoXI and downstream metabolites. In fact, in the *Arabidopsis* CHLH-silenced RNAi line the downstream intermediates, such as Mg-ProtoXI and protochlorophyllide (Pchlide), showed decreasing steady-state levels, whereas ProtoIX content increased approximately three-fold after a 4-d repression of *CHLH* gene (Schlicke et al., 2014). As *CHLH* silencing caused a slight accumulation of the PhANGs *LHCB1.2*, *RbcS*, and plastocyanin mRNA levels, the phototoxic Mg-ProtoIX was questioned as a candidate for a plastid-to-nucleus signaling molecule (Schlicke et al., 2014), who proposed other tetrapyrrole pathway intermediates as retrograde signals (Mochizuki et al., 2008; Schlicke et al., 2014). However, Mg-ProtoIX level has to be strictly regulated, as its overaccumulation particularly during the dark-to-light transition leads to the generation of singlet oxygen ($^1O_2$), triggering oxidative stress responses and the activation of jasmonate and salicylate pathways (Chen et al., 2016).

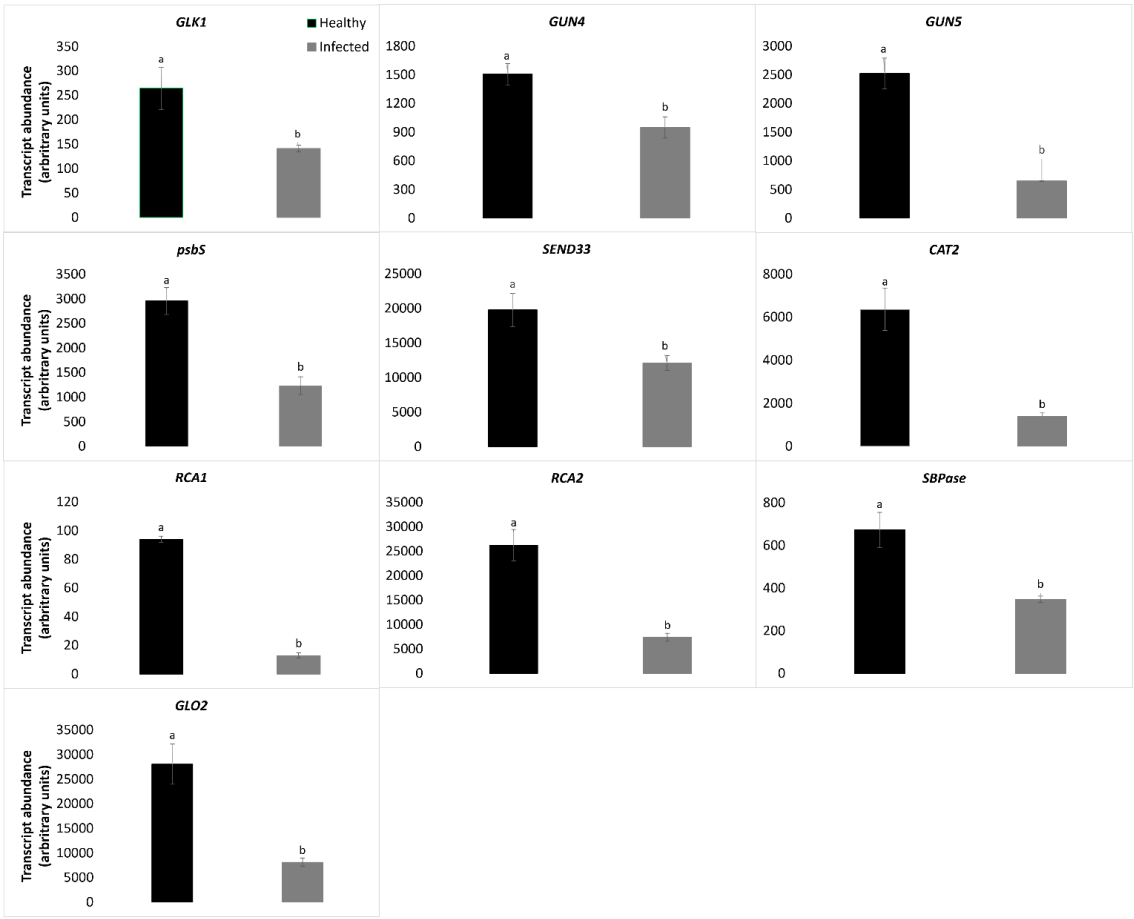

Figure 6. Expression analysis of photosynthesis, antioxidant enzymes and photorespiration genes in tomato midribs by RT-qPCR. The mean normalized expression (MNE) of each gene is plotted as the transcript abundance compared with the *UPL3* expression level (set as 100). Results are expressed as mean ± SE (n=3). Different letters indicate statistically significant differences ($P \leq 0.05$) among the conditions (one-way ANOVA followed by Tukey's test).

Taken together, the repression of *GUN4* and *CHLH/GUN5* genes was consistent with *GLK1* downregulation, suggesting a negative impact on chlorophyll content and photosynthesis in the infected plants. Thus, we determined the level of pigments in infected and healthy tomato leaves. Consistent with downregulation of *GLKs*, and key genes of the tetrapyrrole pathway, the chlorophyll content was significantly reduced in the '*Ca*. P. solani'-infected leaves (Figure 7).

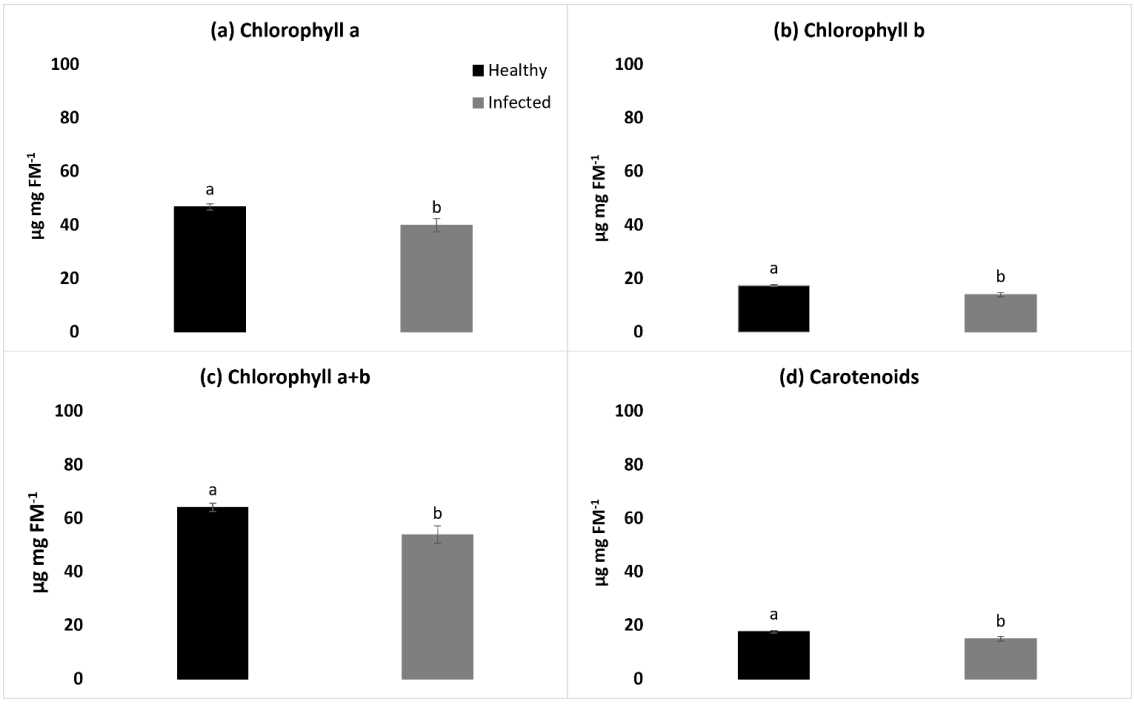

Figure 7. The concentration of chlorophyll and carotenoids was analytically determined according to Lichtenthaler (1987) of tomato plants cv. Micro-Tom grown in two different conditions, healthy and infected. Results are expressed as mean ± SE (n = 5). The different letters in the bars indicate statistically significant differences ($P \leq 0.05$) among conditions (one-way ANOVA followed by Tukey's test).

Specifically, chlorophyll a (Chl a), chlorophyll b (Chl b), and total chlorophyll (Chl a + b) levels declined by 14.5%, 19.8%, and 15.8%, respectively, compared to healthy controls (Figure 7a-c). Carotenoid (Car) content also decreased by 15.3% in infected plants (Figure 7d). These reductions are consistent with the downregulation of genes involved in chloroplast development and pigment biosynthesis, including *GLK1, GUN4*, and *GUN5*. Repression of these pathways impairs chloroplast function and reduces photosynthetic capacity in infected plants.

Thus, we focused on the expression of chloroplast genes directly involved in photosynthesis. Phytoplasmas might disrupt the normal functioning of the electron transport chain, leading to a decrease in the flow of electrons. This can result in reduced

ATP and NADPH production, which are used during the CO_2-fixing Calvin-Benson-Bassham (CBB) cycle. We observed the downregulation of *psbS* (LOC101260830), encoding the photosystem II subunit S PsbS, a small tylakoid protein associated with PSII (Figure 6). Although PsbS is not directly involved in light capture, it plays a crucial role in non-photochemical quenching (NPQ), a key photoprotective mechanism. NPQ is one of the most critical mechanisms for minimizing photo-oxidative damage, safely dissipating excess energy from singlet excited chlorophylls in the antenna complex as heat, thereby protecting the chloroplast under high light conditions (Correa-Galvis et al., 2016). *PsbS* expression strongly enhances NPQ and supports photoprotection under high light or rapidly fluctuating conditions, without significantly affecting steady-state net CO_2 assimilation. Noteworthy, under NPQ suppression, as observed when flg22 induces decrease in PsbS abundance, energy is driven into the production of ROS, in particular singlet oxygen at the PSII (Göhre et al., 2012). Rice plants deficient in the PsbS protein had higher levels of chloroplastic O_2^- and H_2O_2 and were more resistant to the fungus *Magnaporthe oryzae* infection (Zulfugarov et al., 2016), This outcome suggests that dysfunction in the electron transport chain can lead to the overproduction of reactive oxygen species, and cause oxidative stress, damaging chloroplast membranes and proteins, further impairing photosynthesis. On the other hand, chloroplastic ROS can contribute to immunity (Littlejohn et al., 2021) and could be part of the response of the plant to the presence of phytoplasma.

Additionally, the gene *SEND33* (LOC778301) was confirmed to be downregulated (Figure 6). *SEND33* encodes ferredoxin-I, an iron-sulfur protein that serves as an electron carrier, transferring electrons from photosystem I (PSI) to various enzymes involved in carbon fixation and other metabolic pathways (Hase et al., 2006). As regards photosynthesis, electrons from ferredoxin are utilized in linear electron transfer (LET) by the enzyme Ferredoxin-$NADP^+$ reductase (FNR) to reduce $NADP^+$ to NADPH, which in turn is used to reduce 1,3-bisphosphoglycerate during the CBB cycle (Buchert et al.,

2020). Alternatively, electrons from ferredoxin or NADPH can re-enter the photosynthetic electron transfer chain to reduce plastoquinone, via cyclic electron transfer (CET) (Munekage et al., 2004; Yamori et al., 2015). Our outcome suggests disruption of the ETC, potentially leading to decreased photosynthetic efficiency, resulting in lower rates of carbon fixation and reduced energy availability for the plant. Disruption of the ETC, potentially reducing photosynthetic efficiency and carbon fixation, may be linked to impaired regulation of electron partitioning by PGR5, a key mediator of PSI redox balance through its control of LET and CET.

Then, the expression of genes encoding key players of the CBB cycle was focused. Key genes related to CBB cycle were also confirmed to be downregulated in response to the '*Ca.* P. solani' infection. Among these, the sedoheptulose-1,7-bisphosphatase gene (*SBPase*, LOC100316873), is specific to the CBB cycle and plays a key regulatory role in RuBP regeneration under light-saturated conditions (Hammel et al., 2020). Moreover, two paralogs of ribulose bisphosphate carboxylase/oxygenase activase (*RCA1*, LOC101250725 and *RCA2*, LOC101249777) were downregulated in response to the phytoplasma challenge. RCA plays a crucial role in regulating Rubisco by inducing conformational changes that restore its catalytic activity, primarily by removing inhibitory sugar phosphates including ribulose-1,5-bisphosphate (RuBP) from its active sites (Nagarajan & Gill, 2018; Sparrow-Muñoz et al., 2023; Waheeda et al., 2023).

Taken together, these findings supported a scenario where disruption of the ETC (and CET) is paralleled by impairment of CBB cycle, leading to decreased photosynthetic efficiency and reduced energy availability for the plant. These outcomes were corroborated by a reduction in net CO_2 assimilation rate (A) and instantaneous carboxylation efficiency (EiC), as shown in the following Figures 8a and 9f. Additionally, the A-Ci response curve, presented in Figure 9, further supports these results.

2.3.5 Phytoplasma infection impairs CO_2 fixation parameters and A/Ci response curve

We subsequently assessed the impact of '*Ca.* P. solani' infection on carbon fixation, which led to a 42.8% decrease in net CO_2 assimilation (Figure 8a). Similar reductions in photosynthetic CO_2 uptake have been reported in plants challenged with phytoplasmas, often linked to disrupted source/sink dynamics and altered chloroplast function (Maust et al., 2003). In contrast, stomatal conductance (gs), leaf transpiration rate (E), intercellular CO_2 concentration (Ci), and the Ci/Ca ratio remained unaffected under the experimental conditions (Figures 8b-e), suggesting that stomatal limitations were not the primary cause of reduced assimilation. However, the instantaneous in vivo carboxylation efficiency of Rubisco (EiC) significantly decreased by 43.1% in infected plants (Figure 8f), consistent with impaired mesophyll or biochemical capacity, a common hallmark of phytoplasma-induced metabolic reprogramming.

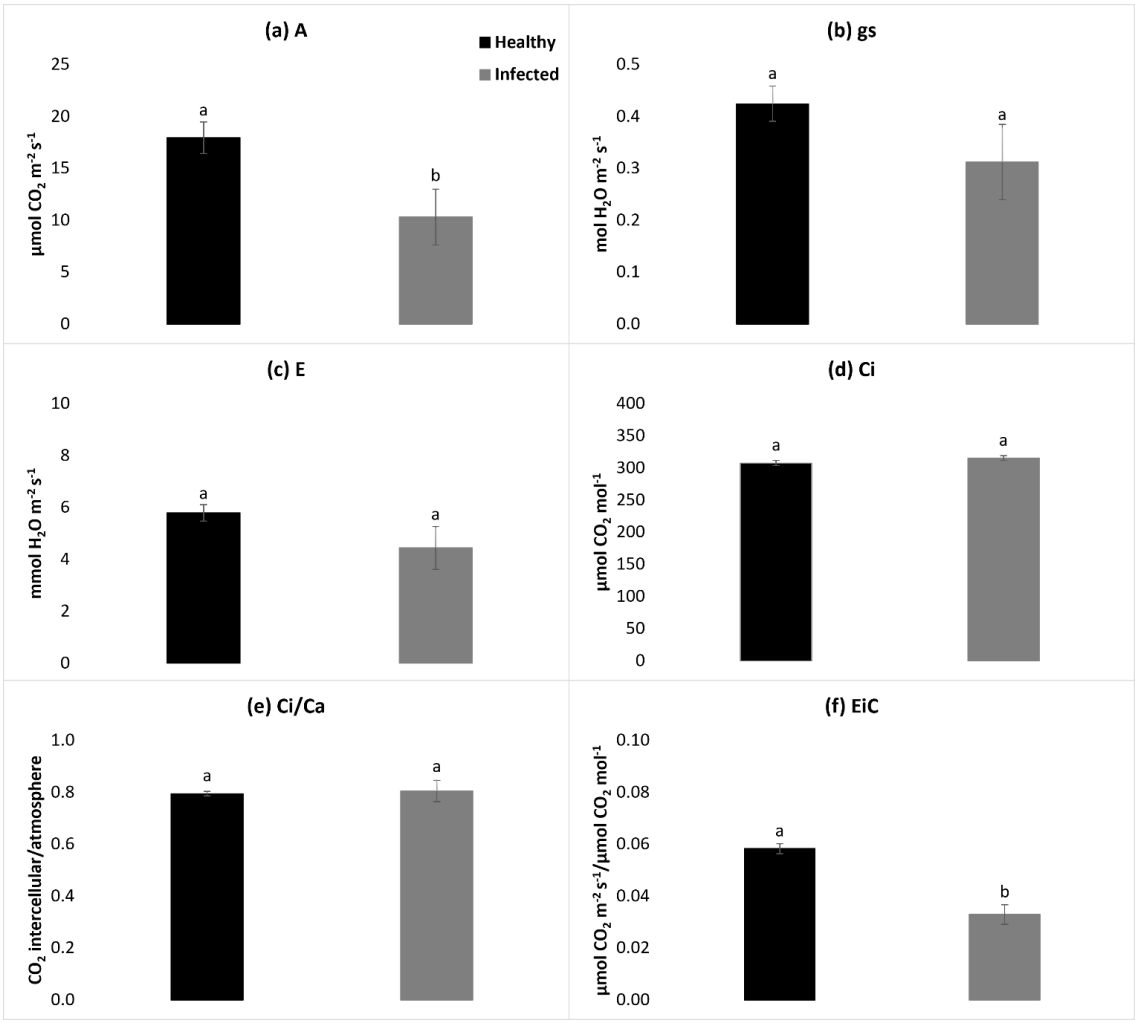

Figure 8. Effect of phytoplasma infection on (a) A, net CO_2 assimilation; (b) gs, stomatal conductance; (c) E, leaf transpiration rate; (d) Ci, intercellular CO_2 concentration; (e) Ci/Ca (ratio of intercellular and atmosphere CO_2 concentration) and (f) instantaneous carboxylation efficiency (EiC). Results are expressed as mean ± SE (n = 5). The different letters in the bars indicate statistically significant differences ($P \leq 0.05$) among conditions (one-way ANOVA followed by Tukey's test).

The effect of the infection on CO_2 assimilation was further examined through an A/Ci response (Figure 9). Such analysis is associated with leaf biochemistry *via* the model proposed by (Farquhar et al., 1980) and is commonly utilized to deduce the biochemical constraints of photosynthesis. At low concentrations of CO_2 (50, 100, 200, and 300 µmol

mol^{-1}), infection had no significant effect on net CO_2 assimilation (A). Differently from healthy, assimilation in infected plants reached a plateau between 300 and 400 µmol CO_2 mol^{-1} and decreased as CO_2 concentration was raised up to 600 µmol CO_2 mol^{-1}, showing that high intracellular CO_2 did not restore photosynthesis. The reduction in carbon fixation observed in phytoplasma-infected plants is a consequence of a multifaceted disruption of photosynthetic processes, spanning from light harvesting and electron transport to enzymatic activity and regulatory signaling, rather than a direct limitation in CO_2 availability.

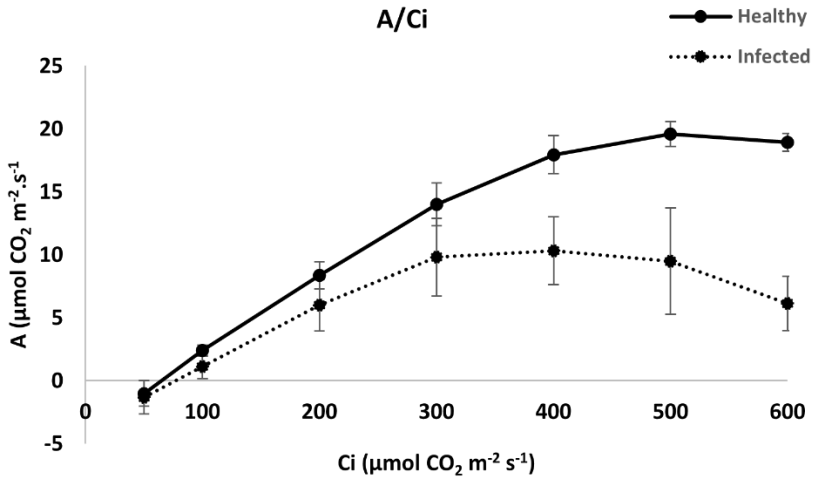

Figure 9. Effect of phytoplasma infection on the net CO_2 assimilation rate (A) at a given intercellular CO_2 concentration (Ci). The A-Ci response is expressed as mean ± SE (n = 5).

2.3.6 Phytoplasma infection impairs light curve and electron transport rate

The coordination between photochemical energy supply and carbon fixation in photosynthesis is reflected in the relationship between net CO_2 assimilation (A) and light intensity (PPFD), as well as the electron transport rate (ETR). According to (Wang et al., 2025), light intensity strongly affects the CO_2 assimilation rate (A) by modulating stomatal conductance (gs), mesophyll conductance (gm), the activation state of Rubisco,

and the electron transport rate (ETR). This aligns with established findings that both stomatal and non-stomatal factors influence photosynthetic efficiency under varying light conditions (Flexas et al., 2004; Yamori et al., 2011). In our study, the reduction in A was associated with downregulation of *RCA* (Salvucci & Crafts-Brandner, 2004) (Salvucci & Crafts-Brandner, 2004), and a pronounced suppression of genes involved in regulating the electron transport rate (Munekage et al., 2002).

To investigate the physiological impact of gene downregulation associated with chloroplast development and pigment biosynthesis in response to *'Ca.* P. solani' infection, light response curves (A/PPFD) and electron transport rate (ETR) were measured (Figure 10). In the A/PPFD curve (Figure 10a), the initial phase (20-100 µmol photons m^{-2} s^{-1}) displayed a linear relationship, with the slope, representing the chloroplastic light-use efficiency (Φ), showing no significant differences between healthy and phytoplasma-infected plants. This pattern reflects the efficiency of photosystems in utilizing absorbed light for photochemistry under non-saturating light (Baker, 2008). At higher photon flux densities (200-500 µmol photons m^{-2} s^{-1}), photosynthetic rates in infected plants stabilized, reaching a maximum (light saturation point) beyond which further increases in PPFD did not enhance photosynthesis. In contrast, healthy plants continued to exhibit an increase in photosynthetic activity up to 500 µmol photons m^{-2} s^{-1}, indicating a broader dynamic range of light responsiveness.
The electron transport rate (ETR), one of the main sources of ROS in plant cells (Foyer et al., 1994), was also analyzed (Figure 10b). The ETR values of infected plants were markedly lower than those of the healthy control, regardless of CO_2 concentration. The reductions in ETR were 10.7, 11.8, 13.7, 15.9, 23.2, 15.4, and 15.4% at CO_2 concentrations of 50, 100, 200, 300, 400, 500, and 600 µmol CO_2 mol^{-1}, respectively. However, ETR remained responsive to increasing CO_2, suggesting that ATP and NADPH production were impaired, but not completely disrupted. This partial impairment still

allowed for some degree of reductive power and energy transfer to support carbon fixation in the CBB (Yamori & Shikanai, 2016).

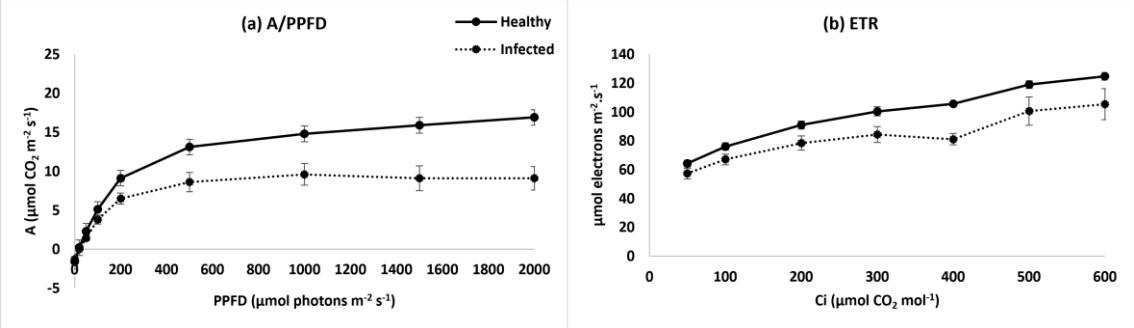

Figure 10. (a) Effect of phytoplasma infection on A (light response curve) and (b) electron transfer rate (ETR). Results are expressed as mean ± SE (n=5).

Lastly, we focused on the modulation of hydrogen peroxide (H_2O_2) scavenging pathways in response to phytoplasma infection. The gene encoding glycolate oxidase 2 (*GLO2*, LOC100134875), along with its co-expressed homolog glycolate oxidase 1 (*GLO1*, LOC544106), identified in the pink module, encodes a key peroxisomal enzyme involved in the conversion of glycolate to glyoxylate during photorespiration, a process that generates H_2O_2 as a by-product (Xu et al., 2018) was found to be downregulated in the RT-qPCR experiment (Figure 6 and Table 1), respectively. Phytoplasma infection disrupts peroxisomal metabolism in tomato, as evidenced by glycolate accumulation in phloem exudates and downregulation of genes associated with glycolate oxidation, including glycolate oxidase. These alterations suggest a suppression of photorespiratory H_2O_2 production. However, the concurrent increase in total H_2O_2 levels indicates that alternative sources, such as chloroplasts or apoplastic NADPH oxidases, may compensate for the reduced peroxisomal ROS output. This uncoupling of photorespiration from ROS accumulation reflects a broader reprogramming of redox homeostasis in response to infection (Marco et al., 2021). Consistently, the gene encoding catalase 2 (*CAT2*, LOC543585), which detoxifies H_2O_2 by catalyzing its

conversion into water and oxygen, was also downregulated. The effect of the repression of key genes that participate in ROS-scavenging system on H_2O_2 and MDA contents, which are markers of oxidative stress, were also evaluated. In response to the infection, the levels of H_2O_2 in both midrib and leaf lamina showed significant increases (Figures 11a-b). However, the infection had no impact on the levels of MDA in both healthy and infected conditions. Nonetheless, a significant increase on MDA was observed in leaf lamina compared to midrib enriched (Figures 11c-d).

PhANGs, such as LHCB and *RbcS*, are responsive to retrograde signals (Griffin & Toledo-Ortiz, 2022; Wu & Bock, 2021). The expression of these genes is repressed in response to disrupted pigment biosynthesis and/or impaired plastid gene expression (PGE) (Wu & Bock, 2021). Recent evidence demonstrates that chloroplast-derived hydrogen peroxide (H_2O_2) functions as a direct retrograde signal, moving from chloroplasts to the nucleus to regulate gene expression in response to high light. Using the fluorescent H_2O_2 sensor HyPer2 in *Nicotiana benthamiana* (Exposito-Rodriguez et al., 2017) showed that nuclear H_2O_2 accumulation and subsequent gene expression depend on photosynthetic H_2O_2 production in chloroplasts closely associated with nuclei, bypassing the cytosol. Additionally, genes associated with radiation response (e.g., phytochrome B1, LOC101262847), chloroplast-related processes (e.g., heme-binding-like protein At3g10130, LOC101251239). The chloroplast-localized heme-binding-like protein At3g10130, part of the SOUL family, likely contributes to heme homeostasis and redox balance in tomato, like its *Arabidopsis* homolog SOUL4, which binds heme and mitigates oxidative stress. Its phosphorylation suggests environmentally responsive regulations (Lundquist et al., 2012). Consistently, the downregulation of high light-responsive genes, including *FtsH protease* (LOC778337), points to a broader disruption of plastidial stress-response pathways (Supplemental files: Tables S5-6). This further underscores the impact of phytoplasma infection on both retrograde and anterograde signaling pathways, leading transcriptomic reprogramming

of genes regulating photomorphogenic alterations clustered in the blue module, as discussed in the following section. The downregulation of these key components points to a disturbance in light signal transduction and chloroplast function, which are crucial for regulating plant growth, development, and physiological processes.

Phytoplasma infection markedly suppressed photosynthetic performance, as evidenced by a reduced net CO_2 assimilation rate (A) across increasing light intensities (APPFD) (Figure 10a). This impairment was accompanied by a decline in electron transport rate (ETR; Figure 10b), indicating that both efficiency of the photosynthetic electron transport chain and carbon fixation were compromised. We observed the downregulation of the photosystem II subunit S (*psbS*, LOC101260830), a chlorophyll a/b binding protein. Although *PsbS* is not directly involved in light harvesting, it is essential for regulating non-photochemical quenching (NPQ), a vital photoprotective mechanism. NPQ helps prevent photo-oxidative damage by safely dissipating excess excitation energy from singlet chlorophylls in the antenna complexes as heat, thereby safeguarding chloroplast function under light stress (Correa-Galvis et al., 2016). *PsbS* expression strongly enhances NPQ and supports photoprotection under high light or rapidly fluctuating conditions, without significantly affecting steady-state net CO_2 assimilation. As a result, stomatal regulation via intercellular CO_2 concentration (Ci) remained unchanged (Głowacka et al., 2018) as demonstrated in Figure 8d. Noteworthy, under NPQ suppression energy is driven into the production of ROS, in particular singlet oxygen at the PSII (Göhre et al., 2012). Additionally, the gene *SEND33* (LOC778301) which encodes ferredoxin-I, an iron-sulfur protein that serves as an electron carrier, transferring electrons from photosystem I (PSI) to various enzymes involved in carbon fixation and other metabolic pathways, was found to be downregulated in our RT-qPCR analyses conducted in independent experiments (Figure 6).

Key genes related to carbon fixation were confirmed downregulated in response to the ‘Ca. P. solani’ infection. Among these, the sedoheptulose-1,7-bisphosphatase gene

(*SBPase*, LOC100316873), plays a key regulatory role in RuBP regeneration under light-saturated conditions (Hammel et al., 2020). Moreover, two paralogs of ribulose bisphosphate carboxylase/oxygenase activase (*RCA1*, LOC101250725 and *RCA2*, LOC101249777) were downregulated in response to the phytoplasma challenge. RCA plays a crucial role in regulating Rubisco by inducing conformational changes that restore its catalytic activity, primarily by removing inhibitory sugar phosphates including ribulose-1,5-bisphosphate (RuBP) from its active sites (Nagarajan & Gill, 2018; Sparrow-Muñoz et al., 2023; Waheeda et al., 2023). These findings were corroborated by a reduction in net CO_2 assimilation rate (A) and instantaneous carboxylation efficiency (EiC), as shown in Figures 8a and 8f. Additionally, the A-Ci response curve, presented in Figure 10a, further supports these results.

2.3.7 Phytoplasma infection alters redox homeostasis without triggering severe oxidative damage

Chloroplasts are major sources of ROS, primarily via overexcitation of PSII and electron leakage to molecular oxygen through PSI under conditions of impaired photochemical and non-photochemical quenching (Havaux et al., 1991; Li & Kim, 2022). In phytoplasma-infected tomato leaves, we observed transcriptional downregulation of several genes encoding components of the chloroplast electron transport chain key sites of ROS generation coinciding with a significant increase in H_2O_2 accumulation across both midrib-enriched and lamina tissues (Figures 11a-b), in line with previous reports linking ETC disruption to ROS overproduction (Lu & Yao, 2018; Moreau et al., 2020; Mühlenbock et al., 2008; Sano et al., 2014; Serrano et al., 2016; Stael et al., 2015). Notably, this increases in H_2O_2 occurred in the absence of elevated malondialdehyde (MDA) levels, a classical marker of lipid peroxidation and irreversible oxidative damage (Figures 11c-d), suggesting a controlled ROS accumulation rather than widespread oxidative stress. This points to a potential signaling role for H_2O_2 in the infected tissues,

rather than its function as a cytotoxic by-product (Schmidt et al., 2020). Consistent with this, the electron transport rate (ETR) remained partially active (Figure 10b), indicating that photosynthetic function, though suppressed, is not fully compromised allowing for continued ROS generation. These findings raise the possibility that phytoplasma may interfere with or co-opt the host antioxidant machinery to limit ROS scavenging and promote localized H_2O_2 accumulation as a means of manipulating host signaling. Alternatively, the host plant itself may actively modulate its scavenging system to sustain H_2O_2 production as part of a defense priming strategy, leveraging ROS as a retrograde signal to activate nuclear stress-responsive and immune genes (Foyer & Noctor, 2005; Mittler, 2017). Such redox modulation has also been proposed in other biotic interactions, where plants adjust ROS-scavenging pathways to maintain a delicate balance between activating defense responses and preserving photosynthetic integrity, particularly under stress conditions (Foyer & Noctor, 2005; Mittler et al., 2011; Pogány et al., 2009). This trade-off suggests a strategic shift in redox homeostasis, allowing controlled ROS accumulation to function as signaling molecules without triggering oxidative damage.

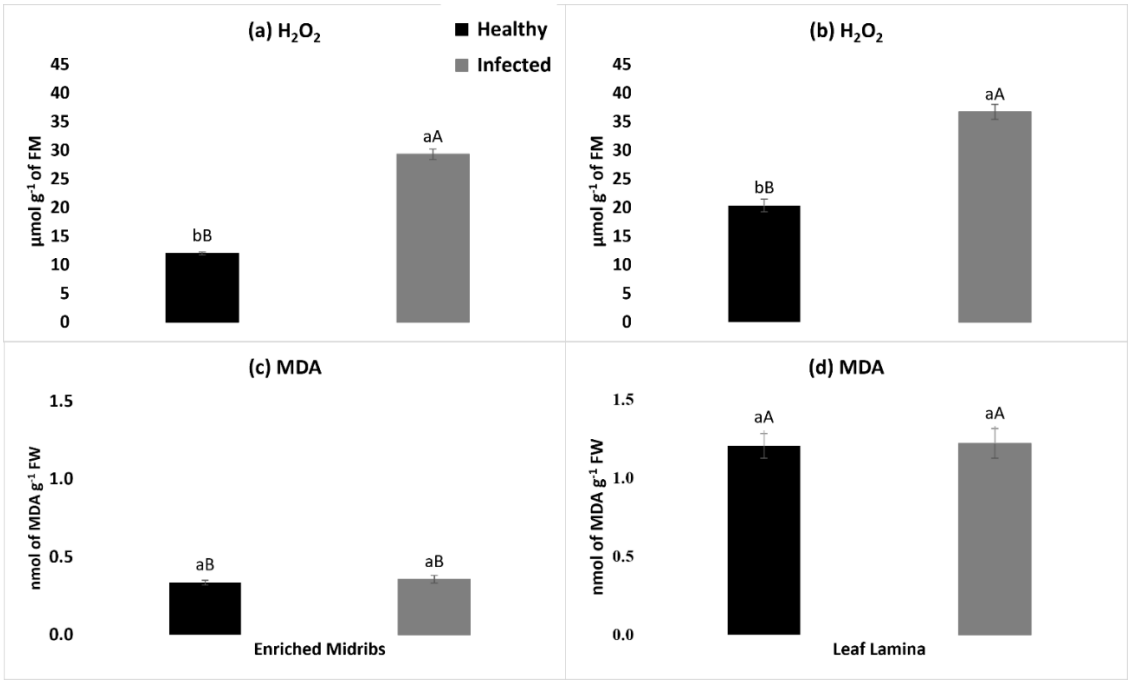

Figure 11. (a) Hydrogen peroxide (H_2O_2) concentration in midrib-enriched (b) H_2O_2 concentration in leaf lamina, (c) malondialdehyde (MDA) concentration in midrib-enriched, and (d) MDA concentration in leaf lamina of healthy and phytoplasma-infected. FM: fresh matter. Results are expressed as mean ± SE (n=5). The different lower-case letters in the bars indicate statistically significant differences between healthy and infected, the different upper-case letters indicate significative differences between enriched leaf midribs and leaf lamina ($P < 0.05$) (two-way ANOVA followed by Tukey's test).

The genes encoding Catalase 2 (*CAT2*, 543585) and glutathione reductase (*GR*, 100301931), both members of the brown module, were significantly downregulated, indicative of a potential reduction in H_2O_2 detoxification capacity and glutathione cycling. Such reduction was further suggested by the downregulation of *GGP*, key gene in the ascorbate biosynthetic pathway (Table 2), which plays an important role in protecting plants by maintaining ascorbate pool and ascorbate redox state. Despite its downregulation, *GR* maintained moderate expression levels (average expression = 1570), possibly preserving basal redox homeostasis. Notably, *CAT2* exhibited the highest

basal expression across the dataset (average expression = 9750), underscoring its constitutive role in antioxidative metabolism (Table 2).

In contrast, ascorbate oxidase (AO, 778230), clustered in the pink module, was upregulated, pointing to a transcriptional shift toward enhanced apoplastic ROS scavenging. This trend was corroborated by the upregulation of a transmembrane ascorbate ferroreductase (LOC101259568) within the same module, suggesting increased apoplastic ascorbate turnover. Conversely, a paralog of L-ascorbate oxidase (LOC101251411) in the turquoise module was downregulated, reflecting module-specific regulation of the ascorbate pathway. Different regulations might reflect different subcellular localization of the proteins. Further evidence for a possible differential subcellular regulation was provided by the upregulation of L-ascorbate peroxidase 3 (LOC101264282) in the turquoise module. Although lowly expressed (average expression = 110), L-ascorbate peroxidase 3 (homolog to *Arabidopsis* AT4G35000, *APX3*) likely contributes to intracellular H_2O_2 detoxification, potentially compensating for reduced CAT2 activity (Najami et al., 2008). The overexpression of nucleobase-ascorbate transporter (LOC101262812) and S-formylglutathione hydrolase (LOC101260331), point to increased ascorbate flux and turnover (Table 2). L-ascorbate (vitamin C) is the most abundant soluble antioxidant in plants and serves as an essential cofactor in numerous enzymatic reactions (Fenech et al., 2019; Smirnoff, 2018). Ascorbate levels vary depending on the tissue type (Franceschi & Tarlyn, 2002; Lorence et al., 2004; Müller-Moulé, 2008; Zhang et al., 2011) and dynamically adjust in response to environmental factors, especially light (Bartoli, 2006; Page et al., 2012; Plumb et al., 2018). Also, glutathione peroxidase (*GPXle-2*, LOC101267098), a cytosolic peroxidase within the brown module, was moderately upregulated, suggesting compensation for reduced catalase activity. Meanwhile, multiple glutathione S-transferases (GSTs) displayed module-dependent expression changes, indicating a nuanced regulation of glutathione-mediated detoxification pathways.

Collectively, our data suggests that the antioxidant response involves a coordinated transcriptional reprogramming of redox-associated genes, tailored to distinct subcellular compartments (Chan et al., 2016). The upregulation of genes associated with the ascorbate-glutathione cycle and apoplastic ROS scavenging pathways, alongside selective downregulation of key cytosolic enzymes, reflects a dynamic and spatially regulated redox adjustment in response to '*Ca*. P. solani' infection. For instance, glutathione biosynthesis depends on enzyme isoforms localized in the chloroplasts, cytosol, and mitochondria (Chan et al., 2013), reflecting the need for compartmental cooperation, while the activity of cytosolic ascorbate peroxidases is modulated by the chloroplast's redox status (Karpinski et al., 1997).

Table 2. Genes involved in oxidative stress co-expressed in different modules for the comparison of infected vs. healthy plants.

Gene Symbol/ Locus ID	Transcript	Gene description	Module	Log2Fold Change	Average expression	FDR*
CAT2	NM_001247257.2	catalase_2	brown	-2.70	9750	0.01
GR	NM_001247314.2	glutathione reductase,_chloroplastic	brown	-1.25	1570	0.00
AO	NM_001247900.2	ascorbate_oxidase	pink	1.43	1080	0.02
LOC101259568	XM_004228699.4	probable transmembrane ascorbate ferrireductase 3	turquoise	2.64	14	0.02
LOC101251411	XM_004228587.3	L-ascorbate_oxidase homolog	turquoise	-6.13	9	0.00
APX3	XM_004232456.3	L-ascorbate_peroxidase 3	turquoise	1.91	110	0.00
LOC101262812	XM_004238656.4	nucleobase-ascorbate transporter 7	turquoise	1.91	175	0.00
LOC101260331	XM_004236537.4	S-formylglutathione hydrolase	turquoise	0.57	1383	0.00
GPXle-2	NM_001321493.1	glutathione_peroxidase	brown	0.84	1595	0.01

*False Discovery Rate

2.3.8 Co-expression analysis identified blue module genes associated with hormone signaling and photomorphogenesis

The blue module comprises 2,688 genes, including 2,245 from *Solanum lycopersicum* and 443 from *'Ca.* P. solani', out of the 549 genes annotated in the reference genome (GCA_000970375). Of the differentially expressed genes, 381 were derived from *Solanum lycopersicum* and 170 from *'Ca.* P. solani'. Notably, 168 of the phytoplasma DEGs were assigned to the blue module, with only two to the turquoise module, underscoring a highly coordinated transcriptional program during host colonization. While the *Solanum* genes in this module were significantly enriched in several KEGG pathways particularly MAPK signaling and plant hormone signal transduction no KEGG or GO term enrichment was observed for the phytoplasma genes. Functional enrichment results are presented in Figure 12 and Supplemental Tables S8-S10.

Solanum genes in the blue module were significantly enriched in several KEGG pathways, including MAPK signaling (sly04016) and plant hormone signal transduction (sly04075) (Figure 12a; Supplemental files: Table S8). The gene *MAPK8* (LOC100736510), involved in early defense signaling and H_2O_2 production, was upregulated mirroring responses seen in *Nerium indicum* with witches' broom disease (Wang et al., 2022). Additionally, the ethylene response factor *ERF C.3* (LOC101247461) and an ethylene receptor homolog (LOC543588) were also upregulated, highlighting the activation of ethylene-mediated defense pathways. MAPK8 functions in a conserved signaling cascade that activates transcription factors such as ERFs (Dubois et al., 2015). Among them, ERF C.3, belonging to the AP2/ERF superfamily, is involved in ethylene-mediated gene regulation and may play a role in defense-related transcriptional reprogramming. Beyond stress signaling, genes of this family also regulate key biological processes such as growth, development, and secondary metabolism (Tang et al., 2024). A pronounced differential expression of ethylene signaling-related genes has been observed in Mexican lime infected with '*Ca*. P. aurantifolia'. These include genes encoding *AP2/ERF-*

like transcription factors, ethylene-responsive transcription factors and ethylene-induced esterases (Mardi et al., 2015). Meanwhile, ethylene receptor homologs, which act as negative regulators of ethylene signaling, may be differentially regulated during infection, reflecting either activation of defense pathways or pathogen-mediated suppression.

Our co-expression network analysis revealed key genes regulating hormonal responses during phytoplasma infection, including the gene encoding for *GID1*-like gibberellin receptor (*GID1*, LOC100736493), *IAA10* protein (LOC543544), *ERF C.3* (LOC101247461), and an ethylene receptor homolog (LOC543588). These genes are components of both the plant hormone signal transduction and MAPK signaling pathways, highlighting the integration of hormonal and kinase cascades in defense regulation (Meng & Zhang, 2013). Except for *IAA10*, which was downregulated, all were upregulated and are involved in gibberellin, ethylene, and auxin signaling (Table 3 Supplemental files; Table S8). During phytoplasma infection, these hormonal pathways interact with MAPK signaling to modulate defense responses (Liu et al., 2018). Gibberellin signaling via GID1 influences growth-defense trade-offs by regulating DELLA proteins, which modulate defense gene expression (De Vleesschauwer et al., 2014). Ethylene signaling components, including ethylene receptors and ERF transcription factors, regulate stress-responsive genes and pathogen defense. Auxin signaling, through IAA10 and related AUX/IAA proteins, controls developmental gene expression and is often reprogrammed during pathogen attack to balance growth and immunity (Korasick et al., 2014; Navarro et al., 2008). The crosstalk between these hormonal pathways and MAPK cascades enables dynamic reprogramming of gene expression, facilitating a balanced modulation of growth suppression and defense activation in response to phytoplasma infection.

A subset of genes was associated with biological processes (BP) related to development, potentially reflecting morphogenic responses to the infection. This

response may be mediated by retrograde signaling, as suggested by gene expression changes observed in retrograde signaling-associated genes within the brown module. Enriched GO terms included floral organ morphogenesis (GO:0048444), pattern specification process (GO:0007389), sulfur compound biosynthetic process (GO:0044272), anatomical structure morphogenesis (GO:0009653), regulation of developmental process (GO:0050793), plant organ development (GO:0099402), shoot system development (GO:0048367), system development (GO:0048731), multicellular organism development (GO:0007275), anatomical structure development (GO:0048856), developmental process (GO:0032502), multicellular organismal process (GO:0032501), cellular response to chemical stimulus (GO:0070887), response to organic substance (GO:0010033), and response to chemical (GO:0042221) (Figure 12b and Supplemental files: Table S9). These biological processes encompass pathways regulating the growth and development of above-ground organs.

Notably, the downregulation of the gene encoding for CLAVATA1 (*CLV1*, LOC101266413), plays a critical role in maintaining the balance between stem cell maintenance and differentiation within meristematic tissues. Its downregulation disrupts this equilibrium, leading to uncontrolled shoot and root proliferation (Clark et al., 1997). Furthermore, the upregulation of scarecrow-like protein 15 (*SCL15*, LOC101251641), WUSCHEL-related homeobox 3-like (*WOX3-like*, LOC101266096), and 1-aminocyclopropane-1-carboxylate oxidase (*ACO2*, LOC101251255) suggests significant alterations in plant development and stress responses. SCL15 affects root and shoot architecture, contributing to abnormal growth patterns like witches' broom, while WOX3-like, involved in stem cell regulation (Clark et al., 1997; Somssich et al., 2016), promotes excessive meristem proliferation. *ACO2*, which regulates ethylene biosynthesis, may disrupt hormonal balance and promoting altered growth and leaf yellowing, a typical symptom observed in phytoplasma-infected plants. In tomato plants infected with potato purple top (PPT) phytoplasma, infection triggers profound

alterations in carbohydrate metabolism and hormone signaling that culminate in premature senescence and abnormal shoot proliferation. Notably, starch degradation is impaired, leading to chloroplast degradation and leaf senescence (Wei et al., 2022). This is accompanied by the transcriptional upregulation of senescence-associated genes, including *Sl-ASN* (asparagine synthetase) and *Sl-TPS* (trehalose-6-phosphate synthase), which are key markers of sugar and stress-responsive pathways. Concurrently, phytoplasma infection disrupts phloem transport, resulting in sucrose accumulation in leaf axils and impaired source-to-sink allocation. These metabolic disturbances, coupled with imbalances in phytohormones such as cytokinins and auxins, are thought to underlie hallmark symptoms of phytoplasma infection, including leaf yellowing, stunting, and the proliferation of axillary shoots characteristic of witches'-broom (Wei et al., 2022). In *Arabidopsis*, WUSCHEL promotes the maintenance of stem cells in shoot and floral meristems (Ikeda et al., 2009), while the CLV genes (CLV1, CLV2, and CLV3) function to limit stem cell proliferation (Clark et al., 1997; Somssich et al., 2016). The antagonistic interaction between WUS-mediated activation and CLV-mediated repression establishes a dynamic regulatory feedback loop that is critical for maintaining stem cell homeostasis and ensuring the precise spatial and temporal control of stem cell proliferation (Brand et al., 2000; Yadav et al., 2013). Previous studies have shown that carotenoid-derived signaling molecules regulate shoot branching, with strigolactones identified as key regulators (Yoshimura et al., 2018). In this context, the downregulation of the strigolactones receptor DWARF14-like (D14-like, LOC101259838) contributes to excessive shoot proliferation, hormonal imbalances, and impaired defense responses, thereby facilitating pathogen dissemination. D14-like proteins also interact with auxin, gibberellin, and ethylene pathways, suggesting broader reprogramming of plant development (Jiang et al., 2013). Additionally, the upregulation of the transcription factor *HHO5*-like (LOC101255362), a stress-induced repressor in the GARP-type HHO family, likely suppresses growth-related genes and alters nutrient and hormone

signaling, redirecting resources toward defense or potentially being exploited by the pathogen to reduce growth and alter plant architecture (Li et al., 2021)

Several GO terms belonging to cellular component (CC) were also enriched (Figure 12c and Supplemental files: Table S10). Terms related to membrane structures, particularly those involved in the plasma membrane (GO:0005886), cell periphery (GO:0071944), and plasmodesmata/cell junctions (GO:005911 and GO:0009506), were highly enriched. Notably, the downregulation of CLV1, a key receptor kinase controlling meristem homeostasis (Stone et al., 1998), likely promotes uncontrolled shoot proliferation, characteristic of witches' broom symptoms. Concurrently, the G-type lectin S-receptor-like kinase and ethylene receptor homolog were upregulated, indicating activation of hormone-mediated defense signaling. Defense-related proteins, such as ribonuclease T2 (Singh et al., 2020), acidic endochitinase, polygalacturonase-like proteins, and osmotin-like proteins, were consistently enriched across extracellular region (GO:0005576) and cell wall (GO:0005618) terms, highlighting a substantial remodeling of the extracellular environment in response to infection. The upregulation of expansin further supports structural modifications (Samalova et al., 2022), facilitating pathogen movement (Samalova et al., 2022; Sampedro & Cosgrove, 2005). Carbohydrate-active enzymes, including beta-1,3-glucanase and glucan endo-1,3-beta-glucosidase 6, were associated with multiple GO categories and may contribute both to cell wall degradation and defense (Perrot et al., 2022). Furthermore, retrograde signaling components related to the endoplasmic reticulum membrane (GO:0005789) and nuclear membrane network were also modulated, suggesting that intracellular communication and stress responses are impacted. During *'Ca.* P. solani' infection, several genes associated with the endoplasmic reticulum (ER) membrane, including 7-dehydrocholesterol reductase, DAD-1 protein and E3 ubiquitin-protein ligase RMA1H1-like, are differentially expressed, reflecting a coordinated host response to pathogen-induced stress (Table 3). 7-dehydrocholesterol reductase may contribute to sterol-

mediated membrane remodeling, which is essential for cellular signaling and could play a role in plant responses to biotic stress (Schaller, 2003). Although no direct evidence currently links DAD1 to phytoplasma-plant interactions, its established role in maintaining ER homeostasis and cell viability under biotic stress suggests a potential involvement in the host response to infection. Given that phytoplasma infection induces widespread transcriptional reprogramming, hormonal imbalance, and likely ER stress, upregulation of DAD1 may reflect an adaptive response to preserve ER function and prevent premature cell death during pathogen colonization (Howell, 2013; J. Liu & Howell, 2016). Upregulation of E3 ubiquitin ligases indicates activation of ER-associated degradation pathways, facilitating clearance of misfolded proteins (Liu & Li, 2014). Collectively, these changes suggest that phytoplasma infection elicits ER stress responses and membrane-associated defense mechanisms to maintain cellular homeostasis.

Several transporters, including ABC transporter family proteins and proline/GABA transporters, were upregulated, potentially adjusting cellular homeostasis under infection stress. The transcriptional landscape reveals a coordinated activation of immune responses, extensive remodeling of cell walls and membrane structures, and disruption of meristematic regulation, collectively contributing to pathogen accommodation and symptom development during phytoplasma infection (Wei et al., 2013).

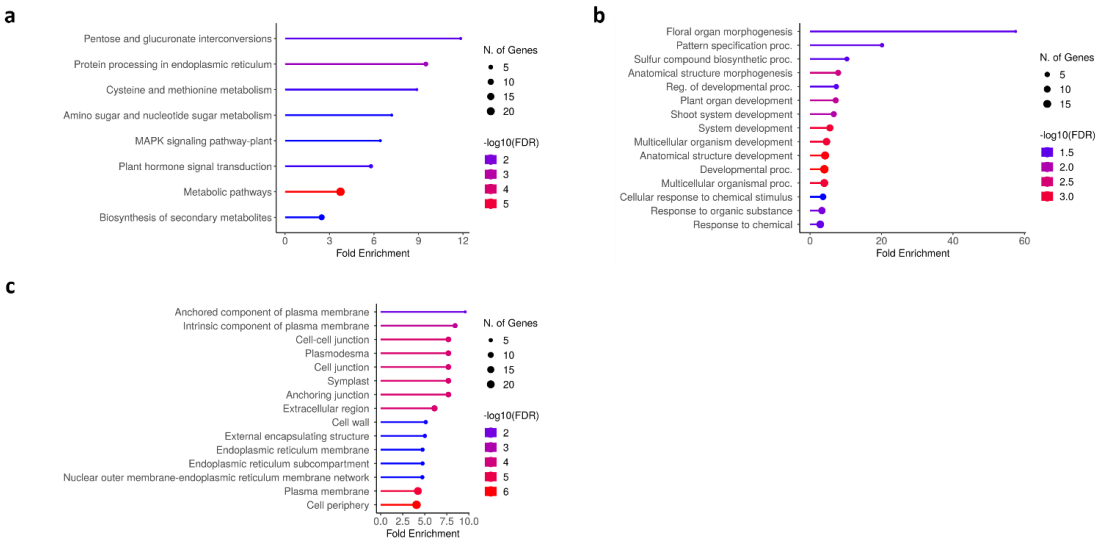

Figure 12. KEGG-enriched pathways and GO terms clustered in the blue ME. (a) KEGG pathways, (b) biological process, and (c) cellular component. Columns and rows represent fold enrichment; round size represents the number of genes; color bar from blue to red represents increasing significance in -log10 (FDR).

All genes from the phytoplasma strain GCA_000970375 were grouped within the blue module (Supplemental files: Table S11). Currently, limited information is available about phytoplasma genes and their roles in the infection process. In our study, we identified several genes, including AAA+ ATPase (S284_02860), MutT/nudix family protein (S284_00330), pyruvate dehydrogenase (S284_00520), Zn-dependent hydrolase (S284_05000), ABC transporter ATPase component (S284_00320), and others, which may disrupt various plant physiological processes (Table 3). These genes may interfere with plant protein homeostasis, nucleotide integrity, metabolism and ion balance, weakening plant defenses, stress responses and immune functions, ultimately supporting phytoplasma survival and immune evasion (Miura et al., 2012). AAA+ ATPases are thought to assist in protein unfolding and degradation, potentially modulating host proteostasis and interfering with protein-based defense mechanisms (Kube et al., 2012). Members of the MutT/Nudix hydrolase family, known for their role in hydrolyzing potentially toxic nucleotide derivatives, may alter nucleotide metabolism,

thereby disrupt DNA/RNA synthesis and interfere with plant immune signaling pathways (Breuer et al., 2023). The presence of a pyruvate dehydrogenase (PDH) gene in several phytoplasma genomes suggests the capacity to reprogram host carbon metabolism, potentially redirecting carbon fluxes to support bacterial survival and colonization (MacLean et al., 2011; Oshima et al., 2004). Zn-dependent hydrolases, upregulated during infection, likely degrade host macromolecules such as proteins and nucleic acids, facilitating nutrient release and within the phloem. These hydrolases may also suppress plant immunity by targeting defense-related proteins or detoxifying ROS and antimicrobial secondary metabolites, thus enabling pathogen persistence under stress conditions (Kube et al., 2012).

Additional genes implicated in host interaction include the ABC transporter ATPase, which may regulate nutrient and toxin transport across the pathogen membrane (Lane et al., 2016), and the cation-transporting P-type ATPase, which likely influences host ion homeostasis and stress responses (Maejima et al., 2014). Genomic plasticity in phytoplasmas is potentially enhanced by mobile genetic elements such as phage integrases, which contribute to gene acquisition and adaptation under host-imposed selective pressures (Bai et al., 2006; Music et al., 2019). Furthermore, cold shock proteins may assist phytoplasmas in tolerating temperature fluctuations or other abiotic stresses within the host, while Fe-S cluster assembly proteins likely support essential metabolic functions and redox balance critical for pathogen survival (Kube et al., 2012; Oshima et al., 2004).

Gene co-expression network analysis revealed significant correlated expression patterns between *Solanum* genes primarily within the brown and blue modules and phytoplasma genes clustered in the blue module. These coordinated expression profiles are associated with regulation of chloroplast function, chlorophyll biosynthesis, phytohormone signaling pathways, and anatomical traits, suggesting that phytoplasma infection may induce photomorphogenic responses in the host plant.

Table 3. Genes involved in hormonal signal transduction, growth and development, metabolism and ion balance for the comparison infected vs. healthy plants.

Gene Symbol/ Locus ID	Transcript	Gene description	Module	Log2Fold Change	Average expression	FDR*
MAPK8	XM_010317553.3	mitogen-activated protein kinase 8, transcript variant X1	blue	0.88	1087	0.00
ERF C.3	XM_004247302.4	ethylene response factor C.3	blue	2.20	35	0.00
ETR4	NM_001247276.2	ethylene receptor homolog	blue	0.89	658	0.03
GID1b-1	NM_001247838.2	putative GID1-like gibberellin receptor	blue	0.83	768	0.01
IAA10	NM_001279126.1	IAA10_protein	blue	-1.49	319	0.00
CLV1	XM_004238322.4	receptor protein kinase CLAVATA1	blue	-1.06	2439	0.00
SCL15	XM_004232335.4	scarecrow-like_protein_15	blue	0.82	974	0.03
WOX3-like	XM_004251403.4	WUSCHEL-related homeobox 3-like	blue	2.98	20	0.03
ACO2	NM_001329913.1	1 aminocyclopropane 1 carboxylate oxidase	blue	1.94	194	0.02
D14-like	XM_004238045.4	alpha/beta-hydrolase DWARF14-like	blue	-1.06	1557	0.00
HH05	XM_004233591.3	transcription factor HHO5-like	blue	1.65	73	0.01
LOC101248602	XM_004228414.4	7-dehydrocholesterol reductase	blue	0.61	3896	0.05
DAD1	NM_001246888.1	dad-1 protein	blue	0.51	645	0.00
101253976	XM_004251741.4	E3 ubiquitin-protein ligase RMA1H1-like	blue	2.41	24	0.00
PETE	NM_001309263.1	plastocyanin, chloroplastic	blue	-0.82	5674	0.03
S284_02860	NC_022588.1	predicted AAA+ ATPase	blue	12.33	711	0.00
S284_00330	NC_022588.1	MutT/nudix family protein	blue	13.25	690	0.00
S284_00520	NC_022588.1	Pyruvate dehydrogenase E1 component (AcoA/PdhA, alpha subunit), putative fragment	blue	12.61	443	0.00
S284_05000	NC_022588.1	Zn-dependent hydrolase	blue	12.48	404	0.00
S284_00320	NC_022588.1	ABC transporter, ATPase component	blue	12.07	305	0.00

*False Discovery Rate

2.3.9 Phytoplasma infection altered biomass production and allocation

The coordinated transcriptomic and phenotypic reprogramming triggered by 'Ca. P. solani' infection resulted in a pronounced increase in shoot dry mass (SDM) in symptomatic plants (Figure 13a), a response consistent with previous reports of pathogen-induced source/sink imbalances (Dermastia, 2019). However, no significant alteration was observed in root dry mass (RDM), as shown in Figure 13b. The infection led to impaired carbon fixation and reduced assimilate translocation from source to sink tissues, as evidenced by a marked reduction in fruit dry mass (FDM) (Figure 13c and Figure 14), a phenomenon previously reported in phytoplasma-infected tomato and apple plants (De Marco et al., 2021; Musetti et al., 2013). Although shoot biomass was increased, the net effect of root, shoot, and fruit dry mass combined indicated that total dry mass (TDM) remained higher in healthy plants (Figure 13d), reinforcing the notion that phytoplasma infection compromises carbon partitioning efficiency (Pagliari et al., 2017). The shoot/root dry mass ratio remained unaffected (Figure 13e), suggesting that root allocation is not preferentially altered.

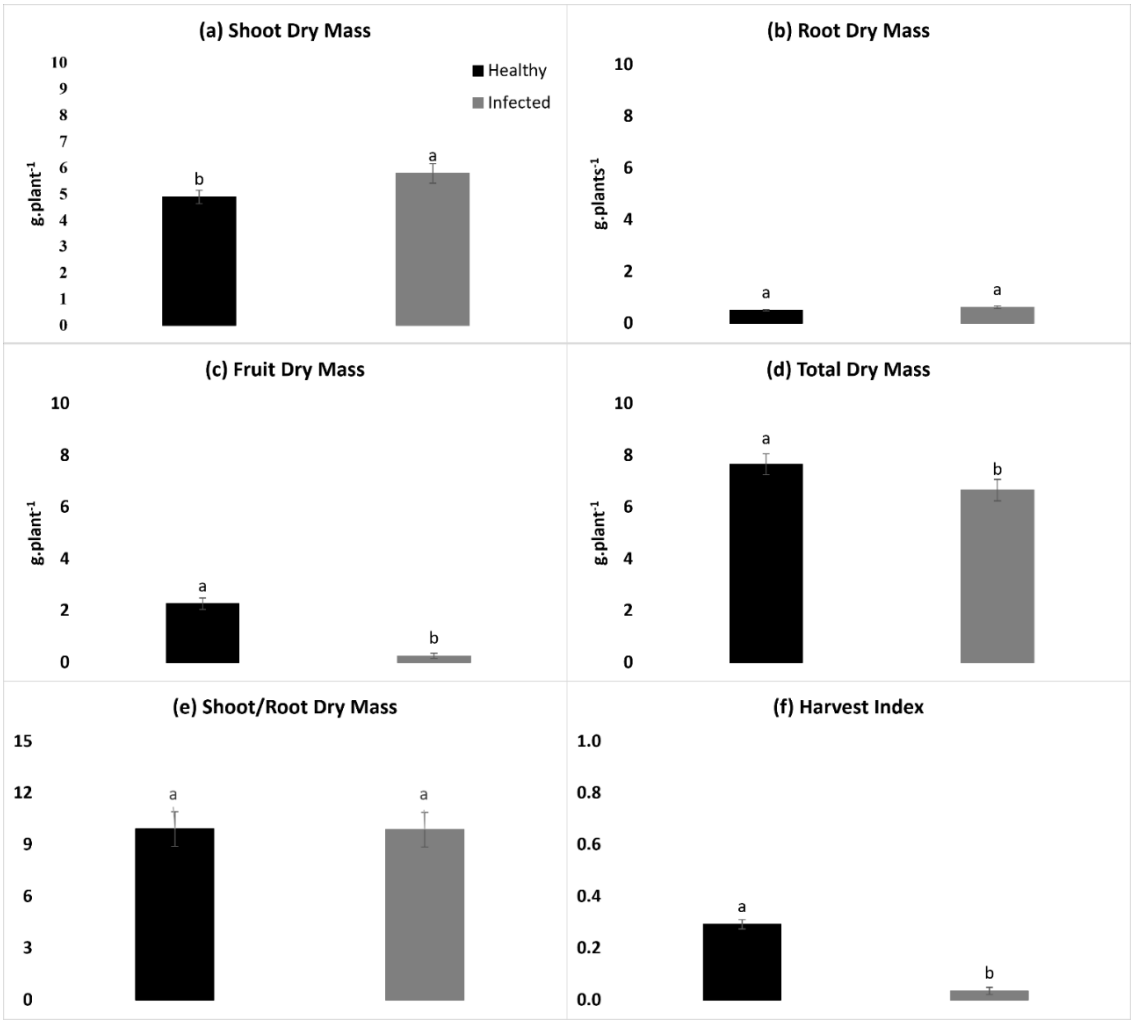

Figure 13. Shoot, root, fruits and total dry mass, shoot/root ratio and harvest index of tomato plants cv. Micro-Tom grown in two different conditions, healthy and phytoplasma infected. Results are expressed as mean ± SE (n = 8). The different letters in the bars indicate statistically significant differences ($P < 0.05$) among conditions (one-way ANOVA followed by Tukey's test).

The harvest index (HI), a key physiological indicator reflecting the efficiency of assimilate allocation to yield structures, was dramatically reduced, showing an 8-fold decrease in infected plants (Figure 13f and Figure 14), highlighting the strong negative impact of '*Ca*. P. solani' on productivity and carbon use efficiency.

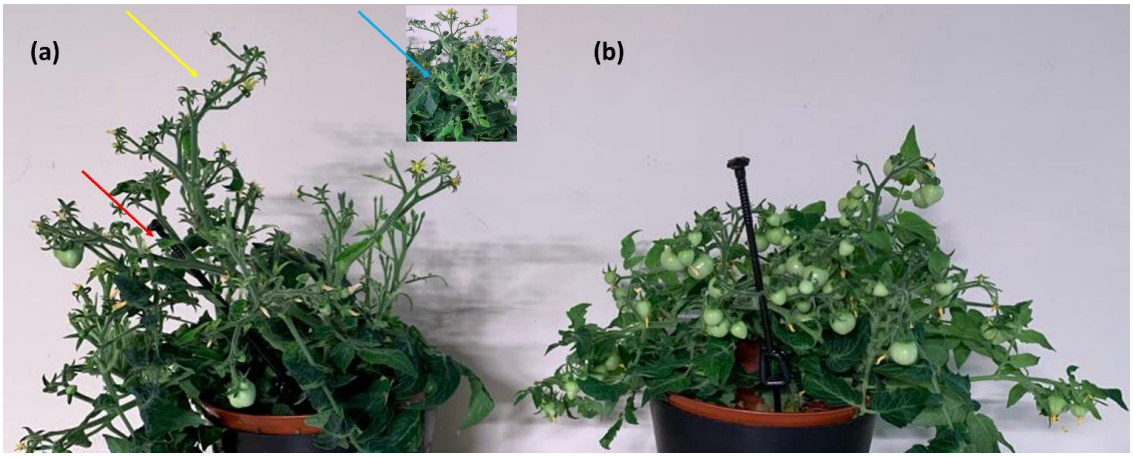

Figure 14. Micro-Tom plants in response to phytoplasma infection 5 weeks after grafting. (a) infected plants with classic phytoplasma symptoms. Red arrow: leaf growth and development impairment, followed by discoloration. Yellow arrow: a branch showing phyllody (abnormal development of the flowers), followed by the witches' broom growth (proliferation of auxiliary shoots), abnormal elongation of internodes, flower malformation and sterility. Blue arrow in the insert: a closeup of leaves and branches. (b) healthy plants, showing normal growth and development of leaves, branches, and fruits.

2.3.9 Hub genes identified in co-expression networks provide insight into the regulatory mechanisms underlying the plant response to phytoplasma.

Identifying hub genes in gene regulatory or co-expression networks offers significant insights into the molecular mechanisms underlying complex biological processes, including development, stress responses, and pathogen defense. Hub genes typically characterized by a high degree of connectivity are thought to function as key regulators or bottlenecks within biological networks, often controlling the expression or activity of multiple downstream targets (Barabási & Oltvai, 2004; Jeong et al., 2001). Their central position makes them ideal candidates for understanding system-wide changes in response to environmental or developmental cues.

In the context of plant-pathogen interactions, hub genes frequently represent crucial components of defense signaling pathways, such as those involving salicylic acid, jasmonic acid, or reactive oxygen species (Mine et al., 2018; Pieterse et al., 2012; Tsuda & Katagiri, 2010). For example, network analyses in *Arabidopsis* and other species have revealed that key transcription factors and signaling kinases often occupy hub positions, orchestrating the expression of broad defensive gene sets (De Vleesschauwer et al., 2014). By targeting such genes for functional validation, researchers can identify potential master regulators that may serve as biomarkers or targets for crop improvement.

Moreover, hub gene identification supports the discovery of novel regulatory components that might not be evident from differential expression analysis alone. These genes may not show strong expression changes individually but play essential coordinating roles in broader modules of co-expressed genes (Langfelder & Horvath, 2008). As such, incorporating hub gene analysis into systems biology approaches improves the resolution and interpretability of transcriptomic data, particularly when integrated with phenotypic or physiological traits (Serin et al., 2016).

After identifying co-expressed gene modules, the brown and blue modules displayed distinct, coordinated expression patterns. Hub genes were defined based on intramodular connectivity, with top-ranked genes in the brown module selected as candidate key regulators of module-specific functions (Supplemental files: Tables S11 and S12).

GGP (GDP-L-galactose phosphorylase, 101055572) emerged as the most highly connected gene within the brown module (Table 4). This gene, which resulted significantly downregulated in the infected plants, encodes a cytosolic key enzyme in the L-galactose pathway of ascorbate biosynthesis, a principal route for vitamin C production essential for redox homeostasis and antioxidant defense (Fenech et al., 2021). Its role as a hub gene suggests a critical regulatory function in the pathway and

in orchestrating cellular responses to oxidative stress. In the tomato knockout *Slggp1* mutant the ascorbate content is significantly decreased (Baldet *et al.*, 2013). Wang et al. (2013) demonstrated that antisense-mediated knockdown of *SlGGP* compromises the ascorbate-dependent ROS scavenging system, underscoring its essential role in maintaining redox homeostasis and conferring tolerance to chilling stress. Their findings highlight *SlGGP* as a key regulator of the ascorbate pool and redox state, crucial for protecting tomato plants under low-temperature conditions. (Baldet et al., 2024; Y. Wang et al., 2013),. Another highly connected gene, glutathione reductase (*GR*, 100301931), is a core component of the glutathione-ascorbate cycle. It catalyzes the regeneration of reduced glutathione (GSH), a major cellular antioxidant (Foyer & Noctor, 2011; Hasanuzzaman et al., 2020). Taken together, these outcomes seem to highlight a photosynthesis-related network modified by deep changes in redox regulation.

Several genes involved in photosynthesis and chloroplast function were downregulated. Notably, components of the cytochrome b6f complex, which mediates electron transport and establishes the proton gradient across the thylakoid membrane for ATP synthesis, were repressed. Likewise, PROTON GRADIENT REGULATION 5 (*PRG5*, LOC101262255), a gene vital for cyclic electron flow and protection of photosystem I from oxidative damage, was downregulated in response to infection (Munekage et al., 2002; Suorsa et al., 2012; Takagi & Miyake, 2018). In *Arabidopsis pgr5* mutants lacking the PGR5/PGRL1-dependent pathway, cyclic electron transport is impaired, leading to a diminished proton motive force (pmf) and reduced photosynthetic efficiency (Wang & Shikanai, 2019).

Additional repressed genes include those encoding ribulose bisphosphate carboxylase/oxygenase activase (LOC101249777), essential for carbon fixation (Salvucci & Crafts-Brandner, 2004), and psbP-domain-containing proteins (LOC101259835), which contribute to the stabilization of photosystem II (Ifuku, 2015). Genes involved in pigment metabolism, such as LCY1 (lycopene cyclase; LOC544104) and pheophytinase

(LOC101268836), as well as key regulators of circadian rhythms and light signaling-including REVEILLE 7 and 8 (LOC101255972, LOC101253545), CONSTANS-LIKE transcription factors (LOC101254370, LOC101265452), and phytochrome A-associated F-box protein (LOC101247753) were also downregulated. This pattern points to extensive transcriptional reprogramming affecting not only the photosynthetic apparatus but also light perception and circadian regulation (Hsu et al., 2013).

Furthermore, genes encoding transporters such as PLASMA MEMBRANE INTRINSIC PROTEIN 1-5 (*PIP1-5*, LOC544086), boron transporter (*BOR1*, LOC101260863), and the K^+ efflux antiporter (*KEA3*, LOC101265888) were downregulated, reflecting disruptions in ion and nutrient homeostasis (Takano et al., 2008; Uflewski et al., 2024). This coordinated transcriptional shift aligns with a wide retrograde signaling response, whereby chloroplast dysfunction is likely resulting from impaired electron transport and increased ROS production triggers stress signaling to the nucleus for reprogramming nuclear gene expression.

Table 4. Gene symbol/Locus ID, connectivity (degree), transcript ID, gene description, Log_2 fold change, average expression for top 15 hub genes in the brown module for the comparison infected vs. healthy.

Gene Symbol / Locus ID	Degree	Transcript	Gene description	Log2 Fold Change	Expression Average	FDR*
GGP	923	NM_001279216.1	GDP-L-galactose_phosphorylase	-2.84	15063	0.00
LOC101262255	876	XM_004247716.4	protein_PROTON_GRADIENT_REGULATION_5,_chloroplastic	-4.24	1366	0.00
LOC101249777	869	XM_010314058.3	ribulose_bisphosphate_carboxylase/oxygenase_activase,_chloroplastic	-3.17	59577	0.00
LOC101259835	860	XM_004237678.4	psbP_domain-containing_protein_4,_chloroplastic	-2.88	691	0.00
LOC101247753	840	XM_004247374.3	phytochrome_A-associated_F-box_protein	-1.09	584	0.01
LOC101265888	819	XM_004250774.4	K(+)_efflux_antiporter_3,_chloroplastic	-2.37	773	0.00
LOC101255972	811	XM_004235342.3	protein_REVEILLE_7	-6.18	1233	0.00
LCY1	800	NM_001247297.2	lycopene_beta-cyclase,_transcript_variant_1	-1.92	1168	0.01
PIP1-5	798	NM_001247210.2	plasma_membrane_intrinsic_protein_1.5	-1.98	14968	0.00
LOC101254370	798	XM_004235757.3	zinc_finger_protein_CONSTANS-LIKE_16	-1.65	3759	0.00

LOC101253545	798	XM_004249460.4	protein_REVEILLE_8	-7.89	1172	0.00
LOC101265452	798	XM_004243376.4	zinc_finger_protein_CONSTANS-LIKE_4	-5.05	424	0.02
GR	789	NM_001247314.2	glutathione_reductase,_chloroplastic	-1.25	1570	0.01
LOC101260863	788	XM_004229320.4	boron_transporter_1,_transcript_variant_X1	-6.17	1349	0.00
LOC101268836	779	XM_004233480.3	pheophytinase,_chloroplastic	-2.67	264	0.00

*False Discovery Rate

The identification of *GGP1* and *GR* as highly connected hub genes supports this model. Their prominence suggests that a compensatory mechanism aimed at mitigating oxidative stress and maintaining cellular homeostasis is altered. Simultaneously, the suppression of photosynthesis-related genes may reflect downregulation of anterograde signaling, as the plant reallocates resources from chloroplast function toward defense responses (Pogson et al., 2008). Together, these findings highlight the complex interplay between retrograde and anterograde signaling pathways during pathogen-induced reprogramming of chloroplast-associated processes.

2.3.10 Host and pathogen hub gene expression reveals dual transcriptional strategies during 'Ca. P. solani' Infection

The blue module revealed a striking contrast to the transcriptional patterns observed in the brown module, underscoring the complexity of host-pathogen interactions during *'Ca.* P. solani' infection. The brown module hub genes were predominantly downregulated *Solanum*-encoded genes involved in photosynthesis, pigment biosynthesis, ion transport, and redox balance, many of which are regulated through retrograde and anterograde signaling (Chan et al., 2016; Crawford et al., 2018; Pogson et al., 2008); the hub genes of the blue module were enriched with *'Ca.* P. solani' transcripts (Table 5 and Supplemental files; Table S13).

The top five hub genes in the blue module, all derived from the phytoplasma genome, suggest that these microbial genes are tightly co-expressed and highly active during infection, potentially reflecting core virulence or survival functions within the

host plant. Their high connectivity in the network implies that they are central players in the phytoplasma's transcriptional program during host colonization. The strong upregulation of ABC transporters, AAA+ ATPase, Zn-dependent hydrolases, and exopolyphosphatase-related proteins indicate active transport, detoxification, and energy-dependent processes that may support nutrient acquisition, stress tolerance, and manipulation of host physiology. These genes likely contribute to the phytoplasma's ability to survive, proliferate, and modulate the host environment to its advantage during systemic infection. Remarkably, all hub genes were of phytoplasma origin and consistently upregulated, indicating a pathogen-driven reprogramming of the host transcriptome (MacLean et al., 2014; Sugio et al., 2011).

Table 5. Gene symbol/Locus ID, connectivity (degree), transcript ID, gene description, Log_2 fold change, average expression for top 5 hub genes in the blue module for the comparison infected vs. healthy.

Locus ID	Degree	Transcript	Gene description	Log2 Fold-Change	Average Expression	FDR*
S284_05000	1095	NC_022588.1	Zn-dependent hydrolase	12.48	404	0.00
S284_01140	1098	NC_022588.1	Amino acid ABC superfamily, permease	9.14	40	0.00
S284_02160	1098	NC_022588.1	AAA+ ATPase	8.84	32	0.00
S284_02050	1102	NC_022588.1	Exopolyphosphatase-related protein	10.90	135	0.00
S284_05170	1106	NC_022588.1	ABC transporter subunit, partial CDS	10.36	93	0.00

*False Discovery Rate

These hub genes included a Zn-dependent hydrolase (S284_05000), an amino acid ABC superfamily permease (S284_01140), an AAA+ ATPase (S284_02160), an exopolyphosphatase-related protein (S284_02050), and ABC transporter subunit (S284_05170). These proteins likely play essential roles in phytoplasma viability and pathogenicity by contributing to nutrient acquisition, stress adaptation, and RNA metabolism within the host cellular environment (Kube et al., 2012; Music et al., 2019; Oshima et al., 2004).

The *Solanum* plastocyanin gene *PETE* (*LOC544053*), expressed in the blue module, was significantly downregulated in response to infection (Table 3). Plastocyanin is a small, copper-containing protein that functions as a mobile electron carrier in the thylakoid lumen, transferring electrons from the cytochrome b6f complex to Photosystem I (PSI) during the light-dependent reactions of photosynthesis (Pesaresi et al., 2009; Weigel et al., 2003; Wu et al., 2025). This step is essential for sustaining the photosynthetic ETC, which enables the reduction of $NADP^+$ to NADPH and supports ATP synthesis through the maintenance of a proton gradient across the thylakoid membrane. In the LET pathway, electrons from ferredoxin are used by ferredoxin-$NADP^+$ reductase (FNR) to produce NADPH, which is then used to reduce 1,3-bisphosphoglycerate in the Calvin-Benson-Bassham (CBB) cycle (Buchert et al., 2020). Alternatively, electrons from ferredoxin or NADPH can re-enter the ETC via CET, enhancing the proton gradient without NADPH production (Munekage et al., 2004; Yamori et al., 2015). The observed downregulation of *PETE*, along with key components of the cytochrome b6f complex and *PROTON GRADIENT REGULATION 5* (*PGR5*, *LOC101262255*), suggests a disruption of both LET and CET pathways. Given that PGR5 (hub gene) plays a critical role in balancing electron flow and maintaining PSI redox homeostasis, its repression likely contributes to a weakened proton motive force (pmf), resulting in impaired photosynthetic efficiency and reduced carbon fixation (Munekage et al., 2002; Suorsa et al., 2012; Takagi & Miyake, 2018). This coordinated repression of photosynthesis-related genes points to a broader physiological reprogramming, possibly initiated by the downregulation of *PETE* in the blue module. Given its central role in electron transport, *PETE* may act upstream, influencing the expression of genes in the brown module and modulating the activity of phytoplasma genes. The tight co-expression patterns between *PETE*, chloroplast-related genes, and pathogen-responsive elements suggest a pathogen-driven interference in chloroplast function and retrograde signaling. This is further supported by the widespread repression of chloroplast-

associated genes in the brown module, consistent with previous findings that phytoplasma effectors target host transcription factors and organellar processes to hijack host metabolism and suppress defense responses (Sugio et al., 2011; Tan et al., 2016). Together, these findings highlight plastid redox status as a potential regulatory hub linking host-pathogen interactions, energy metabolism, and gene expression reprogramming.

2.4 Conclusions

Our results demonstrate that *'Ca.* P. solani' infection triggers a profound reprogramming of plant physiology, primarily by disrupting chloroplast biogenesis and function. This leads to marked morphological alterations in above ground tissues and a substantial decline in photosynthetic capacity. These systemic alterations underscore the chloroplast's emerging role as both a metabolic hub and a central player in stress signaling.

Through WGCNA, we uncovered two transcriptional modules with distinct physiological relevance. The brown module, enriched in host genes, is defined by hub genes such as GGP and glutathione reductase, which play critical roles in ascorbate-glutathione-mediated redox buffering. Their high intramodular connectivity suggests regulatory importance in coordinating oxidative stress responses and retrograde signaling from damaged chloroplasts. The concurrent downregulation of key photosynthetic and transporter genes reflects a stress-induced shift from energy production to cellular protection, a hallmark of defense reprogramming.

In contrast, the blue module displays a marked enrichment of phytoplasma genes. Notably, host genes within this module including those encoding transporters and RNA-processing proteins are significantly upregulated. Such transcriptional signatures are consistent with pathogen-mediated reprogramming of host cellular functions; whereby microbial effectors hijack nutrient transport and RNA metabolism to facilitate

colonization and suppress host defenses. The coordinated expression of these genes supports a model in which the pathogen actively modulates host gene expression to promote its own survival while disrupting chloroplast-associated defense pathways critical hubs of immune signaling in plants. The blue module reflects the host's integrated response to phytoplasma infection, marked by the activation of hormone signaling pathways and suppression of photosynthetic processes. Upregulated hormone-related genes suggest enhanced defense signaling, while downregulation of chloroplast genes points to disrupted electron transport and redox balance highlighting the module's role in coordinating defense, energy metabolism, and host-pathogen interactions.

Altogether, these findings highlight the centrality of chloroplasts not only in photosynthesis but also in immunity and stress integration. By dissecting host and pathogen contributions at the systems level, we provide a framework for understanding how intracellular communication pathways, especially those involving redox balance and retrograde signaling, are modulated during phytoplasma infection. Future research should explore how restoring key hub gene functions might enhance resistance or mitigate the physiological decline observed in infected plants.

2.5 Supplemental files

Table S1. Representative cycle threshold (Ct) values obtained by qPCR for healthy and phytoplasma-infected samples. Each condition was assessed using three biological replicates and two technical replicates per sample.

Condition	Ct
Healthy*	0.00
Infected	23.07

*Each condition was assessed using three biological replicates and two technical replicates per sample.

Table S2. Gene and primer sequences for expression analysis and RNA-seq validation.

Gene NCBI ID	Gene Symbol	NCBI Reference Sequence	Forward primer 5'-3'	Reverse primer 5'-3'
LOC101253257**	ERF017	XM_004251654.4	TTTTTCCGGGGTTCGATGACT	GGTGATGGTTGTGGTGACGA
LOC101260941**	PECTINESTERASE	XM_010323554.2	CCTCTACGTCCACTCACTTCG	GAACAACAGCTGCATTACCAAAAA
LOC101253545**	REVEILLE8	XM_004249460.4	CCCGGACTTTGAACCCATTAAAAA	ACCACCTGTAGGAAGACCGA
LOC101246763**	FRO6	XM_004230336.4	CAGCCTTCATTGGAGGAGGG	ACATCCTTTGAAGCCAGGGG
LOC101262053**	JAR1*	XM_004248027.4 XM_010328700.2	GCAAATTCTCCAGTCGGCCT	ACGATATAAACCTGCGAAATTGGT
LOC104647958**	Ferritin-1	XM_010323864.3	AACGTCCATGCTGTAGCCTC	CCATGTCCTTGGCCAACTCT
LOC101244176**	ChlH alias GUN5	XM_004236562.4	GAACCTCAGGAAGGATGGCA	ACAACGTACGTACCTGAGCA
LOC101248619**	CHLN	NM_001309378.1	TGCTCTGGAGGAGTGAGTGA	AGACACACAAATAGGACACACTGA
LOC101265194**	OPT3	XM_019211035.2	GTGGGGCTTGTTGTTTGCAT	TGTCATATCCGGGTTGCTGATT
LOC101250725	RCA1*	XM_010327541.3 XM_004246367.4	GGCTACCTCCATCTCAACCA	GCCAAAGAAGGCTGTTGGTG
LOC101249777	RCA2	XM_010314058.3	AGATGCTAACGCTGATGCCA	AGTTGACATGTCGCGCTTTT
LOC101250491	RCA3	XM_004235825.4	AAGACTCCGGAGGTGCTGA	AGGCTTCCAGTGTTTGCTCTC
LOC101268337	RBCS4*	XM_026029055.1 NM_001309210.1	GAATTCGAGACTGAGCACGGA	ATGGGCAACTTCCACATGGT
LOC101252496	GUN4	XM_004241362.4	AAGCAGCGGTTAACGAGGA	CCGTCGCTGTATTTCCTCCA
LOC101244176	ChlH alias GUN5	XM_004236562.4	GAACCTCAGGAAGGATGCCA	ACAACGTACGTACCTGACCA
LOC100316873	SBPase	NM_001247656.1	GCTTCTCTTTGAGGCCTTGAC	AAATCCTCCTTCAGCAGGGC
LOC101055587	GLK1	NM_001279264.1	TCCACATCATCAACGGGTACA	GATACGGGTGGTATGCCTGG
LOC101260830	psbS	NM_001309257.1	CTACCCCTCCTACTGGCCTT	TCCAAACAATGGACCTCCTTCA
LOC778301	SEND33	NM_001247130.1	GGGCTGGTTCTTGCTCATCT	ATCCAGCAGCTTCTTGGTCC
LOC543585	CAT2	NM_001247257.2	TGGCAAACGCGAGAAGTGTA	AAGCGTTCTTGTCTGTCGGG
LOC100134875	GLO2	NM_001347977.1	GTATCCCCGTGTTCCTGGAT	TTGGTCGCCCAATAAACACG
AF248959	16Sstol	---	AGGGTAGCTAAAGCGTAAGC	CATCAACCCTACCTTAGACG

*This primer pair amplifies every gene transcript variant. **Buoso et al., (2019)

Table S3. Experimental validation of a subset of genes embedded in different modules, regulated by phytoplasma infection. Shown are the log2 fold-change values from RNA-seq and RT-qPCR.

				Log$_2$(Fold-Change)	
Locus ID	**Gene Symbol**	**Gene description**	**Comparison**	**RNA-seq**	**qRT-PCR**
LOC101253257*	ERF017	Ethylene-responsive transcription factor ERF017	Infected vs Healthy	3.49	3.51
LOC101260941*	PECTINESTERASE	Pectinesterase	Infected vs Healthy	3.68	2.46
LOC101253545*	REVEILLE8	Protein REVEILLE 8	Infected vs Healthy	-8.47	-8.22
LOC101246763*	FRO6	Ferric reduction oxidase 6, FRO6	Infected vs Healthy	-6.04	-5.12
LOC101262053*	JAR1*	Jasmonic acid-amido synthetase JAR1	Infected vs Healthy	-0.14	-0.29
LOC104647958*	Ferritin-1	Ferritin-1, chloroplastic	Infected vs Healthy	-0.18	-1.69
LOC101244176*	ChlH alias GUN5	Magnesium chelatase H subunit ChlH, chloroplastic	Infected vs Healthy	-4.67	-5.10
LOC101248619*	CHLN	Nicotianamine synthase-like	Infected vs Healthy	-1.72	-1,12
LOC101265194*	OPT3	Oligopeptide transporter 3	Infected vs Healthy	-0.32	-0,19
LOC101250725	RCA1	ribulose bisphosphate carboxylase/oxygenase activase 1, chloroplastic	Infected vs Healthy	-8.26	-6.15
LOC101249777	RCA2	ribulose bisphosphate carboxylase/oxygenase activase, chloroplastic	Infected vs Healthy	-3.59	-4.32
LOC101250491	RCA3	ribulose bisphosphate carboxylase/oxygenase activase, chloroplastic	Infected vs Healthy	-0.513	0,470
LOC101268337	RBCS4	ribulose bisphosphate carboxylase small chain 3B, chloroplastic-like	Infected vs Healthy	-1.41	-1.62
LOC101252496	GUN4	tetrapyrrole-binding protein, chloroplastic	Infected vs Healthy	-2.46	-2.58
LOC101244176	ChlH alias GUN5	Magnesium chelatase H subunit	Infected vs Healthy	-4.10	-5.10
LOC100316873	SBPase	chloroplast sedoheptulose-1,7-bisphosphatase	Infected vs Healthy	-1.34	-1.38

*Buoso et al., (2019)

Table S4. Enrichment, number of genes, pathways genes, fold enrichment, KEGG pathway description and gene NCBI ID for the DEGs of brown module.

Enrichment FDR	nGenes	Pathway Genes	Fold Enrichment	Description	Locus ID	LOG_2 (Fold-change)
Carbon fixation in photosynthetic organisms (sly00710)						
7.20E-23	18	38	35.1	fructose_1,6-bisphosphate_aldolase_1	101246870	-2.78
				phosphoenolpyruvate_carboxylase-like	101248407	-1.42
				malate_dehydrogenase,_glyoxysomal	101249428	0.53
				glyceraldehyde-3-phosphate_dehydrogenase_B,_chloroplastic-like	101249445	-2.70
				fructose-bisphosphate_aldolase	101249787	-2.82
				triosephosphate_isomerase,_chloroplastic,_transcript_variant_X2	101250846	-2.58
				phosphoribulokinase,_chloroplastic	101255322	-1.43
				fructose-1,6-bisphosphatase_1,_chloroplastic	101260852	-1.42
				glyceraldehyde-3-phosphate_dehydrogenase_B,_chloroplastic	101264004	-1.02
				ribulose-phosphate_3-epimerase,_chloroplastic,_transcript_variant_X1	101264109	-0.94
				fructose-1,6-bisphosphatase,_chloroplastic	101264273	-1.53
				glutamate--glyoxylate_aminotransferase_2	101265236	-1.97
				glyceraldehyde-3-phosphate_dehydrogenase_A,_chloroplastic	101266713	-1.14
				pyruvate,_phosphate_dikinase,_chloroplastic	101267346	-2.47
				ribulose_bisphosphate_carboxylase_small_chain_3B,_chloroplastic-like,_transcript_variant_X1	101268337	-1.33
				cytosolic_NADP-malic_enzyme	543522	0.74
				ribulose_bisphosphate_carboxylase_small_chain_2A,_chloroplastic	543974	-0.69
				NADP-malic_enzyme	544164	-1.64
Carotenoid biosynthesis (sly00906)						
6.42E-07	6	17	26.2	xanthoxin_dehydrogenase,_transcript_variant_X1	101254297	-0.69
				lycopene_beta_cyclase,_chloroplastic	101267662	-0.97
				phytoene_synthase_2,_chloroplastic,_transcript_variant_X1	543964	-0.73
				phytoene_synthase_1,_chloroplastic,_transcript_variant_4	543988	-2.39
				lycopene_beta-cyclase,_transcript_variant_1	544104	-1.92
				beta-carotene_hydroxylase	544133	-4.05

Glyoxylate and dicarboxylate metabolism (sly00630)						
2.06E-13	13	44	21.9	glycerate_dehydrogenase	100191110	-1.58
				Hop-interacting_protein_THI032,_transcript_variant_X1	101055519	-1.81
				aconitate_hydratase,_cytoplasmic	101248455	0.58
				phosphoglycolate_phosphatase_1B,_chloroplastic	101249417	-1.18
				malate_dehydrogenase,_glyoxysomal	101249428	0.53
				serine_hydroxymethyltransferase_7-like	101250548	-0.67
				oxalate--CoA_ligase	101251259	-4.22
				serine_hydroxymethyltransferase,_mitochondrial,_transcript_variant_X1	101254439	-1.24
				glutamate--glyoxylate_aminotransferase_2	101265236	-1.97
				ribulose_bisphosphate_carboxylase_small_chain_3B,_chloroplastic-like,_transcript_variant_X1	101268337	-1.33
				catalase_2	543585	-2.70
				ribulose_bisphosphate_carboxylase_small_chain_2A,_chloroplastic	543974	-0.69
				glutamine_synthetase,_transcript_variant_1	543998	-1.33
Pentose phosphate pathway (sly00030)						
8.27E-07	7	29	17.9	fructose_1,6-bisphosphate_aldolase_1	101246870	-2.78
				fructose-bisphosphate_aldolase	101249787	-2.82
				glucose-6-phosphate_1-dehydrogenase,_chloroplastic	101253589	-0.66
				fructose-1,6-bisphosphatase_1,_chloroplastic	101260852	-1.42
				NADP-dependent_glyceraldehyde-3-phosphate_dehydrogenase,_transcript_variant_X1	101262732	-3.42
				ribulose-phosphate_3-epimerase,_chloroplastic,_transcript_variant_X1	101264109	-0.94
				fructose-1,6-bisphosphatase,_chloroplastic	101264273	-1.53
Sulfur metabolism (sly00920)						
5.08E-04	4	18	16.5	serine_acetyltransferase_1,_chloroplastic	101245503	-1.22
				bifunctional_L-3-cyanoalanine_synthase/cysteine_synthase_2,_mitochondrial	101255033	-1.02
				ATP_sulfurylase_1,_chloroplastic	101256557	-0.97
				5'-adenylylsulfate_reductase_3,_chloroplastic	101257319	-1.65
Nitrogen metabolism (sly00910)						
3.52E-03	3	14	15.9	high_affinity_nitrate_transporter_2.4-like	101247028	-2.40

				glutamine_synthetase,_transcript_variant_1	543998	-1.33
				nitrite_reductase	778325	-1.81
Carbon metabolism (sly01200)						
4.23E-25	30	149	14.9	glycerate_dehydrogenase	100191110	-1.58
				Hop-interacting_protein_THI032,_transcript_variant_X1	101055519	-1.81
				serine_acetyltransferase_1,_chloroplastic	101245503	-1.22
				fructose_1,6-bisphosphate_aldolase_1	101246870	-2.78
				phosphoenolpyruvate_carboxylase-like	101248407	-1.42
				aconitate_hydratase,_cytoplasmic	101248455	0.58
				phosphoglycolate_phosphatase_1B,_chloroplastic	101249417	-1.18
				malate_dehydrogenase,_glyoxysomal	101249428	0.53
				glyceraldehyde-3-phosphate_dehydrogenase_B,_chloroplastic-like	101249445	-2.70
				fructose-bisphosphate_aldolase	101249787	-2.82
				serine_hydroxymethyltransferase_7-like	101250548	-0.67
				triosephosphate_isomerase,_chloroplastic,_transcript_variant_X2	101250846	-2.58
				glucose-6-phosphate_1-dehydrogenase,_chloroplastic	101253589	-0.66
				serine_hydroxymethyltransferase,_mitochondrial,_transcript_variant_X1	101254439	-1.24
				bifunctional_L-3-cyanoalanine_synthase/cysteine_synthase_2,_mitochondrial	101255033	-1.02
				phosphoribulokinase,_chloroplastic	101255322	-1.43
				fructose-1,6-bisphosphatase_1,_chloroplastic	101260852	-1.42
				NADP-dependent_glyceraldehyde-3-phosphate_dehydrogenase,_transcript_variant_X1	101262732	-3.42
				glyceraldehyde-3-phosphate_dehydrogenase_B,_chloroplastic	101264004	-1.02
				ribulose-phosphate_3-epimerase,_chloroplastic,_transcript_variant_X1	101264109	-0.94
				fructose-1,6-bisphosphatase,_chloroplastic	101264273	-1.53
				glutamate--glyoxylate_aminotransferase_2	101265236	-1.97
				glyceraldehyde-3-phosphate_dehydrogenase_A,_chloroplastic	101266713	-1.14
				pyruvate_dehydrogenase_E1_component_subunit_beta-	101266731	-0.84

				1,_mitochondrial,_transcript_variant_X1		
				pyruvate,_phosphate_dikinase,_chloroplastic	101267346	-2.47
				ribulose_bisphosphate_carboxylase_small_chain_3B,_chloroplastic-like,_transcript_variant_X1	101268337	-1.33
				cytosolic_NADP-malic_enzyme	543522	0.74
				catalase_2	543585	-2.70
				ribulose_bisphosphate_carboxylase_small_chain_2A,_chloroplastic	543974	-0.69
				NADP-malic_enzyme	544164	-1.64
Cyanoamino acid metabolism (sly00460)						
5.67E-03	3	17	13.1	serine_hydroxymethyltransferase_7-like	101250548	-0.67
				serine_hydroxymethyltransferase,_mitochondrial,_transcript_variant_X1	101254439	-1.24
				bifunctional_L-3-cyanoalanine_synthase/cysteine_synthase_2,_mitochondrial	101255033	-1.02
Zeatin biosynthesis (sly00908)						
6.06E-03	3	18	12.4	zeatin_O-glucosyltransferase-like	101258941	-4.25
				UDP-glycosyltransferase_73C3-like	101261675	-8.66
				zeatin_O-xylosyltransferase	101262709	-1.36
Alanine aspartate and glutamate metabolism (sly00250)						
3.20E-03	4	30	9.9	Hop-interacting_protein_THI032,_transcript_variant_X1	101055519	-1.81
				amidophosphoribosyltransferase,_chloroplastic	101250934	-1.52
				glutamate--glyoxylate_aminotransferase_2	101265236	-1.97
				glutamine_synthetase,_transcript_variant_1	543998	-1.33
Fructose and mannose metabolism (sly00051)						
1.73E-03	5	45	8.2	fructose_1,6-bisphosphate_aldolase_1	101246870	-2.78
				fructose-bisphosphate_aldolase	101249787	-2.82
				triosephosphate_isomerase,_chloroplastic,_transcript_variant_X2	101250846	-2.58
				fructose-1,6-bisphosphatase_1,_chloroplastic	101260852	-1.42
				fructose-1,6-bisphosphatase,_chloroplastic	101264273	-1.53
Porphyrin metabolism (sly00860)						
5.67E-03	4	36	8.2	chlorophyllide_a_oxygenase,_chloroplastic-like	101244441	-3.22
				protein_STAY-GREEN_LIKE,_chloroplastic	101252980	-1.75
				putative_magnesium-protoporphyrin_monomethyl_ester_cyclase	101257518	-2.29
				chlorophyllase-2,_chloroplastic	101258376	1.56

Citrate cycle (TCA cycle) (sly00020)						
6.06E-03	4	38	7.8	aconitate_hydratase,_cytoplasmic	101248455	0.58
				malate_dehydrogenase,_glyoxysomal	101249428	0.53
				ATP-citrate_synthase_alpha_chain_protein_2,_transcript_variant_X2	101258745	1.35
				pyruvate_dehydrogenase_E1_component_subunit_beta-1,_mitochondrial,_transcript_variant_X1	101266731	-0.84
Biosynthesis of amino acids (sly01230)						
1.71E-07	13	124	7.8	serine_acetyltransferase_1,_chloroplastic	101245503	-1.22
				fructose_1,6-bisphosphate_aldolase_1	101246870	-2.78
				aconitate_hydratase,_cytoplasmic	101248455	0.58
				fructose-bisphosphate_aldolase	101249787	-2.82
				serine_hydroxymethyltransferase_7-like	101250548	-0.67
				triosephosphate_isomerase,_chloroplastic,_transcript_variant_X2	101250846	-2.58
				serine_hydroxymethyltransferase,_mitochondrial,_transcript_variant_X1	101254439	-1.24
				bifunctional_L-3-cyanoalanine_synthase/cysteine_synthase_2,_mitochondrial	101255033	-1.02
				ribulose-phosphate_3-epimerase,_chloroplastic,_transcript_variant_X1	101264109	-0.94
				anthranilate_synthase_alpha_subunit_2,_chloroplastic	101265030	1.01
				glutamate--glyoxylate_aminotransferase_2	101265236	-1.97
				3-phosphoshikimate_1-carboxyvinyltransferase_2	101265440	-1.51
				glutamine_synthetase,_transcript_variant_1	543998	-1.33
Biosynthesis of amino acids (sly01230)						
1.71E-07	13	124	7.8	serine_acetyltransferase_1,_chloroplastic	101245503	-1.22
				fructose_1,6-bisphosphate_aldolase_1	101246870	-2.78
				aconitate_hydratase,_cytoplasmic	101248455	0.58
				fructose-bisphosphate_aldolase	101249787	-2.82
				serine_hydroxymethyltransferase_7-like	101250548	-0.67
				triosephosphate_isomerase,_chloroplastic,_transcript_variant_X2	101250846	-2.58
				serine_hydroxymethyltransferase,_mitochondrial,_transcript_variant_X1	101254439	-1.24
				bifunctional_L-3-cyanoalanine_synthase/cysteine_synthase_2,_mitochondrial	101255033	-1.02

				ribulose-phosphate_3-epimerase,_chloroplastic,_transcript_variant_X1	101264109	-0.94
				anthranilate_synthase_alpha_subunit_2,_chloroplastic	101265030	1.01
				glutamate--glyoxylate_aminotransferase_2	101265236	-1.97
				3-phosphoshikimate_1-carboxyvinyltransferase_2	101265440	-1.51
				glutamine_synthetase,_transcript_variant_1	543998	-1.33
Pyruvate metabolism (sly00620)						
7.09E-04	6	58	7.7	phosphoenolpyruvate_carboxylase-like	101248407	-1.42
				malate_dehydrogenase,_glyoxysomal	101249428	0.53
				pyruvate_dehydrogenase_E1_component_subunit_beta-1,_mitochondrial,_transcript_variant_X1	101266731	-0.84
				pyruvate,_phosphate_dikinase,_chloroplastic	101267346	-2.47
				cytosolic_NADP-malic_enzyme	543522	0.74
				NADP-malic_enzyme	544164	-1.64
Cysteine and methionine metabolism (sly00270)						
2.38E-04	7	68	7.6	serine_acetyltransferase_1,_chloroplastic	101245503	-1.22
				nicotianamine_synthase-like	101248619	-1.38
				malate_dehydrogenase,_glyoxysomal	101249428	0.53
				bifunctional_L-3-cyanoalanine_synthase/cysteine_synthase_2,_mitochondrial	101255033	-1.02
				1,2-dihydroxy-3-keto-5-methylthiopentene_dioxygenase_1,_transcript_variant_1	101255136	-2.44
				S-adenosylmethionine_decarboxylase_2,_transcript_variant_X1	101260400	-2.43
				glyoxisomal_malate_dehydrogenase	778286	-1.12
Glycolysis/Gluconeogenesis (sly00010)						
1.08E-04	8	82	7.2	fructose_1,6-bisphosphate_aldolase_1	101246870	-2.78
				fructose-bisphosphate_aldolase	101249787	-2.82
				triosephosphate_isomerase,_chloroplastic,_transcript_variant_X2	101250846	-2.58
				fructose-1,6-bisphosphatase_1,_chloroplastic	101260852	-1.42
				NADP-dependent_glyceraldehyde-3-phosphate_dehydrogenase,_transcript_variant_X1	101262732	-3.42
				fructose-1,6-bisphosphatase,_chloroplastic	101264273	-1.53
				pyruvate_dehydrogenase_E1_component_subunit_beta-	101266731	-0.84

				1,_mitochondrial,_transcript_variant_X1		
				pyruvate,_phosphate_dikinase,_chloroplastic	101267346	-2.47
Biosynthesis of secondary metabolites (sly01110)						
2.79E-30	63	733	6.4	glycerate_dehydrogenase	100191110	-1.58
				GDP-mannose_3',5'-epimerase,_GME2	100316874	-0.95
				starch_synthase_III	100316882	-0.88
				GDP-mannose_3',5'-epimerase,_GME1	100316902	-1.80
				Hop-interacting_protein_THI032,_transcript_variant_X1	101055519	-1.81
				GDP-L-galactose_phosphorylase	101055572	-2.84
				magnesium-chelatase_subunit_ChlH,_chloroplastic	101244176	-4.10
				chlorophyllide_a_oxygenase,_chloroplastic-like	101244441	-3.22
				serine_acetyltransferase_1,_chloroplastic	101245503	-1.22
				fructose_1,6-bisphosphate_aldolase_1	101246870	-2.78
				aconitate_hydratase,_cytoplasmic	101248455	0.58
				nicotianamine_synthase-like	101248619	-1.38
				phosphoglycolate_phosphatase_1B,_chloroplastic	101249417	-1.18
				malate_dehydrogenase,_glyoxysomal	101249428	0.53
				fructose-bisphosphate_aldolase	101249787	-2.82
				serine_hydroxymethyltransferase_7-like	101250548	-0.67
				triosephosphate_isomerase,_chloroplastic,_transcript_variant_X2	101250846	-2.58
				amidophosphoribosyltransferase,_chloroplastic	101250934	-1.52
				(+)-neomenthol_dehydrogenase,_transcript_variant_X1	101251042	-2.18
				protein_STAY-GREEN_LIKE,_chloroplastic	101252980	-1.75
				solanesyl_diphosphate_synthase	101253007	-2.13
				vinorine_synthase-like	101253503	-4.16
				glucose-6-phosphate_1-dehydrogenase,_chloroplastic	101253589	-0.66
				xanthoxin_dehydrogenase,_transcript_variant_X1	101254297	-0.69
				serine_hydroxymethyltransferase,_mitochondrial,_transcript_variant_X1	101254439	-1.24
				bifunctional_L-3-cyanoalanine_synthase/cysteine_synthase_2,_mitochondrial	101255033	-1.02
				ATP_sulfurylase_1,_chloroplastic	101256557	-0.97
				putative_magnesium-protoporphyrin_monomethyl_ester_cyclase	101257518	-2.29

				chlorophyllase-2,_chloroplastic	101258376	1.56
				ATP-citrate_synthase_alpha_chain_protein_2,_transcript_variant_X2	101258745	1.35
				5-amino-6-(5-phospho-D-ribitylamino)uracil_phosphatase,_chloroplastic	101258773	-1.32
				zeatin_O-glucosyltransferase-like	101258941	-4.25
				probable_3-beta-hydroxysteroid-Delta(8),Delta(7)-isomerase	101259646	0.49
				fructose-1,6-bisphosphatase_1,_chloroplastic	101260852	-1.42
				1-acyl-sn-glycerol-3-phosphate_acyltransferase_2-like,_transcript_variant_X1	101261177	-2.03
				anthocyanidin_3-O-glucosyltransferase_5	101261193	-11.17
				UDP-glycosyltransferase_73C3-like	101261675	-8.66
				zeatin_O-xylosyltransferase	101262709	-1.36
				2-phytyl-1,4-beta-naphthoquinone_methyltransferase,_chloroplastic,_transcript_variant_X1	101263675	-0.56
				ribulose-phosphate_3-epimerase,_chloroplastic,_transcript_variant_X1	101264109	-0.94
				fructose-1,6-bisphosphatase,_chloroplastic	101264273	-1.53
				anthranilate_synthase_alpha_subunit_2,_chloroplastic	101265030	1.01
				glutamate--glyoxylate_aminotransferase_2	101265236	-1.97
				3-phosphoshikimate_1-carboxyvinyltransferase_2	101265440	-1.51
				pyruvate_dehydrogenase_E1_component_subunit_beta-1,_mitochondrial,_transcript_variant_X1	101266731	-0.84
				vinorine_synthase	101266953	-1.56
				pyruvate,_phosphate_dikinase,_chloroplastic	101267346	-2.47
				lycopene_beta_cyclase,_chloroplastic	101267662	-0.97
				(+)-neomenthol_dehydrogenase-like,_transcript_variant_X3	101268235	-6.35
				ribulose_bisphosphate_carboxylase_small_chain_3B,_chloroplastic-like,_transcript_variant_X1	101268337	-1.33
				gibberellin_20-oxidase-1	543553	-2.10
				catalase_2	543585	-2.70
				1-deoxy-D-xylulose-5-phosphate_reductoisomerase	543682	-1.09
				inositol-3-phosphate_synthase	543809	-3.62
				sucrose_synthase	543961	1.26
				phytoene_synthase_2,_chloroplastic,_transcript_variant_X1	543964	-0.73
				ribulose_bisphosphate_carboxylase_small_chain_2A,_chloroplastic	543974	-0.69

				phytoene_synthase_1,_chloroplastic,_transcript_variant_4	543988	-2.39
				ADP-glucose_pyrophosphorylase_large_subunit	544039	-0.84
				lycopene_beta-cyclase,_transcript_variant_1	544104	-1.92
				beta-carotene_hydroxylase	544133	-4.05
				allene_oxide_synthase	606711	-1.90
				glyoxisomal_malate_dehydrogenase	778286	-1.12
Biosynthesis of cofactors (sly01240)						
3.74E-05	11	145	5.6	GDP-mannose_3',5'-epimerase, GME2	100316874	-0.95
				GDP-mannose_3',5'-epimerase, GME1	100316902	-1.80
				GDP-L-galactose_phosphorylase	101055572	-2.84
				4-hydroxyphenylpyruvate_dioxygenase	101245475	-0.64
				quinolinate_synthase,_chloroplastic	101246910	-1.29
				serine_hydroxymethyltransferase_7-like	101250548	-0.67
				serine_hydroxymethyltransferase,_mitochondrial,_transcript_variant_X1	101254439	-1.24
				probable_pyridoxal_5'-phosphate_synthase_subunit_PDX1	101257782	-1.66
				5-amino-6-(5-phospho-D-ribitylamino)uracil_phosphatase,_chloroplastic	101258773	-1.32
				2-phytyl-1,4-beta-naphthoquinone_methyltransferase,_chloroplastic,_transcript_variant_X1	101263675	-0.56
Metabolic pathways (sly01100)						
4.29E-37	89	1238	5.3	2-phytyl-1,4-beta-naphthoquinone_methyltransferase,_chloroplastic,_transcript_variant_X1	100191110	-0.56
				glutathione_reductase,_chloroplastic	100301931	-1.25
				GDP-mannose_3',5'-epimerase, GME2	100316874	-0.95
				starch_synthase_III	100316882	-0.88
				GDP-mannose_3',5'-epimerase, GME1	100316902	-1.80
				Hop-interacting_protein_THI032,_transcript_variant_X1	101055519	-1.81
				GDP-L-galactose_phosphorylase	101055572	-2.84
				cytochrome_b6-f_complex_iron-sulfur_subunit,_chloroplastic	101243864	-0.89
				probable_polyamine_oxidase_5	101244015	-1.96

				magnesium-chelatase_subunit_ChlH,_chloroplastic	101244176	-4.10
				chlorophyllide_a_oxygenase,_chloroplastic-like	101244441	-3.22
				4-hydroxyphenylpyruvate_dioxygenase	101245475	-0.64
				serine_acetyltransferase_1,_chloroplastic	101245503	-1.22
				fructose_1,6-bisphosphate_aldolase_1	101246870	-2.78
				quinolinate_synthase,_chloroplastic	101246910	-1.29
				phosphoenolpyruvate_carboxylase-like	101248407	-1.42
				aconitate_hydratase,_cytoplasmic	101248455	0.58
				nicotianamine_synthase-like	101248619	-1.38
				phosphoglycolate_phosphatase_1B,_chloroplastic	101249417	-1.18
				malate_dehydrogenase,_glyoxysomal	101249428	0.53
				glyceraldehyde-3-phosphate_dehydrogenase_B,_chloroplastic-like	101249445	-2.70
				fructose-bisphosphate_aldolase	101249787	-2.82
				serine_hydroxymethyltransferase_7-like	101250548	-0.67
				triosephosphate_isomerase,_chloroplastic,_transcript_variant_X2	101250846	-2.58
				amidophosphoribosyltransferase,_chloroplastic	101250934	-1.52
				oxalate--CoA_ligase	101251259	-4.22
				probable_polyamine_oxidase_2	101252005	-1.52
				sulfoquinovosyl_transferase_SQD2	101252422	-0.90
				ATP_synthase_gamma_chain,_chloroplastic	101253342	-0.71
				vinorine_synthase-like	101253503	-4.16
				glucose-6-phosphate_1-dehydrogenase,_chloroplastic	101253589	-0.66
				xanthoxin_dehydrogenase,_transcript_variant_X1	101254297	-0.69
				serine_hydroxymethyltransferase,_mitochondrial,_transcript_variant_X1	101254439	-1.24
				bifunctional_L-3-cyanoalanine_synthase/cysteine_synthase_2,_mitochondrial	101255033	-1.02
				1,2-dihydroxy-3-keto-5-methylthiopentene_dioxygenase_1,_transcript_variant_1	101255136	-2.44
				phosphoribulokinase,_chloroplastic	101255322	-1.43
				ATP_sulfurylase_1,_chloroplastic	101256557	-0.97
				5'-adenylylsulfate_reductase_3,_chloroplastic	101257319	-1.65

				putative_magnesium-protoporphyrin_monomethyl_ester_cyclase	101257518	-2.29
				probable_pyridoxal_5'-phosphate_synthase_subunit_PDX1	101257782	-1.66
				chlorophyllase-2,_chloroplastic	101258376	1.56
				ATP-citrate_synthase_alpha_chain_protein_2,_transcript_variant_X2	101258745	1.35
				5-amino-6-(5-phospho-D-ribitylamino)uracil_phosphatase,_chloroplastic	101258773	-1.32
				phosphoinositide_phosphatase_SAC3-like,_transcript_variant_X1	101259347	-0.39
				probable_3-beta-hydroxysteroid-Delta(8),Delta(7)-isomerase	101259646	0.49
				S-adenosylmethionine_decarboxylase_2,_transcript_variant_X1	101260400	-2.43
				photosystem_II_subunit_S	101260830	-2.13
				fructose-1,6-bisphosphatase_1,_chloroplastic	101260852	-1.42
				1-acyl-sn-glycerol-3-phosphate_acyltransferase_2-like,_transcript_variant_X1	101261177	-2.03
				galactinol_synthase_1	101261450	-2.99
				L-tryptophan--pyruvate_aminotransferase_1-like	101262607	-4.41
				NADP-dependent_glyceraldehyde-3-phosphate_dehydrogenase,_transcript_variant_X1	101262732	-3.42
				UDP-glucuronic_acid_decarboxylase_6,_transcript_variant_X1	101263507	0.45
				2-phytyl-1,4-beta-naphthoquinone_methyltransferase,_chloroplastic,_transcript_variant_X1	101263675	-0.56
				glyceraldehyde-3-phosphate_dehydrogenase_B,_chloroplastic	101264004	-1.02
				ribulose-phosphate_3-epimerase,_chloroplastic,_transcript_variant_X1	101264109	-0.94
				fructose-1,6-bisphosphatase,_chloroplastic	101264273	-1.53
				probable_polygalacturonase_At1g80170	101264436	-2.14
				anthranilate_synthase_alpha_subunit_2,_chloroplastic	101265030	1.01
				glutamate--glyoxylate_aminotransferase_2	101265236	-1.97
				3-phosphoshikimate_1-carboxyvinyltransferase_2	101265440	-1.51
				ferredoxin	101265784	-2.18
				allantoate_deiminase_2	101266592	-1.40

				glyceraldehyde-3-phosphate_dehydrogenase_A,_chloroplastic	101266713	-1.14
				pyruvate_dehydrogenase_E1_component_subunit_beta-1,_mitochondrial,_transcript_variant_X1	101266731	-0.84
				digalactosyldiacylglycerol_synthase_1,_chloroplastic-like	101266854	-1.23
				vinorine_synthase	101266953	-1.56
				pyruvate,_phosphate_dikinase,_chloroplastic	101267346	-2.47
				lycopene_beta_cyclase,_chloroplastic	101267662	-0.97
				ribulose_bisphosphate_carboxylase_small_chain_3B,_chloroplastic-like,_transcript_variant_X1	101268337	-1.33
				cytosolic_NADP-malic_enzyme	543522	0.74
				gibberellin_20-oxidase-1	543553	-2.10
				catalase_2	543585	-2.70
				1-deoxy-D-xylulose-5-phosphate_reductoisomerase	543682	-1.09
				inositol-3-phosphate_synthase	543809	-3.62
				GTP_cyclohydrolase_1	543831	-0.93
				glycerol-3-phosphate_acyltransferase,_transcript_variant_X3	543901	-0.66
				sucrose_synthase	543961	1.26
				phytoene_synthase_2,_chloroplastic,_transcript_variant_X1	543964	-0.73
				ribulose_bisphosphate_carboxylase_small_chain_2A,_chloroplastic	543974	-0.69
				phytoene_synthase_1,_chloroplastic,_transcript_variant_4	543988	-2.39
				glutamine_synthetase,_transcript_variant_1	543998	-1.33
				ADP-glucose_pyrophosphorylase_large_subunit	544039	-0.84
				lycopene_beta-cyclase,_transcript_variant_1	544104	-1.92
				beta-carotene_hydroxylase	544133	-4.05
				NADP-malic_enzyme	544164	-1.64
				allene_oxide_synthase	606711	-1.90
				glyoxisomal_malate_dehydrogenase	778286	-1.12
				nitrite_reductase	778325	-1.81

Table S5. GO enrichment, number of genes, pathways genes, fold enrichment, biological process and gene NCBI ID for the DEGs of brown module.

Enrichment FDR	nGenes	Pathway Genes	Fold Enrichment	Description	Locus ID	Log_2 (Fold-change)
GO:0016109 tetraterpenoid & GO:0016117 carotenoid biosynthetic proc.						
3.18E-06	6	16	27.8	phytoene_synthase_2,_chloroplastic,_transcript_variant_X1	543964	-0.73
				phytoene_synthase_1,_chloroplastic,_transcript_variant_4	543988	-2.39
				lycopene_beta-cyclase,_transcript_variant_1	544104	-1.92
				beta-carotene_hydroxylase	544133	-4.05
				ABC1-like_kinase_1,_transcript_variant_X1	101243810	-0.93
				lycopene_beta_cyclase,_chloroplastic	101267662	-0.97
GO:0016108 tetraterpenoid & GO:0016116 carotenoid metabolic proc.						
5.02E-07	7	20	26.0	phytoene_synthase_2,_chloroplastic,_transcript_variant_X1	543964	-0.73
				phytoene_synthase_1,_chloroplastic,_transcript_variant_4	543988	-2.39
				lycopene_beta-cyclase,_transcript_variant_1	544104	-1.92
				prolycopene_isomerase,_chloroplastic	101247017	2.02
				beta-carotene_hydroxylase	544133	-4.05
				ABC1-like_kinase_1,_transcript_variant_X1	101243810	-0.93
				lycopene_beta_cyclase,_chloroplastic	101267662	-0.97
GO:0006006 glucose metabolic proc.						
1.23E-06	8	34	17.5	glyceraldehyde-3-phosphate_dehydrogenase_A,_chloroplastic	101266713	-1.14
				glyceraldehyde-3-phosphate_dehydrogenase_B,_chloroplastic	101264004	-1.02
				GDP-L-galactose_phosphorylase	101055572	-2.84
				fructose-1,6-bisphosphatase_1,_chloroplastic	101260852	-1.42
				triosephosphate_isomerase,_chloroplastic,_transcript_variant_X2	101250846	-2.58
				fructose-1,6-bisphosphatase,_chloroplastic	101264273	-1.53
				glyceraldehyde-3-phosphate_dehydrogenase_B,_chloroplastic-like	101249445	-2.70
				glucose-6-phosphate_1-dehydrogenase,_chloroplastic	101253589	-0.66
GO:0006721 terpenoid metabolic proc.						
6.37E-06	11	100	8.2	phytoene_synthase_2,_chloroplastic,_transcript_variant_X1	543964	-0.73
				gibberellin_20-oxidase-1	543553	-2.10

				phytoene_synthase_1,_chloroplastic,_transcript_variant_4	543988	-2.39
				1-deoxy-D-xylulose-5-phosphate_reductoisomerase	543682	-1.09
				lycopene_beta-cyclase,_transcript_variant_1	544104	-1.92
				xanthoxin_dehydrogenase,_transcript_variant_X1	101254297	-0.69
				(E)-beta-ocimene_synthase	101247865	-2.08
				prolycopene_isomerase,_chloroplastic	101247017	-2.02
				beta-carotene_hydroxylase	544133	-4.05
				ABC1-like_kinase_1,_transcript_variant_X1	101243810	-0.93
				lycopene_beta_cyclase,_chloroplastic	101267662	-0.97
GO:0005996 monosaccharide metabolic proc.						
3.78E-06	12	115	7.7	ribulose-phosphate_3-epimerase,_chloroplastic,_transcript_variant_X1	101264109	-0.94
				glyceraldehyde-3-phosphate_dehydrogenase_A,_chloroplastic	101266713	-1.14
				UDP-glucuronic_acid_decarboxylase_6,_transcript_variant_X1	101263507	0.45
				glyceraldehyde-3-phosphate_dehydrogenase_B,_chloroplastic	101264004	-1.02
				alpha-mannosidase	100500729	0.47
				GDP-L-galactose_phosphorylase	101055572	-2.84
				fructose-1,6-bisphosphatase_1,_chloroplastic	101260852	-1.42
				triosephosphate_isomerase,_chloroplastic,_transcript_variant_X2	101250846	-2.58
				fructose-1,6-bisphosphatase,_chloroplastic	101264273	-1.53
				glyceraldehyde-3-phosphate_dehydrogenase_B,_chloroplastic-like	101249445	-2.70
				galactinol_synthase_1	101261450	-2.99
				glucose-6-phosphate_1-dehydrogenase,_chloroplastic	101253589	-0.66
GO:0009416 response to light stimulus & GO:0009314 response to radiation						
2.26E-08	18	184	7.3	FtsH_protease	778337	-7.33
				gibberellin_20-oxidase-1	543553	-2.10
				FtsH-like_protein_precursor	100037730	-1.25
				CONSTANS_interacting_protein_1	778334	-4.05
				uncharacterized_LOC101250355	101250355	-2.37
				heme-binding-like_protein_At3g10130,_chloroplastic	101251239	-1.48
				phytochrome_B1	101262847	-1.06
				galactinol_synthase_1	101261450	-2.99
				protein_PLASTID_MOVEMENT_IMPAIRED_2	101261382	-2.46

				calcium_sensing_receptor,_chloroplastic	101268560	-2.31
				photosystem_II_subunit_S	101260830	-2.13
				omega-6_fatty_acid_desaturase	101265653	-2.85
				root_phototropism_protein_2 protein_FAR-RED_ELONGATED_HYPOCOTYL_3,_transcript_variant_X1	101259171 101256896	-3.81 -0.39
				phytochrome_F,_transcript_variant_X1	101259349	-0.48
				ABC1-like_kinase_1,_transcript_variant_X1	101243810	-0.93
				protein_PROTON_GRADIENT_REGULATION_5,_chloroplastic	101262255	-4.24
				cytochrome_b6-f_complex_iron-sulfur_subunit,_chloroplastic	101243864	-0.89
GO:0044283 small molecule biosynthetic proc.						
3.65E-11	31	434	5.3	bifunctional_L-3-cyanoalanine_synthase/cysteine_synthase_2,_mitochondrial	101255033	-1.02
				serine_hydroxymethyltransferase_7-like	101250548	-0.67
				serine_hydroxymethyltransferase,_mitochondrial,_transcript_variant_X1	101254439	-1.24
				gibberellin_20-oxidase-1	543553	-2.10
				palmitoyl-monogalactosyldiacylglycerol_delta-7_desaturase,_chloroplastic	101250586	-3.29
				ATP-citrate_synthase_alpha_chain_protein_2,_transcript_variant_X2	101258745	1.35
				lycopene_beta-cyclase,_transcript_variant_1	544104	-1.92
				xanthoxin_dehydrogenase,_transcript_variant_X1	101254297	-0.69
				allene_oxide_synthase	606711	-1.90
				3-phosphoshikimate_1-carboxyvinyltransferase_2	101265440	-1.51
				inositol-3-phosphate_synthase	543809	-3.62
				probable_pyridoxal_5'-phosphate_synthase_subunit_PDX1	101257782	-1.66
				GTP_cyclohydrolase_1	543831	-0.93
				solanesyl_diphosphate_synthase	101253007	-2.13
				fructose-1,6-bisphosphatase_1,_chloroplastic	101260852	-1.42
				triosephosphate_isomerase,_chloroplastic,_transcript_variant_X2	101250846	-2.58
				lycopene_beta_cyclase,_chloroplastic	101267662	-0.97
				fructose-1,6-bisphosphatase,_chloroplastic	101264273	-1.53
				Hop-interacting_protein_THI032,_transcript_variant_X1	101055519	-1.81
				glutamine_synthetase,_transcript_variant_1	543998	-1.33
				linoleate_9S-lipoxygenase-like	107648852	-1.76

				nicotianamine_synthase-like	101248619	-1.38
				phytoene_synthase_2,_chloroplastic,_transcript_variant_X1	543964	-0.73
				S-adenosylmethionine_decarboxylase_2,_transcript_variant_X1	101260400	-2.43
				phytoene_synthase_1,_chloroplastic,_transcript_variant_4	543988	-2.39
				glutamate--glyoxylate_aminotransferase_2	101265236	-1.97
				anthranilate_synthase_alpha_subunit_2,_chloroplastic	101265030	1.01
				5-amino-6-(5-phospho-D-ribitylamino)uracil_phosphatase,_chloroplastic	101258773	-1.32
				1,2-dihydroxy-3-keto-5-methylthiopentene_dioxygenase_1,_transcript_variant_1	101255136	-2.44
				serine_acetyltransferase_1,_chloroplastic	101245503	-1.22
				2-phytyl-1,4-beta-naphthoquinone_methyltransferase,_chloroplastic,_transcript_variant_X1	101263675	-0.56
GO:0015979 photosynthesis						
6.19E-06	16	228	5.2	FtsH_protease	778337	-7.33
				FtsH-like_protein_precursor	100037730	-1.25
				protein_PROTON_GRADIENT_REGULATION_5,_chloroplastic	101262255	-4.24
				uncharacterized_protein_ycf39	101252442	-0.98
				ATP_synthase_gamma_chain,_chloroplastic	101253342	-0.71
				ribulose_bisphosphate_carboxylase_small_chain_3B,_chloroplastic-like,_transcript_variant_X1	101268337	-1.33
				photosystem_I_assembly_factor_PSA3,_chloroplastic	101249783	-0.63
				ribulose_bisphosphate_carboxylase_small_chain_2A,_chloroplastic	543974	-0.69
				photosystem_II_subunit_S	101260830	-2.13
				omega-6_fatty_acid_desaturase	101265653	-2.85
				solanesyl_diphosphate_synthase	101253007	-2.13
				ABC1-like_kinase_1,_transcript_variant_X1	101243810	-0.93
				fructose-1,6-bisphosphatase_1,_chloroplastic	101260852	-1.42
				putative_magnesium-protoporphyrin_monomethyl_ester_cyclase	101257518	-2.29
				psbP_domain-containing_protein_7,_chloroplastic,_transcript_variant_X1	101246302	-1.03
				cytochrome_b6-f_complex_iron-sulfur_subunit,_chloroplastic	101243864	-0.89
GO:0009628 response to abiotic stimulus						
3.20E-08	28	486	4.3	FtsH_protease	778337	-7.33
				gibberellin_20-oxidase-1	543553	-2.10

				heat_shock_70_kDa_protein_5	101255185	-1.67
				FtsH-like_protein_precursor	100037730	-1.25
				CONSTANS_interacting_protein_1	778334	-4.05
				plasma_membrane_intrinsic_protein_1.5	544086	-1.98
				uncharacterized_LOC101250355	101250355	-2.37
				heme-binding-like_protein_At3g10130,_chloroplastic	101251239	-1.48
				GAI-like_protein	543881	-0.70
				phytochrome_B1	101262847	-1.06
				galactinol_synthase_1	101261450	-2.99
				glutamine_synthetase,_transcript_variant_1	543998	-1.33
				putative_pentatricopeptide_repeat-containing_protein_At1g56570	101248822	0.94
				protein_PLASTID_MOVEMENT_IMPAIRED_2	101261382	-2.46
				calcium_sensing_receptor,_chloroplastic	101268560	-2.31
				photosystem_II_subunit_S	101260830	-2.13
				VPS41	544040	-0.74
				omega-6_fatty_acid_desaturase	101265653	-2.85
				vernalization_insensitive_3	101055574	-0.52
				root_phototropism_protein_2	101259171	-3.81
				protein_FAR-RED_ELONGATED_HYPOCOTYL_3,_transcript_variant_X1	101256896	-0.39
				phytochrome_F,_transcript_variant_X1	101259349	-0.48
				uncharacterized_LOC101264030,_transcript_variant_X1	101264030	-1.75
				ABC1-like_kinase_1,_transcript_variant_X1	101243810	-0.93
				fructose-1,6-bisphosphatase_1,_chloroplastic	101260852	-1.42
				protein_PROTON_GRADIENT_REGULATION_5,_chloroplastic	101262255	-4.24
				30S_ribosomal_protein_S1,_transcript_variant_X1	101267163	-1.33
				cytochrome_b6-f_complex_iron-sulfur_subunit,_chloroplastic	101243864	-0.89
GO:0006091 generation of precursor metabolites and energy						
3.99E-06	22	413	4.0	FtsH_protease	778337	-7.33
				ribulose-phosphate_3-epimerase,_chloroplastic,_transcript_variant_X1	101264109	-0.94
				FtsH-like_protein_precursor	100037730	-1.25
				protein_PROTON_GRADIENT_REGULATION_5,_chloroplastic	101262255	-4.24
				triosephosphate_isomerase,_chloroplastic,_transcript_variant_X2	101250846	-2.58
				aconitate_hydratase,_cytoplasmic	101248455	0.58
				ADP-glucose_pyrophosphorylase_large_subunit	544039	-0.84
				glyoxisomal_malate_dehydrogenase	778286	-1.12

				fructose_1,6-bisphosphate_aldolase_1	101246870	-2.78
				uncharacterized_protein_ycf39	101252442	-0.98
				fructose-bisphosphate_aldolase	101249787	-2.82
				malate_dehydrogenase,_glyoxysomal	101249428	0.53
				ATP_synthase_gamma_chain,_chloroplastic	101253342	-0.71
				photosystem_I_assembly_factor_PSA3,_chloroplastic	101249783	-0.63
				quinolinate_synthase,_chloroplastic	101246910	-1.29
				glucose-6-phosphate_1-dehydrogenase,_chloroplastic	101253589	-0.66
				pyruvate_dehydrogenase_E1_component_subunit_beta-1,_mitochondrial,_transcript_variant_X1	101266731	-0.84
				omega-6_fatty_acid_desaturase	101265653	-2.85
				phosphoenolpyruvate_carboxylase-like	101248407	-1.42
				ABC1-like_kinase_1,_transcript_variant_X1	101243810	-0.93
				fructose-1,6-bisphosphatase_1,_chloroplastic	101260852	-1.42
				ferredoxin	101265784	-2.18
GO:0044281 small molecule metabolic proc.						
3.97E-15	61	1245	3.6	bifunctional_L-3-cyanoalanine_synthase/cysteine_synthase_2,_mitochondrial	101255033	-1.02
				serine_hydroxymethyltransferase_7-like	101250548	-0.67
				ATP_synthase_gamma_chain,_chloroplastic	101253342	-0.71
				serine_hydroxymethyltransferase,_mitochondrial,_transcript_variant_X1	101254439	-1.24
				gibberellin_20-oxidase-1	543553	-2.10
				quinolinate_synthase,_chloroplastic	101246910	-1.29
				1-deoxy-D-xylulose-5-phosphate_reductoisomerase	543682	-1.09
				ribulose-phosphate_3-epimerase,_chloroplastic,_transcript_variant_X1	101264109	-0.94
				palmitoyl-monogalactosyldiacylglycerol_delta-7_desaturase,_chloroplastic	101250586	-3.29
				glyceraldehyde-3-phosphate_dehydrogenase_A,_chloroplastic	101266713	-1.14
				UDP-glucuronic_acid_decarboxylase_6,_transcript_variant_X1	101263507	0.45
				ATP-citrate_synthase_alpha_chain_protein_2,_transcript_variant_X2	101258745	1.35
				lycopene_beta-cyclase,_transcript_variant_1	544104	-1.92

				xanthoxin_dehydrogenase,_transcript_variant_X1	101254297	-0.69
				allene_oxide_synthase	606711	-1.90
				glyceraldehyde-3-phosphate_dehydrogenase_B,_chloroplastic	101264004	-1.02
				cytosolic_NADP-malic_enzyme	543522	0.74
				3-phosphoshikimate_1-carboxyvinyltransferase_2	101265440	-1.51
				inositol-3-phosphate_synthase	543809	-3.62
				alpha-mannosidase	100500729	0.47
				GDP-L-galactose_phosphorylase	101055572	-2.84
				probable_pyridoxal_5'-phosphate_synthase_subunit_PDX1	101257782	-1.66
				GTP_cyclohydrolase_1	543831	-0.93
				4-hydroxyphenylpyruvate_dioxygenase	101245475	-0.64
				solanesyl_diphosphate_synthase	101253007	-2.13
				fructose-1,6-bisphosphatase_1,_chloroplastic	101260852	-1.42
				1,2-dihydroxy-3-keto-5-methylthiopentene_dioxygenase_1,_transcript_variant_1	101255136	-2.44
				triosephosphate_isomerase,_chloroplastic,_transcript_variant_X2	101250846	-2.58
				lycopene_beta_cyclase,_chloroplastic	101267662	-0.97
				probable_acetyltransferase_NATA1-like	101258115	0.40
				fructose-1,6-bisphosphatase,_chloroplastic	101264273	-1.53
				aconitate_hydratase,_cytoplasmic	101248455	0.58
				NADP-malic_enzyme	544164	-1.64
				glyceraldehyde-3-phosphate_dehydrogenase_B,_chloroplastic-like	101249445	-2.70
				Hop-interacting_protein_THI032,_transcript_variant_X1	101055519	-1.81
				galactinol_synthase_1	101261450	-2.99
				glutamine_synthetase,_transcript_variant_1	543998	-1.33
				pyruvate,_phosphate_dikinase,_chloroplastic	101267346	-2.47
				linoleate_9S-lipoxygenase-like	107648852	-1.76
				nicotianamine_synthase-like	101248619	-1.38
				glyoxisomal_malate_dehydrogenase	778286	-1.12
				fructose_1,6-bisphosphate_aldolase_1	101246870	-2.78
				amidophosphoribosyltransferase,_chloroplastic	101250934	-1.52
				fructose-bisphosphate_aldolase	101249787	-2.82
				malate_dehydrogenase,_glyoxysomal	101249428	0.53
				allantoate_deiminase_2	101266592	-1.40
				phytoene_synthase_2,_chloroplastic,_transcript_variant_X1	543964	-0.73

				S-adenosylmethionine_decarboxylase_2,_transcript_variant_X1	101260400	-2.43
				phytoene_synthase_1,_chloroplastic,_transcript_variant_4	543988	-2.39
				R2R3MYB_transcription_factor_117	101263611	-2.15
				glutamate--glyoxylate_aminotransferase_2	101265236	-1.97
				glucose-6-phosphate_1-dehydrogenase,_chloroplastic	101253589	-0.66
				thioredoxin_F1,_chloroplastic-like	101246719	-2.28
				anthranilate_synthase_alpha_subunit_2,_chloroplastic	101265030	1.01
				pyruvate_dehydrogenase_E1_component_subunit_beta-1,_mitochondrial,_transcript_variant_X1	101266731	-0.84
				5-amino-6-(5-phospho-D-ribitylamino)uracil_phosphatase,_chloroplastic	101258773	-1.32
				serine_acetyltransferase_1,_chloroplastic	101245503	-1.22
				thioredoxin_1	101268617	-1.52
				uncharacterized_LOC101267576	101267576	-1.68
				dicarboxylate_transporter_1,_chloroplastic	101250955	-2.88
				2-phytyl-1,4-beta-naphthoquinone_methyltransferase,_chloroplastic,_transcript_variant_X1	101263675	-0.56
GO:0043436 oxoacid metabolic proc.						
1.91E-07	34	761	3.3	bifunctional_L-3-cyanoalanine_synthase/cysteine_synthase_2,_mitochondrial	101255033	-1.02
				serine_hydroxymethyltransferase_7-like	101250548	-0.67
				serine_hydroxymethyltransferase,_mitochondrial,_transcript_variant_X1	101254439	-1.24
				quinolinate_synthase,_chloroplastic	101246910	-1.29
				1-deoxy-D-xylulose-5-phosphate_reductoisomerase	543682	-1.09
				palmitoyl-monogalactosyldiacylglycerol_delta-7_desaturase,_chloroplastic	101250586	-3.29
				ATP-citrate_synthase_alpha_chain_protein_2,_transcript_variant_X2	101258745	1.35
				xanthoxin_dehydrogenase,_transcript_variant_X1	101254297	-0.69
				allene_oxide_synthase	606711	-1.90
				cytosolic_NADP-malic_enzyme	543522	0.74
				3-phosphoshikimate_1-carboxyvinyltransferase_2	101265440	-1.51
				probable_pyridoxal_5'-phosphate_synthase_subunit_PDX1	101257782	-1.66
				4-hydroxyphenylpyruvate_dioxygenase	101245475	-0.64

				1,2-dihydroxy-3-keto-5-methylthiopentene_dioxygenase_1,_transcript_variant_1	101255136	-2.44
				triosephosphate_isomerase,_chloroplastic,_transcript_variant_X2	101250846	-2.58
				probable_acetyltransferase_NATA1-like	101258115	0.40
				aconitate_hydratase,_cytoplasmic	101248455	0.58
				NADP-malic_enzyme	544164	-1.64
				Hop-interacting_protein_THI032,_transcript_variant_X1	101055519	-1.81
				glutamine_synthetase,_transcript_variant_1	543998	-1.33
				pyruvate,_phosphate_dikinase,_chloroplastic	101267346	-2.47
				linoleate_9S-lipoxygenase-like	107648852	-1.76
				nicotianamine_synthase-like	101248619	-1.38
				glyoxisomal_malate_dehydrogenase	778286	-1.12
				fructose_1,6-bisphosphate_aldolase_1	101246870	-2.78
				fructose-bisphosphate_aldolase	101249787	-2.82
				malate_dehydrogenase,_glyoxysomal	101249428	0.53
				R2R3MYB_transcription_factor_117	101263611	-2.15
				glutamate--glyoxylate_aminotransferase_2	101265236	-1.97
				anthranilate_synthase_alpha_subunit_2,_chloroplastic	101265030	1.01
				pyruvate_dehydrogenase_E1_component_subunit_beta-1,_mitochondrial,_transcript_variant_X1	101266731	-0.84
				serine_acetyltransferase_1,_chloroplastic	101245503	-1.22
				uncharacterized_LOC101267576	101267576	-1.68
				dicarboxylate_transporter_1,_chloroplastic	101250955	-2.88
GO:0006082 organic acid metabolic proc.						
1.33E-07	35	786	3.3	bifunctional_L-3-cyanoalanine_synthase/cysteine_synthase_2,_mitochondrial	101255033	-1.02
				serine_hydroxymethyltransferase_7-like	101250548	-0.67
				serine_hydroxymethyltransferase,_mitochondrial,_transcript_variant_X1	101254439	-1.24
				gibberellin_20-oxidase-1	543553	-2.10
				quinolinate_synthase,_chloroplastic	101246910	-1.29
				1-deoxy-D-xylulose-5-phosphate_reductoisomerase	543682	-1.09
				palmitoyl-monogalactosyldiacylglycerol_delta-7_desaturase,_chloroplastic	101250586	-3.29
				ATP-citrate_synthase_alpha_chain_protein_2,_transcript_variant_X2	101258745	1.35
				xanthoxin_dehydrogenase,_transcript_variant_X1	101254297	-0.69

				allene_oxide_synthase	606711	-1.90
				cytosolic_NADP-malic_enzyme	543522	0.74
				3-phosphoshikimate_1-carboxyvinyltransferase_2	101265440	-1.51
				probable_pyridoxal_5'-phosphate_synthase_subunit_PDX1	101257782	-1.66
				4-hydroxyphenylpyruvate_dioxygenase	101245475	-0.64
				1,2-dihydroxy-3-keto-5-methylthiopentene_dioxygenase_1,_transcript_variant_1	101255136	-2.44
				triosephosphate_isomerase,_chloroplastic,_transcript_variant_X2	101250846	-2.58
				probable_acetyltransferase_NATA1-like	101258115	0.40
				aconitate_hydratase,_cytoplasmic	101248455	0.58
				NADP-malic_enzyme	544164	-1.64
				Hop-interacting_protein_THI032,_transcript_variant_X1	101055519	-1.81
				glutamine_synthetase,_transcript_variant_1	543998	-1.33
				pyruvate,_phosphate_dikinase,_chloroplastic	101267346	-2.47
				linoleate_9S-lipoxygenase-like	107648852	-1.76
				nicotianamine_synthase-like	101248619	-1.38
				glyoxisomal_malate_dehydrogenase	778286	-1.12
				fructose_1,6-bisphosphate_aldolase_1	101246870	-2.78
				fructose-bisphosphate_aldolase	101249787	-2.82
				malate_dehydrogenase,_glyoxysomal	101249428	0.53
				R2R3MYB_transcription_factor_117	101263611	-2.15
				glutamate--glyoxylate_aminotransferase_2	101265236	-1.97
				anthranilate_synthase_alpha_subunit_2,_chloroplastic	101265030	1.01
				pyruvate_dehydrogenase_E1_component_subunit_beta-1,_mitochondrial,_transcript_variant_X1	101266731	-0.84
				serine_acetyltransferase_1,_chloroplastic	101245503	-1.22
				uncharacterized_LOC101267576	101267576	-1.68
				dicarboxylate_transporter_1,_chloroplastic	101250955	-2.88
GO:0019752 carboxylic acid metabolic proc.						
3.38E-07	33	742	3.3	bifunctional_L-3-cyanoalanine_synthase/cysteine_synthase_2,_mitochondrial	101255033	-1.02
				serine_hydroxymethyltransferase_7-like	101250548	-0.67
				serine_hydroxymethyltransferase,_mitochondrial,_transcript_variant_X1	101254439	-1.24
				quinolinate_synthase,_chloroplastic	101246910	-1.29
				1-deoxy-D-xylulose-5-phosphate_reductoisomerase	543682	-1.09

				palmitoyl-monogalactosyldiacylglycerol_delta-7_desaturase,_chloroplastic	101250586	-3.29
				ATP-citrate_synthase_alpha_chain_protein_2,_transcript_variant_X2	101258745	1.35
				xanthoxin_dehydrogenase,_transcript_variant_X1	101254297	-0.69
				allene_oxide_synthase	606711	-1.90
				cytosolic_NADP-malic_enzyme	543522	0.74
				3-phosphoshikimate_1-carboxyvinyltransferase_2	101265440	-1.51
				probable_pyridoxal_5'-phosphate_synthase_subunit_PDX1	101257782	-1.66
				4-hydroxyphenylpyruvate_dioxygenase	101245475	-0.64
				1,2-dihydroxy-3-keto-5-methylthiopentene_dioxygenase_1,_transcript_variant_1	101255136	-2.44
				triosephosphate_isomerase,_chloroplastic,_transcript_variant_X2	101250846	-2.58
				probable_acetyltransferase_NATA1-like	101258115	0.40
				aconitate_hydratase,_cytoplasmic	101248455	0.58
				NADP-malic_enzyme	544164	-1.64
				Hop-interacting_protein_THI032,_transcript_variant_X1	101055519	-1.81
				glutamine_synthetase,_transcript_variant_1	543998	-1.33
				pyruvate,_phosphate_dikinase,_chloroplastic	101267346	-2.47
				linoleate_9S-lipoxygenase-like	107648852	-1.76
				nicotianamine_synthase-like	101248619	-1.38
				glyoxisomal_malate_dehydrogenase	778286	-1.12
				fructose_1,6-bisphosphate_aldolase_1	101246870	-2.78
				fructose-bisphosphate_aldolase	101249787	-2.82
				malate_dehydrogenase,_glyoxysomal	101249428	0.53
				R2R3MYB_transcription_factor_117	101263611	-2.15
				glutamate--glyoxylate_aminotransferase_2	101265236	-1.97
				anthranilate_synthase_alpha_subunit_2,_chloroplastic	101265030	1.01
				pyruvate_dehydrogenase_E1_component_subunit_beta-1,_mitochondrial,_transcript_variant_X1	101266731	-0.84
				serine_acetyltransferase_1,_chloroplastic	101245503	-1.22
				dicarboxylate_transporter_1,_chloroplastic	101250955	-2.88
GO:0042221 response to chemical						
7.06E-09	43	984	3.2	ETHYLENE_INSENSITIVE_3-like_3_protein,_transcript_variant_X2	101249950	-1.26

				serine_hydroxymethyltransferase_7-like	101250548	-0.67
				catalase_2	543585	-2.70
				serine_hydroxymethyltransferase,_mitochondrial,_transcript_variant_X1	101254439	-1.24
				probable_2-oxoglutarate-dependent_dioxygenase_At5g05600	101260801	-1.57
				heat_shock_70_kDa_protein_5	101255185	-1.67
				high_affinity_nitrate_transporter_2.4-like	101247028	-2.40
				EIN3-like_protein	543518	0.40
				S-norcoclaurine_synthase_1	101262127	-4.42
				heptahelical_transmembrane_protein_2-like	101252897	-2.12
				lachrymatory-factor_synthase	101250037	-1.76
				protein_NRT1/_PTR_FAMILY_7.3	101263538	-5.43
				plasma_membrane_intrinsic_protein_1.5	544086	-1.98
				VAN3-binding_protein,_transcript_variant_X1	101254530	-0.63
				senescence-associated_protein_SPA15,_chloroplastic,_transcript_variant_X1	101257426	-1.67
				GAI-like_protein	543881	-0.70
				cell_division_cycle_protein_48_homolog,_transcript_variant_X1	101265798	0.53
				phytochrome_B1	101262847	-1.06
				galactinol_synthase_1	101261450	-2.99
				glutamine_synthetase,_transcript_variant_1	543998	-1.33
				putative_pentatricopeptide_repeat-containing_protein_At1g56570	101248822	0.94
				auxin-responsive_protein_SAUR21-like	101251524	-3.09
				sugar_transporter_ERD6-like_5,_transcript_variant_X7	104645435	-1.18
				protein_DETOXIFICATION_40	101255252	0.80
				gibberellin_20-oxidase-1	543553	-2.10
				mitochondrial_carrier_protein_MTM1,_transcript_variant_X2	101253663	-1.24
				protein_DETOXIFICATION_14-like,_transcript_variant_X1	101261991	-2.41
				auxin-responsive_protein_SAUR32	101246226	-1.65
				protein_RESPONSE_TO_LOW_SULFUR_3-like	101268660	-5.32
				calcium_sensing_receptor,_chloroplastic	101268560	-2.31
				small_auxin-up_protein_58	101055583	-4.24
				IAA7_protein	543542	-2.06
				zinc_finger_protein_3	101258965	-1.16
				auxin_response_factor_19	100498663	-0.67
				uncharacterized_LOC101264030,_transcript_variant_X1	101264030	-1.75
				ABC1-like_kinase_1,_transcript_variant_X1	101243810	-0.93

				fructose-1,6-bisphosphatase_1,_chloroplastic	101260852	-1.42
				glutathione_reductase,_chloroplastic	100301931	-1.25
				30S_ribosomal_protein_S1,_transcript_variant_X1	101267163	-1.33
				protein_DETOXIFICATION_18	101265483	-1.44
				protein_DETOXIFICATION_24	101257226	-1.78
				protein_DETOXIFICATION_27	101265986	-1.87
				uncharacterized_LOC101257239	101257239	-2.33
GO:0006629 lipid metabolic proc.						
3.18E-06	32	789	3.0	digalactosyldiacylglycerol_synthase_1,_chloroplastic-like	101266854	-1.23
				lipid_phosphate_phosphatase_epsilon_2,_chloroplastic	101244637	-1.50
				phytoene_synthase_2,_chloroplastic,_transcript_variant_X1	543964	-0.73
				gibberellin_20-oxidase-1	543553	-2.10
				uncharacterized_LOC101252498	543988	-5.54
				1-deoxy-D-xylulose-5-phosphate_reductoisomerase	543682	-1.09
				palmitoyl-monogalactosyldiacylglycerol_delta-7_desaturase,_chloroplastic	101250586	-3.29
				ATP-citrate_synthase_alpha_chain_protein_2,_transcript_variant_X2	101258745	1.35
				lycopene_beta-cyclase,_transcript_variant_1	544104	-1.92
				xanthoxin_dehydrogenase,_transcript_variant_X1	101254297	-0.69
				allene_oxide_synthase	606711	-1.90
				probable_3-beta-hydroxysteroid-Delta(8),Delta(7)-isomerase	101259646	0.49
				solanesyl_diphosphate_synthase	101253007	-2.13
				sulfoquinovosyl_transferase_SQD2	101252422	-0.90
				(E)-beta-ocimene_synthase	101247865	-2.08
				malate_dehydrogenase,_glyoxysomal	101249428	0.53
				phospholipase_A1-II_1	101243853	1.46
				R2R3MYB_transcription_factor_117	101263611	-2.15
				prolycopene_isomerase,_chloroplastic	101247017	-2.02
				inositol-3-phosphate_synthase	543809	-3.62
				beta-carotene_hydroxylase	544133	-4.05
				omega-3_fatty_acid_desaturase	544203	-1.44
				uncharacterized_LOC101250128,_transcript_variant_X2	101250128	-3.39
				omega-6_fatty_acid_desaturase	101265653	-2.85
				phosphoinositide_phosphatase_SAC3-like,_transcript_variant_X1	101259347	-0.39
				ABC1-like_kinase_1,_transcript_variant_X1	101243810	-0.93
				glycerol-3-phosphate_acyltransferase,_transcript_variant_X3	543901	-0.66
				cyprosin	101258304	-1.99

				lycopene_beta_cyclase,_chloroplastic	101267662	-0.97
				3-oxo-5-alpha-steroid_4-dehydrogenase_1	101255051	-4.58
				very-long-chain_enoyl-CoA_reductase	101255353	-6.68
				phosphomethylethanolamine_N-methyltransferase,_transcript_variant_X1	101247110	-2.73
GO:0055085 transmembrane transport						
1.33E-07	41	1031	3.0	protein_DETOXIFICATION_40	101255252	0.80
				monosaccharide-sensing_protein_2-like	101261393	-1.09
				protein_DETOXIFICATION_14-like,_transcript_variant_X1	101261991	-2.41
				inorganic_phosphate_transporter_2-1,_chloroplastic	101267311	-2.04
				vacuolar_cation/proton_exchanger_3-like	101265339	-2.00
				protein_DETOXIFICATION_18	101265483	-1.44
				mitochondrial_carnitine/acylcarnitine_carrier-like_protein,_transcript_variant_2	101262875	-2.05
				protein_DETOXIFICATION_24	101257226	-1.78
				amino_acid_transporter_AVT1D-like	101255449	-0.90
				protein_DETOXIFICATION_27	101265986	-1.87
				tonoplast_dicarboxylate_transporter-like	101257524	-6.01
				mitochondrial_adenine_nucleotide_transporter_ADNT1,_transcript_variant_X2	101268329	-2.68
				protein_PIN-LIKES_7-like	101263965	-2.35
				phosphoenolpyruvate/phosphate_translocator_2,_chloroplastic	101255257	-1.73
				mitochondrial_carrier_protein_MTM1,_transcript_variant_X2	101253663	-1.24
				putative_glycerol-3-phosphate_transporter_1	101259222	-3.20
				mitochondrial_outer_membrane_protein_porin_of_36_kDa-like	101246039	-2.08
				low_affinity_sulfate_transporter_3,_transcript_variant_X2	101245940	-3.48
				calcium-transporting_ATPase_1	101260132	0.60
				cyclic_nucleotide-gated_ion_channel_1-like,_transcript_variant_X1	101250508	0.81
				probable_sulfate_transporter_4.2-like	101257470	-0.68
				high_affinity_nitrate_transporter_2.4-like	101247028	-2.40
				probable_anion_transporter_6,_chloroplastic	101258970	-2.05
				protein_NRT1/_PTR_FAMILY_6.2	101268119	-2.28
				mitochondrial_carrier_protein_CoAc1	101253108	-0.48
				protein_NRT1/_PTR_FAMILY_7.3	101263538	-5.43
				plasma_membrane_intrinsic_protein_1.5	544086	-1.98

				solute_carrier_family_35_member_F2,_transcript_variant_X1	101258401	-1.02
				cation/H(+)_antiporter_20	101249848	-8.28
				sulfate_transporter_3.1	101264062	-2.71
				cation/calcium_exchanger_1	101248713	-1.89
				sulfate_transporter_3.1-like	101253320	-5.74
				aquaporin-5,_transcript_variant_X2	101251423	-3.32
				aquaporin_SIP1-2-like	101244430	0.73
				protein_NUCLEAR_FUSION_DEFECTIVE_4	101244433	-1.13
				cationic_amino_acid_transporter_7,_chloroplastic	101245518	-2.33
				protein_NRT1/_PTR_FAMILY_4.4-like	101268640	-2.79
				dicarboxylate_transporter_1,_chloroplastic	101250955	-2.88
				protein_NRT1/_PTR_FAMILY_6.4	101253972	-2.59
				protein_NRT1/_PTR_FAMILY_8.3-like,_transcript_variant_X1	101252061	1.43
				protein_PIN-LIKES_3-like,_transcript_variant_X1	101247117	-2.27

Table S6. GO enrichment, number of genes, pathways genes, fold enrichment, cellular component and gene NCBI ID for the DEGs of brown module.

Enrichment FDR	nGenes	Pathway Genes	Fold Enrichment	Description	Locus ID	LOG_2 (Fold-change)
GO:0009534 chloroplast thylakoid & GO:0031976 plastid thylakoid						
2.46E-15	25	203	9.14	ATP_synthase_gamma_chain,_chloroplastic	101253342	-0.71
				FtsH_protease	778337	-7.33
				uncharacterized_LOC101257421	101257421	-1.44
				uncharacterized_LOC101249904	101249904	-0.68
				uncharacterized_LOC101268563	101268563	-1.58
				light-harvesting_complex-like_protein_OHP2,_chloroplastic,_transcript_variant_X3	101253996	-1.41
				allene_oxide_synthase	606711	-1.90
				FtsH-like_protein_precursor	100037730	-1.25
				photosystem_II_subunit_S	101260830	-2.13
				light-harvesting_complex-like_protein_OHP1,_chloroplastic	101262449	-1.88
				early_light_inducible_protein	101257109	-3.49
				uncharacterized_LOC101252420	101252420	-3.30
				glutamine_synthetase,_transcript_variant_1	543998	-1.33
				PSII-associated_proline-rich_protein	543930	-1.48
				uncharacterized_LOC101259889	101259889	-2.17
				uncharacterized_protein_ycf39	101252442	-0.98
				photosystem_I_assembly_factor_PSA3,_chloroplastic	101249783	-0.63
				protein_LOW_PSII_ACCUMULATION_2,_chloroplastic	101250094	-0.76
				calcium_sensing_receptor,_chloroplastic	101268560	-2.31
				uncharacterized_LOC101259757	101259757	-1.37
				uncharacterized_LOC101250133	101250133	-3.67
				probable_plastid-lipid-associated_protein_8,_chloroplastic	101260745	-2.75
				putative_magnesium-protoporphyrin_monomethyl_ester_cyclase	101257518	-2.29
				dicarboxylate_transporter_1,_chloroplastic	101250955	-2.88
				cytochrome_b6-f_complex_iron-sulfur_subunit,_chloroplastic	101243864	-0.89
GO:0009941 chloroplast envelope						
2.45E-12	20	166	8.94	digalactosyldiacylglycerol_synthase_1,_chloroplastic-like	101266854	-1.23
				FtsH_protease	778337	-7.33
				allene_oxide_synthase	606711	-1.90

				FtsH-like_protein_precursor	100037730	-1.25
				protein_CHUP1,_chloroplastic	101267989	-1.24
				sulfoquinovosyl_transferase_SQD2	101252422	-0.90
				ADP-glucose_pyrophosphorylase_large_subunit	544039	-0.84
				glutamine_synthetase,_transcript_variant_1	543998	-1.33
				ATP_synthase_gamma_chain,_chloroplastic	101253342	-0.71
				photosystem_I_assembly_factor_PSA3,_chloroplastic	101249783	-0.63
				CBBY-like_protein	101257160	-1.14
				uncharacterized_LOC101253367,_transcript_variant_X1	101253367	-0.60
				beta-carotene_hydroxylase	544133	-4.05
				uncharacterized_LOC101259757	101259757	-1.37
				omega-6_fatty_acid_desaturase	101265653	-2.85
				translation_initiation_factor_IF-2,_chloroplastic	101254504	-0.91
				probable_plastid-lipid-associated_protein_8,_chloroplastic	101260745	-2.75
				putative_magnesium-protoporphyrin_monomethyl_ester_cyclase	101257518	-2.29
				dicarboxylate_transporter_1,_chloroplastic	101250955	-2.88
				cytochrome_b6-f_complex_iron-sulfur_subunit,_chloroplastic	101243864	-0.89
GO:0009535 chloroplast thylakoid membrane & GO:0055035 plastid thylakoid membrane						
7.92E-12	20	179	8.29	ATP_synthase_gamma_chain,_chloroplastic	101253342	-0.71
				FtsH_protease	778337	-7.33
				uncharacterized_LOC101249904	101249904	-0.68
				uncharacterized_LOC101268563	101268563	-1.58
				light-harvesting_complex-like_protein_OHP2,_chloroplastic,_transcript_variant_X3	101253996	-1.41
				allene_oxide_synthase	606711	-1.90
				FtsH-like_protein_precursor	100037730	-1.25
				photosystem_II_subunit_S	101260830	-2.13
				light-harvesting_complex-like_protein_OHP1,_chloroplastic	101262449	-1.88
				early_light_inducible_protein	101257109	-3.49
				uncharacterized_LOC101252420	101252420	-3.30
				glutamine_synthetase,_transcript_variant_1	543998	-1.33
				PSII-associated_proline-rich_protein	543930	-1.48
				uncharacterized_LOC101259889	101259889	-2.17
				photosystem_I_assembly_factor_PSA3,_chloroplastic	101249783	-0.63

				calcium_sensing_receptor,_chloroplastic	101268560	-2.31
				uncharacterized_LOC101259757	101259757	-1.37
				uncharacterized_LOC101250133	101250133	-3.67
				putative_magnesium-protoporphyrin_monomethyl_ester_cyclase	101257518	-2.29
				cytochrome_b6-f_complex_iron-sulfur_subunit,_chloroplastic	101243864	-0.89
GO:0042651 thylakoid membrane						
9.70E-12	21	204	7.64	ATP_synthase_gamma_chain,_chloroplastic	101253342	-0.71
				FtsH_protease	778337	-7.33
				uncharacterized_LOC101249904	101249904	-0.68
				uncharacterized_LOC101268563	101268563	-1.58
				light-harvesting_complex-like_protein_OHP2,_chloroplastic,_transcript_variant_X3	101253996	-1.41
				allene_oxide_synthase	606711	-1.90
				FtsH-like_protein_precursor	100037730	-1.25
				photosystem_II_subunit_S	101260830	-2.13
				light-harvesting_complex-like_protein_OHP1,_chloroplastic	101262449	-1.88
				early_light_inducible_protein	101257109	-3.49
				uncharacterized_LOC101252420	101252420	-3.30
				glutamine_synthetase,_transcript_variant_1	543998	-1.33
				PSII-associated_proline-rich_protein	543930	-1.48
				uncharacterized_LOC101259889	101259889	-2.17
				photosystem_I_assembly_factor_PSA3,_chloroplastic	101249783	-0.63
				calcium_sensing_receptor,_chloroplastic	101268560	-2.31
				uncharacterized_LOC101259757	101259757	-1.37
				uncharacterized_LOC101250133	101250133	-3.67
				putative_magnesium-protoporphyrin_monomethyl_ester_cyclase	101257518	-2.29
				psbP_domain-containing_protein_7,_chloroplastic,_transcript_variant_X1	101246302	-1.03
				cytochrome_b6-f_complex_iron-sulfur_subunit,_chloroplastic	101243864	-0.89
GO:0009526 plastid envelope						
6.47E-17	32	316	7.51	digalactosyldiacylglycerol_synthase_1,_chloroplastic-like	101266854	-1.23
				ATP_synthase_gamma_chain,_chloroplastic	101253342	-0.71
				FtsH_protease	778337	-7.33
				uncharacterized_LOC101249904	101249904	-0.68

				uncharacterized_LOC101268563	101268563	-1.58
				light-harvesting_complex-like_protein_OHP2,_chloroplastic,_transcript_variant_X3	101253996	-1.41
				allene_oxide_synthase	606711	-1.90
				FtsH-like_protein_precursor	100037730	-1.25
				protein_CHUP1,_chloroplastic	101267989	-1.24
				photosystem_II_subunit_S	101260830	-2.13
				light-harvesting_complex-like_protein_OHP1,_chloroplastic	101262449	-1.88
				sulfoquinovosyl_transferase_SQD2	101252422	-0.90
				early_light_inducible_protein	101257109	-3.49
				uncharacterized_LOC101252420	101252420	-3.30
				ADP-glucose_pyrophosphorylase_large_subunit	544039	-0.84
				glutamine_synthetase,_transcript_variant_1	543998	-1.33
				PSII-associated_proline-rich_protein	543930	-1.48
				uncharacterized_LOC101259889	101259889	-2.17
				photosystem_I_assembly_factor_PSA3,_chloroplastic	101249783	-0.63
				CBBY-like_protein	101257160	-1.14
				calcium_sensing_receptor,_chloroplastic	101268560	-2.31
				uncharacterized_LOC101253367,_transcript_variant_X1	101253367	-0.60
				beta-carotene_hydroxylase	544133	-4.05
				uncharacterized_LOC101259757	101259757	-1.37
				omega-6_fatty_acid_desaturase	101265653	-2.85
				translation_initiation_factor_IF-2,_chloroplastic	101254504	-0.91
				uncharacterized_LOC101250133	101250133	-3.67
				probable_plastid-lipid-associated_protein_8,_chloroplastic	101260745	-2.75
				fructose-1,6-bisphosphatase_1,_chloroplastic	101260852	-1.42
				putative_magnesium-protoporphyrin_monomethyl_ester_cyclase	101257518	-2.29
				dicarboxylate_transporter_1,_chloroplastic	101250955	-2.88
				cytochrome_b6-f_complex_iron-sulfur_subunit,_chloroplastic	101243864	-0.89
GO:0042170 plastid membrane						
2.65E-12	23	234	7.29	digalactosyldiacylglycerol_synthase_1,_chloroplastic-like	101266854	-1.23
				ATP_synthase_gamma_chain,_chloroplastic	101253342	-0.71
				FtsH_protease	778337	-7.33
				uncharacterized_LOC101249904	101249904	-0.68

				uncharacterized_LOC101268563	101268563	-1.58
				light-harvesting_complex-like_protein_OHP2,_chloroplastic,_transcript_variant_X3	101253996	-1.41
				allene_oxide_synthase	606711	-1.90
				FtsH-like_protein_precursor	100037730	-1.25
				protein_CHUP1,_chloroplastic	101267989	-1.24
				photosystem_II_subunit_S	101260830	-2.13
				light-harvesting_complex-like_protein_OHP1,_chloroplastic	101262449	-1.88
				early_light_inducible_protein	101257109	-3.49
				uncharacterized_LOC101252420	101252420	-3.30
				glutamine_synthetase,_transcript_variant_1	543998	-1.33
				PSII-associated_proline-rich_protein	543930	-1.48
				uncharacterized_LOC101259889	101259889	-2.17
				photosystem_I_assembly_factor_PSA3,_chloroplastic	101249783	-0.63
				calcium_sensing_receptor,_chloroplastic	101268560	-2.31
				beta-carotene_hydroxylase	544133	-4.05
				uncharacterized_LOC101259757	101259757	-1.37
				uncharacterized_LOC101250133	101250133	-3.67
				putative_magnesium-protoporphyrin_monomethyl_ester_cyclase	101257518	-2.29
				cytochrome_b6-f_complex_iron-sulfur_subunit,_chloroplastic	101243864	-0.89
GO:0009570 chloroplast stroma & GO:0009532 plastid stroma						
1.63E-09	18	191	6.99	uncharacterized_LOC101249904	101249904	-0.68
				ribulose_bisphosphate_carboxylase/oxygenase_activase_1,_chloroplastic,_transcript_variant_X2	101250725	-7.68
				uncharacterized_LOC101252420	101252420	-3.30
				ADP-glucose_pyrophosphorylase_large_subunit	544039	-0.84
				glutamine_synthetase,_transcript_variant_1	543998	-1.33
				prostamide/prostaglandin_F_synthase	101248840	-0.78
				photosystem_I_assembly_factor_PSA3,_chloroplastic	101249783	-0.63
				CBBY-like_protein	101257160	-1.14
				uncharacterized_LOC101253367,_transcript_variant_X1	101253367	-0.60
				clp_protease_adapter_protein_ClpF,_chloroplastic,_transcript_variant_X1	101251088	-0.95
				translation_initiation_factor_IF-2,_chloroplastic	101254504	-0.91

				ABC1-like_kinase_1,_transcript_variant_X1	101243810	-0.93
				glycerol-3-phosphate_acyltransferase,_transcript_variant_X3	543901	-0.66
				fructose-1,6-bisphosphatase_1,_chloroplastic	101260852	-1.42
				glutathione_reductase,_chloroplastic	100301931	-1.25
				30S_ribosomal_protein_S1,_transcript_variant_X1	101267163	-1.33
				uncharacterized_LOC101254243	101254243	-1.08
				uncharacterized_LOC101264805	101264805	-0.98
GO:0009579 thylakoid						
9.10E-13	27	315	6.36	ATP_synthase_gamma_chain,_chloroplastic	101253342	-0.71
				FtsH_protease	778337	-7.33
				uncharacterized_LOC101257421	101257421	-1.44
				uncharacterized_LOC101249904	101249904	-0.68
				uncharacterized_LOC101268563	101268563	-1.58
				light-harvesting_complex-like_protein_OHP2,_chloroplastic,_transcript_variant_X3	101253996	-1.41
				allene_oxide_synthase	606711	-1.90
				FtsH-like_protein_precursor	100037730	-1.25
				photosystem_II_subunit_S	101260830	-2.13
				light-harvesting_complex-like_protein_OHP1,_chloroplastic	101262449	-1.88
				ribulose_bisphosphate_carboxylase/oxygenase_activase_1,_chloroplastic,_transcript_variant_X2	101250725	-7.68
				early_light_inducible_protein	101257109	-3.49
				uncharacterized_LOC101252420	101252420	-3.30
				glutamine_synthetase,_transcript_variant_1	543998	-1.33
				PSII-associated_proline-rich_protein	543930	-1.48
				uncharacterized_LOC101259889	101259889	-2.17
				uncharacterized_protein_ycf39	101252442	-0.98
				photosystem_I_assembly_factor_PSA3,_chloroplastic	101249783	-0.63
				protein_LOW_PSII_ACCUMULATION_2,_chloroplastic	101250094	-0.76
				calcium_sensing_receptor,_chloroplastic	101268560	-2.31
				uncharacterized_LOC101259757	101259757	-1.37
				uncharacterized_LOC101250133	101250133	-3.67
				probable_plastid-lipid-associated_protein_8,_chloroplastic	101260745	-2.75

				putative_magnesium-protoporphyrin_monomethyl_ester_cyclase	101257518	-2.29
				psbP_domain-containing_protein_7,_chloroplastic,_transcript_variant_X1	101246302	-1.03
				dicarboxylate_transporter_1,_chloroplastic	101250955	-2.88
				cytochrome_b6-f_complex_iron-sulfur_subunit,_chloroplastic	101243864	-0.89
GO:0034357 photosynthetic membrane						
3.86E-10	21	248	6.28	ATP_synthase_gamma_chain,_chloroplastic	101253342	-0.71
				FtsH_protease	778337	-7.33
				uncharacterized_LOC101249904	101249904	-0.68
				uncharacterized_LOC101268563	101268563	-1.58
				light-harvesting_complex-like_protein_OHP2,_chloroplastic,_transcript_variant_X3	101253996	-1.41
				allene_oxide_synthase	606711	-1.90
				FtsH-like_protein_precursor	100037730	-1.25
				photosystem_II_subunit_S	101260830	-2.13
				light-harvesting_complex-like_protein_OHP1,_chloroplastic	101262449	-1.88
				early_light_inducible_protein	101257109	-3.49
				uncharacterized_LOC101252420	101252420	-3.30
				glutamine_synthetase,_transcript_variant_1	543998	-1.33
				PSII-associated_proline-rich_protein	543930	-1.48
				uncharacterized_LOC101259889	101259889	-2.17
				photosystem_I_assembly_factor_PSA3,_chloroplastic	101249783	-0.63
				calcium_sensing_receptor,_chloroplastic	101268560	-2.31
				uncharacterized_LOC101259757	101259757	-1.37
				uncharacterized_LOC101250133	101250133	-3.67
				putative_magnesium-protoporphyrin_monomethyl_ester_cyclase	101257518	-2.29
				psbP_domain-containing_protein_7,_chloroplastic,_transcript_variant_X1	101246302	-1.03
				cytochrome_b6-f_complex_iron-sulfur_subunit,_chloroplastic	101243864	-0.89
GO:0009536 plastid & GO:0009507 chloroplast						
4.20E-34	76	957	5.89	digalactosyldiacylglycerol_synthase_1,_chloroplastic-like	101266854	-1.23
				uncharacterized_LOC101262956	101262956	-1.30
				presequence_protease_1,_chloroplastic/mitochondrial-like,_transcript_variant_X2	101250549	-1.82
				pheophytinase,_chloroplastic	101268836	-2.67

				ATP_synthase_gamma_chain,_chloroplastic	101253342	-0.71
				FtsH_protease	778337	-7.33
				uncharacterized_LOC101257421	101257421	-1.44
				protein_LOW_PSII_ACCUMULATION_2,_chloroplastic	101250094	-0.76
				quinolinate_synthase,_chloroplastic	101246910	-1.29
				uncharacterized_LOC101249904	101249904	-0.68
				glyceraldehyde-3-phosphate_dehydrogenase_A,_chloroplastic	101266713	-1.14
				uncharacterized_LOC101268563	101268563	-1.58
				magnesium-chelatase_subunit_ChlH,_chloroplastic	101244176	-4.10
				light-harvesting_complex-like_protein_OHP2,_chloroplastic,_transcript_variant_X3	101253996	-1.41
				allene_oxide_synthase	606711	-1.90
				FtsH-like_protein_precursor	100037730	-1.25
				glyceraldehyde-3-phosphate_dehydrogenase_B,_chloroplastic	101264004	-1.02
				protein_CHUP1,_chloroplastic	101267989	-1.24
				clp_protease_adapter_protein_ClpF,_chloroplastic,_transcript_variant_X1	101251088	-0.95
				cytosolic_NADP-malic_enzyme	543522	0.74
				uncharacterized_LOC101259047	101259047	-1.25
				photosystem_II_subunit_S	101260830	-2.13
				tetrapyrrole-binding_protein,_chloroplastic	101252496	-1.97
				uncharacterized_LOC101259757	101259757	-1.37
				probable_anion_transporter_6,_chloroplastic	101258970	-2.05
				phosphoenolpyruvate_carboxylase-like	101248407	-1.42
				uncharacterized_LOC101250133	101250133	-3.67
				solanesyl_diphosphate_synthase	101253007	-2.13
				phosphoribulokinase,_chloroplastic	101255322	-1.43
				light-harvesting_complex-like_protein_OHP1,_chloroplastic	101262449	-1.88
				ribulose_bisphosphate_carboxylase/oxygenase_activase_1,_chloroplastic,_transcript_variant_X2	101250725	-7.68
				sulfoquinovosyl_transferase_SQD2	101252422	-0.90
				early_light_inducible_protein	101257109	-3.49
				protein_PROTON_GRADIENT_REGULATION_5,_chloroplastic	101262255	-4.24
				ferredoxin	101265784	-2.18

				senescence-associated_protein_SPA15,_chloroplastic,_transcript_variant_X1	101257426	-1.67
				NADP-malic_enzyme	544164	-1.64
				glyceraldehyde-3-phosphate_dehydrogenase_B,_chloroplastic-like	101249445	-2.70
				uncharacterized_LOC101252420	101252420	-3.30
				ADP-glucose_pyrophosphorylase_large_subunit	544039	-0.84
				glutamine_synthetase,_transcript_variant_1	543998	-1.33
				PSII-associated_proline-rich_protein	543930	-1.48
				uncharacterized_LOC101259889	101259889	-2.17
				uncharacterized_protein_ycf39	101252442	-0.98
				malate_dehydrogenase,_glyoxysomal	101249428	0.53
				prostamide/prostaglandin_F_synthase	101248840	-0.78
				starch_synthase_III	100316882	-0.88
				phytoene_synthase_2,_chloroplastic,_transcript_variant_X1	543964	-0.73
				ribulose_bisphosphate_carboxylase_small_chain_3B,_chloroplastic-like,_transcript_variant_X1	101268337	-1.33
				photosystem_I_assembly_factor_PSA3,_chloroplastic	101249783	-0.63
				uncharacterized_LOC101252498	543988	-5.54
				ribulose_bisphosphate_carboxylase_small_chain_2A,_chloroplastic	543974	-0.69
				CBBY-like_protein	101257160	-1.14
				calcium_sensing_receptor,_chloroplastic	101268560	-2.31
				uncharacterized_LOC101253367,_transcript_variant_X1	101253367	-0.60
				lycopene_beta-cyclase,_transcript_variant_1	544104	-1.92
				anthranilate_synthase_alpha_subunit_2,_chloroplastic	101265030	1.01
				beta-carotene_hydroxylase	544133	-4.05
				omega-6_fatty_acid_desaturase	101265653	-2.85
				translation_initiation_factor_IF-2,_chloroplastic	101254504	-0.91
				probable_plastid-lipid-associated_protein_8,_chloroplastic	101260745	-2.75
				putative_leucine-rich_repeat-containing_protein_DDB_G0290503,_transcript_variant_X1	101265150	-0.79
				ABC1-like_kinase_1,_transcript_variant_X1	101243810	-0.93
				glycerol-3-phosphate_acyltransferase,_transcript_variant_X3	543901	-0.66

				elongation_factor_G,_chloroplastic	101245683	-1.80
				fructose-1,6-bisphosphatase_1,_chloroplastic	101260852	-1.42
				sulfate_transporter_3.1	101264062	-2.71
				glutathione_reductase,_chloroplastic	100301931	-1.25
				sulfate_transporter_3.1-like	101253320	-5.74
				30S_ribosomal_protein_S1,_transcript_variant_X1	101267163	-1.33
				uncharacterized_LOC101254243	101254243	-1.08
				putative_magnesium-protoporphyrin_monomethyl_ester_cyclase	101257518	-2.29
				dicarboxylate_transporter_1,_chloroplastic	101250955	-2.88
				cytochrome_b6-f_complex_iron-sulfur_subunit,_chloroplastic	101243864	-0.89
				2-phytyl-1,4-beta-naphthoquinone_methyltransferase,_chloroplastic,_transcript_variant_X1	101263675	-0.56
				uncharacterized_LOC101264805	101264805	-0.98
GO:0048046 apoplast						
0.001012352	8	108	5.50	glyceraldehyde-3-phosphate_dehydrogenase_A,_chloroplastic	101266713	-1.14
				glyceraldehyde-3-phosphate_dehydrogenase_B,_chloroplastic	101264004	-1.02
				phosphoenolpyruvate_carboxylase-like	101248407	-1.42
				glyceraldehyde-3-phosphate_dehydrogenase_B,_chloroplastic-like	101249445	-2.70
				glutamine_synthetase,_transcript_variant_1	543998	-1.33
				uncharacterized_LOC101253367,_transcript_variant_X1	101253367	-0.60
				probable_xyloglucan_endotransglucosylase/hydrolase_protein_30	101263927	-2.01
				fructose-1,6-bisphosphatase_1,_chloroplastic	101260852	-1.42
GO:0031984 organelle subcompartment						
3.23E-13	35	524	4.96	lipid_phosphate_phosphatase_epsilon_2,_chloroplastic	101244637	-1.50
				ATP_synthase_gamma_chain,_chloroplastic	101253342	-0.71
				FtsH_protease	778337	-7.33
				uncharacterized_LOC101257421	101257421	-1.44
				palmitoyl-monogalactosyldiacylglycerol_delta-7_desaturase,_chloroplastic	101250586	-3.29
				uncharacterized_LOC101249904	101249904	-0.68
				uncharacterized_LOC101268563	101268563	-1.58

				light-harvesting_complex-like_protein_OHP2,_chloroplastic,_transcript_variant_X3	101253996	-1.41
				allene_oxide_synthase	606711	-1.90
				FtsH-like_protein_precursor	100037730	-1.25
				photosystem_II_subunit_S	101260830	-2.13
				cellulose_synthase-like_protein_H1	101259456	-3.99
				light-harvesting_complex-like_protein_OHP1,_chloroplastic	101262449	-1.88
				early_light_inducible_protein	101257109	-3.49
				signal_peptide_peptidase-like_4,_transcript_variant_X1	101252725	0.62
				signal_peptide_peptidase-like	101259808	0.82
				cell_division_cycle_protein_48_homolog,_transcript_variant_X1	101265798	0.53
				novel_plant_SNARE_13-like	101248280	-0.62
				uncharacterized_LOC101252420	101252420	-3.30
				glutamine_synthetase,_transcript_variant_1	543998	-1.33
				PSII-associated_proline-rich_protein	543930	-1.48
				uncharacterized_LOC101259889	101259889	-2.17
				uncharacterized_protein_ycf39	101252442	-0.98
				photosystem_I_assembly_factor_PSA3,_chloroplastic	101249783	-0.63
				protein_LOW_PSII_ACCUMULATION_2,_chloroplastic	101250094	-0.76
				calcium_sensing_receptor,_chloroplastic	101268560	-2.31
				uncharacterized_LOC101268558,_transcript_variant_X1	101268558	0.41
				inactive_leucine-rich_repeat_receptor-like_protein_kinase_CORYNE,_transcript_variant_X1	101055499	-0.46
				uncharacterized_LOC101259757	101259757	-1.37
				NADPH--cytochrome_P450_reductase	101247036	-1.43
				uncharacterized_LOC101250133	101250133	-3.67
				probable_plastid-lipid-associated_protein_8,_chloroplastic	101260745	-2.75
				putative_magnesium-protoporphyrin_monomethyl_ester_cyclase	101257518	-2.29
				dicarboxylate_transporter_1,_chloroplastic	101250955	-2.88
				cytochrome_b6-f_complex_iron-sulfur_subunit,_chloroplastic	101243864	-0.89
GO:0031967 organelle envelope & GO:0031975 envelope						
1.79E-12	35	563	4.61	digalactosyldiacylglycerol_synthase_1,_chloroplastic-like	101266854	-1.23
				ATP_synthase_gamma_chain,_chloroplastic	101253342	-0.71

				FtsH_protease	778337	-7.33
				uncharacterized_LOC101246002,_transcript_variant_X1	101246002	-1.01
				uncharacterized_LOC101249904	101249904	-0.68
				uncharacterized_LOC101268563	101268563	-1.58
				light-harvesting_complex-like_protein_OHP2,_chloroplastic,_transcript_variant_X3	101253996	-1.41
				allene_oxide_synthase	606711	-1.90
				FtsH-like_protein_precursor	100037730	-1.25
				protein_CHUP1,_chloroplastic	101267989	-1.24
				photosystem_II_subunit_S	101260830	-2.13
				light-harvesting_complex-like_protein_OHP1,_chloroplastic	101262449	-1.88
				sulfoquinovosyl_transferase_SQD2	101252422	-0.90
				early_light_inducible_protein	101257109	-3.49
				uncharacterized_LOC101252420	101252420	-3.30
				ADP-glucose_pyrophosphorylase_large_subunit	544039	-0.84
				glutamine_synthetase,_transcript_variant_1	543998	-1.33
				PSII-associated_proline-rich_protein	543930	-1.48
				nuclear_envelope-associated_protein_2,_transcript_variant_X1	101263162	-0.86
				uncharacterized_LOC101259889	101259889	-2.17
				photosystem_I_assembly_factor_PSA3,_chloroplastic	101249783	-0.63
				CBBY-like_protein	101257160	-1.14
				mitochondrial_outer_membrane_protein_porin_of_36_kDa-like	101246039	-2.08
				calcium_sensing_receptor,_chloroplastic	101268560	-2.31
				uncharacterized_LOC101253367,_transcript_variant_X1	101253367	-0.60
				beta-carotene_hydroxylase	544133	-4.05
				uncharacterized_LOC101259757	101259757	-1.37
				omega-6_fatty_acid_desaturase	101265653	-2.85
				translation_initiation_factor_IF-2,_chloroplastic	101254504	-0.91
				uncharacterized_LOC101250133	101250133	-3.67
				probable_plastid-lipid-associated_protein_8,_chloroplastic	101260745	-2.75
				fructose-1,6-bisphosphatase_1,_chloroplastic	101260852	-1.42
				putative_magnesium-protoporphyrin_monomethyl_ester_cyclase	101257518	-2.29
				dicarboxylate_transporter_1,_chloroplastic	101250955	-2.88

				cytochrome_b6-f_complex_iron-sulfur_subunit,_chloroplastic	101243864	-0.89
GO:0005773 vacuole						
0.000430787	13	253	3.81	vacuolar_cation/proton_exchanger_3-like	101265339	-2.00
				high_affinity_nitrate_transporter_2.4-like	101247028	-2.40
				alpha-mannosidase	100500729	0.47
				plasma_membrane_intrinsic_protein_1.5	544086	-1.98
				signal_peptide_peptidase-like_4,_transcript_variant_X1	101252725	0.62
				amino_acid_transporter_AVT1D-like	101255449	-0.90
				uncharacterized_LOC101250355	101250355	-2.37
				heme-binding-like_protein_At3g10130,_chloroplastic	101251239	-1.48
				serine_carboxypeptidase-like	101258820	-1.62
				protein_NRT1/_PTR_FAMILY_8.3-like,_transcript_variant_X1	101252061	1.43
				tobamovirus_multiplication_protein_2A,_transcript_variant_X1	101262238	-0.46
				tonoplast_dicarboxylate_transporter-like	101257524	-6.01
				uncharacterized_LOC101257239	101257239	-2.33
GO:0031090 organelle membrane						
2.22E-09	40	940	3.16	digalactosyldiacylglycerol_synthase_1,_chloroplastic-like	101266854	-1.23
				lipid_phosphate_phosphatase_epsilon_2,_chloroplastic	101244637	-1.50
				ATP_synthase_gamma_chain,_chloroplastic	101253342	-0.71
				FtsH_protease	778337	-7.33
				peroxisomal_membrane_protein_11B	101259820	-2.47
				palmitoyl-monogalactosyldiacylglycerol_delta-7_desaturase,_chloroplastic	101250586	-3.29
				uncharacterized_LOC101249904	101249904	-0.68
				uncharacterized_LOC101268563	101268563	-1.58
				light-harvesting_complex-like_protein_OHP2,_chloroplastic,_transcript_variant_X3	101253996	-1.41
				allene_oxide_synthase	606711	-1.90
				FtsH-like_protein_precursor	100037730	-1.25
				protein_CHUP1,_chloroplastic	101267989	-1.24
				vacuolar_cation/proton_exchanger_3-like	101265339	-2.00
				high_affinity_nitrate_transporter_2.4-like	101247028	-2.40
				photosystem_II_subunit_S	101260830	-2.13
				alpha-mannosidase	100500729	0.47

				light-harvesting_complex-like_protein_OHP1,_chloroplastic	101262449	-1.88
				early_light_inducible_protein	101257109	-3.49
				signal_peptide_peptidase-like_4,_transcript_variant_X1	101252725	0.62
				amino_acid_transporter_AVT1D-like	101255449	-0.90
				signal_peptide_peptidase-like	101259808	0.82
				cell_division_cycle_protein_48_homolog,_transcript_variant_X1	101265798	0.53
				protein_NRT1/_PTR_FAMILY_8.3-like,_transcript_variant_X1	101252061	1.43
				novel_plant_SNARE_13-like	101248280	-0.62
				uncharacterized_LOC101252420	101252420	-3.30
				glutamine_synthetase,_transcript_variant_1	543998	-1.33
				PSII-associated_proline-rich_protein	543930	-1.48
				uncharacterized_LOC101259889	101259889	-2.17
				photosystem_I_assembly_factor_PSA3,_chloroplastic	101249783	-0.63
				mitochondrial_outer_membrane_protein_porin_of_36_kDa-like	101246039	-2.08
				calcium_sensing_receptor,_chloroplastic	101268560	-2.31
				arabinosyltransferase_RRA3	101253890	0.53
				inactive_leucine-rich_repeat_receptor-like_protein_kinase_CORYNE,_transcript_variant_X1	101055499	-0.46
				beta-carotene_hydroxylase	544133	-4.05
				uncharacterized_LOC101259757	101259757	-1.37
				NADPH--cytochrome_P450_reductase	101247036	-1.43
				uncharacterized_LOC101250133	101250133	-3.67
				tobamovirus_multiplication_protein_2A,_transcript_variant_X1	101262238	-0.46
				putative_magnesium-protoporphyrin_monomethyl_ester_cyclase	101257518	-2.29
				cytochrome_b6-f_complex_iron-sulfur_subunit,_chloroplastic	101243864	-0.89

Table S7. GO enrichment, number of genes, pathways genes, fold enrichment, molecular function and gene NCBI ID for the DEGs of brown module.

Enrichment FDR	nGenes	Pathway Genes	Fold Enrichment	Description	Locus ID	LOG_2 (Fold-change)
GO:0015301 anion:anion antiporter activity & GO:0140323 solute:anion antiporter activity						
2.25E-04	4	10	29.7	low_affinity_sulfate_transporter_3,_transcript_variant_X2	101245940	-3.48
				probable_sulfate_transporter_4.2-like	101257470	-0.68
				sulfate_transporter_3.1	101264062	-2.71
				sulfate_transporter_3.1-like	101253320	-5.74
GO:0008271 secondary active sulfate transmembrane transporter activity & GO:0015116 sulfate transmembrane transporter activity						
9.44E-04	4	15	19.8	low_affinity_sulfate_transporter_3,_transcript_variant_X2	101245940	-3.48
				probable_sulfate_transporter_4.2-like	101257470	-0.68
				sulfate_transporter_3.1	101264062	-2.71
				sulfate_transporter_3.1-like	101253320	-5.74
GO:0050661 NADP binding						
5.05E-04	7	62	8.4	1-deoxy-D-xylulose-5-phosphate_reductoisomerase	543682	-1.09
				glyceraldehyde-3-phosphate_dehydrogenase_A,_chloroplastic	101266713	-1.14
				glyceraldehyde-3-phosphate_dehydrogenase_B,_chloroplastic	101264004	-1.02
				glucose-6-phosphate_1-dehydrogenase,_chloroplastic	101253589	-0.66
				NADPH--cytochrome_P450_reductase	101247036	-1.43
				glutathione_reductase,_chloroplastic	100301931	-1.25
				glyceraldehyde-3-phosphate_dehydrogenase_B,_chloroplastic-like	101249445	-2.70
GO:0015103 inorganic anion transmembrane transporter activity						
2.37E-04	8	75	7.9	low_affinity_sulfate_transporter_3,_transcript_variant_X2	101245940	-3.48
				probable_sulfate_transporter_4.2-like	101257470	-0.68
				high_affinity_nitrate_transporter_2.4-like	101247028	-2.40
				protein_NRT1/_PTR_FAMILY_7.3	101263538	-5.43
				sulfate_transporter_3.1	101264062	-2.71
				sulfate_transporter_3.1-like	101253320	-5.74
				phosphoenolpyruvate/phosphate_translocator_2,_chloroplastic	101255257	-1.73
				mitochondrial_outer_membrane_protein_porin_of_36_kDa-like	101246039	-2.08

GO:0051287 NAD binding						
1.08E-04	10	108	6.9	glyceraldehyde-3-phosphate_dehydrogenase_A,_chloroplastic	101266713	-1.14
				UDP-glucuronic_acid_decarboxylase_6,_transcript_variant_X1	101263507	0.45
				glyceraldehyde-3-phosphate_dehydrogenase_B,_chloroplastic	101264004	-1.02
				glyceraldehyde-3-phosphate_dehydrogenase_B,_chloroplastic-like	101249445	-2.70
				GDP-mannose_3',5'-epimerase	100316902	-1.80
				glycerate_dehydrogenase	100191110	-1.58
				cytosolic_NADP-malic_enzyme	543522	0.74
				GDP-mannose_3',5'-epimerase	100316874	-0.95
				uncharacterized_LOC101244164	101244164	-1.05
				NADP-malic_enzyme	544164	-1.64
GO:0008509 anion transmembrane transporter activity						
5.18E-05	11	121	6.7	low_affinity_sulfate_transporter_3,_transcript_variant_X2	101245940	-3.48
				probable_sulfate_transporter_4.2-like	101257470	-0.68
				high_affinity_nitrate_transporter_2.4-like	101247028	-2.40
				protein_NRT1/_PTR_FAMILY_7.3	101263538	-5.43
				sulfate_transporter_3.1	101264062	-2.71
				sulfate_transporter_3.1-like	101253320	-5.74
				mitochondrial_carnitine/acylcarnitine_carrier-like_protein,_transcript_variant_2	101262875	-2.05
				phosphoenolpyruvate/phosphate_translocator_2,_chloroplastic	101255257	-1.73
				mitochondrial_outer_membrane_protein_porin_of_36_kDa-like	101246039	-2.08
				tonoplast_dicarboxylate_transporter-like	101257524	-6.01
				dicarboxylate_transporter_1,_chloroplastic	101250955	-2.88
GO:0015297 antiporter activity						
5.18E-05	12	143	6.2	low_affinity_sulfate_transporter_3,_transcript_variant_X2	101245940	-3.48
				probable_sulfate_transporter_4.2-like	101257470	-0.68
				vacuolar_cation/proton_exchanger_3-like	101265339	-2.00
				sulfate_transporter_3.1	101264062	-2.71
				sulfate_transporter_3.1-like	101253320	-5.74
				protein_DETOXIFICATION_40	101255252	0.80

				phosphoenolpyruvate/phosphate_translocator_2,_chloroplastic	101255257	-1.73
				protein_DETOXIFICATION_14-like,_transcript_variant_X1	101261991	-2.41
				cation/H(+)_antiporter_20	101249848	-8.28
				protein_DETOXIFICATION_18	101265483	-1.44
				protein_DETOXIFICATION_24	101257226	-1.78
				protein_DETOXIFICATION_27	101265986	-1.87
GO:0051536 iron-sulfur cluster binding and GO:0051540 metal cluster binding						
2.25E-04	10	122	6.1	quinolinate_synthase,_chloroplastic	101246910	-1.29
				aconitate_hydratase,_cytoplasmic	101248455	0.58
				nitrite_reductase	778325	-1.81
				amidophosphoribosyltransferase,_chloroplastic	101250934	-1.52
				CDGSH_iron-sulfur_domain-containing_protein	101244055	-1.98
				uncharacterized_LOC101254243	101254243	-1.08
				ferredoxin	101265784	-2.18
				chlorophyllide_a_oxygenase,_chloroplastic-like	101244441	-3.22
				uncharacterized_LOC101267576	101267576	-1.68
				cytochrome_b6-f_complex_iron-sulfur_subunit,_chloroplastic	101243864	-0.89
GO:0016830 carbon-carbon lyase activity						
2.37E-04	10	125	5.9	S-adenosylmethionine_decarboxylase_2,_transcript_variant_X1	101260400	-2.43
				UDP-glucuronic_acid_decarboxylase_6,_transcript_variant_X1	101263507	0.45
				phosphoenolpyruvate_carboxylase-like	101248407	-1.42
				fructose_1,6-bisphosphate_aldolase_1	101246870	-2.78
				fructose-bisphosphate_aldolase	101249787	-2.82
				ribulose_bisphosphate_carboxylase_small_chain_3B,_chloroplastic-like,_transcript_variant_X1	101268337	-1.33
				kinesin-like_protein_KIN-14B	543974	-1.62
				cytosolic_NADP-malic_enzyme	543522	0.74
				anthranilate_synthase_alpha_subunit_2,_chloroplastic	101265030	1.01
				NADP-malic_enzyme	544164	-1.64
GO:0015291 secondary active transmembrane transporter activity						
2.11E-07	19	241	5.8	monosaccharide-sensing_protein_2-like	101261393	-1.09
				low_affinity_sulfate_transporter_3,_transcript_variant_X2	101245940	-3.48
				inorganic_phosphate_transporter_2-1,_chloroplastic	101267311	-2.04

				probable_sulfate_transporter_4.2-like	101257470	-0.68
				vacuolar_cation/proton_exchanger_3-like	101265339	-2.00
				probable_anion_transporter_6,_chloroplastic	101258970	-2.05
				protein_NRT1/_PTR_FAMILY_6.2	101268119	-2.28
				sulfate_transporter_3.1	101264062	-2.71
				sulfate_transporter_3.1-like	101253320	-5.74
				protein_NRT1/_PTR_FAMILY_4.4-like	101268640	-2.79
				protein_NRT1/_PTR_FAMILY_6.4	101253972	-2.59
				protein_NRT1/_PTR_FAMILY_8.3-like,_transcript_variant_X1	101252061	1.43
				protein_DETOXIFICATION_40	101255252	0.80
				phosphoenolpyruvate/phosphate_translocator_2,_chloroplastic	101255257	-1.73
				protein_DETOXIFICATION_14-like,_transcript_variant_X1	101261991	-2.41
				cation/H(+)_antiporter_20	101249848	-8.28
				protein_DETOXIFICATION_18	101265483	-1.44
				protein_DETOXIFICATION_24	101257226	-1.78
				protein_DETOXIFICATION_27	101265986	-1.87
GO:0016829 lyase activity						
5.18E-05	19	368	3.8	S-adenosylmethionine_decarboxylase_2,_transcript_variant_X1	101260400	-2.43
				UDP-glucuronic_acid_decarboxylase_6,_transcript_variant_X1	101263507	0.45
				probable_pyridoxal_5'-phosphate_synthase_subunit_PDX1	101257782	-1.66
				phosphoenolpyruvate_carboxylase-like	101248407	-1.42
				aconitate_hydratase,_cytoplasmic	101248455	0.58
				bifunctional_L-3-cyanoalanine_synthase/cysteine_synthase_2,_mitochondrial	101255033	-1.02
				(E)-beta-ocimene_synthase	101247865	-2.08
				fructose_1,6-bisphosphate_aldolase_1	101246870	-2.78
				fructose-bisphosphate_aldolase	101249787	-2.82
				lactoylglutathione_lyase	101251435	-1.91
				ribulose_bisphosphate_carboxylase_small_chain_3B,_chloroplastic-like,_transcript_variant_X1	101268337	-1.33
				ribulose_bisphosphate_carboxylase_small_chain_2A,_chloroplastic	543974	-0.69
				L-tryptophan--pyruvate_aminotransferase_1-like	101262607	-4.41

				allene_oxide_synthase	606711	-1.90
				glutamate--glyoxylate_aminotransferase_2	101265236	-1.97
				cytosolic_NADP-malic_enzyme	543522	0.74
				anthranilate_synthase_alpha_subunit_2,_chloroplastic	101265030	1.01
				strictosidine_synthase_1	101244135	-2.30
				NADP-malic_enzyme	544164	-1.64
GO:0015318 inorganic molecular entity transmembrane transporter activity						
9.40E-05	22	502	3.3	monosaccharide-sensing_protein_2-like	101261393	-1.09
				low_affinity_sulfate_transporter_3,_transcript_variant_X2	101245940	-3.48
				calcium-transporting_ATPase_1	101260132	0.60
				inorganic_phosphate_transporter_2-1,_chloroplastic	101267311	-2.04
				probable_sulfate_transporter_4.2-like	101257470	-0.68
				vacuolar_cation/proton_exchanger_3-like	101265339	-2.00
				high_affinity_nitrate_transporter_2.4-like	101247028	-2.40
				probable_anion_transporter_6,_chloroplastic	101258970	-2.05
				protein_NRT1/_PTR_FAMILY_6.2	101268119	-2.28
				protein_NRT1/_PTR_FAMILY_7.3	101263538	-5.43
				plasma_membrane_intrinsic_protein_1.5	544086	-1.98
				sulfate_transporter_3.1	101264062	-2.71
				sulfate_transporter_3.1-like	101253320	-5.74
				protein_NRT1/_PTR_FAMILY_4.4-like	101268640	-2.79
				protein_NRT1/_PTR_FAMILY_6.4	101253972	-2.59
				protein_NRT1/_PTR_FAMILY_8.3-like,_transcript_variant_X1	101252061	1.43
				probable_magnesium_transporter_NIPA4	101246186	-0.92
				ATP_synthase_gamma_chain,_chloroplastic	101253342	-0.71
				phosphoenolpyruvate/phosphate_translocator_2,_chloroplastic	101255257	-1.73
				mitochondrial_outer_membrane_protein_porin_of_36_kDa-like	101246039	-2.08
				cyclic_nucleotide-gated_ion_channel_1-like,_transcript_variant_X1	101250508	0.81
				aquaporin_SIP1-2-like	101244430	0.73
GO:0015075 ion transmembrane transporter activity						
2.37E-04	21	514	3.0	monosaccharide-sensing_protein_2-like	101261393	-1.09
				low_affinity_sulfate_transporter_3,_transcript_variant_X2	101245940	-3.48

				calcium-transporting_ATPase_1	101260132	0.60
				probable_sulfate_transporter_4.2-like	101257470	-0.68
				vacuolar_cation/proton_exchanger_3-like	101265339	-2.00
				high_affinity_nitrate_transporter_2.4-like	101247028	-2.40
				protein_NRT1/_PTR_FAMILY_6.2	101268119	-2.28
				protein_NRT1/_PTR_FAMILY_7.3	101263538	-5.43
				sulfate_transporter_3.1	101264062	-2.71
				sulfate_transporter_3.1-like	101253320	-5.74
				mitochondrial_carnitine/acylcarnitine_carrier-like_protein,_transcript_variant_2	101262875	-2.05
				protein_NRT1/_PTR_FAMILY_4.4-like	101268640	-2.79
				protein_NRT1/_PTR_FAMILY_6.4	101253972	-2.59
				protein_NRT1/_PTR_FAMILY_8.3-like,_transcript_variant_X1	101252061	1.43
				probable_magnesium_transporter_NIPA4	101246186	-0.92
				ATP_synthase_gamma_chain,_chloroplastic	101253342	-0.71
				phosphoenolpyruvate/phosphate_translocator_2,_chloroplastic	101255257	-1.73
				mitochondrial_outer_membrane_protein_porin_of_36_kDa-like	101246039	-2.08
				cyclic_nucleotide-gated_ion_channel_1-like,_transcript_variant_X1	101250508	0.81
				tonoplast_dicarboxylate_transporter-like	101257524	-6.01
				dicarboxylate_transporter_1,_chloroplastic	101250955	-2.88
GO:0022804 active transmembrane transporter activity						
2.73E-04	21	521	3.0	monosaccharide-sensing_protein_2-like	101261393	-1.09
				low_affinity_sulfate_transporter_3,_transcript_variant_X2	101245940	-3.48
				calcium-transporting_ATPase_1	101260132	0.60
				inorganic_phosphate_transporter_2-1,_chloroplastic	101267311	-2.04
				probable_sulfate_transporter_4.2-like	101257470	-0.68
				vacuolar_cation/proton_exchanger_3-like	101265339	-2.00
				probable_anion_transporter_6,_chloroplastic	101258970	-2.05
				protein_NRT1/_PTR_FAMILY_6.2	101268119	-2.28
				sulfate_transporter_3.1	101264062	-2.71
				sulfate_transporter_3.1-like	101253320	-5.74
				protein_NRT1/_PTR_FAMILY_4.4-like	101268640	-2.79

				protein_NRT1/_PTR_FAMILY_6.4	101253972	-2.59
				protein_NRT1/_PTR_FAMILY_8.3-like,_transcript_variant_X1	101252061	1.43
				protein_DETOXIFICATION_40	101255252	0.80
				phosphoenolpyruvate/phosphate_translocator_2,_chloroplastic	101255257	-1.73
				protein_DETOXIFICATION_14-like,_transcript_variant_X1	101261991	-2.41
				cation/H(+)_antiporter_20	101249848	-8.28
				protein_DETOXIFICATION_18	101265483	-1.44
				protein_DETOXIFICATION_24	101257226	-1.78
				protein_DETOXIFICATION_27	101265986	-1.87
				cytochrome_b6-f_complex_iron-sulfur_subunit,_chloroplastic	101243864	-0.89
GO:0016491 oxidoreductase activity						
6.73E-08	60	1813	2.5	NAD(P)H:quinone_oxidoreductase	101265773	2.25
				glyoxisomal_malate_dehydrogenase	778286	-1.12
				glycerate_dehydrogenase	100191110	-1.58
				catalase_2	543585	-2.70
				gibberellin_20-oxidase-1	543553	-2.10
				probable_2-oxoglutarate-dependent_dioxygenase_At5g05600	101260801	-1.57
				cytochrome_P450_71A3-like	101248089	-3.58
				1-deoxy-D-xylulose-5-phosphate_reductoisomerase	543682	-1.09
				palmitoyl-monogalactosyldiacylglycerol_delta-7_desaturase,_chloroplastic	101250586	-3.29
				glyceraldehyde-3-phosphate_dehydrogenase_A,_chloroplastic	101266713	-1.14
				lycopene_beta-cyclase,_transcript_variant_1	544104	-1.92
				cytochrome_P450_CYP736A12	101245153	1.67
				xanthoxin_dehydrogenase,_transcript_variant_X1	101254297	-0.69
				allene_oxide_synthase	606711	-1.90
				glyceraldehyde-3-phosphate_dehydrogenase_B,_chloroplastic	101264004	-1.02
				cytosolic_NADP-malic_enzyme	543522	0.74
				NADP-dependent_glyceraldehyde-3-phosphate_dehydrogenase,_transcript_variant_X1	101262732	-3.42
				NADPH--cytochrome_P450_reductase	101247036	-1.43
				probable_polyamine_oxidase_5	101244015	-1.96
				probable_polyamine_oxidase_2	101252005	-1.52

				4-hydroxyphenylpyruvate_dioxygenase	101245475	-0.64
				glutathione_reductase,_chloroplastic	100301931	-1.25
				1,2-dihydroxy-3-keto-5-methylthiopentene_dioxygenase_1,_transcript_variant_1	101255136	-2.44
				protein_PROTON_GRADIENT_REGULATION_5,_chloroplastic	101262255	-4.24
				thioredoxin_1	101268617	-1.52
				3-oxo-5-alpha-steroid_4-dehydrogenase_1	101255051	-4.58
				very-long-chain_enoyl-CoA_reductase	101255353	-6.68
				cytochrome_P450_77_A20	101250470	-3.68
				uncharacterized_LOC101244164	101244164	-1.05
				NADP-malic_enzyme	544164	-1.64
				glyceraldehyde-3-phosphate_dehydrogenase_B,_chloroplastic-like	101249445	-2.70
				linoleate_9S-lipoxygenase-like	107648852	-1.76
				(+)-neomenthol_dehydrogenase-like,_transcript_variant_X3	101268235	-6.35
				ferric_reduction_oxidase_6	101246763	-5.48
				nitrite_reductase	778325	-1.81
				5'-adenylylsulfate_reductase_3,_chloroplastic	101257319	-1.65
				malate_dehydrogenase,_glyoxysomal	101249428	0.53
				ribulose_bisphosphate_carboxylase_small_chain_3B,_chloroplastic-like,_transcript_variant_X1	101268337	-1.33
				ribulose_bisphosphate_carboxylase_small_chain_2A,_chloroplastic	543974	-0.69
				uncharacterized_protein_At5g39865	101265209	-0.34
				plant_cysteine_oxidase_2,_transcript_variant_X1	101247510	2.01
				NAD(P)H-quinone_oxidoreductase_subunit_M,_chloroplastic	101247812	-1.32
				prolycopene_isomerase,_chloroplastic	101247017	-2.02
				glucose-6-phosphate_1-dehydrogenase,_chloroplastic	101253589	-0.66
				thioredoxin_F1,_chloroplastic-like	101246719	-2.28
				beta-carotene_hydroxylase	544133	-4.05
				omega-3_fatty_acid_desaturase	544203	-1.44
				uncharacterized_LOC101250128,_transcript_variant_X2	101250128	-3.39
				pyruvate_dehydrogenase_E1_component_subunit_beta-	101266731	-0.84

				1,_mitochondrial,_transcript_variant_X1		
				glutaredoxin_domain-containing_cysteine-rich_protein_1	101252103	-6.24
				3-oxoacyl-[acyl-carrier-protein]_reductase_FabG	101245297	-1.90
				(+)-neomenthol_dehydrogenase,_transcript_variant_X1	101251042	-2.18
				ferredoxin	101265784	-2.18
				putative_magnesium-protoporphyrin_monomethyl_ester_cyclase	101257518	-2.29
				lycopene_beta_cyclase,_chloroplastic	101267662	-0.97
				short-chain_dehydrogenase_TIC_32,_chloroplastic	101263363	-3.71
				NAD(P)H-quinone_oxidoreductase_subunit_O,_chloroplastic,_transcript_variant_X1	101250560	-1.45
				chlorophyllide_a_oxygenase,_chloroplastic-like	101244441	-3.22
				uncharacterized_LOC101267576	101267576	-1.68
				cytochrome_b6-f_complex_iron-sulfur_subunit,_chloroplastic	101243864	-0.89
GO:0022857 transmembrane transporter activity						
2.91E-05	41	1251	2.4	monosaccharide-sensing_protein_2-like	101261393	-1.09
				low_affinity_sulfate_transporter_3,_transcript_variant_X2	101245940	-3.48
				calcium-transporting_ATPase_1	101260132	0.60
				inorganic_phosphate_transporter_2-1,_chloroplastic	101267311	-2.04
				probable_sulfate_transporter_4.2-like	101257470	-0.68
				vacuolar_cation/proton_exchanger_3-like	101265339	-2.00
				high_affinity_nitrate_transporter_2.4-like	101247028	-2.40
				probable_anion_transporter_6,_chloroplastic	101258970	-2.05
				protein_NRT1/_PTR_FAMILY_6.2	101268119	-2.28
				protein_NRT1/_PTR_FAMILY_7.3	101263538	-5.43
				plasma_membrane_intrinsic_protein_1.5	544086	-1.98
				sulfate_transporter_3.1	101264062	-2.71
				sulfate_transporter_3.1-like	101253320	-5.74
				mitochondrial_carnitine/acylcarnitine_carrier-like_protein,_transcript_variant_2	101262875	-2.05
				amino_acid_transporter_AVT1D-like	101255449	-0.90

				protein_NRT1/_PTR_FAMILY_4.4-like	101268640	-2.79
				protein_NRT1/_PTR_FAMILY_6.4	101253972	-2.59
				protein_NRT1/_PTR_FAMILY_8.3-like,_transcript_variant_X1	101252061	1.43
				mitochondrial_adenine_nucleotide_transporter_ADNT1,_transcript_variant_X2	101268329	-2.68
				probable_magnesium_transporter_NIPA4	101246186	-0.92
				protein_DETOXIFICATION_40	101255252	0.80
				probable_purine_permease_10	101261573	-0.90
				ATP_synthase_gamma_chain,_chloroplastic	101253342	-0.71
				phosphoenolpyruvate/phosphate_translocator_2,_chloroplastic	101255257	-1.73
				protein_DETOXIFICATION_14-like,_transcript_variant_X1	101261991	-2.41
				putative_glycerol-3-phosphate_transporter_1	101259222	-3.20
				mitochondrial_outer_membrane_protein_porin_of_36_kDa-like	101246039	-2.08
				cyclic_nucleotide-gated_ion_channel_1-like,_transcript_variant_X1	101250508	0.81
				mitochondrial_carrier_protein_CoAc1	101253108	-0.48
				solute_carrier_family_35_member_F2,_transcript_variant_X1	101258401	-1.02
				cation/H(+)_antiporter_20	101249848	-8.28
				protein_DETOXIFICATION_18	101265483	-1.44
				aquaporin-5,_transcript_variant_X2	101251423	-3.32
				aquaporin_SIP1-2-like	101244430	0.73
				protein_DETOXIFICATION_24	101257226	-1.78
				protein_NUCLEAR_FUSION_DEFECTIVE_4	101244433	-1.13
				cationic_amino_acid_transporter_7,_chloroplastic	101245518	-2.33
				protein_DETOXIFICATION_27	101265986	-1.87
				tonoplast_dicarboxylate_transporter-like	101257524	-6.01
				dicarboxylate_transporter_1,_chloroplastic	101250955	-2.88
				cytochrome_b6-f_complex_iron-sulfur_subunit,_chloroplastic	101243864	-0.89
GO:0005215 transporter activity						
4.75E-05	41	1289	2.4	monosaccharide-sensing_protein_2-like	101261393	-1.09
				low_affinity_sulfate_transporter_3,_transcript_variant_X2	101245940	-3.48
				calcium-transporting_ATPase_1	101260132	0.60
				inorganic_phosphate_transporter_2-1,_chloroplastic	101267311	-2.04

				probable_sulfate_transporter_4.2-like	101257470	-0.68
				vacuolar_cation/proton_exchanger_3-like	101265339	-2.00
				high_affinity_nitrate_transporter_2.4-like	101247028	-2.40
				probable_anion_transporter_6,_chloroplastic	101258970	-2.05
				protein_NRT1/_PTR_FAMILY_6.2	101268119	-2.28
				protein_NRT1/_PTR_FAMILY_7.3	101263538	-5.43
				plasma_membrane_intrinsic_protein_1.5	544086	-1.98
				sulfate_transporter_3.1	101264062	-2.71
				sulfate_transporter_3.1-like	101253320	-5.74
				mitochondrial_carnitine/acylcarnitine_carrier-like_protein,_transcript_variant_2	101262875	-2.05
				amino_acid_transporter_AVT1D-like	101255449	-0.90
				protein_NRT1/_PTR_FAMILY_4.4-like	101268640	-2.79
				dicarboxylate_transporter_1,_chloroplastic	101250955	-2.88
				protein_NRT1/_PTR_FAMILY_6.4	101253972	-2.59
				protein_NRT1/_PTR_FAMILY_8.3-like,_transcript_variant_X1	101252061	1.43
				mitochondrial_adenine_nucleotide_transporter_ADNT1,_transcript_variant_X2	101268329	-2.68
				probable_magnesium_transporter_NIPA4	101246186	-0.92
				protein_DETOXIFICATION_40	101255252	0.80
				probable_purine_permease_10	101261573	-0.90
				ATP_synthase_gamma_chain,_chloroplastic	101253342	-0.71
				phosphoenolpyruvate/phosphate_translocator_2,_chloroplastic	101255257	-1.73
				phosphoenolpyruvate/phosphate_translocator_2,_chloroplastic	101261991	-1.73
				putative_glycerol-3-phosphate_transporter_1	101259222	-3.20
				mitochondrial_outer_membrane_protein_porin_of_36_kDa-like	101246039	-2.08
				cyclic_nucleotide-gated_ion_channel_1-like,_transcript_variant_X1	101250508	0.81
				mitochondrial_carrier_protein_CoAc1	101253108	-0.48
				solute_carrier_family_35_member_F2,_transcript_variant_X1	101258401	-1.02
				cation/H(+)_antiporter_20	101249848	-8.28
				protein_DETOXIFICATION_18	101265483	-1.44
				aquaporin-5,_transcript_variant_X2	101251423	-3.32

				aquaporin_SIP1-2-like	101244430	0.73
				protein_DETOXIFICATION_24	101257226	-1.78
				protein_NUCLEAR_FUSION_DEFECTIVE_4	101244433	-1.13
				cationic_amino_acid_transporter_7,_chloroplastic	101245518	-2.33
				protein_DETOXIFICATION_27	101265986	-1.87
				tonoplast_dicarboxylate_transporter-like	101257524	-6.01
				cytochrome_b6-f_complex_iron-sulfur_subunit,_chloroplastic	101243864	-0.89

Table S8. GO enrichment, number of genes, pathways genes, fold enrichment, KEGG pathway and gene NCBI ID for the DEGs of blue (*Solanum lycopersicum* genes) module.

Enrichment FDR	nGenes	Pathway Genes	Fold Enrichment	Pathway	Locus ID	LOG_2 (FOLD-CHANGE)
Path:sly00040 Pentose and glucuronate interconversions						
2.24E-02	3	51	11.8	probable_pectate_lyase_12	101257697	1.95
				polygalacturonase-like	101263946	3.38
				probable_pectate_lyase_P18	778293	1.81
Path:sly04141 Protein processing in endoplasmic reticulum						
3.08E-03	5	106	9.5	dnaJ_protein_ERDJ3B	101246562	0.65
				E3_ubiquitin-protein_ligase_RMA1H1-like	101253976	2.41
				calreticulin-3-like	101262304	1.11
				endoplasmin_homolog	101265819	0.57
				dad-1_protein	543753	0.51
Path:sly00270 Cysteine and methionine metabolism						
3.33E-02	3	68	8.9	1-aminocyclopropane-1-carboxylate_oxidase	101251255	1.94
				S-adenosylmethionine_decarboxylase_proenzyme-like	101262142	-0.74
				homocysteine_S-methyltransferase_2,_transcript_variant_X2	101262954	0.96
Path:sly00520 Amino sugar and nucleotide sugar metabolism						
4.56E-02	3	84	7.2	UDP-arabinopyranose_mutase_1-like	101252141	6.42
				acidic_endochitinase	101253788	1.75
				GDP-mannose_4,6_dehydratase_1	101266709	0.73
Path:sly04016 MAPK signaling pathway-plant						
4.64E-02	3	94	6.4	mitogen-activated_protein_kinase_8,_transcript_variant_X1	100736510	0.88

				ethylene_response_factor_C.3	101247461	2.20
				ethylene_receptor_homolog	543588	0.89
Path:sly04075 Plant hormone signal transduction						
3.33E-02	4	139	5.8	putative_GID1-like_gibberellin_receptor	100736493	0.83
				ethylene_response_factor_C.3	101247461	2.20
				IAA10_protein	543544	-1.49
				ethylene_receptor_homolog	543588	0.89
Path:sly01100 Metabolic pathways						
1.86E-06	23	1238	3.7	mevalonate_disphosphate_decarboxylase	100134900	0.96
				UMP-CMP_kinase_3	101243930	0.57
				ATP-citrate_synthase_alpha_chain_protein_2	101246135	1.17
				probable_adenylate_kinase_7,_mitochondrial	101246297	1.33
				glucan_endo-1,3-beta-glucosidase_6	101246556	0.88
				7-dehydrocholesterol_reductase	101248602	0.61
				5-formyltetrahydrofolate_cyclo-ligase-like_protein_COG0212	101249350	-0.80
				sulfoquinovosyl_transferase_SQD2	101249508	-0.94
				cytochrome_P450_81D1-like	101250559	1.19
				1-aminocyclopropane-1-carboxylate_oxidase	101251255	1.94
				UDP-arabinopyranose_mutase_1-like	101252141	6.42
				glutamyl-tRNA_reductase_1,_chloroplastic-like	101252440	1.02
				acidic_endochitinase	101253788	1.75
				probable_pectate_lyase_12	101257697	1.95
				S-adenosylmethionine_decarboxylase_proenzyme-like	101262142	-0.74
				homocysteine_S-methyltransferase_2,_transcript_variant_X2	101262954	0.96
				polygalacturonase-like	101263946	3.38
				peroxidase_P7	101264425	1.40
				GDP-mannose_4,6_dehydratase_1	101266709	0.73
				dad-1_protein	543753	0.51
				plastocyanin,_chloroplastic	544053	-0.82
				aromatic_amino_acid_decarboxylase_2	778256	1.18
				probable_pectate_lyase_P18	778293	1.81
Path:sly01110 Biosynthesis of secondary metabolites						
4.64E-02	9	733	2.5	mevalonate_disphosphate_decarboxylase	100134900	0.96

				ATP-citrate_synthase_alpha_chain_protein_2	101246135	1.17
				probable_adenylate_kinase_7,_mitochondrial	101246297	1.33
				7-dehydrocholesterol_reductase	101248602	0.61
				cytochrome_P450_81D1-like	101250559	1.19
				1-aminocyclopropane-1-carboxylate_oxidase	101251255	1.94
				glutamyl-tRNA_reductase_1,_chloroplastic-like	101252440	1.02
				homocysteine_S-methyltransferase_2,_transcript_variant_X2	101262954	0.96
				peroxidase_P7	101264425	1.40

Table S9. Go enrichment, number of genes, pathways genes, fold enrichment, biological process and gene NCBI ID for the blue (*Solanum lycopersicum* genes) module.

Enrichment FDR	nGenes	Pathway Genes	Fold Enrichment	GO Terms	Locus ID	Log_2 (FoldChange)
GO:0048444 floral organ morphogenesis						
3.15E-02	2	7	57.5	putative_GID1-like_gibberellin_receptor	100736493	0.83
				transcription_factor_HHO5-like	101255362	1.65
GO:0007389 pattern specification proc.						
3.01E-02	3	30	20.1	transcription_factor_HHO5-like	101255362	1.65
				receptor_protein_kinase_CLAVATA1	101266413	-1.06
				auxin-regulated_protein,_transcript_variant_X1	543701	1.07
GO:0044272 sulfur compound biosynthetic proc.						
3.36E-02	4	78	10.3	ATP-citrate_synthase_alpha_chain_protein_2	101246135	1.17
				sulfoquinovosyl_transferase_SQD2	101249508	-0.94
				S-adenosylmethionine_decarboxylase_proenzyme-like	101262142	-0.74
				homocysteine_S-methyltransferase_2,_transcript_variant_X2	101262954	0.96
GO:0009653 anatomical structure morphogenesis						
4.16E-03	7	179	7.9	alpha/beta-hydrolase_DWARF14-like	101259838	-1.06
				putative_GID1-like_gibberellin_receptor	100736493	0.83
				transcription_factor_HHO5-like	101255362	1.65
				expansin	544035	1.95

				auxin-regulated_protein,_transcript_variant_X1	543701	1.07
				probable_carboxylesterase_18	101251935	0.53
				chromatin_assembly_factor_1_subunit_FAS2	101246300	0.84
GO:0050793 reg. of developmental proc.						
3.36E-02	5	137	7.3	1-aminocyclopropane-1-carboxylate_oxidase	101251255	1.94
				scarecrow-like_protein_15	101251641	0.82
				receptor_protein_kinase_CLAVATA1	101266413	-1.06
				EPIDERMAL_PATTERNING_FACTOR-like_protein_6	101248013	1.49
				auxin-regulated_protein,_transcript_variant_X1	543701	1.07
GO:0099402 plant organ development						
6.34E-03	7	196	7.2	polygalacturonase-like	101263946	3.38
				putative_GID1-like_gibberellin_receptor	100736493	0.83
				transcription_factor_HHO5-like	101255362	1.65
				annexin_p34	543564	1.03
				auxin-regulated_protein,_transcript_variant_X1	543701	1.07
				chromatin_assembly_factor_1_subunit_FAS2	101246300	0.84
				WUSCHEL-related_homeobox_3-like	101266096	2.98
GO:0048367 shoot system development						
9.06E-03	7	212	6.6	polygalacturonase-like	101263946	3.38
				alpha/beta-hydrolase_DWARF14-like	101259838	-1.06
				putative_GID1-like_gibberellin_receptor	100736493	0.83
				scarecrow-like_protein_15	101251641	0.82
				transcription_factor_HHO5-like	101255362	1.65
				receptor_protein_kinase_CLAVATA1	101266413	-1.06
				chromatin_assembly_factor_1_subunit_FAS2	101246300	0.84
GO:0048731 system development						
9.29E-04	11	398	5.6	polygalacturonase-like	101263946	3.38
				alpha/beta-hydrolase_DWARF14-like	101259838	-1.06
				putative_GID1-like_gibberellin_receptor	100736493	0.83
				scarecrow-like_protein_15	101251641	0.82
				transcription_factor_HHO5-like	101255362	1.65
				annexin_p34	543564	1.03
				receptor_protein_kinase_CLAVATA1	101266413	-1.06
				auxin-regulated_protein,_transcript_variant_X1	543701	1.07

				chromatin_assembly_factor_1_subunit_FAS2	101246300	0.84
				WUSCHEL-related_homeobox_3-like	101266096	2.98
				1-aminocyclopropane-1-carboxylate_oxidase	101251255	1.94
GO:0007275 multicellular organism development						
9.29E-04	13	567	4.6	polygalacturonase-like	101263946	3.38
				alpha/beta-hydrolase_DWARF14-like	101259838	-1.06
				beta-amyrin_28-monooxygenase	101251676	6.21
				putative_GID1-like_gibberellin_receptor	100736493	0.83
				1-aminocyclopropane-1-carboxylate_oxidase	101251255	1.94
				scarecrow-like_protein_15	101251641	0.82
				transcription_factor_HHO5-like	101255362	1.65
				annexin_p34	543564	1.03
				receptor_protein_kinase_CLAVATA1	101266413	-1.06
				EPIDERMAL_PATTERNING_FACTOR-like_protein_6	101248013	1.49
				auxin-regulated_protein,_transcript_variant_X1	543701	1.07
				chromatin_assembly_factor_1_subunit_FAS2	101246300	0.84
				WUSCHEL-related_homeobox_3-like	101266096	2.98
GO:0048856 anatomical structure development						
5.64E-04	16	764	4.2	polygalacturonase-like	101263946	3.38
				alpha/beta-hydrolase_DWARF14-like	101259838	-1.06
				beta-amyrin_28-monooxygenase	101251676	6.21
				putative_GID1-like_gibberellin_receptor	100736493	0.83
				1-aminocyclopropane-1-carboxylate_oxidase	101251255	1.94
				scarecrow-like_protein_15	101251641	0.82
				transcription_factor_HHO5-like	101255362	1.65
				annexin_p34	543564	1.03
				receptor_protein_kinase_CLAVATA1	101266413	-1.06
				EPIDERMAL_PATTERNING_FACTOR-like_protein_6	101248013	1.49
				expansin	544035	1.95
				ethylene_receptor_homolog	543588	0.89
				auxin-regulated_protein,_transcript_variant_X1	543701	1.07
				probable_carboxylesterase_18	101251935	0.53
				chromatin_assembly_factor_1_subunit_FAS2	101246300	0.84
				WUSCHEL-related_homeobox_3-like	101266096	2.98

GO:0032502 developmental proc.						
4.99E-04	18	904	4.0	transcription_termination_factor_MTEF1,_chloroplastic,_transcript_variant_X2	101255820	-0.66
				polygalacturonase-like	101263946	3.38
				alpha/beta-hydrolase_DWARF14-like	101259838	-1.06
				beta-amyrin_28-monooxygenase	101251676	6.21
				putative_GID1-like_gibberellin_receptor	100736493	0.83
				myb-related_transcription_factor	544120	1.67
				1-aminocyclopropane-1-carboxylate_oxidase	101251255	1.94
				scarecrow-like_protein_15	101251641	0.82
				transcription_factor_HHO5-like	101255362	1.65
				annexin_p34	543564	1.03
				receptor_protein_kinase_CLAVATA1	101266413	-1.06
				EPIDERMAL_PATTERNING_FACTOR-like_protein_6	101248013	1.49
				expansin	544035	1.95
				ethylene_receptor_homolog	543588	0.89
				auxin-regulated_protein,_transcript_variant_X1	543701	1.07
				probable_carboxylesterase_18	101251935	0.53
				chromatin_assembly_factor_1_subunit_FAS2	101246300	0.84
				WUSCHEL-related_homeobox_3-like	101266096	2.98
GO:0032501 multicellular organismal proc.						
9.29E-04	15	756	4.0	polygalacturonase-like	101263946	3.38
				alpha/beta-hydrolase_DWARF14-like	101259838	-1.06
				beta-amyrin_28-monooxygenase	101251676	6.21
				putative_GID1-like_gibberellin_receptor	100736493	0.83
				1-aminocyclopropane-1-carboxylate_oxidase	101251255	1.94
				scarecrow-like_protein_15	101251641	0.82
				transcription_factor_HHO5-like	101255362	1.65
				annexin_p34	543564	1.03
				receptor_protein_kinase_CLAVATA1	101266413	-1.06
				EPIDERMAL_PATTERNING_FACTOR-like_protein_6	101248013	1.49
				auxin-regulated_protein,_transcript_variant_X1	543701	1.07
				G-type_lectin_S-receptor-like_serine/threonine-protein_kinase_At4g27290,_transcript_variant_X1	109121373	0.96
				probable_carboxylesterase_18	101251935	0.53

				chromatin_assembly_factor_1_subunit_FAS2	101246300	0.84
				WUSCHEL-related_homeobox_3-like	101266096	2.98
GO:0070887 cellular response to chemical stimulus						
4.60E-02	9	499	3.6	peptide_methionine_sulfoxide_reductase	101253577	0.72
				putative_GID1-like_gibberellin_receptor	100736493	0.83
				1-aminocyclopropane-1-carboxylate_oxidase	101251255	1.94
				E3_ubiquitin-protein_ligase_RMA1H1-like	101253976	2.41
				annexin_p34	543564	1.03
				alpha/beta-hydrolase_DWARF14-like	101259838	-1.06
				IAA10_protein	543544	-1.49
				ethylene_receptor_homolog	543588	0.89
				ethylene_response_factor_C.3	101247461	2.20
GO:0010033 response to organic substance						
2.42E-02	12	725	3.3	putative_GID1-like_gibberellin_receptor	100736493	0.83
				1-aminocyclopropane-1-carboxylate_oxidase	101251255	1.94
				E3_ubiquitin-protein_ligase_RMA1H1-like	101253976	2.41
				WRKY_transcription_factor_IId-4,_transcript_variant_1	544202	0.73
				annexin_p34	543564	1.03
				alpha/beta-hydrolase_DWARF14-like	101259838	-1.06
				IAA10_protein	543544	-1.49
				ethylene_receptor_homolog	543588	0.89
				auxin-responsive_protein_SAUR71	101265243	-1.69
				50S_ribosomal_protein_L5,_chloroplastic	101250331	-0.56
				ethylene_response_factor_C.3	101247461	2.20
				hexose_transporter_protein	543728	1.27
GO:0042221 response to chemical						
3.01E-02	14	984	2.9	peptide_methionine_sulfoxide_reductase	101253577	0.72
				putative_GID1-like_gibberellin_receptor	100736493	0.83
				1-aminocyclopropane-1-carboxylate_oxidase	101251255	1.94
				E3_ubiquitin-protein_ligase_RMA1H1-like	101253976	2.41
				WRKY_transcription_factor_IId-4,_transcript_variant_1	544202	0.73
				annexin_p34	543564	1.03
				alpha/beta-hydrolase_DWARF14-like	101259838	-1.06
				IAA10_protein	543544	-1.49
				ethylene_receptor_homolog	543588	0.89
				auxin-responsive_protein_SAUR71	101265243	-1.69

				50S_ribosomal_protein_L5,_chloroplastic	101250331	-0.56
				ethylene_response_factor_C.3	101247461	2.20
				hexose_transporter_protein	543728	1.27
				protein_SENSITIVE_TO_PROTON_RHIZOTOXICITY_2	101263182	1.17

Table S10. GO enrichment, number of genes, pathways genes, fold enrichment, cellular component and gene NCBI ID for the blue (*Solanum lycopersicum* genes) module.

Enrichment FDR	nGenes	Pathway Genes	Fold Enrichment	GO Terms	Locus ID	Log_2 (Fold-Change)
GO:0046658 anchored component of plasma membrane						
1.20E-02	4	84	9.6	beta-1,3-glucanase	543986	0.98
				cucumber_peeling_cupredoxin	104648156	1.09
				glucan_endo-1,3-beta-glucosidase_6	101246556	0.88
				uncharacterized_GPI-anchored_protein_At4g28100	101252410	1.37
GO:0031226 intrinsic component of plasma membrane						
3.43E-04	7	167	8.4	beta-1,3-glucanase	543986	0.98
				sulfate_transporter_2.1-like	101267799	-1.50
				uncharacterized_LOC101243717	101243717	0.51
				cucumber_peeling_cupredoxin	104648156	1.09
				glucan_endo-1,3-beta-glucosidase_6	101246556	0.88
				ATPase_WRNIP1	543728	0.71
				uncharacterized_GPI-anchored_protein_At4g28100	101252410	1.37
GO:0005911 cell-cell junction, GO:0009506 plasmodesma, GO:0030054 cell junction, GO:0055044 symplast , GO:0070161 anchoring junction						
5.49E-05	9	236	7.7	probable_LRR_receptor-like_serine/threonine-protein_kinase_At4g36180	101252647	1.36
				receptor_protein_kinase_CLAVATA1	101266413	-1.06
				cysteine-rich_repeat_secretory_protein_60-like	101261625	2.70
				receptor_protein-tyrosine_kinase_CEPR2-like	101253498	-0.73
				receptor-like_protein_kinase_HSL1	101247544	1.04
				uncharacterized_LOC101258515	101258515	0.40
				annexin_p34	543564	1.03
				glucan_endo-1,3-beta-glucosidase_6	101246556	0.88
				ATPase_WRNIP1	543728	0.71

GO:0005576 extracellular region						
5.49E-05	11	363	6.1	ribonuclease_T2	544098	2.06
				acidic_endochitinase	101253788	1.75
				beta-1,3-glucanase	543986	0.98
				polygalacturonase-like	101263946	3.38
				probable_pectate_lyase_P18	778293	1.81
				annexin_p34	543564	1.03
				peroxidase_P7	101264425	1.40
				expansin	544035	1.95
				phytosulfokine_precursor_protein	101262762	3.32
				uncharacterized_LOC104644498	104644498	0.97
				osmotin-like_protein	543971	2.36
GO:0005618 cell wall						
3.74E-02	5	197	5.1	glucan_endo-1,3-beta-glucosidase_6	101246556	0.88
				annexin_p34	543564	1.03
				ribonuclease_T2	544098	2.06
				expansin	544035	1.95
				osmotin-like_protein	543971	2.36
GO:0030312 external encapsulating structure						
3.76E-02	5	201	5.0	glucan_endo-1,3-beta-glucosidase_6	101246556	0.88
				annexin_p34	543564	1.03
				ribonuclease_T2	544098	2.06
				expansin	544035	1.95
				osmotin-like_protein	543971	2.36
GO:0005789 endoplasmic reticulum membrane, GO:0098827 endoplasmic reticulum subcompartment, GO:0042175 nuclear outer membrane-endoplasmic reticulum membrane network						
3.90E-02	5	212	4.7	7-dehydrocholesterol_reductase	101248602	0.61
				uncharacterized_LOC101243717	101243717	0.51
				dad-1_protein	543753	0.51
				E3_ubiquitin-protein_ligase_RMA1H1-like	101253976	2.41
				ethylene_receptor_homolog	543588	0.89
GO:0005886 plasma membrane						
4.84E-06	20	954	4.2	beta-1,3-glucanase	543986	0.98
				CASP-like_protein_1	101247363	1.27
				proline_transporter_2,_transcript_variant_X1	543531	1.40
				G-type_lectin_S-receptor-like_serine/threonine-protein_kinase_CES101	101263011	1.10
				ABC_transporter_G_family_member_6	101268272	3.25

				sulfate_transporter_2.1-like	101267799	-1.50
				SNAP25_homologous_protein_SNAP33,_transcript_variant_X1	101257479	0.64
				uncharacterized_LOC101243717	101243717	0.51
				cucumber_peeling_cupredoxin	104648156	1.09
				glucan_endo-1,3-beta-glucosidase_6	101246556	0.88
				probable_GABA_transporter_2	101262033	1.41
				hexose_transporter_protein	543728	1.27
				probable_serine/threonine-protein_kinase_PBL23	101257017	1.33
				G-type_lectin_S-receptor-like_serine/threonine-protein_kinase_At4g27290,_transcript_variant_X1	109121373	0.96
				lysine_histidine_transporter-like_8	101268233	1.41
				uncharacterized_LOC101258515	101258515	0.40
				protein_response_to_dessication_2	101259002	0.93
				annexin_p34	543564	1.03
				auxin-regulated_protein,_transcript_variant_X1	543701	1.07
				uncharacterized_GPI-anchored_protein_At4g28100	101252410	1.37
GO:0071944 cell periphery						
8.66E-07	24	1189	4.1	beta-1,3-glucanase	543986	0.98
				CASP-like_protein_1	101247363	1.27
				proline_transporter_2,_transcript_variant_X1	543531	1.40
				G-type_lectin_S-receptor-like_serine/threonine-protein_kinase_CES101	101263011	1.10
				ABC_transporter_G_family_member_6	101268272	3.25
				sulfate_transporter_2.1-like	101267799	-1.50
				SNAP25_homologous_protein_SNAP33,_transcript_variant_X1	101257479	0.64
				uncharacterized_LOC101243717	101243717	0.51
				cucumber_peeling_cupredoxin	104648156	1.09
				glucan_endo-1,3-beta-glucosidase_6	101246556	0.88
				probable_GABA_transporter_2	101262033	1.41
				hexose_transporter_protein	543728	1.27
				probable_serine/threonine-protein_kinase_PBL23	101257017	1.33
				G-type_lectin_S-receptor-like_serine/threonine-protein_kinase_At4g27290,_transcript_variant_X1	109121373	0.96

				lysine_histidine_transporter-like_8	101268233	1.41
				uncharacterized_LOC101258515	101258515	0.40
				protein_response_to_dessication_2	101259002	0.93
				annexin_p34	543564	1.03
				ribonuclease_T2	544098	2.06
				expansin	544035	1.95
				auxin-regulated_protein,_transcript_variant_X1	543701	1.07
				uncharacterized_GPI-anchored_protein_At4g28100	101252410	1.37
				exocyst_complex_component_EXO70H1	778219	1.74
				osmotin-like_protein	543971	2.36

Table S11. NCBI gene ID, gene description, and log2 fold-change for 'Ca. P. solani' reference genome GCA_000970375 in the blue module.

NCBI Gene ID	Gene description	Log_2 Fold-Change	Expression Average	FDR*
S284_01820	hypothetical protein	13.24	1334	0.00
S284_01810	hypothetical protein	13.79	1001	0.00
S284_04720	hypothetical protein	13.35	737	0.00
S284_02860	predicted AAA+ ATPase	12.33	711	0.00
S284_00330	MutT/nudix family protein	13.25	690	0.00
S284_02020	predicted ATPase	13.05	602	0.00
S284_00430	hypothetical protein	11.93	537	0.00
S284_00520	Pyruvate dehydrogenase E1 component (AcoA/PdhA, alpha subunit), putative fragment	12.61	443	0.00
S284_00060	hypothetical protein	12.52	417	0.00
S284_05000	Zn-dependent hydrolase	12.48	404	0.00
S284_01860	hypothetical protein, partial CDS	12.19	331	0.00
S284_00320	ABC transporter, ATPase component	12.07	305	0.00
S284_00900	putative phage integrase, partial CDS	11.98	286	0.00
S284_02850	cation uptake P-type ATPase	11.87	265	0.00
S284_00780	hypothetical protein, partial CDS	11.85	261	0.00
S284_00280	hypothetical protein	11.71	237	0.00
S284_04360	hypothetical protein	11.71	237	0.00
S284_04860	hypothetical protein	11.66	229	0.00
S284_04390	hypothetical protein	11.62	222	0.00
S284_01300	hypothetical protein	11.57	216	0.00
S284_02500	AAA+ ATPase, partial CDS	11.52	208	0.00
S284_00410	hypothetical protein, putative fragment	11.47	200	0.00
S284_00980	hypothetical protein	11.46	200	0.00
S284_03180	hypothetical protein	11.44	197	0.00
S284_00630	hypothetical protein, similar to phage tail tape measure protein	11.40	191	0.00
S284_00420	predicted ATPase, HflB-like	11.37	188	0.00

S284_05110	hypothetical protein	11.37	187	0.00
S284_00990	hypothetical protein, partial CDS	11.30	179	0.00
S284_03060	hypothetical protein	11.26	174	0.00
S284_04770	hypothetical protein	11.26	174	0.00
S284_00960	hypothetical protein, partial CDS	11.18	164	0.00
S284_03150	hypothetical protein	11.17	163	0.00
S284_00760	cold shock protein	11.12	158	0.00
S284_04570	Cation-transporting ATPase, E1-E2 family	11.00	145	0.00
S284_02050	Exopolyphosphatase-related protein	10.90	135	0.00
S284_04930	hypothetical protein	10.89	134	0.00
S284_03000	hypothetical protein	10.88	134	0.00
S284_03770	conserved hypothetical protein, phage-associated protein	10.87	133	0.00
S284_03310	predicted Cof-like hydrolase	10.75	122	0.00
S284_02030	probable glycoprotease protein	10.74	121	0.00
S284_02820	predicted metal-dependent phosphohydrolase	10.72	119	0.00
S284_02220	hypothetical protein	10.69	117	0.00
S284_03500	conserved hypothetical protein (phage-associated), partial CDS	10.66	115	0.00
S284_04790	hypothetical protein	10.60	110	0.00
S284_05040	hypothetical protein	10.57	107	0.00
S284_04750	hypothetical protein	10.55	106	0.00
S284_01660	putative transposase, partial CDS	10.55	106	0.00
S284_04490	hypothetical protein	10.55	106	0.00
S284_02890	hypothetical protein	10.54	105	0.00
S284_04170	SUF system FeS assembly protein, NifU family	10.48	101	0.00
S284_01990	hypothetical protein	10.41	96	0.00
S284_00070	conserved hypothetical protein, partial CDS	10.37	94	0.00
S284_05170	ABC transporter subunit, partial CDS	10.36	93	0.00
S284_02650	hypothetical protein	10.35	92	0.00
S284_02070	Exopolyphosphatase-related protein	10.22	84	0.00
S284_05010	uncharacterized protein, DegV family	10.21	84	0.00
S284_03570	hypothetical protein	10.20	83	0.00
S284_02340	hypothetical protein	10.19	83	0.00
S284_03160	Type I restriction-modification system (S subunit), partial CDS	10.14	80	0.00
S284_03250	hypothetical protein, (similar to IcmE protein), partial CDS	10.13	79	0.00
S284_00290	hypothetical protein	10.10	78	0.00
S284_03190	hypothetical protein	10.06	76	0.00
S284_02320	hypothetical protein	8.86	64	0.00
S284_03620	predicted AAA+ ATPase	9.82	64	0.00
S284_00690	hypothetical protein	9.82	64	0.00
S284_02350	hypothetical protein	9.80	63	0.00
S284_04350	hypothetical protein	9.76	62	0.00
S284_03090	hypothetical protein	9.74	61	0.00
S284_03140	predicted AAA+ ATPAse	9.70	59	0.00
S284_04190	similar Tyrosine-tRNA ligase (TyrS), partial CDS	9.70	59	0.00
S284_03790	hypothetical protein, phage-associated	9.68	58	0.00
S284_04290	hypothetical protein, partial CDS	9.65	57	0.00
S284_04200	Diadenosine tetraphosphate hydrolase, putative fragment	9.64	57	0.00
S284_00970	hypothetical protein	9.62	56	0.00
S284_05020	Had superfamily phosphatase, subfamily IIb	9.62	56	0.00
S284_02130	hypothetical protein	9.59	55	0.00

S284_02800	arsenate reductase-like protein	9.58	54	0.00
S284_01870	conserved hypothetical protein, partial CDS	9.52	52	0.00
S284_03810	hypothetical protein, partial CDS	9.51	52	0.00
S284_05120	50S ribosomal protein L20P, partial CDS	9.44	49	0.00
S284_02870	hypothetical protein	9.38	47	0.00
S284_03080	hypothetical protein	9.36	47	0.00
S284_01190	conserved hypothetical protein, partial CDS	9.28	44	0.00
S284_01320	hypothetical protein	9.27	44	0.00
S284_03520	hypothetical protein	9.26	43	0.00
S284_03410	Predicted HD superfamily hydrolase	9.24	43	0.00
S284_02450	hypothetical protein	9.21	42	0.00
S284_01880	conserved hypothetical protein, partial CDS	9.21	42	0.00
S284_02680	hypothetical protein	9.18	41	0.00
S284_04100	conserved hypothetical protein, partial CDS	9.17	41	0.00
S284_01140	Amino acid ABC superfamily, permease	9.14	40	0.00
S284_01170	conserved hypothetical protein, partial CDS	9.11	39	0.00
S284_01160	Amino acid ABC transporter, binding-subunit	9.11	39	0.00
S284_00350	hypothetical protein	9.10	39	0.00
S284_04070	hypothetical protein	9.04	37	0.00
S284_03280	hypothetical protein	9.02	37	0.00
S284_00340	hypothetical protein	8.96	35	0.00
S284_03490	predicted peptidase M20 family	8.96	35	0.00
S284_01280	hypothetical protein	8.93	35	0.00
S284_02160	AAA+ ATPase	8.84	32	0.00
S284_00220	hypothetical protein	8.84	32	0.00
S284_01830	hypothetical protein	8.83	32	0.00
S284_01940	hypothetical protein	8.83	32	0.00
S284_03260	conserved hypothetical protein, partial CDS	8.81	32	0.00
S284_01200	hypothetical protein	8.78	31	0.00
S284_00950	hypothetical protein, partial CDS	8.75	31	0.00
S284_03400	Predicted hydrolase	8.71	30	0.00
S284_03650	hypothetical protein	8.70	29	0.00
S284_01750	type II intron reverse transcriptase, partial sequence	8.69	29	0.00
S284_00080	hypothetical protein	8.68	29	0.00
S284_02620	hypothetical protein	8.60	27	0.00
S284_00440	conserved hypothetical protein, phage-associated protein	8.59	27	0.00
S284_01150	amino acid ABC transporter permease protein, ATP binding	8.56	27	0.00
S284_00920	hypothetical protein	8.44	25	0.00
S284_04280	hypothetical protein	8.41	24	0.00
S284_01910	hypothetical protein	8.39	24	0.00
S284_01770	hypothetical protein	8.37	23	0.00
S284_03420	N6-adenine-specific methylase	8.31	23	0.00
S284_03780	hypothetical protein, partial CDS	8.30	22	0.00
S284_00090	conserved hypothetical protein, partial CDS	8.28	22	0.00
S284_04020	predicted NlpA-family lipoprotein, partial sequence	8.26	22	0.00
S284_04030	ABC-type uncharacterized transport system subunit	8.24	21	0.00
S284_03660	hypothetical protein	8.22	21	0.00
S284_01790	hypothetical protein, partial CDS	8.21	21	0.00
S284_00540	hypothetical protein	8.18	20	0.00
S284_02430	putative cobalamin (vitamin B12) biosynthesis protein	8.10	19	0.00
S284_04040	hypothetical protein	8.05	19	0.00
S284_04240	Cytosine/adenosine deaminase	8.05	19	0.00

S284_04180	Cysteine desulfurase	8.03	19	0.00
S284_00680	DegV family protein	8.00	18	0.00
S284_02610	hypothetical protein	7.91	17	0.00
S284_00830	hypothetical protein	7.91	17	0.00
S284_03940	hypothetical protein	7.85	16	0.00
S284_00230	hypothetical protein, similar to replicative DNA helicase	7.78	16	0.00
S284_03630	hypothetical protein	7.74	15	0.00
S284_00120	hypothetical protein	7.70	15	0.00
S284_01890	hypothetical protein, partial CDS	7.68	14	0.00
S284_01250	conserved hypothetical protein, partial CDS	7.56	13	0.00
S284_02590	hypothetical protein	7.54	13	0.00
S284_03760	hypothetical protein	7.53	13	0.00
S284_00020	hypothetical protein	7.40	12	0.00
S284_00240	hypothetical protein	7.36	12	0.00
S284_04960	Zn-dependent carboxypeptidase	7.35	12	0.00
S284_05200	hypothetical protein, partial CDS	7.23	11	0.00
S284_03430	hypothetical protein	7.15	10	0.00
S284_00890	hypothetical protein	7.01	9	0.00
S284_04820	hypothetical protein	7.01	9	0.00
S284_03450	hypothetical protein	6.81	8	0.00
S284_03440	hypothetical protein	6.74	8	0.00
S284_01740	site-specific DNA methylase, partial CDS	6.72	7	0.00
S284_04940	hypothetical protein	6.58	7	0.00
S284_04150	Amino acid ABC superfamily ATP binding cassette transporter, partial CDS	6.55	7	0.00
S284_02230	hypothetical protein	6.54	7	0.00
S284_02720	hypothetical protein, YrdC-like domain protein	6.49	6	0.00
S284_00200	conserved hypothetical protein, partial CDS	6.42	6	0.00
S284_03530	hypothetical protein	6.34	6	0.00
S284_00130	type I restriction-modification system specificity subunit, partial CDS	6.08	5	0.00
S284_01070	hypothetical protein	6.07	5	0.00
S284_01240	putative Tra5 transposase, partial CDS	5.95	4	0.00
S284_00160	hypothetical protein	5.95	4	0.00
S284_01220	conserved hypothetical protein, partial CDS	5.83	4	0.00
S284_04060	ABC transporter, permease protein	5.64	4	0.00
S284_01800	hypothetical protein	5.61	3	0.00
S284_01700	site-specific DNA methylase	5.41	3	0.00
S284_04080	DEAD/DEAH box helicase family protein, SrmB-like	5.36	3	0.01
S284_02360	DNA gyrase modulator	5.19	3	0.01
S284_04400	hypothetical protein	5.11	2	0.01
S284_01760	NifU-like protein	4.61	2	0.05

*False Discovery Rate

Table S12. Gene symbol/Locus ID, connectivity (degree), transcript ID, gene description, Log_2 fold change, and average expression of Hub Genes in the brown module.

Gene Symbol / Locus ID	Degree	Transcript	Gene description	Log2 Fold Chance	Expression Average	FDR*
GGP1	923	NM_001279216.1	GDP-L-galactose_phosphorylase	-2.84	15063	0.00
LOC101255495	922	XM_004240048.4	heavy_metal-associated_isoprenylated_plant_protein_39-like,_transcript_variant_X2	-2.37	372	0.00
LOC101262744	912	XM_004228379.4	ACT_domain-containing_protein_ACR4	-2.48	502	0.00
LOC101248189	898	XM_004237389.4	protein_ACTIVITY_OF_BC1_COMPLEX_KINASE_8,_chloroplastic,_transcript_variant_X1	-2.91	3355	0.00
LOC101248735	888	XM_004249939.3	neutral/alkaline_invertase_3,_chloroplastic,_transcript_variant_X1	-1.25	754	0.01
LOC101260400	880	XM_019211965.2	S-adenosylmethionine_decarboxylase_2,_transcript_variant_X1	-2.43	3802	0.00
LOC101255261	879	XM_004233021.4	SAP-like_protein_BP-73	-3.09	171	0.00
LOC104649457	878	XM_010328715.3	uncharacterized_LOC104649457	-2.57	142	0.00
LOC101264030	876	XM_004243371.3	uncharacterized_LOC101264030,_transcript_variant_X1	-1.75	2471	0.01
LOC101262255	876	XM_004247716.4	protein_PROTON_GRADIENT_REGULATION_5,_chloroplastic	-4.24	1366	0.00
LOC101254958	874	XM_004249465.4	dirigent_protein_17-like	-1.72	151	0.00
LOC101255583	872	XM_004237284.4	protochlorophyllide-dependent_translocon_component_52,_chloroplastic	-3.13	1369	0.00
LOC101249777	869	XM_010314058.3	ribulose_bisphosphate_carboxylase/oxygenase_activase,_chloroplastic	-3.17	59577	0.00
LOC101253239	867	XM_004231474.4	myosin-1	-1.34	2829	0.01
LOC101254893	866	XM_004237134.4	pentatricopeptide_repeat-containing_protein_At5g13770,_chloroplastic	-2.76	975	0.00
LOC101248373	865	XM_004253152.4	uncharacterized_LOC101248373	-3.19	433	0.00
LOC101259171	863	XM_004243605.4	root_phototropism_protein_2	-3.81	7611	0.00
LOC101267036	862	XM_004243105.4	pentatricopeptide_repeat-containing_protein_At5g21222	-1.96	984	0.00
LOC101259835	860	XM_004237678.4	psbP_domain-containing_protein_4,_chloroplastic	-2.88	691	0.00
LOC101267969	860	XM_004251535.4	heme-binding-like_protein_At3g10130,_chloroplastic,_transcript_variant_X1	-2.75	493	0.00
LOC101260431	859	XM_004238386.4	protein_NLP4,_transcript_variant_X2	-2.82	466	0.00
LOC101264863	859	XM_004248207.4	probable_aminotransferase_TAT2	-3.48	222	0.00
LOC101247687	858	XM_004233075.4	pheophytinase,_chloroplastic	-1.77	382	0.00
SAMT	856	NM_001247880.1	S-adenosyl-L-methionine:_salicylic_acid_carboxyl_methyltransferase	-2.79	920	0.01
ACI112	853	XM_010325821.2	ACI112_protein,_transcript_variant_X1	-4.20	1065	0.01
LOC101253972	852	XM_004251487.4	protein_NRT1/_PTR_FAMILY_6.4	-2.59	1980	0.01
LOC101246694	849	XM_004251886.4	uncharacterized_LOC101246694	-3.56	153	0.00
LOC101267284	846	XM_004250669.4	uncharacterized_LOC101267284	-5.49	163	0.00

LOC101260988	845	XM_004233119.4	nuclear_transcription_factor_Y_subunit_A-7	-2.23	582	0.01
LOC112940900	843	XR_003245167.1	uncharacterized_LOC112940900,_transcript_variant_X2	-3.37	71	0.00
LOC101247753	840	XM_004247374.3	phytochrome_A-associated_F-box_protein	-1.09	584	0.01
LOC101252682	837	XM_004238187.4	J_domain-containing_protein_required_for_chloroplast_accumulation_response_1	-5.08	1190	0.00
LOC101245047	833	XM_004236307.4	uncharacterized_protein_slr0889	-1.27	410	0.04
LOC101250128	829	XM_010324322.3	uncharacterized_LOC101250128,_transcript_variant_X2	-3.39	264	0.00
LOC101261662	829	XM_010324322.3	uncharacterized_LOC101250128,_transcript_variant_X2	-3.39	264	0.00
LOC101253417	827	XM_004229190.4	probable_protein_phosphatase_2C_40	-1.48	466	0.00
LOC101248786	824	XM_004241939.4	monooxygenase_2,_transcript_variant_X2	-2.31	185	0.00
LOC101265888	819	XM_004250774.4	K(+)_efflux_antiporter_3,_chloroplastic	-2.37	773	0.00
LOC104649471	815	XM_010328799.3	uncharacterized_LOC104649471	-2.90	23	0.01
LOC101268799	813	XM_004247444.4	uncharacterized_LOC101268799	-1.75	2377	0.00
LOC101255972	811	XM_004235342.3	protein_REVEILLE_7	-6.18	1233	0.00
LOC101247705	811	XM_004252665.4	RING-H2_finger_protein_ATL54	-2.47	111	0.02
LOC101262697	810	XM_004252275.4	(6-4)DNA_photolyase	-3.41	102	0.00
LOC101250133	809	XM_004243164.4	uncharacterized_LOC101250133	-3.67	493	0.00
LOC101261177	808	XM_004249151.4	1-acyl-sn-glycerol-3-phosphate_acyltransferase_2-like,_transcript_variant_X1	-2.03	129	0.00
LOC101268014	807	XM_010326165.3	uncharacterized_LOC101268014	-3.21	170	0.00
LOC101247804	806	XM_019213025.2	cytochrome_P450_71A3	-4.12	253	0.00
LCY1	800	NM_001247297.2	lycopene_beta-cyclase,_transcript_variant_1	-1.92	1168	0.01
PIP1-5	798	NM_001247210.2	plasma_membrane_intrinsic_protein_1.5	-1.98	14968	0.00
LOC101254370	798	XM_004235757.3	zinc_finger_protein_CONSTANS-LIKE_16	-1.65	3759	0.00
LOC101253545	798	XM_004249460.4	protein_REVEILLE_8	-7.89	1172	0.00
LOC101265452	798	XM_004243376.4	zinc_finger_protein_CONSTANS-LIKE_4	-5.05	424	0.02
LOC101267310	793	XM_010322557.3	uncharacterized_LOC101267310,_transcript_variant_X1	-5.19	626	0.00
LOC101259539	793	NM_001348160.1	nodulin-related_MtN21_family_protein	-7.61	224	0.00
LOC101244135	792	NM_001317795.1	strictosidine_synthase_1	-2.30	841	0.02
LOC101257226	792	XM_010313878.2	protein_DETOXIFICATION_24	-1.78	391	0.01
LOC101245297	790	XM_004248227.4	3-oxoacyl-[acyl-carrier-protein]_reductase_FabG	-1.90	69	0.03
GR	789	NM_001247314.2	glutathione_reductase,_chloroplastic	-1.25	1570	0.01
LOC101248432	788	XM_004230678.4	uncharacterized_LOC101248432	-7.06	1609	0.00
LOC101260863	788	XM_004229320.4	boron_transporter_1,_transcript_variant_X1	-6.17	1349	0.00
LOC101266162	788	XM_010328310.3	uncharacterized_LOC101266162,_transcript_variant_X2	-1.13	519	0.03
LOC101266835	786	XM_004241999.4	NAD_kinase_2,_chloroplastic	-1.45	1209	0.00
LOC101255146	784	XM_019215949.1	zinc_finger_protein_2-like	-2.21	105	0.00
LOC101256404	783	XM_004246055.4	COP1-interactive_protein_1-like	-1.69	2564	0.00

LOC101249322	783	XM_004232826.4	probable_2-carboxy-D-arabinitol-1-phosphatase	-1.96	311	0.00
LOC101252748	782	XM_004251483.3	clathrin_coat_assembly_protein_AP180-like	-2.21	232	0.00
LOC101257421	782	XM_004232026.4	uncharacterized_LOC101257421	-1.44	201	0.00
LOC101268836	779	XM_004233480.3	pheophytinase,_chloroplastic	-2.67	264	0.00
LOC101252420	779	XM_004228427.4	uncharacterized_LOC101252420	-3.30	260	0.00
LOC101256107	777	XR_742536.3	protein_SPA1-RELATED_4-like,_transcript_variant_X8	-3.27	1335	0.00
LOC101251538	775	XM_004233008.4	CBL-interacting_serine/threonine-protein_kinase_20	-3.11	442	0.00
LOC101264850	775	XM_019214280.2	probable_S-adenosylmethionine-dependent_methyltransferase_At5g38100,_transcript_variant_X2	-2.57	84	0.00
LOC101257583	770	XM_004235229.4	DNA-binding_protein_SMUBP-2	-2.05	1658	0.01
LOC101246606	770	XM_004233008.4	CBL-interacting_serine/threonine-protein_kinase_20	-3.11	442	
LOC104646671	769	XR_740835.3	uncharacterized_LOC104646671	-2.36	1697	0.00
LOC104648235	769	XR_742336.3	uncharacterized_LOC104648235,_transcript_variant_X3	-1.93	252	0.02

*False Discovery Rate

Table S13. Locus ID, connectivity (degree), transcript ID, gene description, Log_2 fold change, and average expression of Hub Genes in the blue module.

Locus ID	Degree	Transcript	Gene description	Log2 Fold-Change	Average Expression	FDR*
S284_00080	1095	NC_022588.1	hypothetical protein	8.68	29	0.00
S284_00230	1095	NC_022588.1	hypothetical protein, similar to replicative DNA helicase	7.78	16	0.00
S284_05000	1095	NC_022588.1	Zn-dependent hydrolase	12.48	404	0.00
S284_05040	1095	NC_022588.1	hypothetical protein	10.57	107	0.00
S284_01660	1096	NC_022588.1	putative transposase, partial CDS	10.55	106	0.00
S284_04400	1096	NC_022588.1	hypothetical protein	5.11	2	0.01
S284_05110	1097	NC_022588.1	hypothetical protein	11.37	187	0.00
S284_00520	1098	NC_022588.1	Pyruvate dehydrogenase E1 component (AcoA/PdhA, alpha subunit), putative fragment	12.61	443	0.00
S284_01140	1098	NC_022588.1	Amino acid ABC superfamily, permease	9.14	40	0.00
S284_02160	1098	NC_022588.1	AAA+ ATPase	8.84	32	0.00
S284_03310	1098	NC_022588.1	predicted Cof-like hydrolase	10.75	122	0.00
S284_04860	1100	NC_022588.1	hypothetical protein	11.66	229	0.00
S284_00130	1101	NC_022588.1	type I restriction-modification system specificity subunit, partial CDS	6.08	5	0.00
S284_02050	1102	NC_022588.1	Exopolyphosphatase-related protein	10.90	135	0.00
S284_03650	1102	NC_022588.1	hypothetical protein	8.70	29	0.00
S284_02340	1104	NC_022588.1	hypothetical protein	10.19	83	0.00

S284_03660	1104	NC_022588.1	hypothetical protein	8.22	21	0.00
S284_01320	1106	NC_022588.1	hypothetical protein	9.27	44	0.00
S284_03150	1106	NC_022588.1	hypothetical protein	11.17	163	0.00
S284_03250	1106	NC_022588.1	hypothetical protein, (similar to IcmE protein), partial CDS	10.13	79	0.00
S284_05170	1106	NC_022588.1	ABC transporter subunit, partial CDS	10.36	93	0.00
S284_02030	1107	NC_022588.1	probable glycoprotease protein	10.74	121	0.00
S284_03280	1107	NC_022588.1	hypothetical protein	9.02	37	0.00
S284_03080	1108	NC_022588.1	hypothetical protein	9.36	47	0.00
S284_02820	1109	NC_022588.1	predicted metal-dependent phosphohydrolase	10.72	119	0.00
S284_04080	1109	NC_022588.1	DEAD/DEAH box helicase family protein, SrmB-like	5.36	3	0.01

*False Discovery Rate

2.6 References

Alexieva, V., Sergiev, I., Mapelli, S., & Karanov, E. (2001). The effect of drought and ultraviolet radiation on growth and stress markers in pea and wheat. *Plant, Cell & Environment*, *24*(12), Article 12. https://doi.org/10.1046/j.1365-3040.2001.00778.x

Bae, G., & Choi, G. (2008). Decoding of Light Signals by Plant Phytochromes and Their Interacting Proteins. *Annual Review of Plant Biology*, *59*(1), 281–311. https://doi.org/10.1146/annurev.arplant.59.032607.092859

Bai, X., Zhang, J., Ewing, A., Miller, S. A., Jancso Radek, A., Shevchenko, D. V., Tsukerman, K., Walunas, T., Lapidus, A., Campbell, J. W., & Hogenhout, S. A. (2006). Living with Genome Instability: The Adaptation of Phytoplasmas to Diverse Environments of Their Insect and Plant Hosts. *Journal of Bacteriology*, *188*(10), Article 10. https://doi.org/10.1128/JB.188.10.3682-3696.2006

Baker, N. R. (2008). Chlorophyll Fluorescence: A Probe of Photosynthesis In Vivo. *Annual Review of Plant Biology*, *59*(1), 89–113. https://doi.org/10.1146/annurev.arplant.59.032607.092759

Baldet, P., Mori, K., Decros, G., Beauvoit, B., Colombié, S., Prigent, S., Pétriacq, P., & Gibon, Y. (2024). Multi-regulated GDP- L -galactose phosphorylase calls the tune in ascorbate biosynthesis. *Journal of Experimental Botany*, *75*(9), 2631–2643. https://doi.org/10.1093/jxb/erae032

Ballaré, C. L. (2014). Light Regulation of Plant Defense. *Annual Review of Plant Biology*, *65*(1), 335–363. https://doi.org/10.1146/annurev-arplant-050213-040145

Barabási, A.-L., & Oltvai, Z. N. (2004). Network biology: Understanding the cell's functional organization. *Nature Reviews Genetics*, *5*(2), 101–113. https://doi.org/10.1038/nrg1272

Bartoli, C. G. (2006). Inter-relationships between light and respiration in the control of ascorbic acid synthesis and accumulation in Arabidopsis thaliana leaves. *Journal of Experimental Botany*, *57*(8), 1621–1631. https://doi.org/10.1093/jxb/erl005

Beck, M., Heard, W., Mbengue, M., & Robatzek, S. (2012). The INs and OUTs of pattern recognition receptors at the cell surface. *Current Opinion in Plant Biology*, *15*(4), 367–374. https://doi.org/10.1016/j.pbi.2012.05.004

Benjamini, Y., & Hochberg, Y. (1995). Controlling the False Discovery Rate: A Practical and Powerful Approach to Multiple Testing. *Journal of the Royal Statistical Society: Series B (Methodological)*, *57*(1), Article 1. https://doi.org/10.1111/j.2517-6161.1995.tb02031.x

Bernardini, C., Santi, S., Mian, G., Levy, A., Buoso, S., Suh, J. H., Wang, Y., Vincent, C., Van Bel, A. J. E., & Musetti, R. (2022). Increased susceptibility to Chrysanthemum Yellows phytoplasma infection in Atcals7ko plants is accompanied by enhanced

expression of carbohydrate transporters. *Planta*, *256*(2), 43. https://doi.org/10.1007/s00425-022-03954-8

Bertaccini, A. (2007). Phytoplasmas: Diversity, taxonomy, and epidemiology. *Frontiers in Bioscience: A Journal and Virtual Library*, *12*, 673–689. https://doi.org/10.2741/2092

Bertaccini, A., & Duduk, B. (2009). Phytoplasma and phytoplasma diseases: A review of recent research. *Phytopathologia Mediterranea*, *48*(3), Article 3.

Bertamini, M., Grando, M. S., & Nedunchezhian, N. (2003). Effects of Phytoplasma Infection on Pigments, Chlorophyll-Protein Complex and Photosynthetic Activities in Field Grown Apple Leaves. *Biologia Plantarum*, *46*(2), 237–242. https://doi.org/10.1023/b:biop.0000022258.49957.9a

Brand, U., Fletcher, J. C., Hobe, M., Meyerowitz, E. M., & Simon, R. (2000). Dependence of Stem Cell Fate in *Arabidopsis* on a Feedback Loop Regulated by *CLV3* Activity. *Science*, *289*(5479), 617–619. https://doi.org/10.1126/science.289.5479.617

Breuer, R., Gomes-Filho, J. V., Yuan, J., & Randau, L. (2023). Transcriptome profiling of Nudix hydrolase gene deletions in the thermoacidophilic archaeon Sulfolobus acidocaldarius. *Frontiers in Microbiology*, *14*, 1197877. https://doi.org/10.3389/fmicb.2023.1197877

Buchert, F., Mosebach, L., Gäbelein, P., & Hippler, M. (2020). PGR5 is required for efficient Q cycle in the cytochrome *b6f* complex during cyclic electron flow. *Biochemical Journal*, *477*(9), 1631–1650. https://doi.org/10.1042/bcj20190914

Buoso, S., Musetti, R., Marroni, F., Calderan, A., Schmidt, W., & Santi, S. (2022). Infection by phloem-limited phytoplasma affects mineral nutrient homeostasis in tomato leaf tissues. *Journal of Plant Physiology*, *271*, 153659. https://doi.org/10.1016/j.jplph.2022.153659

Buoso, S., Pagliari, L., Musetti, R., Martini, M., Marroni, F., Schmidt, W., & Santi, S. (2019). 'Candidatus Phytoplasma solani' interferes with the distribution and uptake of iron in tomato. *BMC Genomics*, *20*(1), Article 1. https://doi.org/10.1186/s12864-019-6062-x

Chan, K. X., Phua, S. Y., Crisp, P., McQuinn, R., & Pogson, B. J. (2016). Learning the Languages of the Chloroplast: Retrograde Signaling and Beyond. *Annual Review of Plant Biology*, *67*(1), 25–53. https://doi.org/10.1146/annurev-arplant-043015-111854

Chan, K. X., Wirtz, M., Phua, S. Y., Estavillo, G. M., & Pogson, B. J. (2013). Balancing metabolites in drought: The sulfur assimilation conundrum. *Trends in Plant Science*, *18*(1), 18–29. https://doi.org/10.1016/j.tplants.2012.07.005

Chen, M., Ji, M., Wen, B., Liu, L., Li, S., Chen, X., Gao, D., & Li, L. (2016). GOLDEN 2-LIKE Transcription Factors of Plants. *Frontiers in Plant Science*, *7*. https://doi.org/10.3389/fpls.2016.01509

Chen, Y., Zhou, B., Li, J., Tang, H., Tang, J., & Yang, Z. (2018). Formation and Change of Chloroplast-Located Plant Metabolites in Response to Light Conditions.

International Journal of Molecular Sciences, *19*(3), 654. https://doi.org/10.3390/ijms19030654

Clark, S. E., Williams, R. W., & Meyerowitz, E. M. (1997). The CLAVATA1 gene encodes a putative receptor kinase that controls shoot and floral meristem size in Arabidopsis. *Cell*, *89*(4), 575–585. https://doi.org/10.1016/s0092-8674(00)80239-1

Correa-Galvis, V., Redekop, P., Guan, K., Griess, A., Truong, T. B., Wakao, S., Niyogi, K. K., & Jahns, P. (2016). Photosystem II Subunit PsbS Is Involved in the Induction of LHCSR Protein-dependent Energy Dissipation in Chlamydomonas reinhardtii. *Journal of Biological Chemistry*, *291*(33), 17478–17487. https://doi.org/10.1074/jbc.M116.737312

Crawford, T., Lehotai, N., & Strand, Å. (2018). The role of retrograde signals during plant stress responses. *Journal of Experimental Botany*, *69*(11), 2783–2795. https://doi.org/10.1093/jxb/erx481

Danon, A., Miersch, O., Felix, G., Op Den Camp, R. G. L., & Apel, K. (2005). Concurrent activation of cell death-regulating signaling pathways by singlet oxygen in *Arabidopsis thaliana*. *The Plant Journal*, *41*(1), 68–80. https://doi.org/10.1111/j.1365-313X.2004.02276.x

De Marco, F., Pagliari, L., Degola, F., Buxa, S. V., Loschi, A., Dinant, S., Le Hir, R., Morin, H., Santi, S., & Musetti, R. (2016). Combined microscopy and molecular analyses show phloem occlusions and cell wall modifications in tomato leaves in response to “Candidatus Phytoplasma solani.” *Journal of Microscopy*, *263*(2), Article 2. https://doi.org/10.1111/jmi.12426

De Vleesschauwer, D., Xu, J., & HÃ¶fte, M. (2014). Making sense of hormone-mediated defense networking: From rice to Arabidopsis. *Frontiers in Plant Science*, *5*. https://doi.org/10.3389/fpls.2014.00611

Dermastia, M. (2019). Plant Hormones in Phytoplasma Infected Plants. *Frontiers in Plant Science*, *10*, 477. https://doi.org/10.3389/fpls.2019.00477

Dobin, A., Davis, C. A., Schlesinger, F., Drenkow, J., Zaleski, C., Jha, S., Batut, P., Chaisson, M., & Gingeras, T. R. (2013). STAR: Ultrafast universal RNA-seq aligner. *Bioinformatics (Oxford, England)*, *29*(1), Article 1. https://doi.org/10.1093/bioinformatics/bts635

Dubois, M., Van Den Broeck, L., Claeys, H., Van Vlierberghe, K., Matsui, M., & Inzé, D. (2015). The ETHYLENE RESPONSE FACTORs ERF6 and ERF11 Antagonistically Regulate Mannitol-Induced Growth Inhibition in Arabidopsis. *Plant Physiology*, *169*(1), 166–179. https://doi.org/10.1104/pp.15.00335

Endeshaw, S. T., Murolo, S., Romanazzi, G., & Neri, D. (2012). Effects of Bois noir on carbon assimilation, transpiration, stomatal conductance of leaves and yield of grapevine (*Vitis vinifera*) cv. Chardonnay. *Physiologia Plantarum*, *145*(2), 286–295. https://doi.org/10.1111/j.1399-3054.2012.01576.x

Eom, J.-S., Chen, L.-Q., Sosso, D., Julius, B. T., Lin, I. W., Qu, X.-Q., Braun, D. M., & Frommer, W. B. (2015). SWEETs, transporters for intracellular and intercellular sugar translocation. *Current Opinion in Plant Biology*, *25*, 53–62. https://doi.org/10.1016/j.pbi.2015.04.005

Exposito-Rodriguez, M., Laissue, P. P., Yvon-Durocher, G., Smirnoff, N., & Mullineaux, P. M. (2017). Photosynthesis-dependent H2O2 transfer from chloroplasts to nuclei provides a high-light signalling mechanism. *Nature Communications*, *8*(1). https://doi.org/10.1038/s41467-017-00074-w

Farquhar, G. D., Von Caemmerer, S., & Berry, J. A. (1980). A biochemical model of photosynthetic CO2 assimilation in leaves of C3 species. *Planta*, *149*(1), 78–90. https://doi.org/10.1007/BF00386231

Faulkner, C., & Robatzek, S. (2012). Plants and pathogens: Putting infection strategies and defence mechanisms on the map. *Current Opinion in Plant Biology*, *15*(6), Article 6. https://doi.org/10.1016/j.pbi.2012.08.009

Fenech, M., Amorim-Silva, V., Esteban Del Valle, A., Arnaud, D., Ruiz-Lopez, N., Castillo, A. G., Smirnoff, N., & Botella, M. A. (2021). The role of GDP-l-galactose phosphorylase in the control of ascorbate biosynthesis. *Plant Physiology*, *185*(4), 1574–1594. https://doi.org/10.1093/plphys/kiab010

Flexas, J., Bota, J., Loreto, F., Cornic, G., & Sharkey, T. D. (2004). Diffusive and Metabolic Limitations to Photosynthesis under Drought and Salinity in C_3 Plants. *Plant Biology*, *6*(3), 269–279. https://doi.org/10.1055/s-2004-820867

Foyer, C. H., Lelandais, M., & Kunert, K. J. (1994). Photooxidative stress in plants. *Physiologia Plantarum*, *92*(4), 696–717. https://doi.org/10.1111/j.1399-3054.1994.tb03042.x

Foyer, C. H., & Noctor, G. (2005). Redox Homeostasis and Antioxidant Signaling: A Metabolic Interface between Stress Perception and Physiological Responses. *The Plant Cell*, *17*(7), 1866–1875. https://doi.org/10.1105/tpc.105.033589

Foyer, C. H., & Noctor, G. (2009). Redox Regulation in Photosynthetic Organisms: Signaling, Acclimation, and Practical Implications. *Antioxidants & Redox Signaling*, *11*(4), 861–905. https://doi.org/10.1089/ars.2008.2177

Foyer, C. H., & Noctor, G. (2011). Ascorbate and Glutathione: The Heart of the Redox Hub. *Plant Physiology*, *155*(1), 2–18. https://doi.org/10.1104/pp.110.167569

Franceschi, V. R., & Tarlyn, N. M. (2002). L -Ascorbic Acid Is Accumulated in Source Leaf Phloem and Transported to Sink Tissues in Plants. *Plant Physiology*, *130*(2), 649–656. https://doi.org/10.1104/pp.007062

Ge, S. X., Jung, D., & Yao, R. (2020). ShinyGO: A graphical gene-set enrichment tool for animals and plants. *Bioinformatics*, *36*(8), Article 8. https://doi.org/10.1093/bioinformatics/btz931

Geng, R., Pang, X., Li, X., Shi, S., Hedtke, B., Grimm, B., Bock, R., Huang, J., & Zhou, W. (2023). PROGRAMMED CELL DEATH8 interacts with tetrapyrrole biosynthesis enzymes and ClpC1 to maintain homeostasis of tetrapyrrole metabolites in

Arabidopsis. *New Phytologist*, *238*(6), 2545–2560. https://doi.org/10.1111/nph.18906

Głowacka, K., Kromdijk, J., Kucera, K., Xie, J., Cavanagh, A. P., Leonelli, L., Leakey, A. D. B., Ort, D. R., Niyogi, K. K., & Long, S. P. (2018). Photosystem II Subunit S overexpression increases the efficiency of water use in a field-grown crop. *Nature Communications*, *9*(1), 868. https://doi.org/10.1038/s41467-018-03231-x

Göhre, V., Jones, A. M. E., Sklenář, J., Robatzek, S., & Weber, A. P. M. (2012). Molecular crosstalk between PAMP-triggered immunity and photosynthesis. *Molecular Plant-Microbe Interactions: MPMI*, *25*(8), 1083–1092. https://doi.org/10.1094/MPMI-11-11-0301

Griffin, J. H. C., & Toledo-Ortiz, G. (2022). Plant photoreceptors and their signalling components in chloroplastic anterograde and retrograde communication. *Journal of Experimental Botany*, *73*(21), 7126–7138. https://doi.org/10.1093/jxb/erac220

Hammel, A., Sommer, F., Zimmer, D., Stitt, M., Mühlhaus, T., & Schroda, M. (2020). Overexpression of Sedoheptulose-1,7-Bisphosphatase Enhances Photosynthesis in Chlamydomonas reinhardtii and Has No Effect on the Abundance of Other Calvin-Benson Cycle Enzymes. *Frontiers in Plant Science*, *11*, 868. https://doi.org/10.3389/fpls.2020.00868

Hasanuzzaman, M., Bhuyan, M. H. M., Zulfiqar, F., Raza, A., Mohsin, S., Mahmud, J., Fujita, M., & Fotopoulos, V. (2020). Reactive Oxygen Species and Antioxidant Defense in Plants under Abiotic Stress: Revisiting the Crucial Role of a Universal Defense Regulator. *Antioxidants*, *9*(8), 681. https://doi.org/10.3390/antiox9080681

Hase, T., Schürmann, P., Knaff, D.B. (2006). The Interaction of Ferredoxin with Ferredoxin-Dependent Enzymes. In: Golbeck, J.H. (eds) Photosystem I. Advances in Photosynthesis and Respiration, vol 24. Springer, Dordrecht. https://doi.org/10.1007/978-1-4020-4256-0_28

Havaux, M., Strasser, R. J., & Greppin, H. (1991). A theoretical and experimental analysis of the qP and qN coefficients of chlorophyll fluorescence quenching and their relation to photochemical and nonphotochemical events. *Photosynthesis Research*, *27*(1), 41–55. https://doi.org/10.1007/BF00029975

Heath, R. L., & Packer, L. (1968). Photoperoxidation in isolated chloroplasts. I. Kinetics and stoichiometry of fatty acid peroxidation. *Archives of Biochemistry and Biophysics*, *125*(1), 189–198. https://doi.org/10.1016/0003-9861(68)90654-1

Hernández-Verdeja, T., & Lundgren, M. R. (2024). GOLDEN2-LIKE transcription factors: A golden ticket to improve crops? *PLANTS, PEOPLE, PLANET*, *6*(1), 79–93. https://doi.org/10.1002/ppp3.10412

Hogenhout, S. A., Oshima, K., Ammar, E., Kakizawa, S., Kingdom, H. N., & Namba, S. (2008). Phytoplasmas: Bacteria that manipulate plants and insects. *Molecular*

Plant Pathology, *9*(4), 403–423. https://doi.org/10.1111/j.1364-3703.2008.00472.x

Howell, S. H. (2013). Endoplasmic Reticulum Stress Responses in Plants. *Annual Review of Plant Biology*, *64*(1), 477–499. https://doi.org/10.1146/annurev-arplant-050312-120053

Hren, M., Nikolić, P., Rotter, A., Blejec, A., Terrier, N., Ravnikar, M., Dermastia, M., & Gruden, K. (2009). "Bois noir" phytoplasma induces significant reprogramming of the leaf transcriptome in the field grown grapevine. *BMC Genomics*, *10*(1). https://doi.org/10.1186/1471-2164-10-460

Hsu, P. Y., Devisetty, U. K., & Harmer, S. L. (2013). Accurate timekeeping is controlled by a cycling activator in Arabidopsis. *eLife*, *2*, e00473. https://doi.org/10.7554/eLife.00473

Huang, W., Reyes-Caldas, P., Mann, M., Seifbarghi, S., Kahn, A., Almeida, R. P. P., Béven, L., Heck, M., Hogenhout, S. A., & Coaker, G. (2020). Bacterial Vector-Borne Plant Diseases: Unanswered Questions and Future Directions. *Molecular Plant*, *13*(10), Article 10. https://doi.org/10.1016/j.molp.2020.08.010

Ikeda, M., Mitsuda, N., & Ohme-Takagi, M. (2009). *Arabidopsis* WUSCHEL Is a Bifunctional Transcription Factor That Acts as a Repressor in Stem Cell Regulation and as an Activator in Floral Patterning. *The Plant Cell*, *21*(11), 3493–3505. https://doi.org/10.1105/tpc.109.069997

Jarvis, P., & López-Juez, E. (2013). Biogenesis and homeostasis of chloroplasts and other plastids. *Nature Reviews. Molecular Cell Biology*, *14*(12), Article 12. https://doi.org/10.1038/nrm3702

Jeong, H., Mason, S. P., Barabási, A.-L., & Oltvai, Z. N. (2001). Lethality and centrality in protein networks. *Nature*, *411*(6833), 41–42. https://doi.org/10.1038/35075138

Jiang, L., Liu, X., Xiong, G., Liu, H., Chen, F., Wang, L., Meng, X., Liu, G., Yu, H., Yuan, Y., Yi, W., Zhao, L., Ma, H., He, Y., Wu, Z., Melcher, K., Qian, Q., Xu, H. E., Wang, Y., & Li, J. (2013). DWARF 53 acts as a repressor of strigolactone signalling in rice. *Nature*, *504*(7480), 401–405. https://doi.org/10.1038/nature12870

Kachroo, P., Burch-Smith, T. M., & Grant, M. (2021). An Emerging Role for Chloroplasts in Disease and Defense. *Annual Review of Phytopathology*, *59*, 423–445. https://doi.org/10.1146/annurev-phyto-020620-115813

Karpinski, S., Escobar, C., Karpinska, B., Creissen, G., & Mullineaux, P. M. (1997). Photosynthetic electron transport regulates the expression of cytosolic ascorbate peroxidase genes in Arabidopsis during excess light stress. *The Plant Cell*, *9*(4), 627–640. https://doi.org/10.1105/tpc.9.4.627

Korasick, D. A., Westfall, C. S., Lee, S. G., Nanao, M. H., Dumas, R., Hagen, G., Guilfoyle, T. J., Jez, J. M., & Strader, L. C. (2014). Molecular basis for AUXIN RESPONSE FACTOR protein interaction and the control of auxin response repression. *Proceedings of the National Academy of Sciences of the United States of America*, *111*(14), 5427–5432. https://doi.org/10.1073/pnas.1400074111

Kube, M., Mitrovic, J., Duduk, B., Rabus, R., & Seemüller, E. (2012). Current View on Phytoplasma Genomes and Encoded Metabolism. *The Scientific World Journal*, *2012*, 1–25. https://doi.org/10.1100/2012/185942

Lane, T. S., Rempe, C. S., Davitt, J., Staton, M. E., Peng, Y., Soltis, D. E., Melkonian, M., Deyholos, M., Leebens-Mack, J. H., Chase, M., Rothfels, C. J., Stevenson, D., Graham, S. W., Yu, J., Liu, T., Pires, J. C., Edger, P. P., Zhang, Y., Xie, Y., … Stewart, C. N. (2016). Diversity of ABC transporter genes across the plant kingdom and their potential utility in biotechnology. *BMC Biotechnology*, *16*(1), 47. https://doi.org/10.1186/s12896-016-0277-6

Langfelder, P., & Horvath, S. (2008). WGCNA: An R package for weighted correlation network analysis. *BMC Bioinformatics*, *9*, 559. https://doi.org/10.1186/1471-2105-9-559

Langfelder, P., Zhang, B., & Horvath, S. (2008). Defining clusters from a hierarchical cluster tree: The Dynamic Tree Cut package for R. *Bioinformatics (Oxford, England)*, *24*(5), Article 5. https://doi.org/10.1093/bioinformatics/btm563

Larkin, R. M., Alonso, J. M., Ecker, J. R., & Chory, J. (2003). GUN4, a Regulator of Chlorophyll Synthesis and Intracellular Signaling. *Science*, *299*(5608), 902–906. https://doi.org/10.1126/science.1079978

Lee, I. M., Davis, R. E., & Gundersen-Rindal, D. E. (2000). Phytoplasma: Phytopathogenic mollicutes. *Annual Review of Microbiology*, *54*, 221–255. https://doi.org/10.1146/annurev.micro.54.1.221

Leivar, P., & Monte, E. (2014). PIFs: Systems Integrators in Plant Development. *The Plant Cell*, *26*(1), 56–78. https://doi.org/10.1105/tpc.113.120857

Li, M., & Kim, C. (2022). Chloroplast ROS and stress signaling. *Plant Communications*, *3*(1), Article 1. https://doi.org/10.1016/j.xplc.2021.100264

Li, Q., Zhou, L., Li, Y., Zhang, D., & Gao, Y. (2021). Plant NIGT1/HRS1/HHO Transcription Factors: Key Regulators with Multiple Roles in Plant Growth, Development, and Stress Responses. *International Journal of Molecular Sciences*, *22*(16), 8685. https://doi.org/10.3390/ijms22168685

Lichtenthaler, H. K. (1987). [34] Chlorophylls and carotenoids: Pigments of photosynthetic biomembranes. In *Methods in Enzymology* (Vol. 148, pp. 350–382). Elsevier. https://doi.org/10.1016/0076-6879(87)48036-1

Liebers, M., Cozzi, C., Uecker, F., Chambon, L., Blanvillain, R., & Pfannschmidt, T. (2022). Biogenic signals from plastids and their role in chloroplast development. *Journal of Experimental Botany*, *73*(21), 7105–7125. https://doi.org/10.1093/jxb/erac344

Lill, R. (2009). Function and biogenesis of iron–sulphur proteins. *Nature*, *460*(7257), 831–838. https://doi.org/10.1038/nature08301

Littlejohn, G. R., Breen, S., Smirnoff, N., & Grant, M. (2021). Chloroplast immunity illuminated. *New Phytologist*, *229*(6), Article 6. https://doi.org/10.1111/nph.17076

Liu, J., Guo, Y. Y., Bai, Y. W., Camberato, J. J., Xue, J. Q., & Zhang, R. H. (2018). Effects of Drought Stress on the Photosynthesis in Maize. *Russian Journal of Plant Physiology*, *65*(6), 849–856. https://doi.org/10.1134/S1021443718060092

Liu, J., & Howell, S. H. (2016). Managing the protein folding demands in the endoplasmic reticulum of plants. *New Phytologist*, *211*(2), 418–428. https://doi.org/10.1111/nph.13915

Liu, Y., & Li, J. (2014). Endoplasmic reticulum-mediated protein quality control in Arabidopsis. *Frontiers in Plant Science*, *5*. https://doi.org/10.3389/fpls.2014.00162

Liu, Z., Zhao, J., & Liu, M. (2016). Photosynthetic responses to phytoplasma infection in Chinese jujube. *Plant Physiology and Biochemistry*, *105*, 12–20. https://doi.org/10.1016/j.plaphy.2016.04.003

Lorence, A., Chevone, B. I., Mendes, P., & Nessler, C. L. (2004). *Myo* -Inositol Oxygenase Offers a Possible Entry Point into Plant Ascorbate Biosynthesis. *Plant Physiology*, *134*(3), 1200–1205. https://doi.org/10.1104/pp.103.033936

Love, M. I., Huber, W., & Anders, S. (2014). Moderated estimation of fold change and dispersion for RNA-seq data with DESeq2. *Genome Biology*, *15*(12), Article 12. https://doi.org/10.1186/s13059-014-0550-8

Lu, Y., & Yao, J. (2018). Chloroplasts at the Crossroad of Photosynthesis, Pathogen Infection and Plant Defense. *International Journal of Molecular Sciences*, *19*(12), 3900. https://doi.org/10.3390/ijms19123900

Lundquist, P. K., Poliakov, A., Bhuiyan, N. H., Zybailov, B., Sun, Q., & Van Wijk, K. J. (2012). The Functional Network of the Arabidopsis Plastoglobule Proteome Based on Quantitative Proteomics and Genome-Wide Coexpression Analysis. *Plant Physiology*, *158*(3), 1172–1192. https://doi.org/10.1104/pp.111.193144

Lupi, A. C. D., Lira, B. S., Gramegna, G., Trench, B., Alves, F. R. R., Demarco, D., Peres, L. E. P., Purgatto, E., Freschi, L., & Rossi, M. (2019). Solanum lycopersicum GOLDEN 2-LIKE 2 transcription factor affects fruit quality in a light- and auxin-dependent manner. *PLOS ONE*, *14*(2), e0212224. https://doi.org/10.1371/journal.pone.0212224

MacLean, A. M., Orlovskis, Z., Kowitwanich, K., Zdziarska, A. M., Angenent, G. C., Immink, R. G. H., & Hogenhout, S. A. (2014). Phytoplasma Effector SAP54 Hijacks Plant Reproduction by Degrading MADS-box Proteins and Promotes Insect Colonization in a RAD23-Dependent Manner. *PLoS Biology*, *12*(4), e1001835. https://doi.org/10.1371/journal.pbio.1001835

MacLean, A. M., Sugio, A., Makarova, O. V., Findlay, K. C., Grieve, V. M., Tóth, R., Nicolaisen, M., & Hogenhout, S. A. (2011). Phytoplasma Effector SAP54 Induces Indeterminate Leaf-Like Flower Development in Arabidopsis Plants. *Plant Physiology*, *157*(2), Article 2. https://doi.org/10.1104/pp.111.181586

Maejima, K., Iwai, R., Himeno, M., Komatsu, K., Kitazawa, Y., Fujita, N., Ishikawa, K., Fukuoka, M., Minato, N., Yamaji, Y., Oshima, K., & Namba, S. (2014). Recognition

of floral homeotic MADS domain transcription factors by a phytoplasmal effector, phyllogen, induces phyllody. *The Plant Journal: For Cell and Molecular Biology*, *78*(4), Article 4. https://doi.org/10.1111/tpj.12495

Marco, F. D., Batailler, B., Thorpe, M. R., Razan, F., Le Hir, R., Vilaine, F., Bouchereau, A., Martin-Magniette, M.-L., Eveillard, S., & Dinant, S. (2021). Involvement of SUT1 and SUT2 Sugar Transporters in the Impairment of Sugar Transport and Changes in Phloem Exudate Contents in Phytoplasma-Infected Plants. *International Journal of Molecular Sciences*, *22*(2), Article 2. https://doi.org/10.3390/ijms22020745

Mardi, M., Karimi Farsad, L., Gharechahi, J., & Salekdeh, G. H. (2015). In-Depth Transcriptome Sequencing of Mexican Lime Trees Infected with Candidatus Phytoplasma aurantifolia. *PLOS ONE*, *10*(7), e0130425. https://doi.org/10.1371/journal.pone.0130425

Martín, G., Leivar, P., Ludevid, D., Tepperman, J. M., Quail, P. H., & Monte, E. (2016). Phytochrome and retrograde signalling pathways converge to antagonistically regulate a light-induced transcriptional network. *Nature Communications*, *7*(1), 11431. https://doi.org/10.1038/ncomms11431

Maust, B. E., Espadas, F., Talavera, C., Aguilar, M., Santamaría, J. M., & Oropeza, C. (2003). Changes in Carbohydrate Metabolism in Coconut Palms Infected with the Lethal Yellowing Phytoplasma. *Phytopathology®*, *93*(8), 976–981. https://doi.org/10.1094/phyto.2003.93.8.976

Meng, X., & Zhang, S. (2013). MAPK Cascades in Plant Disease Resistance Signaling. *Annual Review of Phytopathology*, *51*(1), 245–266. https://doi.org/10.1146/annurev-phyto-082712-102314

Mine, A., Seyfferth, C., Kracher, B., Berens, M. L., Becker, D., & Tsuda, K. (2018). The Defense Phytohormone Signaling Network Enables Rapid, High-Amplitude Transcriptional Reprogramming during Effector-Triggered Immunity. *The Plant Cell*, *30*(6), 1199–1219. https://doi.org/10.1105/tpc.17.00970

Mittler, R. (2017). ROS Are Good. *Trends in Plant Science*, *22*(1), 11–19. https://doi.org/10.1016/j.tplants.2016.08.002

Mittler, R., Vanderauwera, S., Suzuki, N., Miller, G., Tognetti, V. B., Vandepoele, K., Gollery, M., Shulaev, V., & Van Breusegem, F. (2011). ROS signaling: The new wave? *Trends in Plant Science*, *16*(6), 300–309. https://doi.org/10.1016/j.tplants.2011.03.007

Miura, C., Sugawara, K., Neriya, Y., Minato, N., Keima, T., Himeno, M., Maejima, K., Komatsu, K., Yamaji, Y., Oshima, K., & Namba, S. (2012). Functional characterization and gene expression profiling of superoxide dismutase from plant pathogenic phytoplasma. *Gene*, *510*(2), 107–112. https://doi.org/10.1016/j.gene.2012.09.001

Mochizuki, N., Brusslan, J. A., Larkin, R., Nagatani, A., & Chory, J. (2001). *Arabidopsis genomes uncoupled 5* (*GUN5*) mutant reveals the involvement of Mg-chelatase

H subunit in plastid-to-nucleus signal transduction. *Proceedings of the National Academy of Sciences*, *98*(4), Article 4. https://doi.org/10.1073/pnas.98.4.2053

Mochizuki, N., Tanaka, R., Tanaka, A., Masuda, T., & Nagatani, A. (2008). The steady-state level of Mg-protoporphyrin IX is not a determinant of plastid-to-nucleus signaling in *Arabidopsis*. *Proceedings of the National Academy of Sciences*, *105*(39), 15184–15189. https://doi.org/10.1073/pnas.0803245105

Moreau, S., Van Aubel, G., Janky, R., & Van Cutsem, P. (2020). Chloroplast Electron Chain, ROS Production, and Redox Homeostasis Are Modulated by COS-OGA Elicitation in Tomato (Solanum lycopersicum) Leaves. *Frontiers in Plant Science*, *11*. https://doi.org/10.3389/fpls.2020.597589

Mühlenbock, P., Szechyńska-Hebda, M., Płaszczyca, M., Baudo, M., Mateo, A., Mullineaux, P. M., Parker, J. E., Karpińska, B., & Karpiński, S. (2008). Chloroplast Signaling and*LESION SIMULATING DISEASE1*Regulate Crosstalk between Light Acclimation and Immunity in*Arabidopsis*. *The Plant Cell*, *20*(9), 2339–2356. https://doi.org/10.1105/tpc.108.059618

Müller-Moulé, P. (2008). An expression analysis of the ascorbate biosynthesis enzyme VTC2. *Plant Molecular Biology*, *68*(1–2), 31–41. https://doi.org/10.1007/s11103-008-9350-4

Munekage, Y., Hashimoto, M., Miyake, C., Tomizawa, K.-I., Endo, T., Tasaka, M., & Shikanai, T. (2004). Cyclic electron flow around photosystem I is essential for photosynthesis. *Nature*, *429*(6991), 579–582. https://doi.org/10.1038/nature02598

Munekage, Y., Hojo, M., Meurer, J., Endo, T., Tasaka, M., & Shikanai, T. (2002). PGR5 Is Involved in Cyclic Electron Flow around Photosystem I and Is Essential for Photoprotection in Arabidopsis. *Cell*, *110*(3), 361–371. https://doi.org/10.1016/S0092-8674(02)00867-X

Musetti, R., Buxa, S. V., De Marco, F., Loschi, A., Polizzotto, R., Kogel, K.-H., & Van Bel, A. J. E. (2013). Phytoplasma-Triggered Ca^{2+} Influx Is Involved in Sieve-Tube Blockage. *Molecular Plant-Microbe Interactions®*, *26*(4), 379–386. https://doi.org/10.1094/MPMI-08-12-0207-R

Musetti, R., Pagliari, L., Mian, G., De Oliveira Cantao, F. R., Bernardini, C., Santi, S., & Van Bel, A. J. E. (2023). The sieve-element endoplasmic reticulum: A focal point of phytoplasma-host plant interaction? *Frontiers in Microbiology*, *14*, 1030414. https://doi.org/10.3389/fmicb.2023.1030414

Music, M. S., Samarzija, I., Hogenhout, S. A., Haryono, M., Cho, S.-T., & Kuo, C.-H. (2019). The genome of “Candidatus Phytoplasma solani” strain SA-1 is highly dynamic and prone to adopting foreign sequences. *Systematic and Applied Microbiology*, *42*(2), Article 2. https://doi.org/10.1016/j.syapm.2018.10.008

Nagarajan, R., & Gill, K. S. (2018). Evolution of Rubisco activase gene in plants. *Plant Molecular Biology*, *96*(1–2), 69–87. https://doi.org/10.1007/s11103-017-0680-y

Najami, N., Janda, T., Barriah, W., Kayam, G., Tal, M., Guy, M., & Volokita, M. (2008). Ascorbate peroxidase gene family in tomato: Its identification and characterization. *Molecular Genetics and Genomics*, *279*(2), 171–182. https://doi.org/10.1007/s00438-007-0305-2

Navarro, L., Bari, R., Achard, P., Lisón, P., Nemri, A., Harberd, N. P., & Jones, J. D. G. (2008). DELLAs Control Plant Immune Responses by Modulating the Balance of Jasmonic Acid and Salicylic Acid Signaling. *Current Biology*, *18*(9), 650–655. https://doi.org/10.1016/j.cub.2008.03.060

Nguyen, C. V., Vrebalov, J. T., Gapper, N. E., Zheng, Y., Zhong, S., Fei, Z., & Giovannoni, J. J. (2014). Tomato *GOLDEN2-LIKE* Transcription Factors Reveal Molecular Gradients That Function during Fruit Development and Ripening. *The Plant Cell*, *26*(2), Article 2. https://doi.org/10.1105/tpc.113.118794

Nomura, H., Komori, T., Uemura, S., Kanda, Y., Shimotani, K., Nakai, K., Furuichi, T., Takebayashi, K., Sugimoto, T., Sano, S., Suwastika, I. N., Fukusaki, E., Yoshioka, H., Nakahira, Y., & Shiina, T. (2012). Chloroplast-mediated activation of plant immune signalling in Arabidopsis. *Nature Communications*, *3*(1), 926. https://doi.org/10.1038/ncomms1926

Oshima, K., Kakizawa, S., Nishigawa, H., Jung, H.-Y., Wei, W., Suzuki, S., Arashida, R., Nakata, D., Miyata, S., Ugaki, M., & Namba, S. (2004). Reductive evolution suggested from the complete genome sequence of a plant-pathogenic phytoplasma. *Nature Genetics*, *36*(1), Article 1. https://doi.org/10.1038/ng1277

Oshima, K., Maejima, K., & Namba, S. (2013). Genomic and evolutionary aspects of phytoplasmas. *Frontiers in Microbiology*, *4*, 230. https://doi.org/10.3389/fmicb.2013.00230

Page, M., Sultana, N., Paszkiewicz, K., Florance, H., & Smirnoff, N. (2012). The influence of ascorbate on anthocyanin accumulation during high light acclimation in *Arabidopsis thaliana*: Further evidence for redox control of anthocyanin synthesis. *Plant, Cell & Environment*, *35*(2), 388–404. https://doi.org/10.1111/j.1365-3040.2011.02369.x

Pagliari, L., Buoso, S., Santi, S., Furch, A. C. U., Martini, M., Degola, F., Loschi, A., Van Bel, A. J. E., & Musetti, R. (2017). Filamentous sieve element proteins are able to limit phloem mass flow, but not phytoplasma spread. *Journal of Experimental Botany*, *68*(13), 3673–3688. https://doi.org/10.1093/jxb/erx199

Perrot, T., Pauly, M., & Ramírez, V. (2022). Emerging Roles of β-Glucanases in Plant Development and Adaptative Responses. *Plants*, *11*(9), 1119. https://doi.org/10.3390/plants11091119

Pesaresi, P., Scharfenberg, M., Weigel, M., Granlund, I., Schröder, W. P., Finazzi, G., Rappaport, F., Masiero, S., Furini, A., Jahns, P., & Leister, D. (2009). Mutants, Overexpressors, and Interactors of Arabidopsis Plastocyanin Isoforms: Revised Roles of Plastocyanin in Photosynthetic Electron Flow and Thylakoid Redox State. *Molecular Plant*, *2*(2), 236–248. https://doi.org/10.1093/mp/ssn041

Pieterse, C. M. J., Van Der Does, D., Zamioudis, C., Leon-Reyes, A., & Van Wees, S. C. M. (2012). Hormonal Modulation of Plant Immunity. *Annual Review of Cell and Developmental Biology*, *28*(1), 489–521. https://doi.org/10.1146/annurev-cellbio-092910-154055

Plumb, W., Townsend, A. J., Rasool, B., Alomrani, S., Razak, N., Karpinska, B., Ruban, A. V., & Foyer, C. H. (2018). Ascorbate-mediated regulation of growth, photoprotection, and photoinhibition in Arabidopsis thaliana. *Journal of Experimental Botany*, *69*(11), 2823–2835. https://doi.org/10.1093/jxb/ery170

Pogány, M., Von Rad, U., Grün, S., Dongó, A., Pintye, A., Simoneau, P., Bahnweg, G., Kiss, L., Barna, B., & Durner, J. (2009). Dual Roles of Reactive Oxygen Species and NADPH Oxidase RBOHD in an Arabidopsis-*Alternaria* Pathosystem. *Plant Physiology*, *151*(3), 1459–1475. https://doi.org/10.1104/pp.109.141994

Pogson, B. J., Woo, N. S., Förster, B., & Small, I. D. (2008). Plastid signalling to the nucleus and beyond. *Trends in Plant Science*, *13*(11), Article 11. https://doi.org/10.1016/j.tplants.2008.08.008

Quaglino, F., Zhao, Y., Casati, P., Bulgari, D., Bianco, P. A., Wei, W., & Davis, R. E. (2013). "Candidatus Phytoplasma solani", a novel taxon associated with stolbur- and bois noir-related diseases of plants. *International Journal of Systematic and Evolutionary Microbiology*, *63*(Pt 8), Article Pt 8. https://doi.org/10.1099/ijs.0.044750-0

Rodríguez-Concepción, M., Ahumada, I., Diez-Juez, E., Sauret-Güeto, S., Lois, L. M., Gallego, F., Carretero-Paulet, L., Campos, N., & Boronat, A. (2001). 1-Deoxy-D-xylulose 5-phosphate reductoisomerase and plastid isoprenoid biosynthesis during tomato fruit ripening. *The Plant Journal*, *27*(3), 213–222. https://doi.org/10.1046/j.1365-313x.2001.01089.x

Salvucci, M. E., & Crafts-Brandner, S. J. (2004). Inhibition of photosynthesis by heat stress: The activation state of Rubisco as a limiting factor in photosynthesis. *Physiologia Plantarum*, *120*(2), 179–186. https://doi.org/10.1111/j.0031-9317.2004.0173.x

Samalova, M., Gahurova, E., & Hejatko, J. (2022). Expansin-mediated developmental and adaptive responses: A matter of cell wall biomechanics? *Quantitative Plant Biology*, *3*, e11. https://doi.org/10.1017/qpb.2022.6

Sampedro, J., & Cosgrove, D. J. (2005). [No title found]. *Genome Biology*, *6*(12), 242. https://doi.org/10.1186/gb-2005-6-12-242

Sano, S., Aoyama, M., Nakai, K., Shimotani, K., Yamasaki, K., Sato, M. H., Tojo, D., Suwastika, I. N., Nomura, H., & Shiina, T. (2014). Light-dependent expression of flg22-induced defense genes in Arabidopsis. *Frontiers in Plant Science*, *5*. https://doi.org/10.3389/fpls.2014.00531

Santi, S., De Marco, F., Polizzotto, R., Grisan, S., & Musetti, R. (2013a). Recovery from stolbur disease in grapevine involves changes in sugar transport and metabolism. *Frontiers in Plant Science*, *4*. https://doi.org/10.3389/fpls.2013.00171

Santi, S., Grisan, S., Pierasco, A., De Marco, F., & Musetti, R. (2013b). Laser microdissection of grapevine leaf phloem infected by stolbur reveals site-specific gene responses associated to sucrose transport and metabolism. *Plant, Cell & Environment*, *36*(2), 343–355. https://doi.org/10.1111/j.1365-3040.2012.02577.x

Schaller, H. (2003). The role of sterols in plant growth and development. *Progress in Lipid Research*, *42*(3), 163–175. https://doi.org/10.1016/s0163-7827(02)00047-4

Schlicke, H., Hartwig, A. S., Firtzlaff, V., Richter, A. S., Glässer, C., Maier, K., Finkemeier, I., & Grimm, B. (2014). Induced Deactivation of Genes Encoding Chlorophyll Biosynthesis Enzymes Disentangles Tetrapyrrole-Mediated Retrograde Signaling. *Molecular Plant*, *7*(7), 1211–1227. https://doi.org/10.1093/mp/ssu034

Schmidt, A., Mächtel, R., Ammon, A., Engelsdorf, T., Schmitz, J., Maurino, V. G., & Voll, L. M. (2020). Reactive oxygen species dosage in Arabidopsis chloroplasts can improve resistance towards *Colletotrichum higginsianum* by the induction of WRKY33. *New Phytologist*, *226*(1), 189–204. https://doi.org/10.1111/nph.16332

Serin, E. A. R., Nijveen, H., Hilhorst, H. W. M., & Ligterink, W. (2016). Learning from Co-expression Networks: Possibilities and Challenges. *Frontiers in Plant Science*, *7*. https://doi.org/10.3389/fpls.2016.00444

Serrano, I., Audran, C., & Rivas, S. (2016). Chloroplasts at work during plant innate immunity. *Journal of Experimental Botany*, *67*(13), 3845–3854. https://doi.org/10.1093/jxb/erw088

Shimizu, T., Kacprzak, S. M., Mochizuki, N., Nagatani, A., Watanabe, S., Shimada, T., Tanaka, K., Hayashi, Y., Arai, M., Leister, D., Okamoto, H., Terry, M. J., & Masuda, T. (2019). The retrograde signaling protein GUN1 regulates tetrapyrrole biosynthesis. *Proceedings of the National Academy of Sciences*, *116*(49), 24900–24906. https://doi.org/10.1073/pnas.1911251116

Singh, N. K., Paz, E., Kutsher, Y., Reuveni, M., & Lers, A. (2020). Tomato T2 ribonuclease LE is involved in the response to pathogens. *Molecular Plant Pathology*, *21*(7), 895–906. https://doi.org/10.1111/mpp.12928

Somssich, M., Je, B. I., Simon, R., & Jackson, D. (2016). CLAVATA-WUSCHEL signaling in the shoot meristem. *Development (Cambridge, England)*, *143*(18), 3238–3248. https://doi.org/10.1242/dev.133645

Sparrow-Muñoz, I., Chen, T. C., & Burgess, S. J. (2023). Recent developments in the engineering of Rubisco activase for enhanced crop yield. *Biochemical Society Transactions*, *51*(2), 627–637. https://doi.org/10.1042/BST20221281

Stael, S., Kmiecik, P., Willems, P., Van Der Kelen, K., Coll, N. S., Teige, M., & Van Breusegem, F. (2015). Plant innate immunity – sunny side up? *Trends in Plant Science*, *20*(1), 3–11. https://doi.org/10.1016/j.tplants.2014.10.002

Stone, J. M., Trotochaud, A. E., Walker, J. C., & Clark, S. E. (1998). Control of meristem development by CLAVATA1 receptor kinase and kinase-associated protein

phosphatase interactions. *Plant Physiology*, *117*(4), 1217–1225. https://doi.org/10.1104/pp.117.4.1217

Sugio, A., Kingdom, H. N., MacLean, A. M., Grieve, V. M., & Hogenhout, S. A. (2011). Phytoplasma protein effector SAP11 enhances insect vector reproduction by manipulating plant development and defense hormone biosynthesis. *Proceedings of the National Academy of Sciences of the United States of America*, *108*(48), Article 48. https://doi.org/10.1073/pnas.1105664108

Sundin, L., Vanholme, R., Geerinck, J., Goeminne, G., Höfer, R., Kim, H., Ralph, J., & Boerjan, W. (2014). Mutation of the Inducible *ARABIDOPSIS THALIANA CYTOCHROME P450 REDUCTASE2* Alters Lignin Composition and Improves Saccharification. *Plant Physiology*, *166*(4), 1956–1971. https://doi.org/10.1104/pp.114.245548

Suorsa, M., Järvi, S., Grieco, M., Nurmi, M., Pietrzykowska, M., Rantala, M., Kangasjärvi, S., Paakkarinen, V., Tikkanen, M., Jansson, S., & Aro, E.-M. (2012). PROTON GRADIENT REGULATION5 Is Essential for Proper Acclimation of *Arabidopsis* Photosystem I to Naturally and Artificially Fluctuating Light Conditions. *The Plant Cell*, *24*(7), 2934–2948. https://doi.org/10.1105/tpc.112.097162

Takagi, D., & Miyake, C. (2018). PROTON GRADIENT REGULATION 5 supports linear electron flow to oxidize photosystem I. *Physiologia Plantarum*, *164*(3), 337–348. https://doi.org/10.1111/ppl.12723

Takano, J., Miwa, K., & Fujiwara, T. (2008). Boron transport mechanisms: Collaboration of channels and transporters. *Trends in Plant Science*, *13*(8), 451–457. https://doi.org/10.1016/j.tplants.2008.05.007

Tan, C. M., Li, C.-H., Tsao, N.-W., Su, L.-W., Lu, Y.-T., Chang, S. H., Lin, Y. Y., Liou, J.-C., Hsieh, L.-C., Yu, J.-Z., Sheue, C.-R., Wang, S.-Y., Lee, C.-F., & Yang, J.-Y. (2016). Phytoplasma SAP11 alters 3-isobutyl-2-methoxypyrazine biosynthesis in *Nicotiana benthamiana* by suppressing *NbOMT1*. *Journal of Experimental Botany*, *67*(14), Article 14. https://doi.org/10.1093/jxb/erw225

Tang, Q., Wei, S., Zheng, X., Tu, P., & Tao, F. (2024). APETALA2/ethylene-responsive factors in higher plant and their roles in regulation of plant stress response. *Critical Reviews in Biotechnology*, *44*(8), 1533–1551. https://doi.org/10.1080/07388551.2023.2299769

Tan, Y., Li, Q., Zhao, Y., Wei, H., Wang, J., Baker, C. J., Liu, Q., & Wei, W. (2021). Integration of metabolomics and existing omics data reveals new insights into phytoplasma-induced metabolic reprogramming in host plants. *PLOS ONE*, *16*(2), Article 2. https://doi.org/10.1371/journal.pone.0246203

Tsuda, K., & Katagiri, F. (2010). Comparing signaling mechanisms engaged in pattern-triggered and effector-triggered immunity. *Current Opinion in Plant Biology*, *13*(4), 459–465. https://doi.org/10.1016/j.pbi.2010.04.006

Uflewski, M., Rindfleisch, T., Korkmaz, K., Tietz, E., Mielke, S., Correa Galvis, V., Dünschede, B., Luzarowski, M., Skirycz, A., Schwarzländer, M., Strand, D. D.,

Hertle, A. P., Schünemann, D., Walther, D., Thalhammer, A., Wolff, M., & Armbruster, U. (2024). The thylakoid proton antiporter KEA3 regulates photosynthesis in response to the chloroplast energy status. *Nature Communications*, *15*(1), 2792. https://doi.org/10.1038/s41467-024-47151-5

Vitali, M., Chitarra, W., Galetto, L., Bosco, D., Marzachì, C., Gullino, M. L., Spanna, F., & Lovisolo, C. (2013). Flavescence dorée phytoplasma deregulates stomatal control of photosynthesis in *Vitis vinifera*. *Annals of Applied Biology*, *162*(3), 335–346. https://doi.org/10.1111/aab.12025

Waheeda, K., Kitchel, H., Wang, Q., & Chiu, P.-L. (2023). Molecular mechanism of Rubisco activase: Dynamic assembly and Rubisco remodeling. *Frontiers in Molecular Biosciences*, *10*, 1125922. https://doi.org/10.3389/fmolb.2023.1125922

Wang, C., & Shikanai, T. (2019). Modification of Activity of the Thylakoid H^+ /K^+ Antiporter KEA3 Disturbs ΔpH-Dependent Regulation of Photosynthesis. *Plant Physiology*, *181*(2), 762–773. https://doi.org/10.1104/pp.19.00766

Wang, L.-Y., Li, D., Deng, Y.-S., Lv, W., & Meng, Q.-W. (2013). Antisense-mediated depletion of tomato GDP-l-galactose phosphorylase increases susceptibility to chilling stress. *Journal of Plant Physiology*, *170*(3), 303–314. https://doi.org/10.1016/j.jplph.2012.10.015

Wang, R., Bai, B., Li, D., Wang, J., Huang, W., Wu, Y., & Zhao, L. (2024). Phytoplasma: A plant pathogen that cannot be ignored in agricultural production—Research progress and outlook. *Molecular Plant Pathology*, *25*(2), Article 2. https://doi.org/10.1111/mpp.13437

Wang, S., Wang, S., Li, M., Su, Y., Sun, Z., & Ma, H. (2022). Combined transcriptome and metabolome analysis of Nerium indicum L. elaborates the key pathways that are activated in response to witches' broom disease. *BMC Plant Biology*, *22*(1), 291. https://doi.org/10.1186/s12870-022-03672-z

Wang, X., Shi, Q., Liu, N., Cao, J., & Huang, W. (2025). Light Intensity Dependence of CO2 Assimilation Is More Related to Biochemical Capacity Rather than Diffusional Conductance. *Plants (Basel, Switzerland)*, *14*(7), 986. https://doi.org/10.3390/plants14070986

Waters, M. T., Wang, P., Korkaric, M., Capper, R. G., Saunders, N. J., & Langdale, J. A. (2009a). GLK transcription factors coordinate expression of the photosynthetic apparatus in Arabidopsis. *The Plant Cell*, *21*(4), Article 4. https://doi.org/10.1105/tpc.108.065250

Waters, M. T., Wang, P., Korkaric, M., Capper, R. G., Saunders, N. J., & Langdale, J. A. (2009b). GLK Transcription Factors Coordinate Expression of the Photosynthetic Apparatus in *Arabidopsis*. *The Plant Cell*, *21*(4), 1109–1128. https://doi.org/10.1105/tpc.108.065250

Weigel, M., Varotto, C., Pesaresi, P., Finazzi, G., Rappaport, F., Salamini, F., & Leister, D. (2003). Plastocyanin Is Indispensable for Photosynthetic Electron Flow in

Arabidopsis thaliana. *Journal of Biological Chemistry*, *278*(33), 31286–31289. https://doi.org/10.1074/jbc.m302876200

Wei, W., Davis, R. E., Nuss, D. L., & Zhao, Y. (2013). Phytoplasmal infection derails genetically preprogrammed meristem fate and alters plant architecture. *Proceedings of the National Academy of Sciences*, *110*(47), 19149–19154. https://doi.org/10.1073/pnas.1318489110

Wei, W., Inaba, J., Zhao, Y., Mowery, J. D., & Hammond, R. (2022). Phytoplasma Infection Blocks Starch Breakdown and Triggers Chloroplast Degradation, Leading to Premature Leaf Senescence, Sucrose Reallocation, and Spatiotemporal Redistribution of Phytohormones. *International Journal of Molecular Sciences*, *23*(3), Article 3. https://doi.org/10.3390/ijms23031810

Wu, G., Bin, S., Chen, J., Li, J., Yi, H., Wei, C., Zheng, H., Chen, C., Lee, B., Wang, X., Yang, W., Hu, Z., & Li, X. (2025). Plastocyanin affects photosynthesis and high light acclimation by modulating redox states of electron transport chain in Chlamydomonas reinhardtii. *Communications Biology*, *8*(1). https://doi.org/10.1038/s42003-025-07904-4

Wu, G.-Z., & Bock, R. (2021). GUN control in retrograde signaling: How GENOMES UNCOUPLED proteins adjust nuclear gene expression to plastid biogenesis. *The Plant Cell*, *33*(3), Article 3. https://doi.org/10.1093/plcell/koaa048

Xue, C., Liu, Z., Dai, L., Bu, J., Liu, M., Zhao, Z., Jiang, Z., Gao, W., & Zhao, J. (2018). Changing Host Photosynthetic, Carbohydrate, and Energy Metabolisms Play Important Roles in Phytoplasma Infection. *Phytopathology®*, *108*(9), Article 9. https://doi.org/10.1094/PHYTO-02-18-0058-R

Yadav, R. K., Perales, M., Gruel, J., Ohno, C., Heisler, M., Girke, T., Jönsson, H., & Reddy, G. V. (2013). Plant stem cell maintenance involves direct transcriptional repression of differentiation program. *Molecular Systems Biology*, *9*(1), 654. https://doi.org/10.1038/msb.2013.8

Yamori, W., Sakata, N., Suzuki, Y., Shikanai, T., & Makino, A. (2011). Cyclic electron flow around photosystem I via chloroplast NAD(P)H dehydrogenase (NDH) complex performs a significant physiological role during photosynthesis and plant growth at low temperature in rice. *The Plant Journal*, *68*(6), 966–976. https://doi.org/10.1111/j.1365-313X.2011.04747.x

Yamori, W., Shikanai, T., & Makino, A. (2015). Photosystem I cyclic electron flow via chloroplast NADH dehydrogenase-like complex performs a physiological role for photosynthesis at low light. *Scientific Reports*, *5*(1). https://doi.org/10.1038/srep13908

Yamori, W., & Shikanai, T. (2016). Physiological Functions of Cyclic Electron Transport Around Photosystem I in Sustaining Photosynthesis and Plant Growth. *Annual Review of Plant Biology*, *67*(1), 81–106. https://doi.org/10.1146/annurev-arplant-043015-112002

Yoshimura, M., Sato, A., Kuwata, K., Inukai, Y., Kinoshita, T., Itami, K., Tsuchiya, Y., & Hagihara, S. (2018). Discovery of Shoot Branching Regulator Targeting Strigolactone Receptor DWARF14. *ACS Central Science*, *4*(2), 230–234. https://doi.org/10.1021/acscentsci.7b00554

Zhang, B., & Horvath, S. (2005). A general framework for weighted gene co-expression network analysis. *Statistical Applications in Genetics and Molecular Biology*, *4*, Article17. https://doi.org/10.2202/1544-6115.1128

Zhang, C., Liu, J., Zhang, Y., Cai, X., Gong, P., Zhang, J., Wang, T., Li, H., & Ye, Z. (2011). Overexpression of SlGMEs leads to ascorbate accumulation with enhanced oxidative stress, cold, and salt tolerance in tomato. *Plant Cell Reports*, *30*(3), 389–398. https://doi.org/10.1007/s00299-010-0939-0

Zhang, X.-F., Li, Z., Lin, H., Cheng, Y., Wang, H., Jiang, Z., Ji, Z., Huang, Z., Chen, H., & Wei, T. (2024). A phytoplasma effector destabilizes chloroplastic glutamine synthetase inducing chlorotic leaves that attract leafhopper vectors. *Proceedings of the National Academy of Sciences*, *121*(22), e2402911121. https://doi.org/10.1073/pnas.2402911121

Zheng, M., Wang, X., Luo, J., Ma, B., Li, D., & Chen, X. (2024). The pleiotropic functions of GOLDEN2-LIKE transcription factors in plants. *Frontiers in Plant Science*, *15*, 1445875. https://doi.org/10.3389/fpls.2024.1445875

Zhu, J., Moreno-Pérez, A., & Coaker, G. (2023). Understanding plant pathogen interactions using spatial and single-cell technologies. *Communications Biology*, *6*(1), Article 1. https://doi.org/10.1038/s42003-023-05156-8

Zulfugarov, I. S., Tovuu, A., Kim, C.-Y., Xuan Vo, K. T., Ko, S. Y., Hall, M., Seok, H.-Y., Kim, Y.-K., Skogstrom, O., Moon, Y.-H., Jansson, S., Jeon, J.-S., & Lee, C.-H. (2016). Enhanced resistance of PsbS-deficient rice (Oryza sativa L.) to fungal and bacterial pathogens. *Journal of Plant Biology*, *59*(6), 616–626. https://doi.org/10.1007/s12374-016-0068-6

Chapter III - Physiological Responses of the Micro-Tom Photomorphogenic Mutant Aurea to Phytoplasmas

Abstract - Phytoplasmas are phloem-limited pathogens that severely impair plant growth, development, and productivity by disrupting source-sink relationships and photosynthetic performance. This study investigated the genotype-dependent physiological responses of tomato (*Solanum lycopersicum* cv. Micro-Tom) to *'Candidatus* Phytoplasma solani' (*'Ca.* P. solani') infection, comparing the wild type and the chlorophyll-deficient *Aurea* mutant. Despite infection-induced reductions in net CO_2 assimilation and photochemical efficiency in both genotypes, the *Aurea* mutant displayed a more stable physiological profile, characterized by sustained water-use efficiency, higher electron transport rates, and less energy dissipation via non-photochemical quenching. Infected *Aurea* plants also maintained higher fruit biomass compared to infected wild type, indicating partial tolerance to phytoplasma infection. These differences are likely linked to the au mutant's altered basal photoprotection and carbon allocation capacity. Overall, the results highlight the critical role of genotype-specific traits in modulating plant responses to phloem-restricted pathogens and offer insights into the physiological mechanisms underlying tolerance to *'Ca.* P. solani'.

3. 1 Introduction

Chloroplasts, the hallmark organelles of algae and plants, are the prototype of all plastids. While they are primarily recognized for their role in photosynthesis, they also serve as key sites for the biosynthesis of essential compounds such as amino acids, nucleotides, lipids, and phytohormones (Chen et al., 2018). As such, chloroplasts are crucial for plant development (Liebers et al., 2022; Pogson et al., 2015) and play a central role in sensing and responding to environmental cues (Dopp et al., 2021; Kleine et al., 2021; Liebers et al., 2022; Wu & Bock, 2021).

Phytoplasma infection disrupts retrograde signaling, downregulating key photosynthesis-associated nuclear genes (PhANGs), such as Light Harvesting Complex (LHCB) and ribulose bisphosphate carboxylase small chain (RbcS), which are responsive to retrograde signals (Buoso et al., 2019; Griffin & Toledo-Ortiz, 2022; Wu & Bock, 2021).

The genes involved in chlorophyll biosynthesis, including *GUN4* and *GUN5* markers for retrograde signaling were also downregulated (Richter et al., 2023).

The identification of *GUN* (GENOMES UNCOUPLED) mutants by (Susek et al., 1993) marked a pivotal starting point in efforts to unravel the mechanisms of retrograde signaling (Dopp et al., 2021; Kleine et al., 2021; Liebers et al., 2022; Wu & Bock, 2021). The *GUN* mutant (Susek et al., 1993) demonstrated that chloroplast-to-nucleus signaling is genetically tractable, and treatments by Norflurazon and lincomycin reduce expression of key photosynthesis-related nuclear genes, particularly LHCB. Phytochrome chromophore-deficient mutants have proven valuable for studying photomorphogenesis, as they exhibit reduced activity of all phytochrome types due to a shared chromophore. This chromophore, 3(E)-phytochromobilin, is synthesized in plastids via the heme branch of the tetrapyrrole pathway, and mutants affecting its biosynthesis have been identified in multiple species (Terry & Kendrick, 1999). The *Aurea* mutant is specifically deficient in 3(E)-phytochromobilin synthase (GUN3) activity (Terry, 1997; Terry & Kendrick, 1999). The *Aurea* mutant, a well-characterized photomorphogenic mutant, exhibits traits typical of chromophore deficiency, including elongated growth, impaired chloroplast development, and reduced chlorophyll and anthocyanin, resulting in a pale yellow-green phenotype (Terry, 1997).

While mature *Aurea* plants show a less severe phytochrome deficiency than seedlings, they still exhibit the characteristic yellow-gold pigmentation that gives the mutant its name (Terry & Kendrick, 1999). The base of each leaflet is nearly white, transitioning to pale green toward the edges, with a distinctive mosaic appearance caused by pale green veins surrounded by yellow interveinal tissue. Chlorophyll content in mature *Aurea* plants ranges from 33% to 61% of wild-type levels, depending on environmental conditions such as light and temperature (Becker et al., 1992; Koornneef et al., 1985; López-Juez et al., 1990). Importantly, this reduction in chlorophyll is not

linked to defective photoinduction of LHCB genes, which remain normally expressed at its developmental stage (Becker et al., 1992).

The Micro-Tom *Aurea* (*GUN3*) mutant is a strategic model for phytoplasma-plant interaction studies because it carries a defect in phytochromobilin synthesis, impairing phytochrome-mediated photomorphogenesis and altering tetrapyrrole metabolism-both processes tightly linked to chloroplast function and retrograde signaling. Since '*Ca* P. solani' infection profoundly disrupts chloroplast biogenesis, photosynthesis, and host physiology, *Aurea* provides a unique genetic background to dissect how impaired plastid-to-nucleus communication modulates physiological responses, resilience, and disease outcomes. We hypothesize that Micro-Tom mutant *Aurea* may exhibit increased tolerance to phytoplasma due to altered GUN3 signaling which enhances light perception and chloroplast-to-nucleus communication, ultimately improving photosynthetic efficiency and pathogen resilience this study aimed to evaluate the physiological responses of the Micro-Tom mutant *Aurea* to infection by '*Ca* P. solani'.

3.2 Material and Methods

3.2.1 Plant growth conditions and phytoplasma detection

Seeds of tomato, mutant *Aurea*, deficient in functional phytochromes (Gavassi et al., 2023) were collected from the fruits of a single plant, placed between two layers of filter paper moistened with 1 mM $CaSO_4$ (Figure 1a), and germinated in darkness at 22 °C. After seven days, uniform seedlings (Figure 1b) were transferred into pots containing 2 liters of half-strength nutrient solution composed of 1.5 mM K_2SO_4, 3 mM KNO_3, 0.5 mM $MgSO_4$, 1.5 mM $CaCl_2$, 0.5 mM NaH_2PO_4, 25 µM H_3BO_3, 1 µM $MnSO_4$, 0.5 µM $ZnSO_4$, 0.3 µM $CuSO_4$, 0.05 µM $(NH_4)_6Mo_7O_{24}$, and 20 µM Fe-EDTA, with the pH adjusted to 6.0 using KOH. For the following four weeks, plants were supplied with full-strength nutrient solution, continuously aerated via an air-pumping system connected to each pot and

replaced every four days. Plants were cultivated in a growth chamber maintained at 23 ± 1 °C under a 16-hour photoperiod, with a photosynthetic photon flux density (PPFD) of 250 µmol m^{-2} s^{-1} at canopy level.

Figure 1. Tomato 'Micro-Tom' seedlings one week after germination are shown in (a), while (b) shows seedlings one week after transplanting into a hydroponic solution and growing under controlled conditions in a growth chamber.

Healthy plants were grafted at the stem base using a lateral grafting technique with shoot tips from either phytoplasma-infected or non-infected donor plants, following the method described by (Buoso et al., 2019) (Figure 2a). Figure 2b shows the plants one week after grafting. Infections were carried out using '*Ca* P. solani', a phytoplasma from the stolbur group (16SrXII-A; (Quaglino et al., 2013), following procedures previously described by (Buoso et al., 2019, 2022). Five weeks post-grafting, the leaf midrib and leaf lamina from the first fully expanded symptomatic or healthy leaves (designated as L2 and L3, with L1 being the youngest not fully expanded leaf) were harvested

separately. Tissues were excised with a sterile scalpel and stored at -80 °C for further analysis.

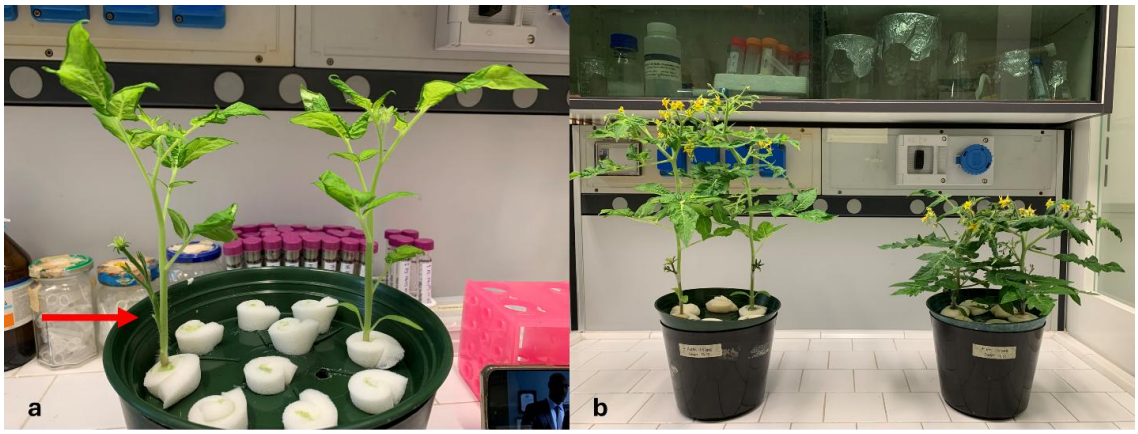

Figure 2. The red arrow in Figure 2a indicates the lateral grafting performed on the Micro-Tom mutant *Aurea* (au), while Figure 2b shows plants one week after grafting on the left au mutants and on the right wild type.

3.2.2 Gas exchange and Chlorophyll Fluorescence in Light Adapted Leaves

Gas exchange and chlorophyll fluorescence parameters were measured in the fifth week after grafting on the terminal leaflet of the first fully expanded (L2) symptomatic leaf of the primary shoot in the infected and healthy plants as described by (Buoso et al., 2022). Gas exchange (GE) and chlorophyll fluorescence (ChlF) measurements were conducted simultaneously using a portable infrared gas analyzer (IRGA; LI-6800, LI-COR Biosciences, Lincoln, NE, USA) equipped with a 2 cm^2 fluorometer leaf chamber (6800-01A) (Figure 3).

Figure 3. Infrared Gas Analyzer (IRGA) with a fluorometer leaf chamber used to simultaneously measure gas exchange and chlorophyll fluorescence.

Measurements were performed with an IRGA in the morning, starting three hours after the onset of the light period. Conditions within the measurement chamber were maintained at a CO_2 concentration of 400 µmol mol^{-1}, a photosynthetic photon flux density (PPFD) of 1200 µmol photons m^{-2} s^{-1}, a flow rate of 500 µmol s^{-1}, and relative humidity of 55%. Gas exchange and chlorophyll fluorescence measurements were performed simultaneously using a portable infrared gas analyzer (IRGA; LI-6800, LI-COR Biosciences, Lincoln, NE, USA) equipped with a 2 cm^2 fluorometer leaf chamber (6800-01A) (Figure 3). Measurements were conducted in the morning, beginning three hours after the onset of the light period. The conditions inside the chamber were set to a CO_2 concentration of 400 µmol CO_2 mol^{-1} air, a photosynthetic photon flux density (PPFD) of 1200 µmol photons m^{-2} s^{-1}, an air flow rate of 500 µmol s^{-1}, and relative humidity maintained at 55%.

The gas exchange parameters recorded included net photosynthetic rate (A, µmol CO_2 m^{-2} s^{-1}), stomatal conductance (gs, mol H_2O m^{-2} s^{-1}), transpiration rate (E, mmol H_2O m^{-2} s^{-1}), and intercellular CO_2 concentration (Ci, µmol CO_2 mol^{-1} air). In addition, instantaneous water use efficiency (WUEi, calculated as A/E; µmol CO_2 $mmol^{-1}$ H_2O) and intrinsic water use efficiency (WUEintr, calculated as A/gs; µmol CO_2 mol^{-1} H_2O) were

determined to assess the balance between carbon assimilation and water loss under phytoplasma infection. Chlorophyll fluorescence parameters were acquired simultaneously and included photochemical quenching (qP, unitless), effective quantum yield of photosystem II (ΦPSII, unitless), electron transport rate (ETR, µmol electrons m^{-2} s^{-1}), quantum yield of CO_2 assimilation (ΦCO_2, unitless), and the parameter 1-qL (unitless), which reflects non-photochemical quenching-like behavior (NPQ-like) in light adapted conditions.

3.2.3 Biomass allocation

The experiment was conducted to determine the dry mass of roots, shoots, and fruits from four plants per condition. Plant organs (roots, shoots, and fruits) were collected and separated. The samples were then oven-dried at 65°C until they reached a constant weight. Subsequently, the dry mass of each organ was measured using an analytical balance with a precision of 0.001 g. The total dry mass was determined by summing the dry masses of roots, shoots, and fruits.

3.2.4 Statistical analysis

Plant biometrics and gene expression data are expressed as mean values ± SE. Statistical analysis was performed, using one-way ANOVA followed by a Tukey test as post hoc multiple comparison ($P \leq 0.05$).

3.3 Results

3.3.1 Genotype-dependent effects of phytoplasma on carbon allocation and fruit development

The impact of 'Ca. P. solani' infection on biomass accumulation differed between genotypes and plant organs. Both the Micro-Tom wild type and the *Aurea* mutant exhibited a significant increase in shoot dry weight upon infection compared with their healthy controls (Figure 4a). Higher root dry weight was also observed for *Aurea* mutant infected compared to both wild type and *Aurea* mutant in healthy conditions. No differences were observed for wild type and *Aurea* infected (Figure 4b).

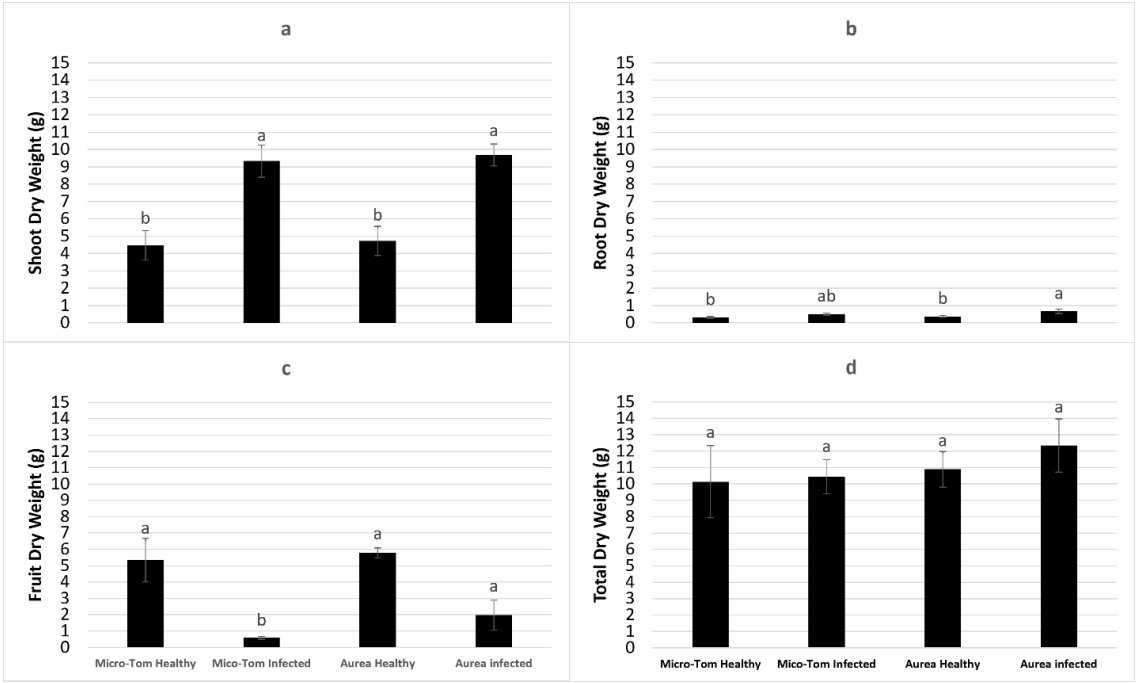

Figure 4. Effect of 'Ca P. solani' infection on carbon allocation in Micro-Tom wild type and the *Aurea* mutant.

Regarding the fruit dry weight (FDW) Micro-Tom healthy and the Mutant Aurea in both conditions showed higher values compared to the Micro-Tom infected (Figures 4c and 5).

Interestingly, no significant differences in total dry weight were found between healthy wild type and *Aurea* plants (Figure 4d), despite the infection's clear negative effect on shoot dry weight in both genotypes (Figure 4a) and its differential impact on fruit dry weight (Figure 4c). These observations suggest that *Aurea* maintains higher photosynthetic activity (Figure 6a) and exhibits distinct photoassimilate allocation patterns, which may underlie a lower sensitivity to phytoplasma infection.

Figure 5. Effect of 'C. P. solani' on fruit development: (a) Micro-Tom wild type under healthy conditions; (b) Micro-Tom wild type under infected conditions; (c) Micro-Tom mutant *Aurea* under healthy conditions; and (d) Micro-Tom mutant *Aurea* under infected conditions.

3.3.2 Genotype-dependent effects of phytoplasma on gas exchange and chlorophyll fluorescence

Figure 6 illustrates the effects of 'C. P. solani' infection on leaf gas exchange parameters and water use efficiency (WUE) in Micro-Tom wild type and *Aurea* mutant plants grown hydroponically. Infected Micro-Tom wild type plants showed significant reductions in net photosynthetic rate (A), stomatal conductance (gs), and transpiration rate (E) compared to healthy controls, reflecting impaired gas exchange capacity. In contrast, the *Aurea* mutant exhibited a moderate decline of these parameters, indicating better-preserved photosynthetic performance. Intercellular CO_2 concentration (Ci) remained stable for wild type and *Aurea* healthy and *Aurea* infected, with a significant reduction observed for the wild type plants in response to the infection (Figure 6a-d).

Divergent patterns in water-use efficiency (WUE) were observed, infected Micro-Tom wild type plants exhibited a marked increase in $WUE_{intrinsic}$ (WUE_i) and $WUE_{instantaneous}$ (WUE_e) likely due to strong stomatal closure observed (Figure 6e-f). In both *Aurea* mutant and wild type healthy and *Aurea* infected, WUE indicators remained unchanged, suggesting more effective stomatal regulation and photosynthetic function under ‘Ca. P. solani’ infection.

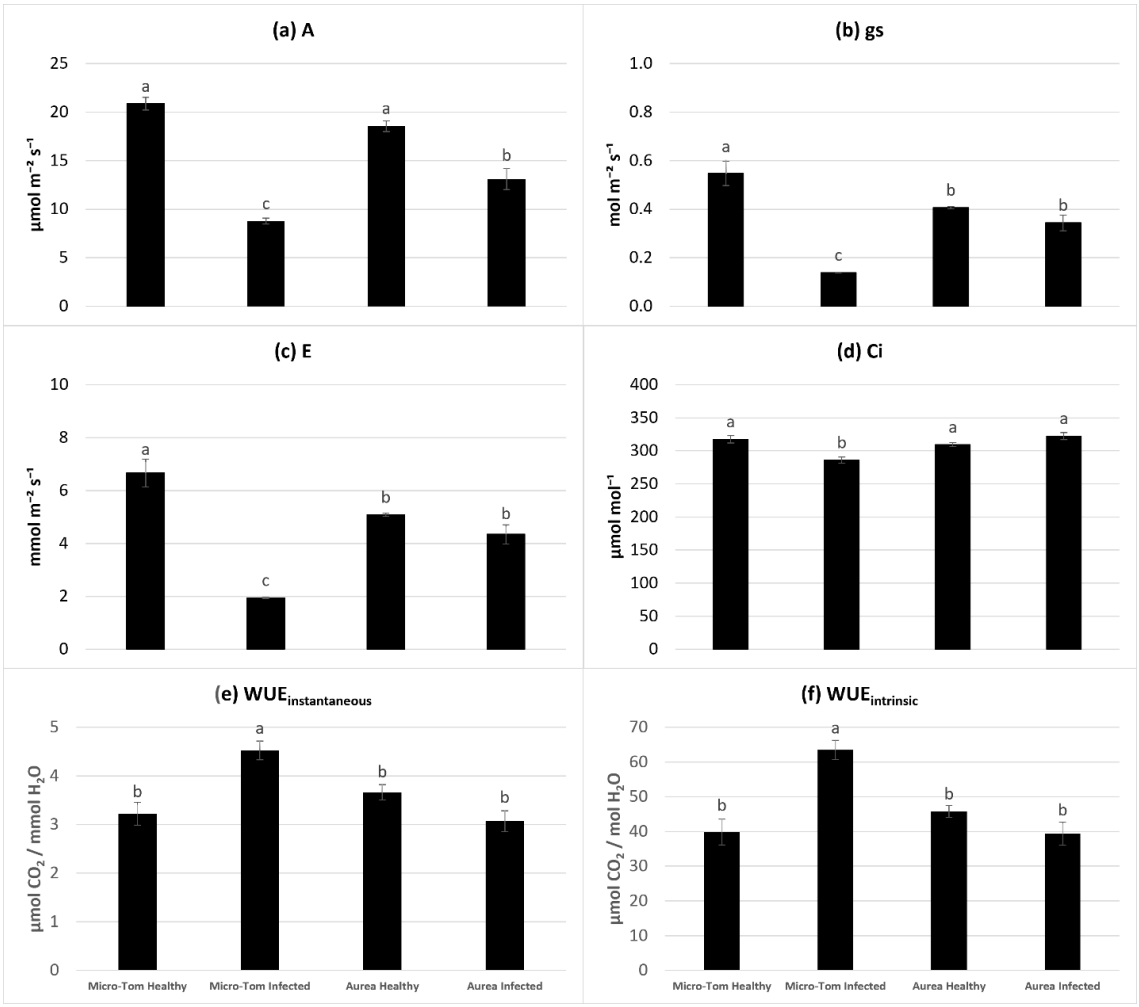

Figure 6. Effect of '*Ca* P. solani' on gas exchange parameters in Micro-Tom wild type and the Aurea (au) mutant: (a) net photosynthetic rate (A, µmol CO_2 m^{-2} s^{-1}), (b) stomatal conductance (gs, mol H_2O m^{-2} s^{-1}), (c) transpiration rate (E, mmol H_2O m^{-2} s^{-1}), (d) intercellular CO_2 concentration (Ci, µmol CO_2 mol^{-1} air). Additionally, the instantaneous Water Use Efficiency (e) ($WUE_{instantaneous}$, calculated as A/E; µmol CO_2 $mmol^{-1}$ H_2O) and (f) $WUE_{intrinsic}$ (calculated as A/gs; µmol CO_2 mol^{-1} H_2O) are presented.

Infection by 'Ca P. solani' led to genotype-dependent alterations in key chlorophyll fluorescence parameters, reflecting disruptions in the photosynthetic electron transport chain and energy conversion efficiency. No significant differences qL a component of non-photochemical quenching (NPQ), which is a mechanism that plants use to protect

themselves from excess light by dissipating surplus energy as heat (Figure 7a). Also, no differences were observed in photochemical quenching (qP; Figure 7b), indicating that the proportion of open PSII reaction centers remained relatively stable. However, ΦPSII (Phi PSII) was significantly reduced in infected plants of both genotypes (Figure 7c). ΦPSII, or the quantum yield of Photosystem II, measures the efficiency with which absorbed light is utilized in the photochemistry of PSII during photosynthesis. Additionally, 1 - qL represents the proportion of absorbed light dissipated as heat through non-photochemical quenching (NPQ). In the healthy *Aurea* mutant, this value is lower, suggesting that, in its basal state, the mutant dissipates less energy as heat, allowing a larger portion of absorbed light to be used for productive photochemistry (Figure 7d). ETR values (Figure 7e) were significantly altered by the infection, the higher value was observed for the mutant healthy mutant *Aurea*, which is aligned with the lower 1 - qL as previously reported (Figure 7d). The quantum yield of CO_2 assimilation (ΦCO_2 or $PhiCO_2$) was also reduced following 'Ca. P. solani' infection. Notably, the Micro-Tom wild-type genotype exhibited a lower ΦCO_2 than the infected *Aurea* mutant (Figure 7f). This suggests a compromised coupling between light capture and carbon fixation, consistent with the observed decrease in net CO_2 assimilation rates (see gas exchange data).

Together, these data indicate that phytoplasma infection impairs the photosynthetic apparatus, primarily by reducing energy conversion efficiency and electron transport. The *Aurea* mutant displayed a more robust photochemical response and superior photoprotection under infection, further supporting less sensitivity compared to the Micro-Tom wild type.

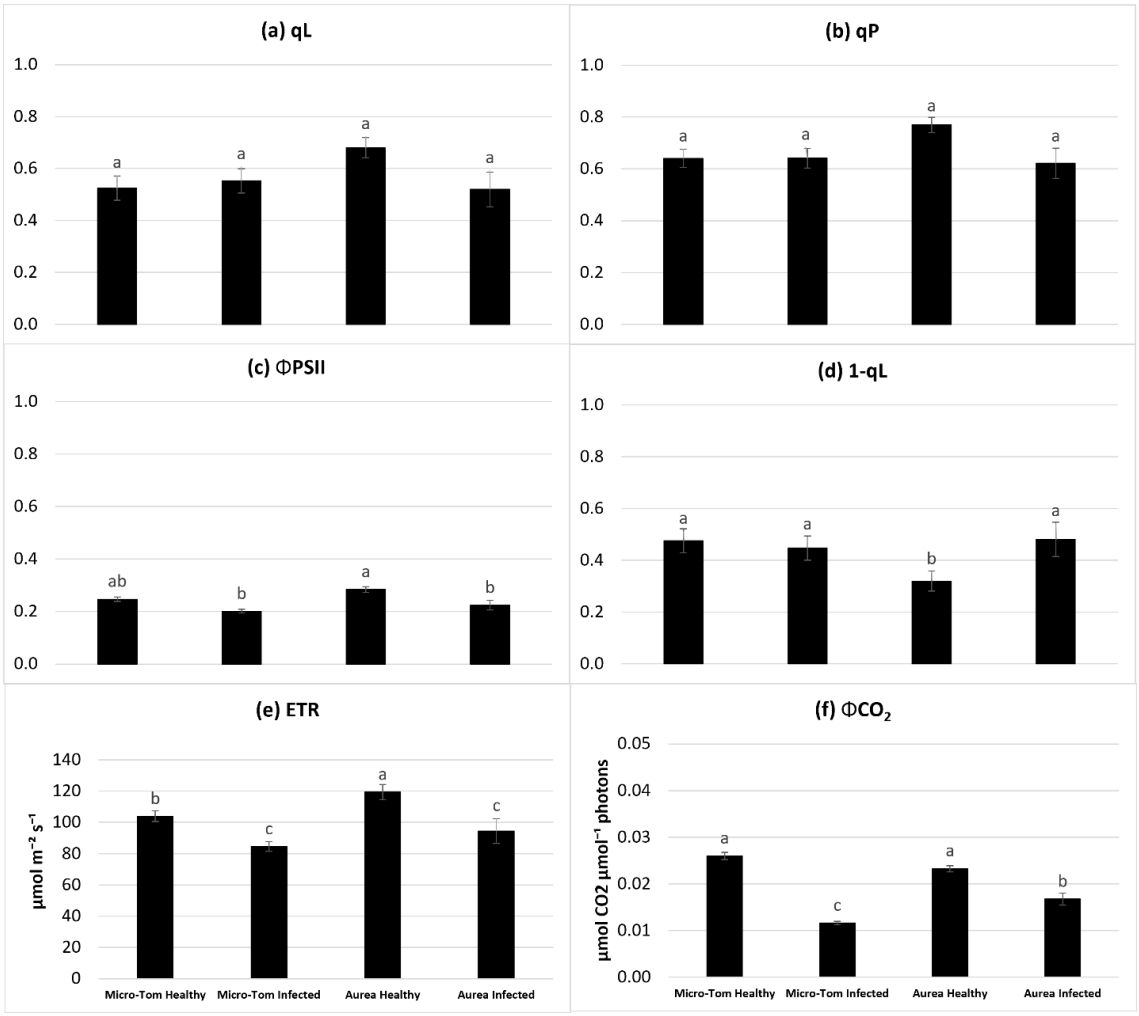

Figure 7. Effect of 'C. P. solani' on chlorophyll fluorescence parameters in Micro-Tom wild type and the Aurea mutant: (a) (qP, unitless), (b) effective quantum yield of photosystem II (ΦPSII, unitless), (c) electron transport rate (ETR, µmol electrons m^{-2} s^{-1}), (d) quantum yield of CO_2 assimilation (ΦCO_2, unitless), (e) 1-qL (unitless), which reflects non-photochemical quenching-like behavior (NPQ-like).

3.4 Discussion

Dry mass was particularly informative for assessing differences in biomass allocation across genotypes. Notably, the *Aurea* mutant exhibited a greater proportion of biomass allocated to the roots in response to the infection. This observation aligns with previous findings that the *Aurea* functional phytochromes deficiency due to impaired

chromophore biosynthesis, particularly affecting phytochrome B (PhyB), a key photoreceptor in red/far-red (R:FR) light signaling (Terry & Kendrick, 1996). In natural conditions, a shift to low R:FR light commonly perceived as shade leads to PhyB inactivation or degradation, triggering physiological adaptations such as increased root and shoot elongation (Ballaré, 2014; Ballaré & Pierik, 2017).

This biomass reallocation may not solely result from altered light perception but could also involve modulation of hormone-mediated signaling pathways, particularly jasmonic acid (JA). Under shade-like conditions (low R:FR), JA-mediated defense responses are typically downregulated to favor growth, allowing plants to prioritize resource acquisition over defense (Campos et al., 2016; Gommers et al., 2017). It is therefore plausible to hypothesize that *Aurea*, due to its constitutively impaired PhyB signaling, similarly suppresses JA-related defense pathways in favor of growth and resource allocation to belowground structures. This hypothesis is consistent with broader evidence of growth-defense trade-offs regulated by phytohormone and light interactions (Campos et al., 2016; Gommers et al., 2017; Huot et al., 2014).

The disruption of phytochrome-mediated signaling in the Micro-Tom *Aurea* mutant influences the physiological response to '*Ca.* P. solani' infection, including more stable photosynthetic traits. This finding suggests that altered plastid-to-nucleus (retrograde) signaling may modulate the transcriptional and physiological response in a way that mitigates pathogen-induced stress. Phytochromes, especially PhyA and PhyB, are central to light perception and integrate external cues to control chloroplast development, carbon allocation, and immunity (Franklin & Quail, 2010). They regulate the activity of PHYTOCHROME INTERACTING FACTORS (PIFs), which in turn repress *GLK1*, a regulator of chloroplast biogenesis and photosynthetic gene expression (Martín et al., 2016). In the absence of functional phytochromes, this regulatory cascade is disrupted, potentially altering the integration of plastid-derived stress signals that normally amplify defense responses (Chan et al., 2016; Hernández-Verdeja & Strand,

2018). Moreover, studies in other systems have shown that moderate attenuation of stress signaling pathways can reduce the metabolic cost of defense, preserving growth and reproductive fitness under biotic stress (Huot et al., 2014). Thus, the partial tolerance observed in *Aurea* may reflect a trade-off strategy where diminished perception of chloroplast stress results in less drastic defense activation, thereby maintaining a better source-sink balance and developmental progression even in the presence of '*Ca.* P. solani'.

3.4.1 Genotype-dependent effects of 'Ca. P. solani' on carbon allocation

The impact of *'Ca.* P. solani' infection on biomass distribution was clearly genotype-dependent, with significant alterations observed in shoot and root dry weight across treatments. Interestingly, both Micro-Tom wild type and the *Aurea* mutant displayed increased shoot dry weight upon infection, which may reflect a compensatory overaccumulation of photoassimilates in source tissues, a common response to phloem-limited pathogens that interfere with carbon translocation (Hogenhout et al., 2008). This phenomenon has been documented in previous studies showing that phytoplasma infections disrupt phloem function, impair assimilate translocation, and cause the accumulation of photoassimilates in source leaves (Buoso et al., 2019). These disruptions often lead to imbalanced nutrient distribution and altered hormonal signaling, ultimately affecting overall plant growth and development (Wang et al., 2020).

Notably, the infected *Aurea* mutant also exhibited higher root dry weight relative to both healthy genotypes, suggesting a more balanced allocation of assimilates between above and below-ground organs. This could indicate a degree of functional carbon partitioning preservation in the *Aurea* mutant despite infection (Bai et al., 2009). Fruit dry weight, in contrast, was markedly reduced by '*Ca.* P. solani' in both genotypes, but the effect was significantly more pronounced in the wild type. While no differences were detected between healthy wild type and *Aurea* plants, the infected *Aurea* mutant

maintained higher fruit biomass compared to infected wild type plants. These results highlight a minor sensitivity in the *Aurea* genotype, likely conferred by physiological traits that sustain carbon assimilation and allocation to sink tissues even under biotic stress.

3.4.2 Genotype dependent effects of 'Ca. P. solani' on gas exchange and chlorophyll fluorescence

Gas exchange measurements revealed a pronounced suppression of photosynthetic function in infected Micro-Tom wild type plants, including reduced net photosynthetic rate (A), stomatal conductance (gs), and transpiration rate (E), consistent with findings by (Buoso et al., 2022). These reductions indicate impaired CO_2 uptake and water vapor exchange, likely driven by pathogen-induced stomatal closure. The *Aurea* mutant, however, exhibited a more moderate decline in these parameters, suggesting better preservation of photosynthetic capacity under infection. Intercellular CO_2 concentration (Ci) decreased significantly in infected wild type plants but remained stable in *Aurea*, reinforcing the notion of more efficient gas exchange regulation in the mutant background.

Water use efficiency (WUE) responses further emphasized this contrast. Infected wild type plants showed elevated intrinsic and instantaneous WUE (WUE_i and WUE_e, respectively), likely reflecting stress-induced stomatal closure that limits CO_2 influx more than water loss (Flexas et al., 2004). While superficially indicative of increased efficiency, this response reflects compromised carbon fixation due to stomatal limitations. By contrast, WUE remained stable in the *Aurea* mutant under infection, suggesting a more controlled stomatal response and better coordination between CO_2 uptake and water loss. Such regulation is consistent with more sustained photosynthetic performance, critical for supporting sink demand and fruit development in response to *'Ca.* P. solani' infection.

Chlorophyll fluorescence analyses provided further insights into genotype-specific photosynthetic adjustments. No significant differences were observed in qP or qL between genotypes or treatments, suggesting the proportion of open PSII reaction centers and excitation energy distribution between photochemistry and heat dissipation remained stable (Maxwell & Johnson, 2000). However, the effective quantum yield of PSII (ΦPSII) was significantly reduced in infected plants of both genotypes, indicating decreased efficiency of light use in photochemical reactions (Baker, 2008). Interestingly, the parameter 1-qL, reflecting the fraction of absorbed light energy dissipated as heat via non-photochemical quenching (NPQ), was lower in healthy *Aurea* plants compared to other treatments. This suggests that, in its basal state, the *Aurea* mutant dissipates less energy as heat, directing more absorbed light toward productive photochemistry. This was supported by higher electron transport rate (ETR) values observed in healthy *Aurea* plants, significantly greater than in other conditions (Genty et al., 1989). The infected *Aurea* plants maintained intermediate ETR levels, indicating more stable photochemical performance compared to infected wild type plants. Furthermore, the quantum yield of CO_2 assimilation (ΦCO_2) was also reduced following infection, particularly in wild type plants, indicating a more severe breakdown in coupling between light harvesting and carbon fixation.

These findings underscore a multifaceted impact of *'Ca.* P. solani' infection on photosynthetic machinery, characterized by disrupted energy conversion, limited electron flow, and constrained carbon assimilation. The *Aurea* mutant retained more functional photochemical processes and better coordinated gas exchange responses, supporting partial tolerance. These physiological advantages likely contribute to more effective source-sink dynamics.

3.6 Conclusions

This study demonstrates that 'Ca. P. solani' infection induces genotype-dependent alterations in carbon allocation and photosynthetic performance. While both the Micro-Tom wild type and the *Aurea* mutant experienced disruptions in photosynthesis and biomass partitioning, the *Aurea* mutant exhibited a more resilient physiological profile. This included stable water-use efficiency, preserved chlorophyll fluorescence parameters, and a less pronounced decline in fruits development. The *Aurea* mutant altered photoprotective responses and sustained energy conversion efficiency suggest that its partial tolerance to phytoplasma infection is linked to an intrinsic ability to maintain source-sink balance and productive photochemistry in response to the infection. These findings underscore the importance of genotype-specific physiological traits in shaping plant responses to 'Ca. P. solani' and offer a valuable framework for investigating the mechanisms underlying tolerance to phytoplasma infection.

3.7 References

Bai, X., Correa, V. R., Toruño, T. Y., Ammar, E.-D., Kamoun, S., & Hogenhout, S. A. (2009). AY-WB phytoplasma secretes a protein that targets plant cell nuclei. *Molecular Plant-Microbe Interactions: MPMI*, *22*(1), Article 1. https://doi.org/10.1094/MPMI-22-1-0018

Baker, N. R. (2008). Chlorophyll Fluorescence: A Probe of Photosynthesis In Vivo. *Annual Review of Plant Biology*, *59*(1), 89–113. https://doi.org/10.1146/annurev.arplant.59.032607.092759

Ballaré, C. L. (2014). Light Regulation of Plant Defense. *Annual Review of Plant Biology*, *65*(1), 335–363. https://doi.org/10.1146/annurev-arplant-050213-040145

Ballaré, C. L., & Pierik, R. (2017). The shade-avoidance syndrome: Multiple signals and ecological consequences. *Plant, Cell & Environment*, *40*(11), 2530–2543. https://doi.org/10.1111/pce.12914

Becker, ThomasW., Foyer, C., & Caboche, M. (1992). Light-regulated expression of the nitrate-reductase and nitrite-reductase genes in tomato and in the phytochrome-deficient aurea mutant of tomato. *Planta*, *188*(1). https://doi.org/10.1007/BF00198937

Bernardini, C., Santi, S., Mian, G., Levy, A., Buoso, S., Suh, J. H., Wang, Y., Vincent, C., Van Bel, A. J. E., & Musetti, R. (2022). Increased susceptibility to Chrysanthemum Yellows phytoplasma infection in Atcals7ko plants is accompanied by enhanced expression of carbohydrate transporters. *Planta*, *256*(2), 43. https://doi.org/10.1007/s00425-022-03954-8

Bertaccini, A. (2007). Phytoplasmas: Diversity, taxonomy, and epidemiology. *Frontiers in Bioscience: A Journal and Virtual Library*, *12*, 673–689. https://doi.org/10.2741/2092

Buoso, S., Musetti, R., Marroni, F., Calderan, A., Schmidt, W., & Santi, S. (2022). Infection by phloem-limited phytoplasma affects mineral nutrient homeostasis in tomato leaf tissues. *Journal of Plant Physiology*, *271*, 153659. https://doi.org/10.1016/j.jplph.2022.153659

Buoso, S., Pagliari, L., Musetti, R., Martini, M., Marroni, F., Schmidt, W., & Santi, S. (2019). 'Candidatus Phytoplasma solani' interferes with the distribution and uptake of iron in tomato. *BMC Genomics*, *20*(1), Article 1. https://doi.org/10.1186/s12864-019-6062-x

Campos, M. L., Yoshida, Y., Major, I. T., De Oliveira Ferreira, D., Weraduwage, S. M., Froehlich, J. E., Johnson, B. F., Kramer, D. M., Jander, G., Sharkey, T. D., & Howe, G. A. (2016). Rewiring of jasmonate and phytochrome B signalling uncouples plant growth-defense tradeoffs. *Nature Communications*, *7*(1). https://doi.org/10.1038/ncomms12570

Chan, K. X., Phua, S. Y., Crisp, P., McQuinn, R., & Pogson, B. J. (2016). Learning the Languages of the Chloroplast: Retrograde Signaling and Beyond. *Annual Review of Plant Biology*, *67*(1), 25–53. https://doi.org/10.1146/annurev-arplant-043015-111854

Chen, Y., Zhou, B., Li, J., Tang, H., Tang, J., & Yang, Z. (2018). Formation and Change of Chloroplast-Located Plant Metabolites in Response to Light Conditions. *International Journal of Molecular Sciences*, *19*(3), 654. https://doi.org/10.3390/ijms19030654

Dopp, I. J., Yang, X., & Mackenzie, S. A. (2021). A new take on organelle-mediated stress sensing in plants. *New Phytologist*, *230*(6), 2148–2153. https://doi.org/10.1111/nph.17333

Flexas, J., Bota, J., Loreto, F., Cornic, G., & Sharkey, T. D. (2004). Diffusive and Metabolic Limitations to Photosynthesis under Drought and Salinity in C_3 Plants. *Plant Biology*, *6*(3), 269–279. https://doi.org/10.1055/s-2004-820867

Franklin, K. A., & Quail, P. H. (2010). Phytochrome functions in Arabidopsis development. *Journal of Experimental Botany*, *61*(1), 11–24. https://doi.org/10.1093/jxb/erp304

Gavassi, M. A., Alves, F. R. R., Monteiro, C. C., Gaion, L. A., Alves, L. R., Prado, R. D. M., Gratão, P. L., & Carvalho, R. F. (2023). Photomorphogenic tomato mutants high-pigment 1 and aurea responses to iron deficiency. *Scientia Horticulturae*, *307*, 111502. https://doi.org/10.1016/j.scienta.2022.111502

Gommers, C. M. M., Keuskamp, D. H., Buti, S., Van Veen, H., Koevoets, I. T., Reinen, E., Voesenek, L. A. C. J., & Pierik, R. (2017). Molecular Profiles of Contrasting Shade Response Strategies in Wild Plants: Differential Control of Immunity and Shoot Elongation. *The Plant Cell*, *29*(2), 331–344. https://doi.org/10.1105/tpc.16.00790

Griffin, J. H. C., & Toledo-Ortiz, G. (2022). Plant photoreceptors and their signalling components in chloroplastic anterograde and retrograde communication. *Journal of Experimental Botany*, *73*(21), 7126–7138. https://doi.org/10.1093/jxb/erac220

Hernández-Verdeja, T., & Strand, Å. (2018). Retrograde Signals Navigate the Path to Chloroplast Development. *Plant Physiology*, *176*(2), Article 2. https://doi.org/10.1104/pp.17.01299

Hogenhout, S. A., Oshima, K., Ammar, E., Kakizawa, S., Kingdom, H. N., & Namba, S. (2008). Phytoplasmas: Bacteria that manipulate plants and insects. *Molecular Plant Pathology*, *9*(4), 403–423. https://doi.org/10.1111/j.1364-3703.2008.00472.x

Huot, B., Yao, J., Montgomery, B. L., & He, S. Y. (2014). Growth–Defense Tradeoffs in Plants: A Balancing Act to Optimize Fitness. *Molecular Plant*, *7*(8), 1267–1287. https://doi.org/10.1093/mp/ssu049

Kleine, T., Nägele, T., Neuhaus, H. E., Schmitz-Linneweber, C., Fernie, A. R., Geigenberger, P., Grimm, B., Kaufmann, K., Klipp, E., Meurer, J., Möhlmann, T., Mühlhaus, T., Naranjo, B., Nickelsen, J., Richter, A., Ruwe, H., Schroda, M., Schwenkert, S., Trentmann, O., … Leister, D. (2021). Acclimation in plants – the Green Hub consortium. *The Plant Journal*, *106*(1), 23–40. https://doi.org/10.1111/tpj.15144

Koornneef, M., Cone, J. W., Dekens, R. G., O'Herne-Robers, E. G., Spruit, C. J. P., & Kendrick, R. E. (1985). Photomorphogenic Responses of Long Hypocotyl Mutants of Tomato. *Journal of Plant Physiology*, *120*(2), 153–165. https://doi.org/10.1016/S0176-1617(85)80019-5

Lee, I. M., Davis, R. E., & Gundersen-Rindal, D. E. (2000). Phytoplasma: Phytopathogenic mollicutes. *Annual Review of Microbiology*, *54*, 221–255. https://doi.org/10.1146/annurev.micro.54.1.221

Liebers, M., Cozzi, C., Uecker, F., Chambon, L., Blanvillain, R., & Pfannschmidt, T. (2022). Biogenic signals from plastids and their role in chloroplast development. *Journal of Experimental Botany*, *73*(21), 7105–7125. https://doi.org/10.1093/jxb/erac344

López-Juez, E., Nagatani, A., Buurmeijer, W. F., Peters, J. L., Furuya, M., Kendrick, R. E., & Wesselius, J. C. (1990). Response of light-grown wild-type and aurea-mutant tomato plants to end-of-day far-red light. *Journal of Photochemistry and Photobiology B: Biology*, *4*(4), 391–405. https://doi.org/10.1016/1011-1344(90)85018-R

Martín, G., Leivar, P., Ludevid, D., Tepperman, J. M., Quail, P. H., & Monte, E. (2016). Phytochrome and retrograde signalling pathways converge to antagonistically regulate a light-induced transcriptional network. *Nature Communications*, *7*(1). https://doi.org/10.1038/ncomms11431

Maxwell, K., & Johnson, G. N. (2000). Chlorophyll fluorescence—A practical guide. *Journal of Experimental Botany*, *51*(345), 659–668. https://doi.org/10.1093/jexbot/51.345.659

Musetti, R., Pagliari, L., Mian, G., De Oliveira Cantao, F. R., Bernardini, C., Santi, S., & Van Bel, A. J. E. (2023). The sieve-element endoplasmic reticulum: A focal point of phytoplasma-host plant interaction? *Frontiers in Microbiology*, *14*, 1030414. https://doi.org/10.3389/fmicb.2023.1030414

Omenge, K., Viscardo, O. C., De Oliveira Cantao, F. R., Santi, S., Van Bel, A. J. E., & Musetti, R. (2025). SEOR2 in Arabidopsis mediates Ca2+ dependent defense against phytoplasmas and reduction of plant growth. *Scientific Reports*, *15*(1), 17829. https://doi.org/10.1038/s41598-025-01374-8

Pogson, B. J., Ganguly, D., & Albrecht-Borth, V. (2015). Insights into chloroplast biogenesis and development. *Biochimica et Biophysica Acta (BBA) - Bioenergetics*, *1847*(9), 1017–1024. https://doi.org/10.1016/j.bbabio.2015.02.003

Quaglino, F., Zhao, Y., Casati, P., Bulgari, D., Bianco, P. A., Wei, W., & Davis, R. E. (2013). "Candidatus Phytoplasma solani", a novel taxon associated with stolbur- and bois noir-related diseases of plants. *International Journal of Systematic and Evolutionary Microbiology*, *63*(Pt 8), Article Pt 8. https://doi.org/10.1099/ijs.0.044750-0

Richter, A. S., Nägele, T., Grimm, B., Kaufmann, K., Schroda, M., Leister, D., & Kleine, T. (2023). Retrograde signaling in plants: A critical review focusing on the GUN pathway and beyond. *Plant Communications*, *4*(1), 100511. https://doi.org/10.1016/j.xplc.2022.100511

Susek, R. E., Ausubel, F. M., & Chory, J. (1993). Signal transduction mutants of arabidopsis uncouple nuclear CAB and RBCS gene expression from chloroplast development. *Cell*, *74*(5), Article 5. https://doi.org/10.1016/0092-8674(93)90459-4

Terry, M. J., & Kendrick, R. E. (1996). The aurea and yellow-green-2 Mutants of Tomato Are Deficient in Phytochrome Chromophore Synthesis. *Journal of Biological Chemistry*, *271*(35), 21681–21686. https://doi.org/10.1074/jbc.271.35.21681

Terry, M. J. (1997). Phytochrome chromophore-deficient mutants. *Plant, Cell & Environment*, *20*(6), Article 6. https://doi.org/10.1046/j.1365-3040.1997.d01-102.x

Terry, M. J., & Kendrick, R. E. (1999). Feedback Inhibition of Chlorophyll Synthesis in the Phytochrome Chromophore-Deficient *aurea* and *yellow-green-2* Mutants of Tomato. *Plant Physiology*, *119*(1), 143–152. https://doi.org/10.1104/pp.119.1.143

Wang, L., Leister, D., & Kleine, T. (2020). Chloroplast development and genomes uncoupled signaling are independent of the RNA-directed DNA methylation pathway. *Scientific Reports*, *10*(1), Article 1. https://doi.org/10.1038/s41598-020-71907-w

Wu, G.-Z., & Bock, R. (2021). GUN control in retrograde signaling: How GENOMES UNCOUPLED proteins adjust nuclear gene expression to plastid biogenesis. *The Plant Cell*, *33*(3), Article 3. https://doi.org/10.1093/plcell/koaa048

Chapter IV - General Conclusions

Phytoplasmas '*Ca*. P. solani', represents a major threat to global crop production due to their unique biological features, complex transmission dynamics, and profound physiological impact on host plants. These cell wall-less bacteria, restricted to sieve elements, exploit the nutrient-rich and immune-privileged environment of the phloem while evading early detection and defense responses. Building on previous work carried out by our research, our integrative analysis combining transcriptomics, co-expression network analysis, and physiological characterization of *S. lycopersicum* cv. Micro-Tom allowed to gain deeper understanding on how '*Ca*. P. solani' infection severely disrupting the host's photosynthetic machinery through repression of key genes involved in chlorophyll biosynthesis, the electron transport chain, and carbon fixation. This approach revealed that the disruption is primarily driven by impaired chloroplast-mediated anterograde and retrograde signaling, which normally coordinates chloroplast function with nuclear gene expression.

Importantly, our findings underscore the pivotal role of chloroplasts not only in energy metabolism but also as signaling hubs in plant immunity, influencing hormone biosynthesis, redox homeostasis, and defense gene activation. In addition to advancing current knowledge, our data demonstrated that the differential physiological responses between Wild-type and *Aurea* mutant plants highlight the critical role of genetic background and photomorphogenic traits in shaping host resilience.The *Aurea* mutant, with its altered light signaling and carbon allocation strategies, maintained a more stable physiological performance under '*Ca*. P. solani' infection, including improved water-use efficiency, sustained electron transport, and greater fruit biomass retention, highlighting genotype-specific mechanisms of tolerance.

Together, this work provides new insights into how phytoplasmas interfere with core plant functions by targeting chloroplast signaling pathways and offers a physiological and molecular framework for understanding tolerance mechanisms. These insights may

support the development of more targeted strategies for phytoplasma disease management, including the development of genotypes with enhanced chloroplast resilience and improved immune signaling.

Acknowledgments

I would like to express my deepest gratitude to my supervisors: Professor Fabio Marroni, Dr. Simonetta Santi, and Professor Rita Musetti. Their support was invaluable, but even more so, they motivated me when my determination faltered, always encouraging me to push myself further and reach my goals. I am especially grateful to Dr. Santi for her patience and guidance throughout my PhD journey, and Professor Marroni for his mentoring and friendship.

I would also like to extend my heartfelt thanks to my PhD colleague, Massimo Guazzini, for his friendship and invaluable assistance with data analysis, as well as for his support in the moments when I needed it most.

A special thank you goes to Dr. Gaia Carminati for her technical support at the beginning of my experiments. To Dr. Alessandra De Francesco, for her true friendship. I also would like to thank Professors Marta Martini and Dr. Paolo Ermacora for providing the phytoplasma strain and access to the growth chamber. My thanks also go to Dr. Chiara Bernardini for her help and exchange experiences. Lastly, I would like to thank the entire Plant Pathology Research Group at the University of Udine for their support, the time we shared in the lab, and the kindness and respect they have always shown me.

I would like to express my deepest gratitude to my three mothers. Yes, believe it or not, I am blessed to have three (Maria, Rosaria, and Flavia) for their unconditional love and support. I am also grateful to my uncle Dr. Antonio Carlos de Oliveira, whose example I have always strived to follow. To my lovely wife Lilian, thank you for your unwavering love, care, and for never giving up on me.

Finally, I want to thank everyone who crossed my path throughout this journey, each contributing in their own way. A special thanks goes to Professor Rogério Falleiros Carvalho from São Paulo State University (UNESP), Brazil, whose support, guidance, and long conversations helped me grow professionally and personally.

List of Publications

Journal of Plant Pathology (2022) 104:1207–1280
https://doi.org/10.1007/s42161-022-01234-8

ABSTRACT

Abstracts of presentations at the XXVII Congress of the Italian Phytopathological Society (SIPaV)

September 21-23, 2022. University of Palermo, Palermo, Italy

Published online: 29 November 2022

Phloem-restricted phytoplasmas impair carbon fixation in tomato

F. Cantao[1], S. Santi[1], F. Marroni[1], M. Guazzini[1], R. Musetti[2]

[1]University of Udine, Department of Agricultural, Food, Environmental and Animal Sciences, Via delle Scienze, 206—33100 Udine; [2]Department of Land, Environment, Agriculture and Forestry (TESAF), University of Padova Agripolis, Viale dell'Università 16 – 35020 Legnaro, Padova, Italy. E-mail: cantao.fernando@spes.uniud.it

Phytoplasmas are prokaryotic obligated parasites of plants that colonize the sieve elements of their host plant, causing alterations in phloem function such as occlusion, nutrients uptake and utilization, impairment of photosynthesis and photo assimilates translocation. Symptoms have been well described and include inhibition and decline of photosynthesis efficiency and alterations in sugar metabolism. Our research group has been investigating the effects of 'Candidatus *Phytoplasma solani*' infection on tomato plants (*Solanum lycopersicum* cv. Micro-Tom) by RNA-sequencing. Analyzing tomato plants grown under different Fe regimes, we demonstrated that infection changes Fe distribution in leaves, affects photosynthetic machinery and perturbs shoot-to-root communication. Moreover, infection impacts mineral nutrient fluxes and alters ion homeostasis of K, Ca, Mg, Fe and Mn. Here, we focus our analysis on the transcriptional regulation of genes involved on carbon fixation and carbon metabolism. A gene co-expression network was investigated with a weighted correlation approach implemented in the R package WGCNA. Gene expression and protein analysis highlighted key genes of carbon fixation pathway and confirmed impairment of carbon metabolism.

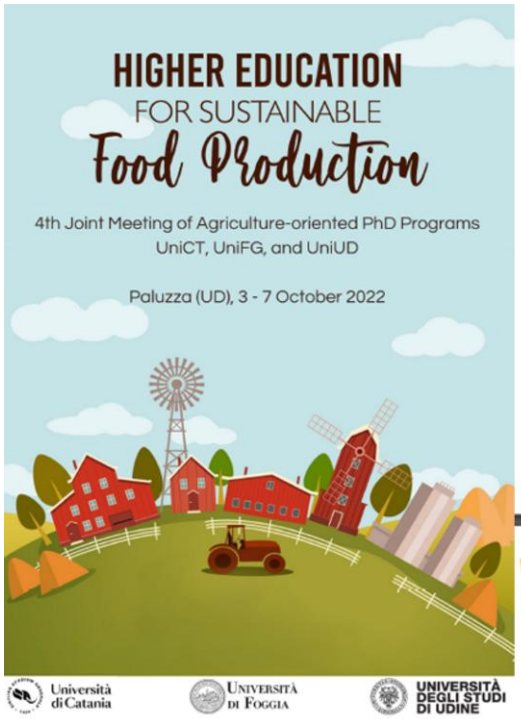

Unlocking the molecular bases of phytoplasmas infection and recovery

Fernando Cantão - cantão.fernando@spes.uniud.it; Simonetta Santi - simonetta.santi@uniud.it; Fabio Marroni - fabio.marroni@uniud.it and Rita Musetti - rita.musetti@unipd.it
[1]Department of Agricultural, Food, Environmental and Animal Sciences, University of Udine
[2]Department of Land, Environment, Agriculture and Forestry (TESAF), University of Padova

Phytoplasmas are prokaryotic phloem-restricted parasites, whose management relies exclusively on the preventive control of the vectors using compulsory insecticide application. In grapevine an interesting aspect of plant-phytoplasma interaction (PPI) is recovery phenomenon, which is a spontaneous remission of symptoms in previously symptomatic plants. Genes modulated in recovered plants can be regarded as promising players on phytoplasma resistance, although the underlying molecular mechanisms are still unknown. The aim of our project is to study the molecular bases of PPI. To reveal transcriptomic changes specifically at the infection site. Transcriptome profiling by RNA-seq was carried out and generated a sub-set of genes differentially regulated in tomato infected midribs and grapevine phloem-cell complexes upon infection and, in case of grapevine, also upon recovery. This has served as foundation for developing a gene co-expression network, evidencing crucial molecular players in the PPI that could then be verified by classical reverse genetics approaches. Grapevine proteomics analysis of the phloem exudates and leaf midrib is planned, thus proteomics coupled with phloem transcriptome profiling will allow us to select the most interesting genes or proteins expressed during the interaction (i.e., phytoplasma effectors and phloem receptors). We expect to

4th Joint Meeting of Agriculture-oriented PhD Programs
3-7 October 2022

set up a platform for silencing or overexpressing candidate genes in tomato, used as experimental test plant. Transgenic plants will be produced, and phenotype analyzed. Project outcomes have the potential to improve significantly basic knowledge on general and specific plant defense mechanisms during phytoplasma infection, leading to the development of more sustainable control strategies.

Journal of Plant Pathology (2023) 105:1237–1323
https://doi.org/10.1007/s42161-023-01500-3

ABSTRACT

Abstracts of presentations at the XXVIII Congress of the Italian Phytopathological Society (SIPaV)

September 18 - 20, 2023. University of Naples "Federico II", Naples, Italy

Published online: 15 November 2023

Transcriptome dynamics underlying AtSEOR2-mediated defense responses of Arabidopsis to phytoplasmas

K. Omenge[1], O.C. Viscardo[2,3], F.R. De Oliveira Cantao[4], S. Santi[4], R. Musetti[2]

[1]Julius Kühn-Institut (JKI) - Federal Research Centre for Cultivated Plants, Institute for Biosafety in Plant Biotechnology (SB), Erwin-Baur-Straße 27, D-06484 Quedlinburg, Germany; [2]Department of Land, Environment, Agriculture and Forestry (TESAF), University of Padova, viale dell'Università 16, 35020 Legnaro (PD), Italy; [3]CREA Centro di Ricerca per la Viticoltura e l'Enologia, via XXVIII Aprile 26, 31015 Conegliano (TV), Italy; [4]University of Udine, Department of Agricultural, Food, Environmental and Animal Sciences, via delle Scienze, 206, 33100 Udine, Italy. E-mail: rita.musetti@unipd.it

Phytoplasmas are bacterial pathogens that inflict significant economic losses on a global scale. Residing in the sieve elements of their host plants, phytoplasmas impair the immune system, altering the development, *via* secretion of effector proteins. Many studies focused on the identification of the effector-mediated mechanisms altering plant physiology following phytoplasma infection. However, the mechanisms underlying the activation of the immune response by the host plant in response to phytoplasmas remain largely unknown. In Arabidopsis, a sieve-element occlusion-related (SEOR) protein, AtSEOR2, is an "effector hub" involved in plant immunity. Arabidopsis mutants expressing unbound AtSEOR2 display reduced phytoplasma titer compared to Col-0 wild type (wt) plants in early infection stage. The present study sought to elucidate the gene expression profiles associated with the AtSEOR2 protein of infected plants. RNA was extracted from the leaves of plants expressing unbound AtSEOR2 protein followed by RNA-seq in an Illumina platform. Comparative transcriptome analysis revealed 1036 differentially expressed genes (DEGs) (893 up- and 143 down-regulated) plants expressing unbound AtSEOR2. DEGs were significantly enriched in two pathways associated with plant immunity. Plants expressing unbound AtSEOR2 exhibited significant upregulation of key genes involved in plant defense, in contrast to wt plants. The observed decrease in phytoplasma titers in plants expressing unbound AtSEOR2 can thus be attributed to a heightened immune response, indicating a stronger immune reaction compared to wt plants. The development of an interaction network between up- and down-regulated DEGs and AtSEOR2 highlights the main metabolic pathways involved in AtSEOR2-mediated defense processes.

5th Joint Meeting of Agriculture-oriented PhD Programs

25-28 September 2023

Presentation#19

Unlocking the physiology and molecular bases of phytoplasmas infection: an update

Fernando Cantão – *cantao.fernando@spes.uniud.it*
Simonetta Santi & Fabio Marroni
University of Udine

The symptoms of phytoplasma infections vary depending on the pathogen phylogenetic group and the host plant. However, leaf discoloration is a common symptom in most phytoplasma diseases. It indicates that the infection affects the chloroplast and its components. In fact, disruptions in the photosynthetic apparatus and the carbohydrate metabolic pathways are the most significant changes in response to the infection. Despite the growing understanding of the chloroplast's role as a target in plant diseases caused by effectors, its precise role during phytoplasma infections remains unclear. RNA-seq was employed to conduct transcriptome profiling in stolbur-infected tomato plants, resulting in the identification of a subset of genes exhibiting differential regulation in infected midribs. A gene co-expression network was performed revealing 14 modules evidencing crucial molecular players in the plant pathogen interaction specially for genes regulating photosynthesis, chlorophyll and carotenoids biosynthesis and photorespiration. Gas exchange (by Infrared Gas Analyzer, IRGA) and chlorophyll, carotenoids, reactive oxygen species (ROS) were analytically determined. The results were consistent with the data obtained from the RNA-Seq analysis. Chloroplasts play a central role in producing energy, hormones, and ROS. Nevertheless, phloem chloroplasts serve distinct functions by prioritizing energy provision over carbon fixation, which is the primary role of mesophyll chloroplasts. New experiments with the Micro-tom Aurea mutant, which carries a mutated allele (gene *Solyc01g008930*) that is unable to respond to light for processes like photomorphogenesis (i.e., chloroplast differentiation) have been started. Integrating transcriptomic profiling, protein expression with photosynthesis phenotyping we expect to better understand the interplay between chloroplasts and stolbur-infection in tomato plants.

Chloroplasts 'retrograde signaling' in phytoplasma infected Micro-Tom: Who switched the lights off?

F.Cantao[1], R. Musetti[2], F. Marroni[1], R. Carvalho[3], S. Santi[1]

[1]Department of Agricultural, Food, Environmental and Animal Sciences, University of Udine, Italy, [2]Department of Land, Environment, Agriculture and Forestry (TESAF), Università di Padova, via delle Università, Legnaro, Italy, [3]Department of Biology, Faculty of Agriculture and Veterinary Sciences, São Paulo State University, Jaboticabal, São Paulo, Brazil

Phytoplasma-infected plants often display a range of symptoms, including the proliferation of auxiliary shoots known as "witches'-broom," abnormal elongation of internodes, yellowing, alterations in leaf and flower morphoanatomy, leading to sterility. Accompanied by a reduction in chlorophylls and carotenoids, yellowing is associated to severely impaired photosynthesis. During the infection, a general downregulation of genes involved in light harvesting and electron flow, as well as carbon fixation has been reported. The chloroplast's role during phytoplasma infection remains unclear, although its function as a target in effector-mediated plant pathologies is becoming more evident. Here we have performed a re-analysis of a previously generated RNA-Seq of Micro-tom leaves, using both the reference build SL3.0 for tomato genome (gene annotation ITAG3.20) and the reference genome GCA_000970375 (strain 284_09) for '*Candidatus* Phytoplasma solani', followed by weighted gene co-expression network analysis. A large cluster of co-expressed genes (called 'brown' module) harbored most of the plant nuclear genes encoding for chloroplast proteins and was enriched in KEGG Pathways as Carbon fixation, Carotenoid biosynthesis and Porphyrin metabolism, Sulphur and Nitrogen metabolism. Glyoxylate and dicarboxylate metabolism, as well as Carbon metabolism and Glycolysis also resulted enriched pathways in this module. Plastids communicate their developmental and physiological status to the nucleus via 'retrograde signalling', controlled by different factors, among which light, tetrapyrrole biosynthesis, redox-state and reactive oxygen species. Signaling during plastid biogenesis has been studied in *gun* (*genomes uncoupled*) mutants for three decades. Analysis of the brown module highlighted the downregulation of several known and putative photosynthesis-associated *GUN* genes in the infected plants. Genes encoding transcription factors such as GOLDEN-LIKE1 and 2 (GLK1 and GLK2) that act downstream of both light and phytohormone signalling were downregulated by the infection. The loci *GUN2-GUN6* encode enzymes and regulators of tetrapyrrole biosynthesis. The mutant Aurea (GUN3, phytochromobilin synthase) affects the signal transduction pathway of phytochrome A and photomorphogenesis. We next, conducted a series of experiments comparing the genotypes of Micro-Tom (Wild-type and Aurea) in healthy and phytoplasma-infected conditions by physiology and biochemical approaches, followed by a new RNA-Seq. We also focused our analysis on a second module of co-expressed genes (called 'blue') composed of phytoplasma and by a relatively large number of *Solanum* genes. Interestingly, the blue module was enriched in KEGG pathways such MAPK signaling pathway-plant, and plant hormone signal transduction. Also, the GO terms, biological process categories related to "floral organ morphogenesis", "anatomical structure morphogenesis" and "plant organ development" were enriched, providing clues to the genes responsible for the differences observed between healthy and infected plants.

frontiers | Frontiers in Microbiology

TYPE Original Research
PUBLISHED 02 February 2023
DOI 10.3389/fmicb.2023.1030414

OPEN ACCESS

EDITED BY
Esther Menendez,
University of Salamanca,
Spain

REVIEWED BY
Claudia S. L. Vicente,
University of Évora, Portugal
Aurelio Ciancio,
Institute for the Sustainable Protection of Plants, Bari branch, Institute for Sustainable Plant Protection (CNR), Italy
Katrin Janik,
Leimburg Research Centre, Italy

*CORRESPONDENCE
Rita Musetti
rita.musetti@unipd.it

SPECIALTY SECTION
This article was submitted to Microbe and Virus Interactions with Plants, a section of the journal Frontiers in Microbiology

RECEIVED 28 August 2022
ACCEPTED 13 January 2023
PUBLISHED 02 February 2023

CITATION
Musetti R, Pagliari L, Mian G, De Oliveira Cantao FR, Bernardini C, Santi S and van Bel AJE (2023) The sieve-element endoplasmic reticulum: A focal point of phytoplasma-host plant interaction?
Front. Microbiol. 14:1030414.
doi: 10.3389/fmicb.2023.1030414

The sieve-element endoplasmic reticulum: A focal point of phytoplasma-host plant interaction?

Rita Musetti[1]*, Laura Pagliari[1], Giovanni Mian[1], Fernando R. De Oliveira Cantao[2], Chiara Bernardini[2], Simonetta Santi[2] and Aart J. E. van Bel[3]

[1]Department of Land, Environment, Agriculture and Forestry (TESAF), Università di Padova, via dell' Università, Legnaro, Italy, [2]Department of Agricultural, Food, Environmental and Animal Sciences, University of Udine, via delle Scienze, Udine, Italy, [3]Institute of Phytopathology, Justus-Liebig University, Giessen, Germany

The rough endoplasmic reticulum (r-ER) is of paramount importance for adaptive responses to biotic stresses due to an increased demand for de novo synthesis of immunity-related proteins and signaling components. In nucleate cells, disturbance of r-ER integrity and functionality leads to the "unfolded protein response" (UPR), which is an important component of innate plant immune signaling. In contrast to an abundance of reports on r-ER responses to biotic challenges, sieve-element endoplasmic reticulum (SE-ER) responses to phytoplasma infection have not been investigated. We found that morphological SE-ER changes, associated with phytoplasma infection, are accompanied by differential expression of genes encoding proteins involved in shaping and anchoring the reticulum. Phytoplasma infection also triggers an increased release of bZIP signals from the (SE-ER)/r-ER and consequent differential expression of UPR-related genes. The modified expression patterns seem to reflect a trade-off between survival of host cells, needed for the phytoplasmic biotrophic lifestyle, and phytoplasmas. Specialized plasmodesmata between sieve element and companion cell may provide a corridor for transfer of phytoplasma effectors inducing UPR-related gene expression in companion cells.

KEYWORDS

Arabidopsis, endoplasmic reticulum, phytoplasma, phytoplasma-host interaction, sieve element, pore-plasmodesma units, sieve-element ER docking sites, unfolded protein response

1. Introduction

Phytoplasmas are phytopathogenic mollicutes associated with numerous economically relevant plant diseases, worldwide (Namba, 2019). Biology of phytoplasmas and host responses to infection are still largely unknown due to the biotrophic lifestyle of these microorganisms which impedes *in vitro* studies (Jiang et al., 2019; Maputsanga et al., 2022). In plants, phytoplasmas reside exclusively in sieve elements (SEs; van Bel and Musetti, 2019; Lewis et al., 2022), highly specialized transport cells, that provide an exceptional physical and chemical environment, favored by phytoplasmas (van Bel et al., 2022). The interaction between phytoplasmas and SE components has barely been investigated thus far (van Bel and Musetti, 2019). Phytoplasmas have a low-size genome, and their survival most likely relies on plant resources, given the absence of many key genes, essential for cell metabolism (Kube et al., 2012; Oshima et al., 2013).

www.nature.com/scientificreports

scientific reports

Check for updates

OPEN

SEOR2 in *Arabidopsis* mediates Ca^{2+} dependent defense against phytoplasmas and reduction of plant growth

Keziah Omenge[1,6], Ottone Carmelo Viscardo[2,3,6], Fernando Rodrigo De Oliveira Cantao[4], Simonetta Santi[4], Aart Jan Eeuwe van Bel[5] & Rita Musetti[2]✉

The *Arabidopsis seor1ko* line, which expresses the protein AtSEOR2 free of its bond with AtSEOR1, exhibits a lower phytoplasma titre as compared to wild type plants. In search for mechanism(s) underlying potential SEOR2-mediated defense responses the transcriptome of healthy wild type and *Atseor1ko* plants was disclosed by RNA sequencing. Comparative transcriptome analysis revealed 1036 differentially expressed genes (DEGs, 893 up- and 143 down-regulated) between the *Atseor1ko* line and the wild type. Sequence annotation and classification of the up-regulated genes identified "plant-pathogen interaction" among the most enriched clusters. The "plant-pathogen interaction" cluster included genes encoding members of the protein kinase superfamily, actors in calcium/calmodulin signaling transduction and WRKY transcription factors. An interaction network analysis and a host-phytoplasma interaction map demonstrated that AtSEOR2 protein could interact with the calcium-binding proteins CAM2 and TCH3. The latter one also turned out to be an indirect target of the $SAP54_{CY}$ phytoplasma effector, which suggests a SEOR2-mediated role of TCH3 in balancing nutrient investments in plant defense and plant growth.

Keywords *Arabidopsis*, AtSEOR2, Effectors, Interaction, Phloem, Plant defense, Phytoplasma

Phytoplasmas are sieve-element (SE) restricted pathogenic prokaryotes[1] causing severe yield and/or quality loss of many economically important crops[2]. Thus far, phytoplasma epidemics are mainly combatted by insect vector control through pesticides, or by removal of symptomatic plants. However, the efficacy of these approaches is limited because chemical control of vector proliferation is often inadequate and natural phytoplasma reservoirs in host plants are unknown or reside in nearby wild plants[3]. Thus, there is an urgent need for novel ways to control phytoplasma infections. Such strategies, however, require a profound knowledge of the complex mechanisms that underlie plant-phytoplasma relationships. Studies on the molecular interaction between phytoplasmas and host plants would provide important information for development of more efficient and sustainable control strategies based on natural plant defense mechanisms[4].

Phytoplasmas heavily affect host physiology by secretion of chemical effectors that weaken the defense responses of the host[5]. Effectors are able to move systemically via the SEs or to migrate cell-to-cell from the SEs to adjacent cells and tissues[6]. Plants dispose of receptor proteins for early recognition of effectors mediating plant immune reactions that counteract host colonization[7]. For phytoplasma-plant host interaction, it is unknown whether and how effector-recognition proteins activate an effector-triggered immunity (ETI). Natural resistance mechanisms to phytoplasma diseases have not yet been detected among cultivated plants, but their existence is likely, given the diverse levels of susceptibility between the genotypes of one species[8–10].

A limited number of studies, mainly making use of model plants, provided a few interesting candidate genes to be exploited in the search for resistance mechanisms against phytoplasma infection[11,12]. Phytoplasma quantification in different lines of *Arabidopsis thaliana* showed that the *Atseor1ko* line, expressing the protein

[1]Institute for Biosafety in Plant Biotechnology (SB), Julius Kühn-Institut (JKI) - Federal Research Centre for Cultivated Plants, Erwin-Baur-Straße 27, 06484 Quedlinburg, Germany. [2]Department of Land, Environment, Agriculture and Forestry (TESAF), University of Padova, Viale Dell'Università 16, 35020 Legnaro, PD, Italy. [3]CREA Centro di Ricerca per la Viticoltura e l'Enologia, Via XXVIII Aprile 26, 31015 Conegliano, TV, Italy. [4]Department of Agricultural, Food, Environmental and Animal Sciences, University of Udine, Via delle Scienze 206, 33100 Udine, Italy. [5]Institute of Phytopathology, Justus-Liebig University, Heinrich-Buff-Ring 26–32, 35392 Giessen, Germany. [6]Keziah Omenge and Ottone Carmelo Viscardo have contributed equally to this work. ✉email: rita.musetti@unipd.it